# Regulation of $GABA_AR$ Signaling and Neuroadaptations in Response to Diazepam

by

**Joshua M. Lorenz-Guertin**

B.S. Grand Valley State University, 2014

Submitted to the Graduate Faculty of

School of Medicine in partial fulfillment

of the requirements for the degree of

Doctor of Philosophy

University of Pittsburgh

2019

UNIVERSITY OF PITTSBURGH

SCHOOL OF MEDICINE

This dissertation was presented

by

**Joshua M. Lorenz-Guertin**

It was defended on

July 26, 2019

and approved by

Michael Palladino, Professor, Pharmacology & Chemical Biology

Alexander Sorkin, Professor, Cell Biology

Simon Watkins, Professor, Cell Biology

Gregg Homanics, Professor, Anesthesiology & Perioperative Medicine

Dissertation Director: Tija Jacob, Assistant Professor, Pharmacology & Chemical Biology

**Regulation of $GABA_AR$ Signaling and Neuroadaptations in Response to Diazepam**

Joshua M. Lorenz-Guertin, PhD

University of Pittsburgh, 2019

Despite 50+ years of use as anxiolytics, anti-convulsants, and sedative/hypnotic agents, the mechanisms underlying benzodiazepine (BZD) tolerance are poorly understood. BZDs potentiate the actions of GABA, the primary inhibitory neurotransmitter in the adult brain, through positive allosteric modulation of γ2 subunit containing GABA type A receptors ($GABA_ARs$). Sustained treatment with BZD drugs is intimately associated with the development of tolerance, dependence, withdrawal and addiction. BZD efficacy diminishes after prolonged or high dose acute exposure, with tolerance to the sedative/hypnotic effects forming most quickly. We investigated the adaptive mechanisms occurring during initial exposure to the classical BZD, Diazepam (DZP), and the molecular signature of the mouse brain during established sedative tolerance. We found cultured neurons treated 24 h with DZP presented no change in surface or synaptic levels of γ2-$GABA_ARs$. In contrast, both γ2 and the key inhibitory synaptic scaffolding protein gephyrin levels were decreased after a single DZP treatment *in vitro* and *in vivo*. Live-imaging and label-free quantitative proteomics further revealed alterations in γ2 subunit surface trafficking, internalization and lysosomal targeting. In comparison, mice treated seven days with DZP had altered $GABA_AR$ subunit composition, reduced responsiveness to DZP, and tonic inhibition was diminished. Furthermore, DZP increased excitatory NMDA receptor subunit levels and function. State of the art mass spectrometry experiments revealed increased CaMKII subunits, which are positive regulators of NMDA receptors and involved in tolerance to other drugs. Downstream bioinformatics analysis confirmed robust synaptic plasticity after DZP. Together, we describe a time-dependent downregulation of synaptic $GABA_AR$ function after initial DZP exposure

followed by an adaptive increase in excitatory neurotransmission, neuronal remodeling and altered synaptic $GABA_AR$ composition.

## Table of Contents

## List of Tables

## List of Figures

**Acknowledgements**

When I began graduate school I did not even know how to pipette correctly. Fast forward five years, and I can safely say I have made meaningful contributions to my field of science. None of this would have been possible without the continued support of my mentor Tija Jacob, who continuously provided me opportunities to grow as a scientist and person. The lab has seen many changes, including a long stint where it was just Dr. Jacob and I, but we remained perseverant and productive. She encouraged me to travel abroad for science and submit for travel awards, and that advice culminated with me traveling to conferences in the U.K., Switzerland and China, among many other U.S. destinations. I think I have had a unique graduate school experience, and I owe much of that to my supportive mentor.

I would also like to thank all of our collaborators who have made my thesis project and publications scientifically diverse and meaningful. Dr. Alan Waggoner, Dr. Ming Zhang, Dr. Marcel Bruchez, and Dr. Brigitte Schmidt all played integral roles in the development and characterization of the novel optical tool $\gamma 2^{pH}$FAP. Dr. Simon Watkins and Dr. Mads Larsen further enriched this project by assisting in imaging applications using this tool in various cell types. Dr. Madeline Wilcox and Dr. Jon Johnson provided important electrophysiology contributions for validation of the $\gamma 2^{pH}$FAP construct. Dr. Nadezda Povysheva in the Johnson lab also performed many key electrophysiology slice experiments in investigating functional changes in neurotransmission occurring with sustained diazepam treatment (7 day treatment protocol) with the help of Aparna Nigam performing animal injections. My research projects took a huge leap towards *in vivo* relevance thanks to the experimental mass spectrometry contributions and guidance by the labs of Dr. Susan Weintraub at the University of Texas San Antonio Health Center

and Dr. Matthew MacDonald at the University of Pittsburgh. I would also like to thank all of my former lab members who have made the everyday lab experience enjoyable and engaging. I want to especially acknowledge Dr. Megan Brady for investing multiple hours teaching me the fundamentals of science and countless techniques. Dr. Sabya Das, Dr. Katarina Vajn and Matthew Bambino had integral roles in many of my publications and work, and for that I thank you! Lastly I want to thank my committee members for continually providing insight and keeping me focused on the ultimate goal of earning a PhD.

# 1.0 Introduction

Chapter adapted from:

1) Lorenz-Guertin, J. M. and T. C. Jacob (2017). GABA type a receptor trafficking and the architecture of synaptic inhibition. Develop Neurobiol
(1) https://doi.org/10.1002/dneu.22536 License Number: 4611921510881

## 1.1 The GABA Type A Receptor

$GABA_A$ receptors ($GABA_ARs$) are ligand-gated ionotropic chloride ($Cl^-$) channels responsible for most fast inhibitory neurotransmission in the mature central nervous system (CNS). Ubiquitous expression supports their central role in regulating most aspects of CNS function. Binding of the neurotransmitter GABA induces $GABA_AR$ ion channel opening, $Cl^-$ influx, and subsequent membrane hyperpolarization **(Fig. 1A)**. These receptors are heteropentameric structures typically composed of two α (α1-6), two β (β1-3), and either a γ (γ1-3) or a δ subunit (2). Subunits share a common structure consisting of a large N-terminal extracellular domain (ECD) that participates in GABA binding, transmembrane domains (TM) comprised of four α-helical regions (TM1-4) and a small extracellular C-terminus **(Fig. 1C)**. The TM regions are connected by a small intracellular loop between TM1-TM2 and a much larger intracellular domain (ICD) between TM3 and TM4 that undergoes extensive post-translational modifications and is key for protein trafficking and function (**Fig. 1C**). The most common $GABA_ARs$ providing fast synaptic inhibition in the mature mammalian cerebral cortex contain α1β2γ2 subunits **(Fig. 1B)** (3). As viewed from outside the cell $GABA_ARs$ are arranged in a counterclockwise subunit

configuration of γ-β-α-β-α **(Fig. 1B)** (4, 5). Despite the great diversity of $GABA_AR$ subunits (α1-6, β1-3, γ1-3, δ, ε, θ, π, ρ1-3) and possible configurations, these receptors produce two types of currents: synaptic (phasic) and tonic. Presynaptic terminal release of GABA onto post-synaptically

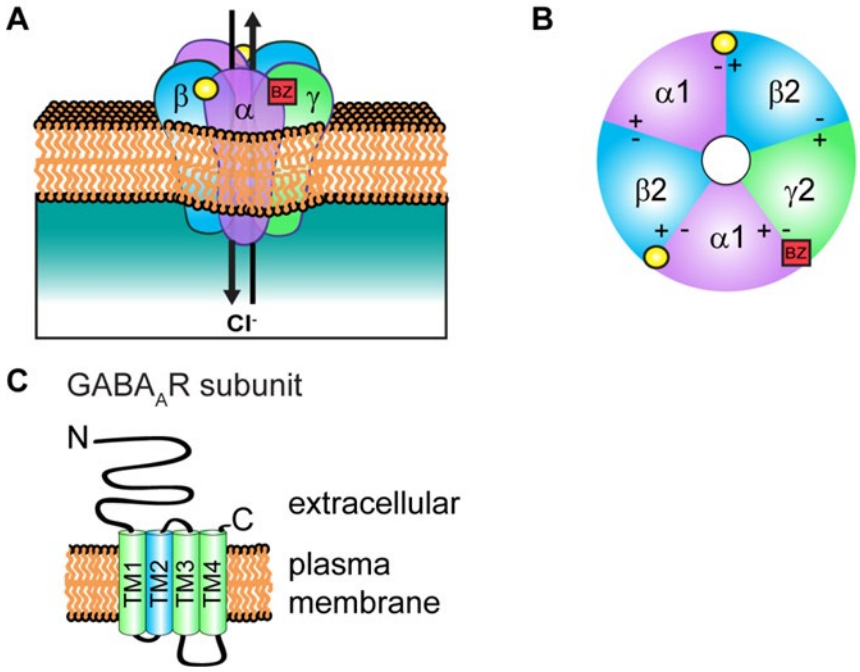


**Figure 1. $GABA_AR$ Structure and Subunit Topology.**

A) A representation of the heteropentameric $GABA_AR$ composed of αβγ subunits. Binding of the neurotransmitter GABA (yellow circle) at the αβ interface triggers ion channel opening and allows the rapid influx of $Cl^-$ and membrane hyper polarization in the mature nervous system. (B) Extracellular representation of the receptor showing all five subunits contributing to the central ion pore and the general binding sites of GABA (yellow circle) and benzodiazepines (BZs) (red square). BZs bind at the interface of an α1/2/3/5 and γ subunit. (C) All subunits have a common topology including an extracellular N-terminal domain, short C-terminal tail, and four transmembrane domains (TM1–4). $GABA_AR$ subunit TM2 (blue) contributes to formation of the receptor ion channel pore, while the intracellular domain (ICD) between TM3 and TM4 contain sites of phosphorylation and protein interactions that modulate channel function and/or trafficking. Adapted from: Lorenz-Guertin, J. M. and T. C. Jacob (2017). GABA type a receptor trafficking and the architecture of synaptic inhibition. Develop Neurobiol..

clustered $GABA_ARs$ triggers fast, transient synaptic currents, while ambient "spill over" GABA generates a persistent tonic current via activation of extrasynaptic receptors. $GABA_AR$ subunit composition therefore determines receptor cell surface localization, electrophysiological properties and drug sensitivities.

In addition to their inhibitory function in the mature CNS, $GABA_ARs$ are of fundamental importance in organization of newly forming circuits by promoting dendritic outgrowth and synaptogenesis. Synapses develop first with the emergence of excitatory GABAergic synaptic signals that drive the subsequent establishment of glutamatergic synapses, before GABA neurotransmission shifts to functioning as an inhibitory signal (6-9). Underlying deficits in GABAergic neurotransmission occur in a wide variety of neurological disorders such as epilepsy, psychiatric disorders (anxiety (10, 11), depression (12, 13), post-traumatic stress disorder (14-17)) and neurodevelopmental disorders including autism (18-21), Fragile X (22, 23) and schizophrenia (24-26). Importantly, pathophysiological events including seizures (27), ischemic stroke (28-30), traumatic brain injury (31) and stress can cause adaptive changes in $GABA_AR$ neurotransmission, compromising GABAergic inhibition and further hampering recovery.

## 1.2 $GABA_AR$ Pharmacology

### 1.2.1 $GABA_AR$ Clinical Agents

The ubiquitous expression of $GABA_ARs$ in the CNS makes these receptors key drug targets to enhance inhibition and globally dampen neuronal activity. Multiple clinically recognized agents exert actions at $GABA_ARs$ specifically or non-specifically including barbiturates, benzodiazepines

(BZDs), benzodiazepine-site ligands, barbiturates, intravenous and volatile anesthetics, ethanol and neuroactive steroids (32). In general these drugs induce distinct conformational states of $GABA_AR$s thereby altering the efficacy of GABA-mediated receptor activation. The site of $GABA_AR$ drug action is highly dependent on $GABA_AR$ subunit composition and binding site interfaces. For example, BZDs bind between the interface of a γ2 subunit and a directly adjacent α1/2/3/5 subunit at the ECD (**Fig. 1B**) (33). In contrast, transmembrane domain interactions between non α/γ subunit interfaces mediate binding drugs like etomidate, propofol, barbiturates, volatile anesthetics, octanol, and neuroactive steroids (34). Importantly, a recent surge in high-resolution $GABA_AR$ structural findings (35-40) have dramatically expanded our molecular understanding of drug binding sites and the physical changes in receptor conformation that mediate downstream signaling and clinical effects. $GABA_AR$ structures for the human β3 homopentamer bound to benzamidine (35), chimeric α5TM/β3ECD bound to the neurosteroid allopregnanolone (37), human α1β2γ2 heteropentamer bound to the benzodiazepine site antagonist Flumazenil (36), the human α1β3γ2 $GABA_AR$ in a lipid bilayer (38), as well as full-length α1β3γ2L bound in different conformations in the presence of a channel-blocker, agonist or competitive antagonist, or the BZDs alprazolam and DZP (39) have all been recently resolved. One notable finding from this work is the physical identification of an additional second low-affinity DZP binding site between the β3/α1 receptor interface (39), consistent with the biphasic response seen in electrophysiology studies using high DZP concentrations (41).

### 1.2.2 **BZD Clinical Use and Tolerance**

No $GABA_AR$ drug class has been more heavily utilized clinically or subject to more intensive research efforts than BZDs. The BZD drug class was first introduced in the 1960's by

the company Hoffman-La Roche with the release of the revolutionary drug chlordiazepoxide (Librium) (42). As compared to the widely-used CNS depressant barbiturate agents, chlordiazepoxide demonstrated significantly less dangerous side effects, most notably respiratory depression. By 1963, the second and more potent BZD, diazepam (DZP; Valium), also entered the marketplace. Before long, DZP became one of the top selling drugs in the history of mankind (43). The wide-spread use of these drugs propagated a need to characterize their pharmacological target and mechanism of action, ultimately leading to the discovery of the $GABA_AR$ (also referred to as the "BZD receptor" up until the early 2000s). Clinically, BZDs are used for their sedative, myorelaxant, anticonvulsant and short term memory loss effects. Multiple BZD type drugs exist with differing pharmacokinetic/pharmacodynamics profiles and some selectivity for specific $GABA_AR$ subtypes.

The classical BZD, DZP, belongs to a subclass of non-selective, long-acting BZDs that includes the drug flurazepam (Dalmane). Intermediate-acting BZDs (example: alprazolam; Xanax) have relatively shorter half-lives compared to DZP and flurazepam and their metabolites, where the elimination half-life may take up to 48 h in humans. A subclass of short-acting BZDs with half-lives of 1-4h are also available, namely midazolam (Versed) and triazolam (Halcion). These differences in half-lives, as well as other characteristics including peak onset time and drug administration options, provide clinicians multiple BZD therapy options to suit the preferred therapeutic outcome. This catalog of BZD drugs is heavily utilized in medicine; in 2008 approximately 5.2% of US adults aged 18-80 used BZDs according to one study (44). Additionally, a more recent survey from 2015-2016 found 12.6% of adults reported BZD use in the last year (45). Shockingly, 25.3 million individuals reported taking the drug as prescribed, while 5.3 million were reported to be misusing the drugs.

The chronic use of BZD drugs manifests in a number of behavioral and physical symptoms including tolerance, withdrawal, addiction and dependence. Requiring a higher dose of a drug to achieve the same therapeutic effect overtime is known as tolerance, and is a hallmark of BZD use. At the molecular level, positive allosteric modulation by BZD enhances $GABA_AR$ inhibition by increasing the binding affinity of GABA and increasing ion channel opening frequency (33). This potentiating effect of BZD is lost after prolonged or high dose acute exposure in animal models and humans, characterized first by a loss of sedative/hypnotic activity followed by the anti-convulsant and potentially anxiolytic properties (46). 2-Deoxyglucose quantitative autoradiography in BZD-treated rats suggests that tolerance initiates in the cerebral cortex (47), a region with diverse roles in sensory and motor processing, anxiety (48), memory (49) and sleep (50). The induction of BZD tolerance occurs in part due to the uncoupling of allosteric actions between GABA and BZD, leading to diminished potentiation of BZD on GABA-induced current and a loss in the ability of GABA to potentiate BZD binding (51, 52). Resolving the neuroadaptations that occur after BZD treatment and the molecular mechanisms regulating $GABA_AR$ function and drug responsiveness will provide a critical step in building towards new treatment paradigms that limit the harmful side effects of BZD agents.

## 1.3 $GABA_AR$ Regulation and Surface Localization

### 1.3.1 Key GABAergic Synapse Components

The confinement of $GABA_ARs$ at synaptic sites is a key step in tuning the strength of phasic inhibition, receptor function and drug response (53) **(Fig. 2)**. The postsynaptic inhibitory

scaffolding protein gephyrin is the main organizer of $GABA_AR$ synaptic localization and density (54), as gephyrin knock out mice exhibit a robust loss of $GABA_AR$ clustering (55), although gephyrin-independent synaptic clustering does occur (56, 57). Gephyrin is a highly conserved 93 kDa protein that is hypothesized to form multimeric complexes which associate with a number of cytoskeletal proteins (58), contributing to its scaffolding function (59). The architecture of gephyrin scaffolding arises from the N-terminal or G-domain of gephyrin participating in dimer-dimer self-associations, while the C-terminal or E-domain forms trimer interactions, likely to create a hexagonal lattice (60, 61). This structure tethers freely-diffusing receptors at synaptic sites through binding $GABA_AR$ α1, α2, α3, α5, β2, and β3 subunits (62-65). The $GABA_AR$ γ2 subunit also plays an important role in gephyrin-receptor attachment, as γ2-knockout mice demonstrate diminished clustering of gephyrin and $GABA_ARs$ (66, 67). Importantly, synaptic $GABA_AR$ clustering can occur independent of γ2 in some cases (68). Functionally, gephyrin acts to confine receptors undergoing diffusion at the cell surface membrane and limit their escape into the extrasynaptic space, a process that is influenced by neuronal activity and $GABA_AR$ specific drugs including DZP (69, 70).

Gephyrin's scaffolding ability is regulated by extensive post-translational modifications. Mass spectrometry studies alone have revealed 22 sites of phosphorylation in gephyrin's C-domain and 1 additional threonine 324 (Thr324) site in the E-domain (71-73). Yet, the exact role of gephyrin phosphorylation is complex and controversial, highlighted by the bidirectional effect of altering gephyrin phosphorylation at the serine (S) 270 site. Initial findings by Tyagarajan et al. (2011) (74) identified phosphorylation of this site by Glycogen Synthase Kinase 3β (GSK3β) to negatively modulate gephyrin clustering via enhanced $Ca^{2+}$-dependent protease calpain-1 mediated degradation. Accordingly, overexpression of a phosphodeficient S270A gephyrin mutant

enhanced both the amplitude and frequency of miniature inhibitory postsynaptic currents (mIPSCs), suggesting increased functional $GABA_AR$ clustering. It was later revealed that the S270 site was also a substrate for the proline-directed serine/threonine kinase, cyclin-dependent kinase 5 (CDK5) (72, 75). Gephyrin synaptic clusters were found to be basally phosphorylated at Ser270 in a CDK5-dependent manner (72), with CDK5 knockdown or inhibition leading to loss of phosphorylated gephyrin clusters and postsynaptic γ2-containing $GABA_A$ receptors (75). To further complicate these findings, S270 is cross-regulated by phosphorylation of a neighboring S268 residue targeted by extracellular signal-regulated kinase 1/2 (ERK1/2) (73) (role for ERK also described in (76)). This study suggested these serine residues control distinct gephyrin clustering dynamics including postsynaptic cluster size and number, again in conjunction with calpain activity. Expanding the role of gephyrin serine site regulation, phosphomutant studies and *in vitro* kinase assays indicate that increased phosphorylation of gephyrin on S305 (mass spectrometry identification by Tyagarajan et al) by the kinase CAMKII is required for activity-dependent inhibitory plasticity (77). Considering the number of additional gephyrin phosphorylation sites identified *in vivo* and the challenges of gephyrin point mutant studies (overexpression concerns), continued multidisciplinary efforts are necessary to resolve the functional relevance of these modifications.

Transynaptic proteins are also key to GABAergic synapses formation and stability. One of the most well characterized trans-synaptic interactions crucial for $GABA_AR$ synapse development is that of neuroligins and neurexins (78) **(Fig. 2)**. Neurexins are found presynaptically and induce differentiation of GABAergic and glutamatergic postsynaptic densities during maturation and plasticity (79, 80), although overexpression of neurexins leads to reduced GABAergic neurotransmission (81). Postsynaptically, different neuroligins (NL1-4) are found at either

glutamatergic or GABAergic synapses and play important scaffolding and receptor recruitment roles. GABAergic synapses primarily rely on NL2 for synapse integrity, and when expressed with recombinant $GABA_A$Rs in HEK cells, NL2 supports formation of functional GABAergic synapses in neuron co-culture systems (82). Moreover, NL2 is critical for GABAergic synapse formation and coding in the retina (83), while enhanced expression of this protein in cerebellar granule cells can accelerate $GABA_A$R synapse development (84, 85) and strengthen inhibitory synaptic function in hippocampal neurons (86).

Our current overall understanding of the proteins involved in inhibitory synapse stability and clustering remains incomplete, as highlighted by two *in vivo* inhibitory synapse proteomic screenings using α2-pHluorin (pH-sensitive GFP) tagged subunit knock-in mice (87) or viral expression of inhibitory fusion proteins including gephyrin (88). These mass spectrometry methods revealed 140 (Uezu, et al. 2016) and 149 (Nakamura, et al. 2016) novel protein components of $GABA_A$R/inhibitory synapses spanning multiple trafficking, stability, and regulatory pathways. Collectively, these studies further validated molecular interactions between $GABA_A$R intracellular loops and the metabotropic glutamate receptor subunit mGluR5, the Dbl family GEF Ephexin, the metabotropic GABA B receptor ($GABA_B$R) auxiliary subunit KCTD12, and initiated characterization of a novel inhibitory synaptic regulator inhibitory synaptic protein 1 (InSyn1). Our lab recently found DZP-induced changes in γ2-$GABA_A$R using label-free quantitative proteomics (details in Chapter 3), identifying new key interactor proteins and changes in their association by a common clinical agent. Future investigations will need to dissect the exact roles of these identified proteins in $GABA_A$R regulation and function.

### 1.3.2 **Extrasynaptic $GABA_ARs$**

While synaptic receptors participate in phasic inhibition, extrasynaptic $GABA_ARs$ are responsible for setting the inhibitory tone of a neuron through the generation of a constant tonic current. Receptors composed of α4βδ or α6βδ subunits are found extrasynaptically and respond to low concentrations of ambient or "spillover" GABA (89-94) **(Fig. 2)**. While hippocampal tonic currents are largely generated by synaptic spillover (95), other GABA sources include astrocytes (96, 97), and neurogliaform cells (98). Furthermore, extrasynaptic $GABA_ARs$ can be spontaneously open in the absence of GABA (99). $GABA_ARs$ incorporating the α5 subunit with βγ2 also represent a large pool of extrasynaptic GABAergic signaling (100, 101), although this receptor subtype can be found clustered both synaptically (63, 102, 103) and extrasynaptically (104). Scaffolding of α5βγ2 $GABA_ARs$ extrasynaptically occurs due to interaction with the ERM (ezrin, radixin, moesin) family protein radixin (104), whereas α5 was recently shown to interact with gephyrin at synaptic sites (63).

It is important to note that $GABA_ARs$ undergo Brownian motion at the surface membrane and are continuously diffusing into and out of the synaptic and extrasynaptic space (105), meaning δ containing $GABA_ARs$ can impact synaptic current, and γ2 $GABA_ARs$ participate in extrasynaptic tonic current. $GABA_AR$ subtype specific protein interactions regulate the degree of confinement at a given location and $GABA_AR$ diffusion dynamics and localization are highly influenced by activity-dependent changes and various signaling cascades (Section 1.5). For instance, radixin acts in a phospho-dependent manner to scaffold α5βγ2 receptors to the actin cytoskeleton ultimately reducing diffusion rates and concentrating channel activity away from axon terminals (106). Bidirectional control of radixin phosphorylation state by the RhoA GTP- and Rho-kinase (ROCK)

dependent pathway is contingent on GABAergic versus glutamatergic activity **(Fig. 2)**. Application of GABA favors radixin phosphorylation and retention of α5-$GABA_A$Rs extrasynaptically, while AMPA treatment leads to dephosphorylation and increased percentage of α5-subunit receptors found synaptically (106). Additional $GABA_A$R subtypes are also subject to synaptic/extrasynaptic exchange following manipulations of the excitatory/inhibitory balance and/or kinase signaling. Gerrow & Triller (2014) identified $GABA_B$R activity increases α2-$GABA_A$Rs diffusion from synapses via PKC activity, allowing α5-$GABA_A$R synaptic accumulation due to available synaptic binding slots (107). PKC-activation also promotes synaptic accumulation of α4-containing $GABA_A$Rs (108), while PKA-activation shifts α4-receptors extrasynaptically **(Fig. 2)** (109). These findings highlight the dynamic nature of $GABA_A$R synaptic/extrasynaptic exchange and the diverse mechanisms to fine-tune GABAergic neurotransmission.

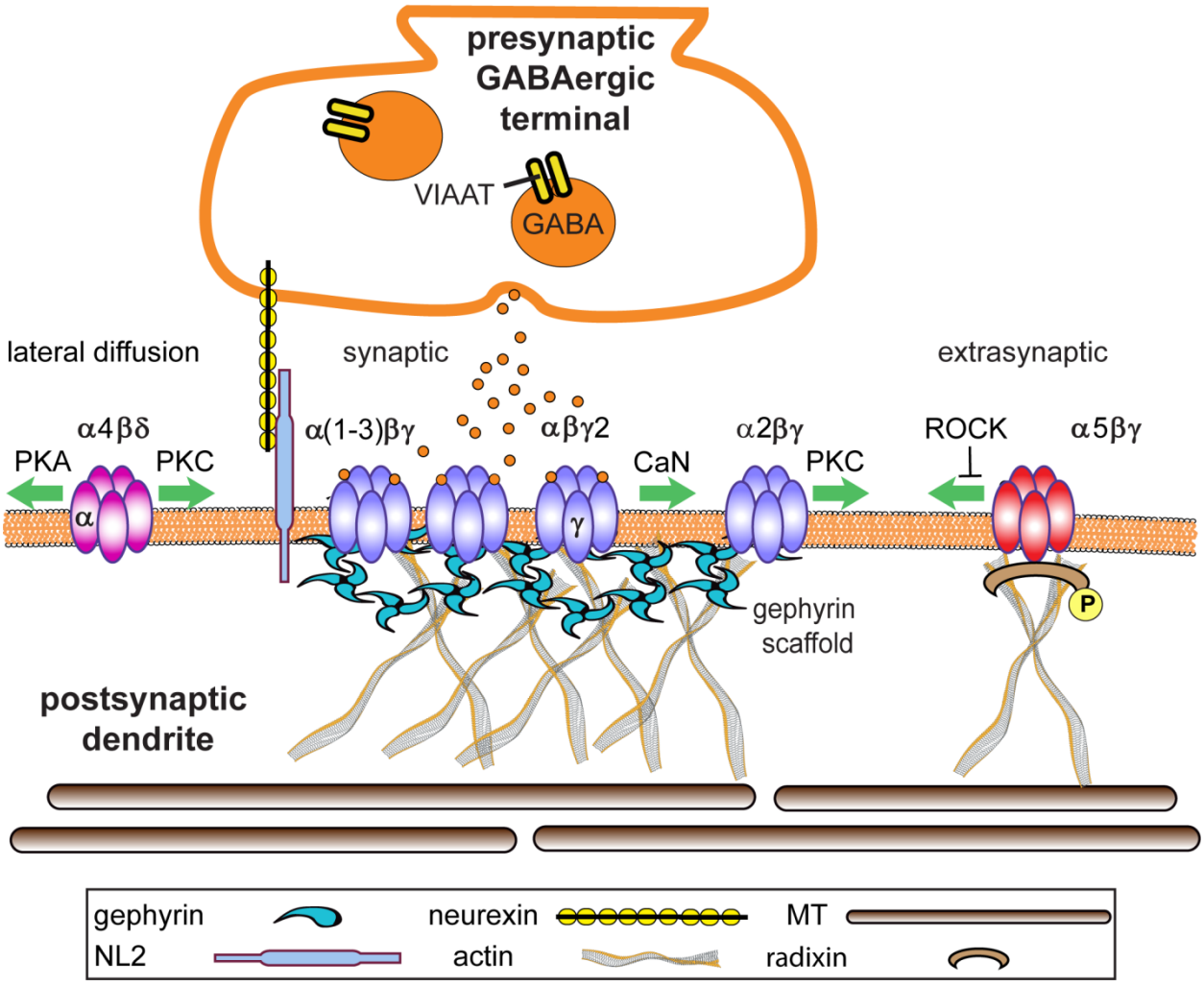


**Figure 2. GABA$_A$R Synapse Structure.**

GABA$_A$Rs composed of α(1–3)βγ subunits are largely synaptically localized via gephyrin interactions and contribute to phasic currents, whereas α(4/6)βδ receptors are extrasynaptic and generate tonic current. α5βγ receptors are found in both locations due to binding with gephyrin at synapses and radixin extrasynaptically. Proteomics and other modern strategies have significantly enriched the complexity of the inhibitory synapse, however the functions of many new components have yet to be defined. Key synaptic adhesion, scaffold and signaling proteins shown. Adapted from: Lorenz-Guertin, J. M. and T. C. Jacob (2017). GABA type a receptor trafficking and the architecture of synaptic inhibition. Develop Neurobiol.

## 1.4 $GABA_AR$ Intracellular Trafficking

### 1.4.1 Assembly and Forward Trafficking

$GABA_AR$ biogenesis is controlled via regulated assembly of subunits into heteropentamers within the endoplasmic reticulum (ER). Due to the diversity of receptors generated in recombinant systems during multiple independent subunit transfections, studies on assembly of concatenated subunit constructs have been a major route for determining receptor configuration. $GABA_AR$ studies using heterologous cells show that a β subunit is required for receptor cell surface expression, while the αβ interface that forms the GABA binding site is required for functional responses. Although unlikely to occur *in vivo*, β1 or β3 homomeric channels form, while other individual subunit expression leads to ER retention (110, 111). Co-expression of γ2 subunits with αβ leads to preferential assembly of αβγ2 receptors (112, 113). Receptor complex formation begins with αβ heterodimer formation, with the N-terminal domains controlling this process. Studies of α1β2γ2 recombinant receptors demonstrate that the N-terminal putative α helical region of the α1 subunit is critical for surface receptor expression, while deletion of the other subunits N-terminal extensions had minimal effects on surface expression (114). Rather, deletion of the β2 α-helix decreased GABA sensitivity and receptor desensitization, while γ2 N-terminal deletions reduced incorporation of γ2 in receptors.

The exit of $GABA_ARs$ from the ER is negatively regulated by constitutive ER-associated degradation (ERAD) (115-117). ERAD recognition of misfolded proteins leads to their dislocation from the ER membrane, ubiquitination via E3 ligases, and proteosomal degradation in the cytoplasm. Chronic neuronal blockade via 24 h tetrodotoxin (TTX) treatment increases β3 subunit $GABA_AR$ ubiquitination and ERAD, leading to reduced receptor cell surface expression and

decreased inhibition (117). Conversely, enhanced neuronal activity diminished β3 subunit ubiquitination and improved receptor stability. Reduced calcium entry via voltage-gated calcium channels (VGCC) also contributes to ubiquitination and degradation of receptor subunits (118), while enhanced VGCC activity promotes β3 S383 phosphorylation and receptor insertion (119), suggesting a mechanistic link to activity-dependent changes. $GABA_AR$ subunit mutations that result in enhanced ERAD contribute to genetically determined epilepsies, or idiopathic generalized epilepsies (IGEs) (120, 121) and altered $GABA_AR$ ERAD is indicated in autism spectrum disorder (ASD) subjects (122)

Once assembled, $GABA_ARs$ undergo transport from the ER to the Golgi apparatus, followed by translocation to the plasma membrane. In the Golgi, the γ2 subunit is subject to palmitoylation by the Golgi-specific DHHC zinc finger enzyme (GODZ), a process important for synaptic $GABA_AR$ maintenance and surface expression (123-125). During Golgi forward transport, $GABA_ARs$ are segregated into distinct vesicles from excitatory glutamatergic AMPA receptors, and are subsequently inserted at the cell surface via specialized Rab GTPases and SNARE complexes SNAP23–syntaxin1A/B–VAMP2 and SNAP25–syntaxin1A/B–VAMP2, respectively (126). Proteins contributing to $GABA_AR$ trafficking from the Golgi to the plasma membrane include Big2 (brefeldin A-inhibited GDP/GTP exchange factor 2) (127), GABARAP (GABA receptor-associated protein) (128), GRIP (Glutamate receptor interacting protein) (129, 130), PRIP1/2 (phospholipase C-related catalytically inactive proteins 1 and 2) (131, 132), GRIF-1 (133), Macoco (134), and NSF (135). Vesicular $GABA_AR$ transport from the trans-Golgi network (TGN) to the plasma membrane relies on the microtubule-dependent molecular motor kinesin KIF5 family (KIF5A, KIF5B, KIF5C) (136).

### 1.4.2 **Internalization, Recycling and Lysosomal Degradation**

Regulated internalization of cell surface receptors is a universal cellular response to moderate signaling and function. $GABA_AR$ internalization occurs through clathrin-mediated endocytosis dependent on dynamin (the GTPase that is responsible for fission of endocytic vesicles from the plasma membrane) and binding of the adaptor protein AP2 to specific $GABA_AR$ subunits **(Fig. 3)** (137), although clathrin-independent endocytosis occurs in heterologous cells and in *C. elegans* (138, 139). The interaction of AP2 with $GABA_ARs$ is partly regulated by PKA and PKC mediated-phosphorylation of serine residues within a highly basic ten amino acid sequence motif in the intracellular loop of the β subunits (S409 in β1, S410 in β2, S408/409 in β3), with increased phosphorylation reducing AP2 and $GABA_AR$ interaction and endocytosis **(Fig. 3)** (140-144). Two additional motifs in the β-subunit appear important for AP2 interactions: 1) a dileucine motif is critical for receptor internalization in HEK cells (145) and 2) three arginine residues (405RRR407) within the β3-subunit intracellular domain are important for AP2-stabilization of receptors at dendritic endocytic zones (146). The importance of phosphoregulation of these residues was revealed by S408/409A homozygous mice (the S/A mutation reduces AP2 interaction, mimicking phosphorylation (147)), which exhibit increased phasic but decreased tonic inhibition, and demonstrate the core phenotypes of autism spectrum disorders (148). Moreover, a common model of fragile X syndrome and autism spectrum disorders, the Fmr1 KO mouse, demonstrates enhanced S408/409 phosphorylation, further providing evidence for deregulation of these sites in disease (148). Accordingly, BZD resistance in epileptic mice undergoing sustained seizures is linked to reductions in PKC phosphorylation of β phosphorylation (148). How specific PKC isoforms participate in phosphoregulation of $GABA_AR$ surface levels and internalization is still unclear. For instance, ethanol induced internalization of α1-containing $GABA_ARs$ is PKCγ dependent (149),

while PKCε reduces $GABA_AR$ sensitivity to ethanol and BZDs by acting at a γ2 S327 residue (150).

The intracellular loop of the γ2 subunit also contains two AP2 interaction domains, a 12 basic amino acid region similar to the β-subunits and a YGYECL motif (144). The Tyr 365/367 within the YGYECL motif are targets of Fyn and other Src family kinases **(Fig. 3)** (151, 152), and phosphorylation at these sites reduce AP2 binding (153). Tyrosine to phenylalanine mutations inhibits AP2 binding to the γ2 subunit, and heterozygous Y365/7F knock-in mice demonstrate surface and synaptic accumulation of $GABA_ARs$ and spatial memory deficits (154). Importantly, homozygous Y365/7F knock-in mice are developmentally lethal, highlighting the importance of these residues in regulating $GABA_AR$ activity. BDNF-induced phosphorylation of the γ2 subunit Y365/7 residues was recently implicated as a promoter of receptor surface expression during hippocampal neurogenesis (155). The authors found heterozygous Y365/7F mice demonstrated an antidepressant-like phenotype and enhanced neurogenesis that could not be further enhanced by BDNF.

A number of noxious stimuli trigger $GABA_AR$ endocytosis including seizure models (156-158), oxygen-glucose deprivation (OGD) conditions (159), and prolonged agonist application (160). Protein phosphatases **(Fig. 3)** have an important role in regulating receptor endocytosis under these conditions. For example, inhibition of the calcium-sensitive phosphatase calcineurin (CaN) by FK506 or serine/threonine protein phosphatase 1 (PP1) and 2A (PP2A) by okadaic acid reverses reduction of surface γ2-subunit containing $GABA_ARs$ and mIPSC amplitude induced by status epilepticus treatments in slice preparations (161). NMDA receptor mediated calcium entry and CaN activation was further shown to decrease surface α2-containing receptors during *in vitro* epileptiform activity by live-cell imaging techniques (162). Activation

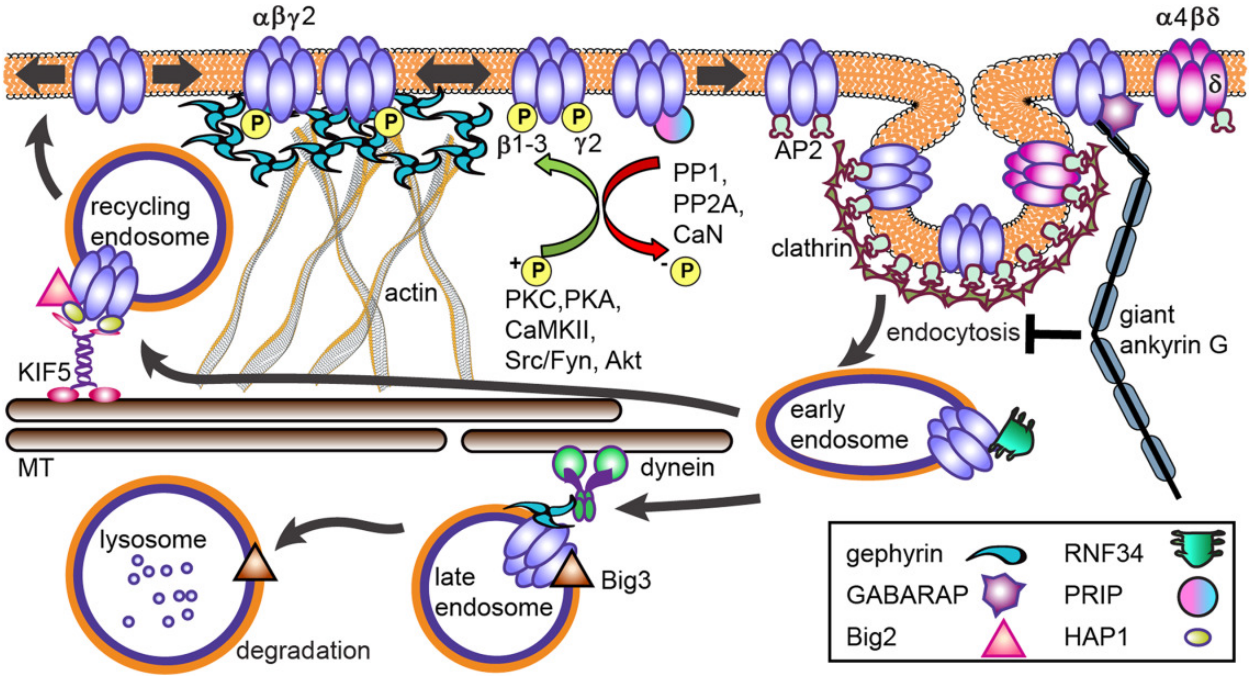


**Figure 3. GABA$_A$R Intracellular Trafficking.**

GABA$_A$Rs composed of α(1-3)βγ subunits are largely synaptically localized via gephyrin interactions and contribute to phasic currents, whereas α(4 or 6)βδ receptors are extrasynaptic and generate tonic current. α5βγ receptors are found in both locations due to binding with gephyrin at synapses and radixin extrasynaptically. Proteomics and other modern strategies have significantly enriched the complexity of the inhibitory synapse, however the functions of many new components have yet to be defined. Reproduced from: Lorenz-Guertin, J. M. and T. C. Jacob (2017). GABA type a receptor trafficking and the architecture of synaptic inhibition. Develop Neurobiol.

of the transient receptor potential cation channel subfamily V member 1 (TRPV1) also appears to cause GABA$_A$R endocytosis in the dentate gyrus of rodents dependent on calcium influx, CaN, and dynamin-activity (163). In addition, inflammation and release of the proinflammatory cytokine tumor necrosis factor-α (TNFα) stimulates GABA$_A$R internalization (α1/2/5, β3, γ2) in a CaN-independent pathway in cultured hippocampal neurons (164). Recent evidence has also recognized

the amyloid β (Aβ) peptide, most commonly associated with the pathogenesis of Alzheimer's disease, as a stimulator of $GABA_AR$ endocytosis (165).

Surface biotinylation assays suggest the majority of constitutively-internalized $GABA_ARs$ rapidly recycle back to the cell surface (70% in 1 h), while significant degradation occurs over longer time scales (6 h) (166). The recycling of $GABA_ARs$ is partly mediated by huntingtin associated protein 1 (HAP1) direct association with the β subunits **(Fig. 3)** (136, 166). HAP1 functions as a kinesin adaptor and localizes to early endosomes containing $GABA_AR$, and thus overexpression of HAP1 promotes receptor surface levels and reverses intracellular accumulation of receptors by constitutive (166) and OGD-induced endocytosis (167). Mutation of the HAP1 protein resulting in polyglutamine expansion, as seen in Huntington's Disease, results in dysregulated transport of $GABA_ARs$ to the cell surface and compromised inhibitory neurotransmission (136). The recycling activity of HAP1 likely arises from its association with the kinesin KIF5 **(Fig. 3)**. Purified complexes of β3-$GABA_AR$/KIF5 and HAP-1/KIF5 are readily immunoprecipitated from rat brain tissue, while acute blockade of KIF5 reduces $GABA_AR$ synaptic levels and signaling strength (136). The integral membrane protein CAML (calcium-modulating cyclophilin ligand) has also been implicated in $GABA_AR$ forward trafficking and recycling via interaction with the γ2 subunit cytoplasmic and fourth transmembrane domain regions (168). CAML-deficient neurons have reduced recycling of internalized $GABA_ARs$ and decreased GABAergic neurotransmission in electrophysiological recordings.

$GABA_ARs$ undergoing constitutive internalization from the cell surface may be subjected to lysosomal-mediated degradation **(Fig. 3)**, a process blocked by the lysosomal proteolytic inhibitor leupeptin (166). Acute leupeptin treatment also increases the size, number, and strength of GABAergic synapses in cortical slices (159). Certain stimuli can also accelerate degradation of

surface $GABA_AR$s. For instance, cultured hippocampal neurons undergo enhanced lysosomal-mediated degradation of α2-containing receptors in response to BZD treatment (169). Ubiquitination of 7 lysine residues within the intracellular loop of the γ2 subunit plays a key role in $GABA_AR$ lysosomal targeting (159). Mutation of these lysines to arginine (K7R) reduced colocalization of receptors at late endosomes, made receptors impervious to leupeptin treatment in heterologous cells, and blocked an OGD-induced loss of surface receptor clusters in neurons (159). The ubiquitin E3-ligase, ring finger protein 34 (RNF34), directly interacts with the intracellular loop of γ2, co-immunoprecipitates with this subunit from brain extracts, and can be found colocalized at GABAergic synapses **(Fig. 3)** (170). Overexpression of RNF34 enhances the rate of γ2-$GABA_AR$ degradation and reduces $GABA_AR$ synaptic cluster size and strength. Interestingly, expression of the γ2 K7R mutant in these experiments did not reverse RNF34-induced degradation of $GABA_AR$s in co-transfected HEK293 cells, but mutation of additional lysine residues in a K8R, K9R, and K10R mutant did. Moreover, RNF34 mediated ubiquitination appears to contribute to both proteasomal and lysosomal degradation of $GABA_AR$s in these cells. The ARF GEF, Brefeldin A-inhibited guanine nucleotide-exchange protein 3 (BIG3), may also be important for lysosomal trafficking of $GABA_AR$s **(Fig. 3)**. BIG3 is primarily expressed in pancreatic islets and the brain, and is found colocalized with lysosomes in neurons. BIG3 KO mice demonstrate increased $GABA_AR$ synaptic size and current, suggesting this protein is involved in negative regulation of $GABA_AR$ levels (171). The exact role of specific $GABA_AR$ subunits, associated E3-ligases and ubiquitination patterns, and lysosomal trafficking proteins that regulate the transition of surface receptors to lysosomes is an important area of future research.

## 1.5 Activity-Dependent Plasticity of $GABA_AR$ Synapses

Synapse plasticity refers to strengthening or weakening of individual synapses in response to changes in stimuli at a local or system level. Two decades of research have uncovered various forms of short and long term plasticity of GABAergic neurotransmission in different brain regions, with underlying cellular and molecular mechanisms being identified both pre- and post-synaptically (172). Persistent changes in synaptic efficacy are generally referred to as long-term potentiation (LTP) and long-term depression (LTD). Traditionally this described excitatory synapse plasticity that produced a respective increase or decrease in synapse strength. However, with growing awareness of GABAergic synapse plasticity, these terms now refer to changes in the gain of either synapse type (for GABAergic synapses, iLTD and iLTP).

$GABA_AR$ postsynaptic plasticity is encompassed by changes in channel function, receptor number or clustering/lateral diffusion, and altered chloride homeostasis (changing the GABA reversal potential/$E_{GABA}$). Tonic inhibition generated by extrasynaptic receptors is also dynamic, with acute and chronic stress inducing changes in cell surface trafficking and subunit specific expression (173). Receptor phosphorylation state is a key means for altering channel function or receptor trafficking via activation of protein kinases (including PKC, PKA, CaMKII, and Src) or phosphatases (CaN, PP1, PP2A) **(Fig. 2)** (174). Investigation of GABAergic postsynaptic plasticity has largely focused on excitation driven changes. Early plasticity studies identified that intracellular application of CaMKII (175) and experimental epilepsy kindling models (176) elevated $GABA_AR$ surface levels and potentiated the inhibitory response. Later studies revealed that moderate NMDA activation of hippocampal neurons promote CaMKIIα translocation to inhibitory synapses and CaMKIIα-dependent insertion of $GABA_ARs$ with concomitant phosphatase-mediated AMPAR (GluR1) removal (177, 178). Aside from NMDAR stimulation,

enhanced VGCC (voltage-gated calcium channel) activity promotes CaMKII phosphorylation of the β3 subunit S383 residue and receptor insertion **(Fig. 3)** (119), suggesting multiple routes for calcium signaling to enhance $GABA_AR$ surface levels. In addition, a quantum dot single-particle tracking study showed that NMDA-induced iLTP required CaMKII phosphorylation of β3 S383 to reduce $GABA_AR$ lateral diffusion and enhance recruitment of the synaptic scaffold protein gephyrin (179). More recently, this experimental approach revealed additional glutamate- and calcium-evoked plasticity of GABAergic synapses. Low glutamate levels stimulate mGluR-driven calcium store release via PKC and IP3 receptors and stabilization of surface $GABA_ARs$, while robust NMDAR activation promoted CaN phosphatase activity and destabilization of postsynaptic $GABA_AR$ (180). This is consistent with earlier findings where glutamate application promotes CaMKIIα translocation to excitatory synapses, enhanced AMPAR surface levels, and reduced plasma membrane $GABA_AR$ levels (178, 181). Glutamate, high levels of neuronal activity, or strong NMDAR activation also reduces plasma membrane $GABA_AR$ cluster size, stimulates receptor lateral mobility, and decreases mIPSC amplitude via CaN (182) and dephosphorylation of the γ2 subunit S327 residue (183). These molecular studies in neuronal culture are consistent with earlier slice and *in vivo* studies showing LTD of GABAergic inhibition via NMDAR activation requires CaN (184) and the γ2 subunit (185). Similar mechanisms for iLTD and iLTP that rely on $GABA_AR$ trafficking are supported by studies in other brain regions such as the deep cerebellar nuclei (186, 187). Together these plasticity studies show that glutamate receptor activation and calcium-sensitive signaling pathways can generate either iLTP or iLTD. Moderate or ambient glutamate signaling promotes kinase activity that stabilizes $GABA_ARs$, while strong stimulation leads to CaN phosphatase activation and receptor diffusion. Ultimately, glutamatergic

activity dictates bidirectional modulation of GABAergic postsynaptic strength and receptor clustering.

Structural reorganization of gephyrin scaffolding is now emerging as a key mechanism of rapid inhibitory synaptic plasticity with changes occurring on a minute timescale (188). Gephyrin post-translational modifications such as phosphorylation and ubiquitination are likely to be central in regulating synapse architecture. A recent organotypic slice culture study of gephyrin dynamics identified that activity patterns promoting NMDAR LTP (carbachol treatment or theta burst stimulation) increase gephyrin cluster size and formation in a CaMKII-dependent manner (77). Furthermore this gephyrin plasticity was associated with enhanced phosphorylation of gephyrin S305, a CaMKII phospho site identified by *in vitro* kinase assay.

On the other spectrum of neuronal activity level, early studies using chronic activity blockade (24 - 48 h TTX treatment) resulted in homeostatic pre- and post-synaptic GABAergic plasticity with decreased $GABA_AR$ synaptic clusters, mIPSC amplitude and frequency (189). *In vivo* chronic sensory deprivation via whisker trimming decreases $GABA_AR$ number and weakens inhibitory synapses (190-192). In contrast, whisker training promotes GABAergic synaptogenesis on dendritic spines, while not on dendritic shafts (193). Analogous findings in the visual cortex (194) indicate that a pool of dynamic GABAergic spine synapses support changes to network activity levels. These chronic *in vivo* protocols reveal how neuronal adaptation operates across a continuum of $GABA_AR$ synaptic plasticity, where reductions in activity lead to loss of inhibition, while learning or heightened neuronal activity strengthens existing GABAergic synapse or initiates new synapse formation. However, some sensory modulation can occur in an inverse fashion, as brief monocular deprivation potentiates iLTP (195), concurrent with increasing gephyrin and $GABA_AR$ perisomatic accumulation (179). Other visual cortex studies indicate that $GABA_AR$

endocytosis contributes to LTD occurring with repetitive firing, while slow membrane oscillations, comparable to activity during sleep state, promote iLTP via exocytosis (196). Similarly, acquisition of a fear response is accompanied by surface $GABA_AR$ decreases (197) and extinction of fear requires $GABA_AR$ insertion (198). Collectively, GABAergic synapse plasticity and rewiring is fundamental for sensory experience adaptation and behavior, with functional changes in inhibition matching structural changes.

### 1.6 Advancing our Understanding of Dynamic $GABA_AR$ Trafficking and Regulation

Considerable scientific progress has revealed a network of molecular mechanisms underlying GABAergic plasticity. Yet, advancement of new and existing methods is promoting major inroads for our understanding of $GABA_AR$ signaling and trafficking. Recent proteomic strategies from other labs has vastly expanded the protein repertoire of GABAergic synapses to nearly 200 proteins by targeted purification of $GABA_ARs$, NL2, or gephyrin and their respective interactomes (87, 88, 199, 200). Microscopy-based approaches encompass the fastest growing means of discovery *in vitro* and *in vivo*, including optogenetically controlled $GABA_ARs$ (201, 202), two-photon based GABA photolysis (203), single-particle-tracking of receptor diffusion (204), quantitative super-resolution imaging of gephyrin (205) and gephyrin recombinant antibody-like proteins (206, 207) or fluorescent super-binding peptides (208). Additionally, proximity ligation assays allow for researchers to detect native protein interactions utilizing widely-available primary antibodies (209, 210), while emerging fluorescence resonance energy transfer methods (FRET) have begun to be applied, as in our recent publication (211). Herein we validate and characterize a new tool to address multiple $GABA_AR$ trafficking questions within a

single assay using a dual fluorescent sensor $GABA_AR$ γ2 subunit to advance our knowledge of basal receptor trafficking and drug-induced neuroadaptive changes.

## 2.0 Designing an Optical Tool to Measure Multistage $GABA_AR$ Trafficking

Chapter adapted from: Lorenz-Guertin, J. M., et al. (2017). A versatile optical tool for studying synaptic GABAA receptor trafficking. J Cell Sci 130: 3933-3945; doi: 10.1242/jcs.205286 (212) https://jcs.biologists.org/content/130/22/3933.long

JL-G performed the biochemistry, fixed- and live-imaging acquisition and analysis. Madeleine R. Wilcox performed the electrophysiology and Madeleine R. Wilcox and Jon W. Johnson performed electrophysiology data analysis.

### 2.1 Introduction

The majority of $GABA_ARs$ are composed of two α, two β, and a γ2 subunit forming a heteropentamer, but considerable subunit heterogeneity may exist (α1-6, β1-3, γ1-3, δ, ε, θ, π, ρ1-3) (53). The γ2 subunit plays a critical role in $GABA_AR$ function, as it is necessary for receptor synaptic targeting and cluster maintenance (67, 213-216), coassembles with nearly all α and β subunits (217), and is the only subunit characterized to undergo ubiquitination leading to lysosomal degradation (159). The degree of γ2-$GABA_AR$ synaptic clustering directly impacts the strength of GABAergic synaptic inhibition and is dynamically regulated by changes in receptor trafficking (53, 218). A number of endogenous and pharmacological agents including GABA, neurosteroids, ethanol, and BZDs are known to influence receptor trafficking (149, 219-226). Despite this knowledge, precise $GABA_AR$ trafficking mechanisms induced by these and other clinically relevant compounds remain underexplored at the molecular level.

Real-time receptor trafficking measurements typically rely on genetically encoded fluorophores to track single protein localization and movement within living cells. In contrast to immunofluorescence based live-cell techniques which require reliable antibodies and are restricted

to measurements of surface proteins (227), fluorescent tags allow for identification of a protein from synthesis through degradation. Despite this advantage, traditional fluorophores still remain limited in their ability to spatially resolve surface from internal populations without the use of total internal reflection fluorescence (TIRF) imaging approaches (228). This issue led to the generation of pH-sensitive fluorescent proteins, such as pHluorin (pHGFP), which exhibit fluorescence in extracellular environments with alkaline pH (pH ~ 7.4), but not in more acidic areas like intracellular vesicles (229). pHGFP is not without limitations, as some discernable signal can be observed in the E.R. where pH can be roughly 7.2 (230). One possible way to resolve protein trafficking occurring at the cell surface from the intracellular space is to use compartment specific high-affinity labeling techniques. We previously described a labeling method utilizing a $GABA_AR$ subunit genetically tagged with an α-bungarotoxin binding site which selectively binds cell-excluded fluorescent bungarotoxin, allowing for selective monitoring of receptor insertion and internalization (231). Unfortunately, the inherent fluorescence of Alexa dye coupled bungarotoxins necessitates extensive washing after labeling to reduce background signal. Furthermore, bungarotoxins were recently shown to function as antagonists of the $GABA_AR$, further complicating the use of this reagent (232). To overcome these obstacles associated with $GABA_AR$ imaging we have employed an innovative paired optical reporter system where two individually non-fluorescent components become highly fluorescent upon binding: a genetically encoded fluorogen-activating peptide (FAP tag) and exogenously applied malachite green (MG) dyes. FAPs are antibody single chain variable fragments (scFvs) which have been characterized to selectively bind MG synthetic dyes with high specificity and affinity (233). These synthetic dyes are non-fluorescent in solution until bound by their respective FAP and can be modified to have distinct characteristics including cell permeability, pH-sensitivity, and various fluorescence

properties (234-238). The FAP-dye system offers many advantages for live-imaging: (i) the dyes can be added directly to a culture dish and saturate the target FAP in seconds; (ii) a number of distinct dyes can be used for the same genetically encoded FAP; and (iii) the dyes are highly specific for their target FAP. Moreover, high affinity MG-FAP binding forms a stable fluorescent module that allows for measurements of receptors undergoing internalization and recycling (239-241). Measuring drug-induced changes in FAP-tagged receptor trafficking has proven largely successful (234, 236, 241-244) placing this technique at the forefront of pharmacological screening.

In order to design a tool to track synaptic $GABA_AR$ internalization and trafficking, we engineered a γ2 subunit encoding a pHGFP and the fluorogen-activating peptide dl5 ($\gamma2^{pH}FAP$) (233, 240, 245, 246). We find that $\gamma2^{pH}FAP$ containing $GABA_ARs$ are trafficked to the cell surface in both HEK293 cells and primary neurons, and are localized appropriately at synapses. We further demonstrate how this construct can be combined with malachite green (MG) dye derivatives to measure alterations in surface localization and intracellular trafficking using high-resolution confocal microscopy approaches. Finally, using these FAP based methods we found that an *in vitro* seizure model induced rapid loss of dye-labeled synaptic $GABA_ARs$ concomitant with enhanced targeting of internalized receptors to lysosomal compartments, key results that were not detectable using pHGFP signal alone. We therefore demonstrate an innovative tool to monitor multistage synaptic $GABA_AR$ trafficking.

## 2.2 Methods and Materials

### 2.2.1 Cell culture and Transfection

All procedures were approved by the University of Pittsburgh Institutional Animal Care and Use Committee. Cortical neurons were prepared from embryonic day 18 Sprague Dawley rats and nucleofected (Lonza, Switzerland) at plating (54). HEK293 cells were maintained in DMEM with 10% FBS (Life Technologies, Carlsbad, CA) and were transfected by nucleofection.

### 2.2.2 DNA Constructs and Antibodies

The *α2*, *β3*, and pH-sensitive GFP tagged γ2 subunit (*γ2$^{pH}$GFP*) plasmids have been previously described (54, 65, 247, 248). The flurogen-activating peptide *dl5* (240) was inserted upstream of *pHGFP* (*γ2$^{pH}$FAP*) separated by a *G-A-P-P-A* amino acid linker. The *EEA1-GFP* was a gift from Silvia Corvera (Addgene plasmid #42307) (249). All constructs were sequenced to confirm the fidelity of final plasmids. The following primary antibodies were used: mouse anti-β-actin (1:2000, A1978, Sigma); rabbit anti-GFP (1:1000, A11122, Invitrogen); rabbit anti-VGAT (1:1000, 131002, Synaptic Systems); mouse anti-EEA1 (1:1000, 610457, BD Biosciences) and immunofluorescence secondary antibodies: goat anti-rabbit Alexa Fluor 641 (1:1000, A21245, Invitrogen); goat anti-mouse Alexa Fluor 405 (1:1000; A31553, Invitrogen).

### 2.2.3 **MG Dyes**

MG dyes were kindly provided by Dr. Alan S. Waggoner, Dr. Ming Zhang, Dr. Marcel P. Bruchez, and Dr. Brigitte F. Schmidt at CMU. The MG dye MG-BTau was synthesized as described in (236, 239) and the MG dye Cy3pH(S/SA)-MG was prepared by the method of (238). The IUPAC name for Cy3pH(S/SA)-MG is 2-((E)-3-((Z)-3,3-dimethyl-5-sulfoindolin-2-ylidene)prop-1-en-1-yl)-1-(6-((3-(4-((4-(dimethylamino)phenyl)(4-(dimethyliminio)cyclohexa-2,5-dien-1-ylidene)methyl)phenoxy)propyl)amino)-6-oxohexyl)-3,3-dimethyl-5-sulfamoyl-3H-indol-1-ium. Structural, synthetic and analytical details for MG-BTau are as described previously (239, 241, 250).

### 2.2.4 **Immunocytochemistry and Confocal Microscopy**

Primary cortical neurons grown on glass coverslips were fixed at days *in vitro* (DIV) 13-14. Neurons were permeabilized and stained with anti-VGAT antibody. Images were taken on a Nikon Ti-E A1 Confocal microscope equipped with a motorized Z-stage and perfect focus system (PFS) using a 60x oil immersion objective (NA 1.49) at 3x zoom. Data were analyzed using NIS Elements software (Nikon, NY). Thresholds were set using binary masks to selectively identify brightly fluorescent objects above background (54). Three dendritic 10 μm regions of interest (ROI) were drawn per neuron to measure synaptic colocalization of pHGFP signal with VGAT in $\gamma 2^{pH}$FAP characterization studies. $\gamma 2^{pH}$GFP control and $\gamma 2^{pH}$FAP expressing neuron pixel intensity and sum area of synapses in $\mu m^2$ was measured and values were normalized to control mean. Fixed EEA1 early endosome studies utilized a 2 min 100 nM MG-BTau dye pulse-labeling protocol in HBS at room temperature. After live cell MG dye incubation steps, cells were washed 5 times to

remove all unbound dye prior to returning the cells to 10°C or 37°C solution for 30 min followed by fixation and immunostaining. Total pixel intensity of MG-BTau labeled receptors colocalized with EEA1 was measured within a cell body ROI. Laser settings were held constant across experiments. The researcher was blinded during image acquisition and data analysis.

### 2.2.5 **Live-Cell Imaging**

Transfected DIV 12-14 cortical neurons or HEK293 cells were plated on MatTek glass-bottom dishes (Ashland, MA). Imaging was performed in HEPES-buffered saline (HBS): 135 mM NaCl, 4.7 mM KCl, 1.2 mM $MgCl_2$, 10 mM HEPES, 2.5 mM $CaCl_2$, 11 mM glucose, pH 7.4 (169). Low pH HBS (pH 6.4-6.8) was similarly prepared, while pH 4.8 saline was a MES-buffered saline: (135 mM NaCl, 4.7 mM KCl, 1.2 mM $MgCl_2$, 10 mM MES, 2.5 mM $CaCl_2$, 11 mM glucose). All dye pulse-labeling steps were performed in HBS at room temperature. Following dye incubation steps, cells were washed 5 times to remove all unbound dye prior to treatment or imaging. All images were taken at room temperature using a 60x objective at a 3x zoom within 10 min of dye washout. Perfusion assays utilizing different pH saline buffers monitored a single cell per assay, while 2-3 cells were imaged in each experimental dish for all other experiments. Researchers were blinded during data analysis where applicable.

Cy3pH(S/SA)-MG dye was used for neuron constitutive trafficking assays. Neurons were pre-incubated in DMSO vehicle control (t0, t30) or 80 μM dynasore (2897, Tocris) 30 min prior to pulse-labeling. After dye exposure, neurons were either immediately imaged (t0) or returned to conditioned media ± the continued presence of dynasore for 30 min at 37°C prior to imaging. Cy3pH(S/SA)-MG dye acquisition was taken sequentially to measure Cy3pH (561 nm excitation) induced MG emission (680 nm) followed by MG (640 nm excitation) induced MG emission (680

nm). Laser settings were then switched to allow for capture of pHGFP (488 nm excitation; 510 nm emission). Individual vesicles were identified using the NIS Elements Spot Detection tool and thresholding analysis. A ROI was drawn around the cell body and binary thresholds were set to selectively capture only pHGFP clusters and $MG_{ex640}$ (MG signal excited by 640 nM) signal above background. Next, spot detection thresholds were set to selectively identify $MG_{ex561}$ (signal excited by 561 nM) fluorescent objects with a minimum circular area of 0.55 $\mu m^2$ and signal above threshold. Colocalization of $MG_{ex561}$ spot signal and $MG_{ex640}$ binary signal was considered a $\gamma 2^{pH}$FAP positive vesicle. To remove contributions of surface synaptic $GABA_A$Rs from these vesicle measurements, $MG_{ex561}$ and $MG_{ex640}$ signals colocalized with pHGFP signals were subtracted. The values reported reflect the total number of $MG_{ex561}$ and $MG_{ex640}$ positive objects (vesicles) identified and the $MG_{561}/MG_{640}$ ratio of each vesicle. Early endosome characterization assays measured colocalization of Cy3-MG objects with EEA1-GFP vesicles to determine the $MG_{561}/MG_{640}$ ratio in these compartments, while all non-associated Cy3-MG objects were placed in the "other" category. A ROUT outlier test (Q = 1.0%) was used in this experimental analysis. For surface Cy3pH(S/SA)-MG pH characterization perfusion assays, the ratio of $MG_{561}/MG_{640}$ was determined by selectively measuring synaptic clusters of $\gamma 2^{pH}$FAP $GABA_A$Rs.

Neuron surface and lysosomal-association assays utilized MG-BTau dye for surface receptor pulse-labeling. For bicuculline-induced seizure assays, neurons were either immediately imaged following 100 nM MG dye incubation (t0) or returned to conditioned media in the presence of 50 µM (-)-bicuculline methiodide (2503, Tocris) or DMSO vehicle control. To label lysosomes, neurons were incubated at 37°C in 50 nM LysoTracker Blue DND-22 (Life Technologies) in conditioned media 30 min prior to imaging. For image analysis, independent ROIs were drawn to capture the soma, three 10 µM sections of dendrite, and the whole cell. Binary thresholds and

colocalization measurements were performed as above to identify MG-BTau, pHGFP synaptic $GABA_AR$ clusters, and lysosomes. Total surface pHGFP expression was determined by taking the entire cell surface signal following background subtraction.

### 2.2.6 **Western Blot**

Transfected and non-transfected DIV 13-14 cortical neurons were lysed using RIPA buffer containing: 50 mM Tris-HCl (pH 8.0), 50 mM NaCl, 1 mM EDTA, 1% Igepal, 0.5% sodium deoxycholate, 0.1% SDS, 10mM NaF, 2 mM sodium orthovanadate, and protease inhibitor cocktail (Sigma, St. Louis, MO), solubilized for 15-30 min at 4°C, and spun at 13,500xg for 15 min to remove the nuclear pellet. BCA protein assay was performed on the supernatant, and equivalent amounts of protein were loaded for SDS-PAGE analysis. After electrophoresis and transfer to nitrocellulose membrane, samples were probed with primary antibody overnight followed by the appropriate HRP-coupled secondary antibody. Blots were visualized using a Biorad Chemicdoc XRS+ following ECL development (Thermo Scientific).

### 2.2.7 **Electrophysiology**

Whole-cell voltage-clamp recordings were performed on HEK293 cells 12-48 h after nucleofection with $GABA_AR$ subunits. Cells were transfected with (a) *EGFP:α2:β3:γ2$^{pH}$GFP* or (b) *EGFP:α2:β3:γ2$^{pH}$FAP* in a 1:1:1:3 ratio to favor the production of γ2 subunit-containing receptors. Pipettes were pulled from borosilicate capillary tubing (Sutter Instruments) to a resistance of 2 – 5 MΩ on a Sutter Instruments-Flaming Brown P-97 electrode puller and fire polished. Unless otherwise indicated, the extracellular solution contained (in mM): 140 NaCl, 4.7

KCl, 1.2 $MgCl_2$, 2.5 $CaCl_2$, 10 HEPES and 11 D-glucose, and was pH adjusted to 7.4 ± 0.05 with NaOH. The intracellular solution contained (in mM): 140 CsCl, 0.1 $CaCl_2$, 10 HEPES, 1.1 EGTA, 2 $MgCl_2$, 2.5 phosphocreatine, 2 ATP-Mg and 1 GTP-Na, and was pH adjusted to 7.2 ± 0.05 with CsOH. Recordings were made from cells expressing *EGFP* identified by epifluorescence illumination on an inverted Zeiss Axioscope microscope. Cells were held at a membrane potential ($V_m$) of -50 mV for all experiments. $V_m$ was corrected for an empirically determined liquid junction potential between the extracellular and intracellular solution of -4 mV. Whole-cell currents were recorded using an Axopatch 200A patch-clamp amplifier (Molecular Devices), low-pass filtered at 5 kHz and sampled at 10 kHz in pClamp10.7 (Molecular Devices). Series resistance was compensated with the prediction and correction circuitry to at least 75% in all experiments. Rapid solution exchange was achieved using an in-house-fabricated 10-barrel fast perfusion system connected to gravity-fed reservoirs similar to the system previously described (251). All experiments were performed at room temperature. Peak currents were measured relative to baseline current prior to agonist application using Clampfit 10.7.

### 2.2.8 **Statistics**

Statistical analysis was performed using GraphPad Prism 6 (GraphPad Software, San Diego, CA) or Microsoft Excel. Unpaired Student's t-tests or one way ANOVA with subsequent post hoc Tukey's test were used to determine significance in indicated imaging studies. Significant differences in data distribution for Cy3pH(S/SA)-MG experiments were determined using the Mann-Whitney test. Paired or unpaired two-tailed Student's t-tests were used to determine significance of differences in electrophysiological studies. All data are reported as mean ± S.E.M. unless otherwise indicated in the text.

## 2.3 Results

### 2.3.1 Expression and Function of γ2$^{pH}$FAP in HEK293 Cells

We began by introducing the dl5 FAP into a previously characterized N-terminal pHGFP γ2-construct (γ2$^{pH}$GFP) that functions comparably to wild-type γ2 (54, 183, 247, 252) **(Fig. 4A)**. The FAP will selectively bind MG dyes with distinct biophysical and fluorescence properties. For example, the MG derivative (2-((4-[(2,5-dioxopyrrolidin-1-yl)oxy]-4-oxobutanoyl}amino)ethanesulfonate; MG-BTau) is cell impermeant, binds to dl5 FAP with high binding affinity (Kd value less than 0.5 nM), and is non-fluorescent until dl5 FAP binding occurs, which causes activation of fluorescence in the far red spectral region (680 nm) (239-241, 250) **(Fig. 4B)**. We first examined if the full length γ2$^{pH}$FAP construct was appropriately expressed in HEK293 cells. $GABA_AR$ β3 subunits were coexpressed in these experiments as a β subunit is required for trafficking of receptors to the cell surface (253). Western blot analysis of non-transfected, γ2$^{pH}$GFP control, and γ2$^{pH}$FAP expressing cells reveal γ2$^{pH}$FAP is ~25 kDa larger than γ2$^{pH}$GFP, consistent with the molecular weight of the dl5 FAP (240) (**Fig. 4C**). Next, we evaluated surface expression and specificity of MG-BTau dye labeling of $GABA_ARs$ in cells transiently transfected with *β3 + γ2$^{pH}$FAP* or *β3 + γ2$^{pH}$GFP*. Addition of MG-BTau to a live-cell culture should swiftly and selectively label surface $GABA_ARs$ containing γ2$^{pH}$FAP. To test this dye based labeling approach, living cells plated on glass-bottom Mattek dishes were pulse-labeled with 250 nM MG-BTau in HEPES-buffered saline (HBS) for 1 min at room temperature, washed 5x times with saline, and then immediately imaged by confocal microscopy. We found that HEK293 cells expressing γ2$^{pH}$FAP demonstrate selective receptor surface labeling by MG-BTau, while γ2$^{pH}$GFP control cells show no cell membrane MG-BTau fluorescence (although occasional low-level

background MG-BTau binding can occur with cellular debris (239)) **(Fig. 4D)**. The majority of cells express heteromeric receptors composed of β3 + γ2 subunits, although a few cells express the γ2 subunit alone, leading to subunit retention in the endoplasmic reticulum (ER) and no MG-BTau signal in $\gamma2^{pH}$FAP cells (**Fig. 4D**, yellow arrowheads). These results highlight key advantages of FAP-fluorogen labeling over pHGFP alone: 1) higher signal-to-noise ratio and 2) the removal of pHGFP intracellular background fluorescence generated by ER localized receptors where pH can be roughly 7.2 (230).

We further investigated the ability of $\gamma2^{pH}$FAP to assemble into functional heteromeric α2β3γ2 $GABA_A$Rs with normal chloride channel activity in response to the endogenous agonist GABA which binds between α and β subunits. Patch clamp recordings were used to determine the GABA dose-response curve for HEK293 cells expressing receptors composed of α2β3$\gamma2^{pH}$GFP or α2β3$\gamma2^{pH}$FAP. Concentration-response analysis revealed these receptors exhibit similar GABA $EC_{50}$ values (α2β3$\gamma2^{pH}$GFP, 22.0 ± 6.2 μM; α2β3$\gamma2^{pH}$FAP, 14.3 ± 8.9 μM; $p > 0.05$) and Hill coefficients (α2β3$\gamma2^{pH}$GFP, 1.14 ± 0.26; α2β3$\gamma2^{pH}$FAP, 0.90 ± 0.29; $p > 0.05$) **(Fig. 5A)**. The $EC_{50}$ values are consistent with previously reported values for receptors containing this subunit composition (254). To directly test if addition of the FAP tag altered drug binding and functional properties of the γ2 subunit, we compared the potentiation response the induced by the BZD, diazepam (DZ/DZP), a $GABA_A$R positive allosteric modulator that binds at

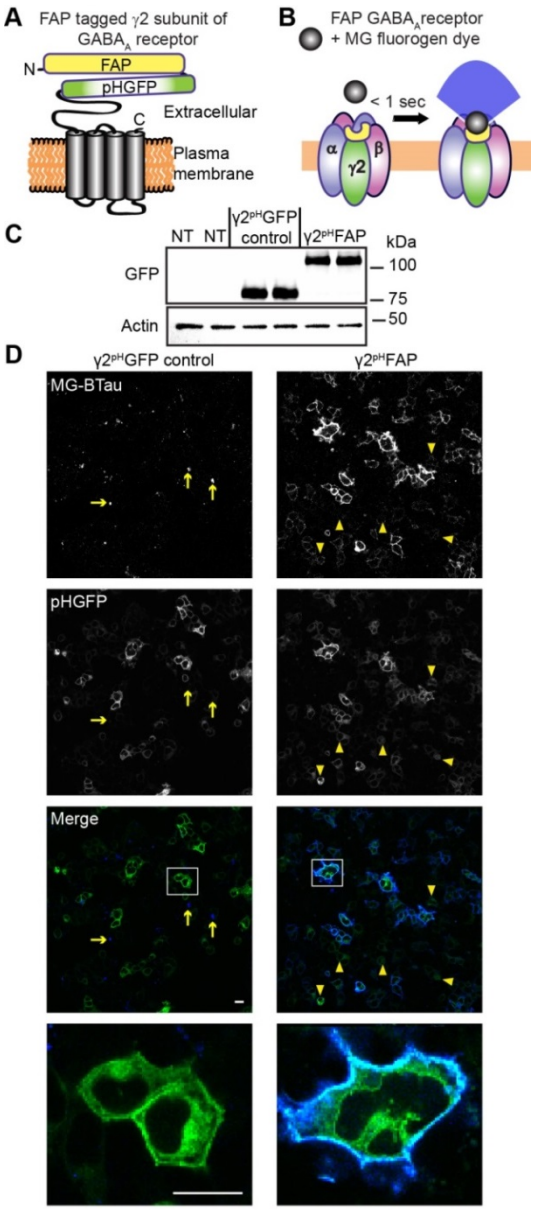


**Figure 4. Novel Optical GABA$_A$R Paired Reporter System.**

(A) The fluorogen activating peptide (FAP) dl5 was inserted upstream of an N-terminal pH-sensitive GFP tag (pHGFP) in a γ2-subunit construct. Cartoon schematic of γ2$^{pH}$FAP subunit. Model not to scale. (B) The MG dye, MG-BTau, is cell impermeant and dark in solution. Fluorescence is generated when MG dye binds to surface receptors containing the γ2$^{pH}$FAP subunit. (C, D) HEK293 cells were transfected with *β3 + γ2$^{pH}$GFP* control or *β3 + γ2$^{pH}$FAP* (β3 subunits are needed to form surface targeted receptors). (C) Representative western blot from NT (non-transfected), β3 + γ2$^{pH}$GFP control and β3 + γ2$^{pH}$FAP expressing cells (*n* = 2 experiments). (D) HEK293 cells

transfected with *β3 + γ2$^{pH}$GFP* control or *β3 + γ2$^{pH}$FAP* were pulse-labeled with 250 nM MG-BTau dye for 1 min prior to live-cell imaging. pHGFP fluorescence is shown in green and MG-BTau is shown in blue in the Merge panels and boxed areas enlarged below. MG-BTau signal is selectively localized at the cell surface in γ2$^{pH}$FAP expressing cells and is absent in γ2$^{pH}$GFP control cells. Note that with double transient transfection (*β3 + γ2$^{pH}$FAP*), some cells contain the γ2$^{pH}$FAP subunit alone (yellow arrowheads), leading to intracellular retention and a pHGFP signal (green) but no MG dye labeling (blue). Scale bars = 20 μm.

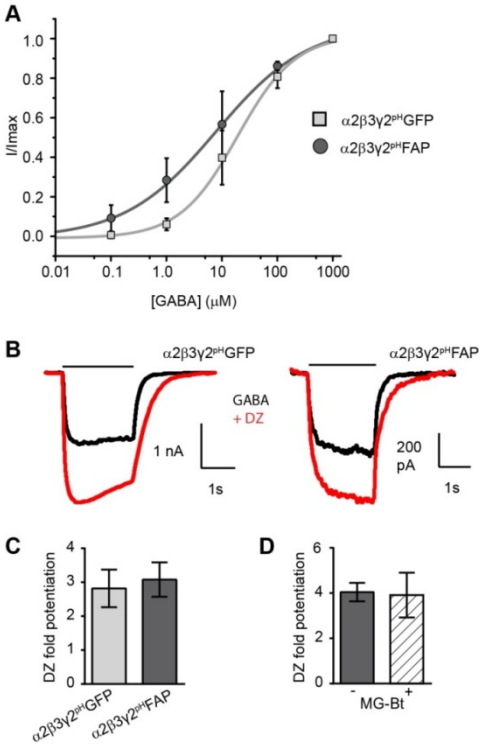


**Figure 5. Recombinant GABA$_A$Rs Containing γ2$^{pH}$FAP Maintain Responsiveness to GABA and the Benzodiazepine Drug Diazepam in HEK293 Cells.**

**(**A) The GABA concentration response curve in α2β3γ2$^{pH}$GFP and α2β3γ2$^{pH}$FAP expressing cells is equivalent. 1s GABA applications were made at ≥120 s intervals and peak response was measured. Curves were fit with the Hill equation, and the $EC_{20}$ was determined. (B) GABA currents are equivalently potentiated by 1 μM DZ (at the GABA $EC_{20}$). Representative traces show responses to application of GABA (black) and of GABA with DZ (DZP) (red). (C) Quantification of DZ potentiation (*n* = 5-8 cells per treatment). (D) DZ potentiation of the GABA response in α2β3γ2$^{pH}$FAP expressing cells is not altered by the presence of 100 nM MG-BTau dye (*n* = 4 cells per treatment). (C,D) Data presented as mean ± S.E.M., Student's t-tests.

the interface of γ2 and specific α subunits (α1, 2, 3 or 5) **(Fig. 5B)** (217). We found no significant difference in the DZ potentiation of the $EC_{20}$ GABA response between α2β3γ2$^{pH}$GFP or α2β3γ2$^{pH}$FAP expressing cells (**Fig. 5C**, Fold DZ potentiation α2β3γ2$^{pH}$GFP = 3.1 ± 0.5, α2β3γ2$^{pH}$FAP = 2.8 ± 0.6; $p > 0.05$**)**. Finally, we tested if binding of a MG dye to the γ2$^{pH}$FAP subunit would interfere with receptor function. We compared the DZ potentiation response of γ2$^{pH}$FAP before and after co-application of MG-BTau. Binding of MG-BTau to the receptors did not alter the response to DZ (**Fig. 5D**, Fold DZ potentiation γ2$^{pH}$FAP without dye = 4.0 ± 0.4, γ2$^{pH}$FAP with dye = 3.9 ± 1.0; $p > 0.05$**)**. Taken together these results suggest $GABA_A$Rs incorporating γ2$^{pH}$FAP maintain normal receptor function and responsiveness to GABA and DZ in the presence of MG dye.

### 2.3.2 γ2$^{pH}$FAP is Clustered at Synapses in Neurons and Can be Used to Monitor Multistage Receptor Trafficking

To confirm that γ2$^{pH}$FAP is fully expressed in cultured neurons, we compared non-transfected rat cortical neurons to those transfected with *γ2$^{pH}$FAP* or *γ2$^{pH}$GFP* control at plating **(Fig. 6)**. Neurons were lysed 14 days after transfection and subsequently immunoblotted with anti-GFP antibody **(Fig. 6A)**, revealing robust expression of γ2$^{pH}$FAP and γ2$^{pH}$GFP as seen in HEK293 cells **(Fig. 4C)**. We then tested if neurons with γ2$^{pH}$FAP $GABA_A$Rs could selectively bind and activate MG-BTau dye fluorescence. Days *in vitro* (DIV) 12 cortical neurons expressing γ2$^{pH}$GFP or γ2$^{pH}$FAP were pulse-labeled with 250 nM MG-BTau dye for 1 min at room temperature, then immediately washed and used for live-cell imaging. Only γ2$^{pH}$FAP expressing neurons demonstrate dye activation and colocalization with pHGFP surface synaptic clusters **(Fig. 6B)**. Furthermore, it is evident that MG-BTau labeling in neurons also has a higher signal-to-noise ratio

than pHGFP due to 1) the continually generated pHGFP signal of diffuse newly inserted extrasynaptic γ2$^{pH}$FAP receptors that are not yet clustered at synapses, which contrasts with the small MG-BTau pulse-labeled extrasynaptic population (if the MG dye was continually present rather than being washed away, its extrasynaptic signal would be more similar to pHGFP) and 2) the low but observable pHGFP background from ER resident γ2$^{pH}$FAP subunits, whereas there is no ER signal from MG-BTau labeling. These data establish MG dyes as a selective label for synaptic γ2$^{pH}$FAP containing $GABA_AR$ populations in living primary cortical neurons.

Synapse formation and receptor clustering are critical for neuronal development and regulation of inhibitory neurotransmission. To determine if γ2$^{pH}$FAP clusters normally at GABAergic synapses in mature neurons, we transfected cortical neurons at DIV 0 with *γ2$^{pH}$GFP* control or *γ2$^{pH}$FAP* and fixed the cells for immunofluorescence studies at DIV 15. We assessed receptor synaptic localization by measuring colocalization of the pHGFP tagged receptors with the vesicular GABA transporter (VGAT), a presynaptic marker of GABAergic synapses **(Fig. 6C)**. Expression of γ2$^{pH}$FAP did not alter presynaptic GABAergic input as indicated by unchanged VGAT levels (intensity) and area compared to control **(Fig. 6D)**. Additionally, the size of postsynaptic GABAergic synapses was not significantly different between constructs, although the mean intensity of γ2$^{pH}$GFP synapses was 20.7% (95% confidence interval) greater than γ2$^{pH}$FAP, likely due to higher overall expression of the control subunit. These results indicate that the full length γ2$^{pH}$FAP construct is expressed, assembles with endogenous subunits into receptors, traffics to synapses, and does not disturb neuronal development.

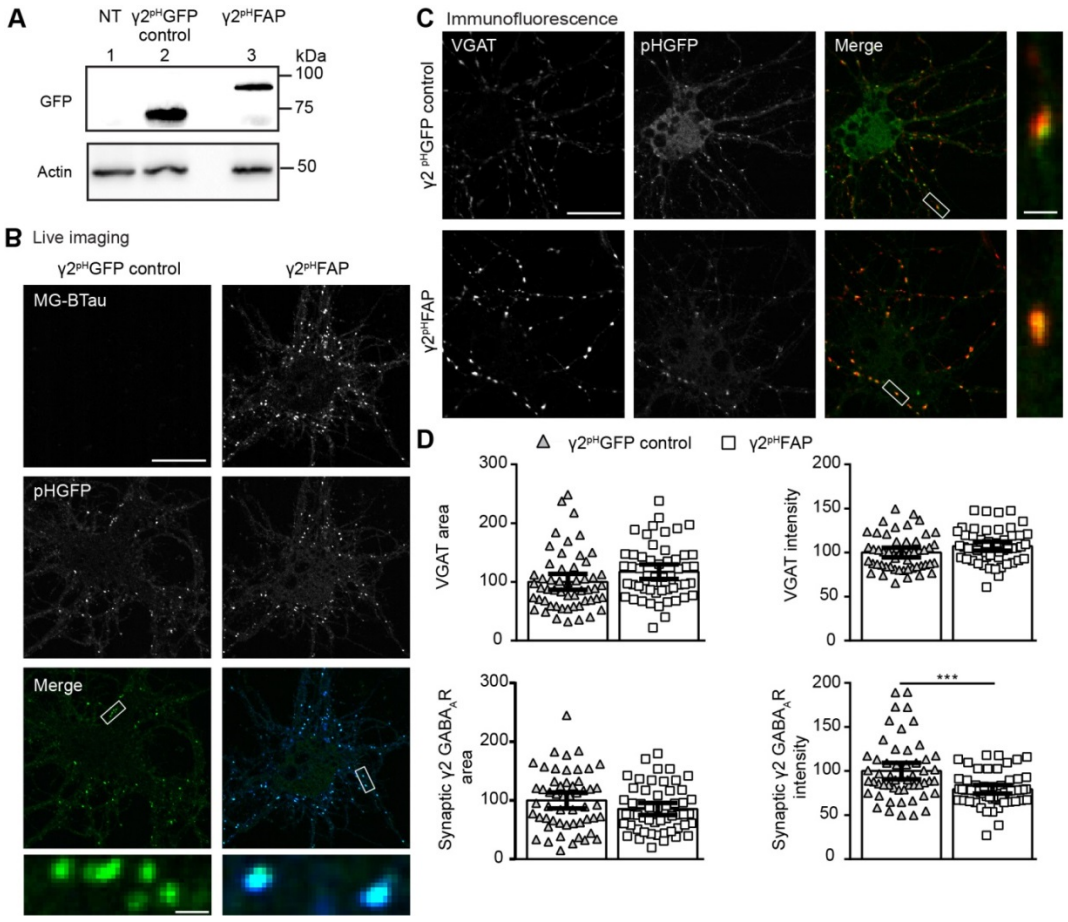


**Figure 6. γ2$^{pH}$FAP is Fully Expressed in Neurons and Appropriately Clustered at GABAergic Synapses.**

(A) Detection of γ2$^{pH}$GFP control and γ2$^{pH}$FAP receptors via western blot in cortical neurons 14 days post-transfection. NT = non-transfected. (*n* = 3 neuronal cultures). (B) DIV 12 neurons expressing γ2$^{pH}$GFP control or γ2$^{pH}$FAP were pulse-labeled with 250 nM MG-BTau dye for 1 min prior to live-cell imaging. Surface $GABA_A$Rs are selectively labeled in γ2$^{pH}$FAP neurons as evidenced by extensive colocalization of the pHGFP signal (green, Merge) and MG-BTau signal (blue, Merge). Note that in γ2$^{pH}$GFP control neurons, surface $GABA_A$Rs are not labeled by MG-BTau dye. Boxed areas enlarged below. (C) Confocal fixed immunofluorescence images of γ2$^{pH}$GFP control and γ2$^{pH}$FAP expressing neurons with presynaptic GABAergic terminals labeled with VGAT antibody. pHGFP fluorescence (green in Merge) shows intracellular γ2 subunit and synaptically localized receptors on dendrites that are colocalized with VGAT (red in Merge). Boxed areas enlarged below. (D) VGAT and surface γ2 containing receptor synaptic clusters were quantified. Scatter plot graphs showing mean area and mean fluorescence intensity in neurons transfected with γ2$^{pH}$GFP control or γ2$^{pH}$FAP. No changes were observed in GABAergic presynaptic terminals as

measured by VGAT area and intensity. Synaptic γ2 $GABA_AR$ measurements were determined from pHGFP signal colocalized with VGAT: synaptic γ2 $GABA_AR$ fluorescence area was equivalent, while the intensity was slightly lower in $\gamma2^{pH}$FAP neurons (***$p < 0.001$, Student's t-test; n = 54-57 neurons from 3 cultures for each condition; error bars represent ± 95% confidence interval). Scale bars: main panels = 20 μm, enlargements = 1 μm.

Having validated and established the application of FAP technology to generate a synaptic $GABA_AR$ reporter system, we first explored the experimental flexibility afforded by the distinct characteristics of available MG dyes to study receptor trafficking. First we examined if MG-BTau labeled surface receptors could be identified in endosomal pathways following internalization. DIV 12-13 $\gamma2^{pH}$FAP neurons were pulse-labeled with 100 nM MG-BTau, transferred to 10°C or 37°C HBS for 30 min, and then fixed and immunostained with the early endosome marker EEA1 **(Fig. 7A)**. Neurons maintained at 37°C demonstrated greater mean intensity and area of MG-BTau colocalized at EEA1 vesicles compared to those kept at 10°C to inhibit internalization, indicating MG-BTau labeling can also be used to track $GABA_AR$ internalized pools **(Fig. 7B)**.

We next investigated the adaptability of $\gamma2^{pH}$FAP with other MG dye applications in live-imaging intracellular trafficking assays. The Cy3pH(S/SA)-MG dye is a dichromophore consisting of a pH-sensitive forester-resonance energy transfer (FRET) donor Cy3pH molecule and an acceptor MG **(Fig. 8A)** (238). Excitation of Cy3pH (561 nm excitation) results in highly efficient FRET to MG and emission is observed at 680 nm, while direct stimulation of MG (640 nm excitation) also results in 680 nm emission, allowing calculation of an emission ratio of $MG_{561}/MG_{640}$ **(Fig. 8A)**. Increasingly acidic environments such as endosomes and lysosomes lead to protonation of Cy3pH and increased fluorescence intensity, enhancing FRET, and the ratio of $MG_{561}/MG_{640}$ (236, 238, 255, 256) The pH sensor dye is cell impermeant like MG-BTau and thus allows for selective labeling of surface γ2-containing $GABA_ARs$. To characterize the pH-

sensitivity of Cy3pH(S/SA)-MG in our γ2$^{pH}$FAP neuronal system, we first performed live-cell imaging perfusion experiments using different pH solutions to simulate receptor progression through an increasingly acidic endolysosomal pathway, as similarly performed in other cell culture methods using Cy3pH(S/SA)-MG (238). Neurons were pulse-labeled with pH sensor dye and then first imaged with pH 7.4 physiological saline, followed by pH 6.8 and pH 4.8 solutions, demonstrating a clear shift in the ratio of $MG_{561}/MG_{640}$ across treatments **(Fig. 8B)**. Quantification of $MG_{561}/MG_{640}$ mean ratios at surface synaptic cluster sites revealed pH 7.4 (0.58 ± 0.01), pH 6.8 (0.69 ± 0.01), and pH 4.8 (0.99 ± 0.02) conditions were significantly different from one another **(Fig. 8C)**. Therefore, Cy3pH(S/SA)-MG labeled γ2$^{pH}$FAP receptors can be readily identified in environments of different acidities using the $MG_{561}/MG_{640}$ ratio.

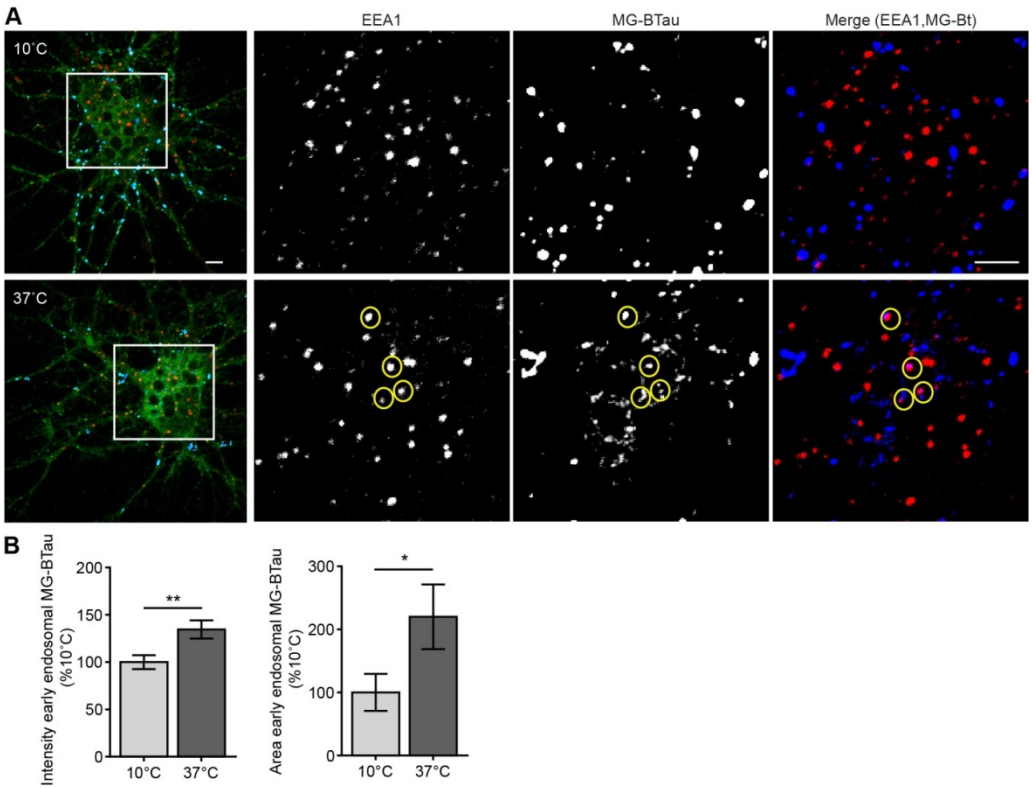


**Figure 7. MG-BTau Dye Signal Shows Trafficking of γ2$^{pH}$FAP GABA$_A$Rs to Early Endosomes.**

(A) DIV 12 γ2$^{pH}$FAP expressing neurons were pulse labeled with 100 nM MG-BTau dye for 2 min, then incubated in HBS at 37°C or 10°C for 30 min prior to fixation. MG-BTau (blue) labeled neurons were permeabilized and stained with early endosome marker EEA1 antibody (red). pHGFP (green) is visible throughout the cell after fixation. Boxed area is enlarged to the right with EEA1 (red), MG-BTau (blue), and Merge panels. Yellow circles show colocalized EEA1 and MG-BTau signal. (B) The intensity and area of MG-BTau labeled receptors colocalized with EEA1-positive intracellular vesicles is increased when endocytosis is not inhibited by 10°C. (*p≤0.05, **p < 0.01, Student's t-test; n = 25 neurons from 3 cultures each condition; error bars represent ± S.E.M.). Scale bars = 5 μm.

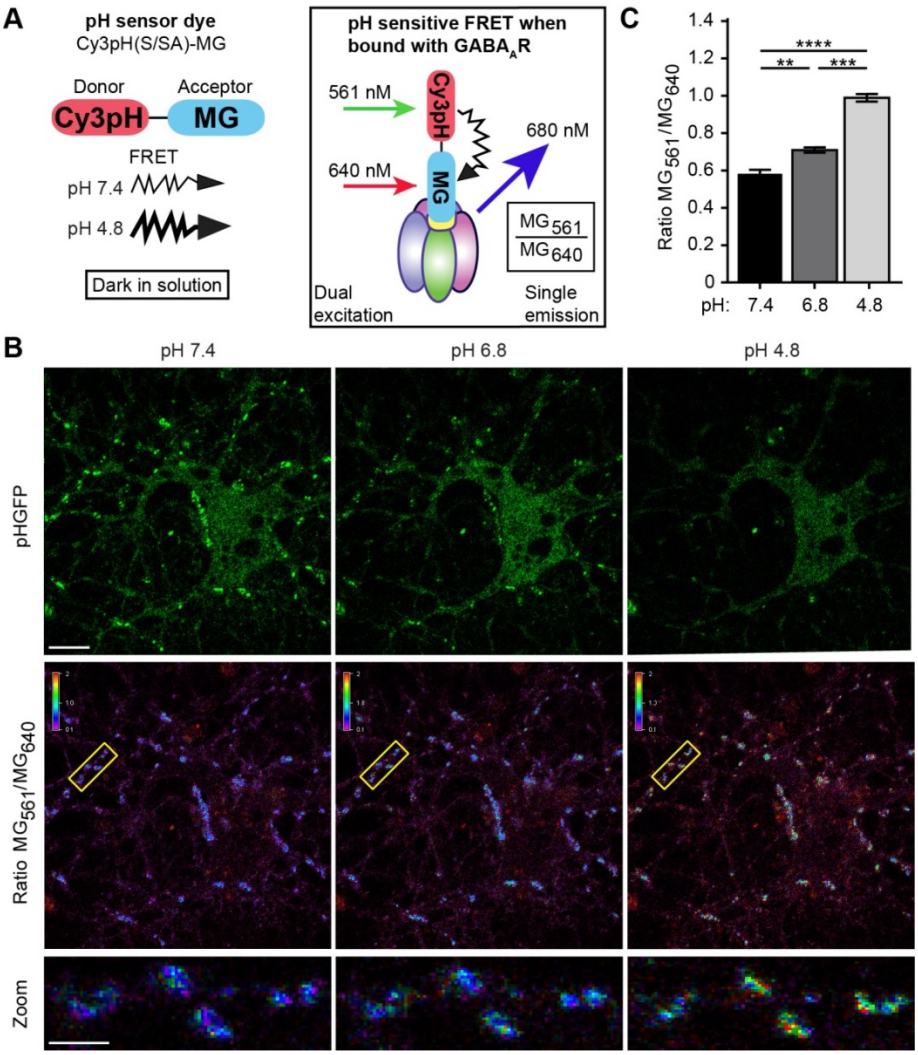


**Figure 8. Cy3pH(S/SA)-MG Dye Bound to Surface γ2$^{pH}$FAP Receptors Displays a pH-Sensitive FRET Signal.**

(A) pH sensor dye Cy3pH(S/SA)-MG is a fluorogen FRET sensor. Increasingly acidic environment enhances Cy3pH fluorescence intensity and FRET. A higher $MG_{561}/MG_{640}$ ratio indicates lower pH. (B) DIV 12-13 γ2$^{pH}$FAP expressing neurons were pulse labeled with 100nM pH sensor dye Cy3pH(S/SA)-MG for 2 mins, then were immediately used for live-imaging. Cells were first perfused with pH 7.4 HBS, then pH 6.8 HBS, and finally MES-buffered saline pH 4.8. Zoomed dendrite images below highlight $MG_{561}/MG_{640}$ ratios at surface synaptic clusters across different acidities. All ratiometric images are on a scale from 0.1 to 2. Scale bars: whole image = 10 µm; zoom image = 2.5 µm. (C) The $MG_{561}/MG_{640}$ ratio of individual surface γ2$^{pH}$FAP $GABA_AR$ synaptic clusters were quantified at each pH (****$p \leq 0.0001$, one way ANOVA followed by post hoc Tukey's test; $n = 41$ synaptic clusters from 4 cells; error bars represent ± S.E.M.

Following pH characterization of Cy3pH(S/SA)-MG, we then utilized this dye to identify localization of internalized $\gamma2^{pH}$FAP receptors in the endosomal-lysosomal system. Acidity increases as intracellular receptors undergo transition from early endosomal/recycling pathways to late endosomal/lysosomal pools **(Fig. 9A)**. We therefore anticipated differences in mean $MG_{561}/MG_{640}$ ratios between these vesicular populations. To examine this effect, we cotransfected $\gamma2^{pH}$FAP neurons with the early endosome marker EEA1-GFP for live-imaging experiments. At DIV 12-13, 10 nM Cy3pH(S/SA)-MG was added directly to the cell culture media and neurons were incubated for 30 min at 37°C prior to imaging. Cells were first perfused with pH 7.4 HBS to acquire $MG_{561}/MG_{640}$ data, then with pH 6.4 solution to eliminate surface $\gamma2^{pH}$FAP (pHGFP) signal (orange stars; **Fig. 9B**) to isolate intracellular EEA1-GFP for image analysis. Cy3pH(S/SA)-MG vesicles colocalized with EEA1-GFP (yellow arrows; **Fig. 9B**) demonstrated a mean $MG_{561}/MG_{640}$ ratio of 0.824 ± 0.012, while all other identified vesicles not-associated with EEA1-GFP (white triangles; **Fig. 9B**) displayed a significantly higher ratio of 0.918 ± 0.016 (Other; **Fig. 9C**). The Cy3pH(S/SA)-MG found in non-EEA1 intracellular sites typically displayed the lowest pH and was in comparably larger vesicular bodies, suggesting lysosomal compartments. These results indicate Cy3pH(S/SA)-MG labeled $\gamma2^{pH}$FAP receptors can be used to decipher the localization of internalized $GABA_AR$ pools along the endosome-lysosome axis.

Next we wanted to elucidate if Cy3pH(S/SA)-MG could be used to monitor the constitutive endolysosomal trafficking of $GABA_ARs$ by using conditions that limit internalization. We compared $\gamma2^{pH}$FAP neurons pulse-labeled with 100 nM Cy3pH(S/SA)-MG dye either immediately after washing (t0) or 30 min later ± the dynamin inhibitor, dynasore (80 μM) at 37°C. Importantly, $GABA_ARs$ have been previously characterized to undergo constitutive dynamin-dependent clathrin mediated endocytosis (137, 257). Images of neurons allowed 30 min of trafficking show

enhanced dye-labeled $GABA_AR$ accumulation within the cell body compared to t0 and to t30 + dynasore **(Fig. 9D)**. The number of $GABA_AR$-positive vesicles inside the neuronal cell body was measured using the spot detection feature in NIS Elements. Quantification confirmed that the total number of vesicles identified at t30 is 78.7 ± 20% greater than at t0 and that vesicle internalization is blocked by dynasore co-treatment **(Fig. 9E)**. To better understand the receptor population distribution along the endosomal-lysosomal trafficking axis, we examined each measured vesicle's respective $MG_{561}/MG_{640}$ ratio using a histogram plot **(Fig. 9F)**. This analysis revealed that the increase in vesicles found at t30 were primarily at lower $MG_{561}/MG_{640}$ ratios, suggesting early endosomal trafficking. Moreover, the vesicle median $MG_{561}/MG_{640}$ ratios were significantly different between all conditions: t0 = 1.31; t30 = 0.767; and t30 + dynasore = 0.826. Interestingly, we found that while dynasore reduced the number of internalized receptors detected back to t0 levels, dynasore treated neurons demonstrated a unique vesicular $MG_{561}/MG_{640}$ ratio profile **(Fig. 9E)**. Dynasore inhibition of clathrin-coated pit formation and endocytosis generates half formed "U" and "O" shaped pits/vesicles associated with the plasma membrane (258). The few vesicles present in t30 + dynasore treated neurons (**Fig. 9D**) are likely to be these structures undergoing partial acidification during the 30 minute experimental period. In summary, $\gamma 2^{pH}FAP$ and the Cy3pH(S/SA)-MG dye reveal significant constitutive clathrin-dependent endocytosis of $GABA_ARs$ that favors early endosomal pathways.

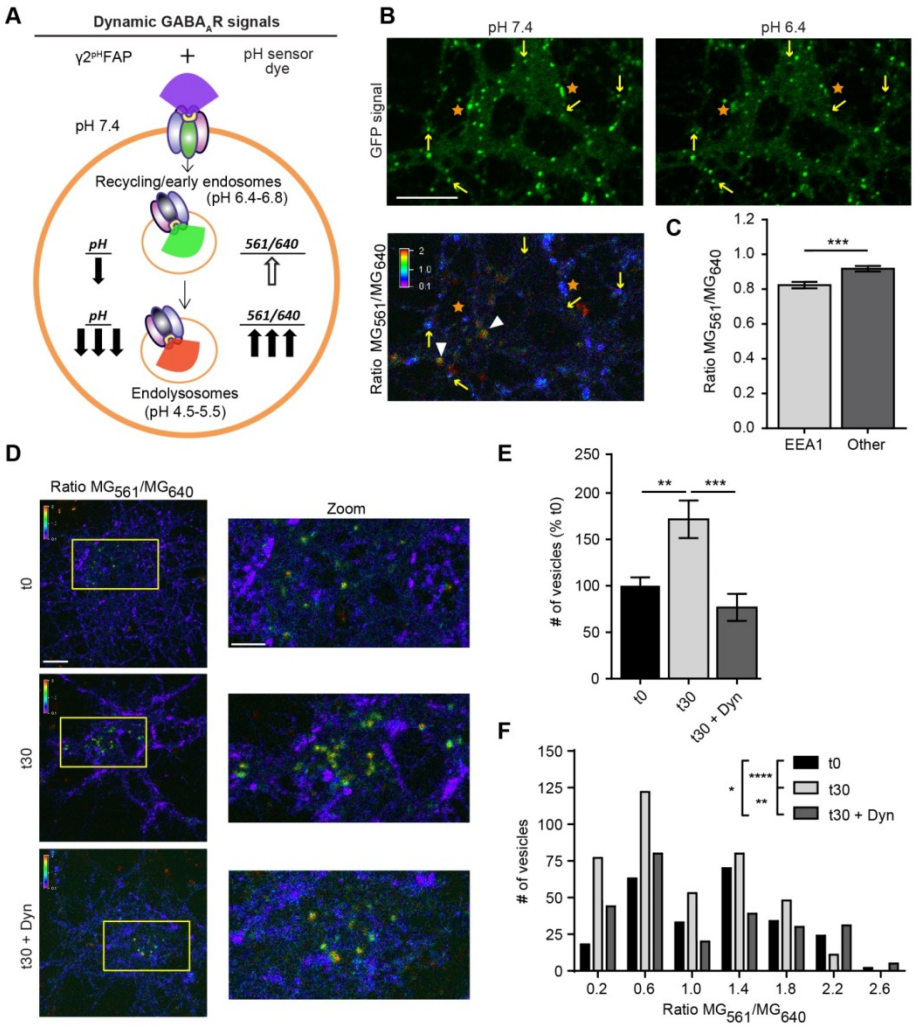


**Figure 9. Constitutive Endolysosomal Trafficking of GABA$_A$Rs can be Measured using the pH-Sensitive Dye Cy3pH(S/SA)-MG and γ2$^{pH}$FAP.**

(A) Application of pH sensor dye to visualize and distinguish intracellular vesicle targeting of internalized GABA$_A$R. Once internalized, the pHGFP signal is immediately quenched, and the increasingly acidic environment enhances Cy3pH fluorescence intensity and FRET. A higher MG$_{561}$/MG$_{640}$ ratio indicates vesicular acidification. Recycling/early endosomal vesicle signal represented as green, late endosome/lysosomes as red to match the MG$_{561}$/MG$_{640}$ ratio heatmap in images. (B) Neurons transfected with *γ2$^{pH}$FAP* and *EEA1-GFP* were incubated in the continuous presence of 10nM Cy3pH(S/SA)-MG dye for 30 min in conditioned media at 37°C and then washed and rapidly imaged. After initial images were taken at pH 7.4, pH 6.4 HBS was perfused onto cells to quench surface pHGFP signal of γ2$^{pH}$FAP and selectively identify EEA1-GFP positive vesicles. Yellow arrows indicate vesicles where EEA1-GFP is colocalized with Cy3pH(S/SA)-MG; white triangles indicate larger Cy3pH(S/SA)-MG vesicular

structures not colocalized with EEA1-GFP (Other); orange stars represent γ2$^{pH}$FAP pHGFP surface signal that is eliminated after pH 6.4 saline perfusion. Scale bar = 10 μm. (C) Quantification of individual intracellular vesicles $MG_{561}/MG_{640}$ ratio at either EEA1-GFP positive sites or other internal compartments (*n* = 243 EEA1-GFP; 511 Other from 9 cells and 2 neuronal cultures; Student's t-test; error bars represent error bars represent ± S.E.M.). (D) Confocal images of pH sensor dye-labeled $GABA_A$Rs at t0, t30 and t30 + dynasore (Dyn, 80 μM), with cell body indicated by yellow outlined region of interest (ROI). Zoomed images of timepoints are shown to right. Scale bars: whole image = 10 μm; zoom image = 5 μm. (E) More intracellular vesicles are quantified at t30 than t0 or t30 + dynasore (one way ANOVA followed by post hoc Tukey's test; error bars represent ± S.E.M.). (F) Histogram analysis reveals most t30 vesicles had lower $MG_{561}/MG_{640}$ ratios and the median values between all conditions were significantly different (Mann-Whitney test) *(n* = 14 neurons per treatment from 3 independent cultures). All ratiometric images are on a scale from 0.1 to 2. *p* values for (C,E,F): *p≤0.05, **p≤0.01, ***p≤0.001, and ****p≤0.0001

### 2.3.3 γ2$^{pH}$FAP Reveals Enhanced $GABA_A$R Synaptic Turnover in an *In Vitro* Bicuculline Seizure Paradigm

We last set out to investigate if the γ2$^{pH}$FAP-dye system could be used to measure pharmacologically-induced changes in $GABA_A$R trafficking in living neurons. Prolonged exposure of the $GABA_A$R antagonist bicuculline is proconvulsant due to sustained dampening of network inhibition, leading to seizure-type activity *in vitro* and *in vivo* (259-262). Multiple hyperexcitable neuronal states have previously been reported to enhance γ2-containing $GABA_A$R internalization and reduce total surface levels at 1 h post induction (156-158, 263). We investigated if the γ2$^{pH}$FAP construct could be used to simultaneously examine multiple stages of receptor trafficking including receptor surface, synaptic, and lysosomal levels following a bicuculline-induced seizure paradigm. At DIV 12-14 γ2$^{pH}$FAP neurons were pulse-labeled with MG-BTau dye and then returned to conditioned media +/- 50 μM bicuculline at 37°C for 1 h. 50 nM LysoTracker was added 30 min prior to the end of treatment to identify association of receptors with lysosomes.

Representative images indicate MG-BTau labels synaptic $GABA_AR$ clusters on the surface of dendrites as seen by colocalization of MG-BTau (blue) and pHGFP (green) **(Fig. 10A,B).** MG-BTau also reveals internalized receptors within the cell body in lysosomes (**Fig. 10C**, Lysotracker in red). These data demonstrate that the binding of MG-BTau to $\gamma2^{pH}$FAP $GABA_ARs$ and its resulting fluorescence is stable even in very low pH environments such as lysosomes, consistent with previous findings using different FAP-tagged receptors colocalized with LysoTracker in cell culture (236). Image analysis uncovered no significant difference in total surface expression of $\gamma2^{pH}$FAP between DMSO control and bicuculline treated cells when measuring pHGFP signal (**Fig. 10D**). There was a trend towards a decrease in synaptic levels of $\gamma2^{pH}$FAP in bicuculline treated neurons (75 ± 13% of control), determined by pHGFP cluster fluorescence, but this was not significant. In contrast, **(Fig. 10E)** shows bicuculline treatment reduced total and synaptic MG-BTau signal by 41 ± 10% and 67 ± 8%, respectively, indicating the population of pulse-labeled $\gamma2^{pH}$FAP receptors had decreased. In support of enhanced receptor turnover, we found that bicuculline treatment increased association of labeled receptors with lysosomes by 107 ± 41% compared to control. These findings suggest that bicuculline-induced seizure activity leads to augmented $GABA_AR$ synaptic turnover, lysosomal targeting, and a compensatory increase in new, non-recycled $GABA_AR$ insertion to

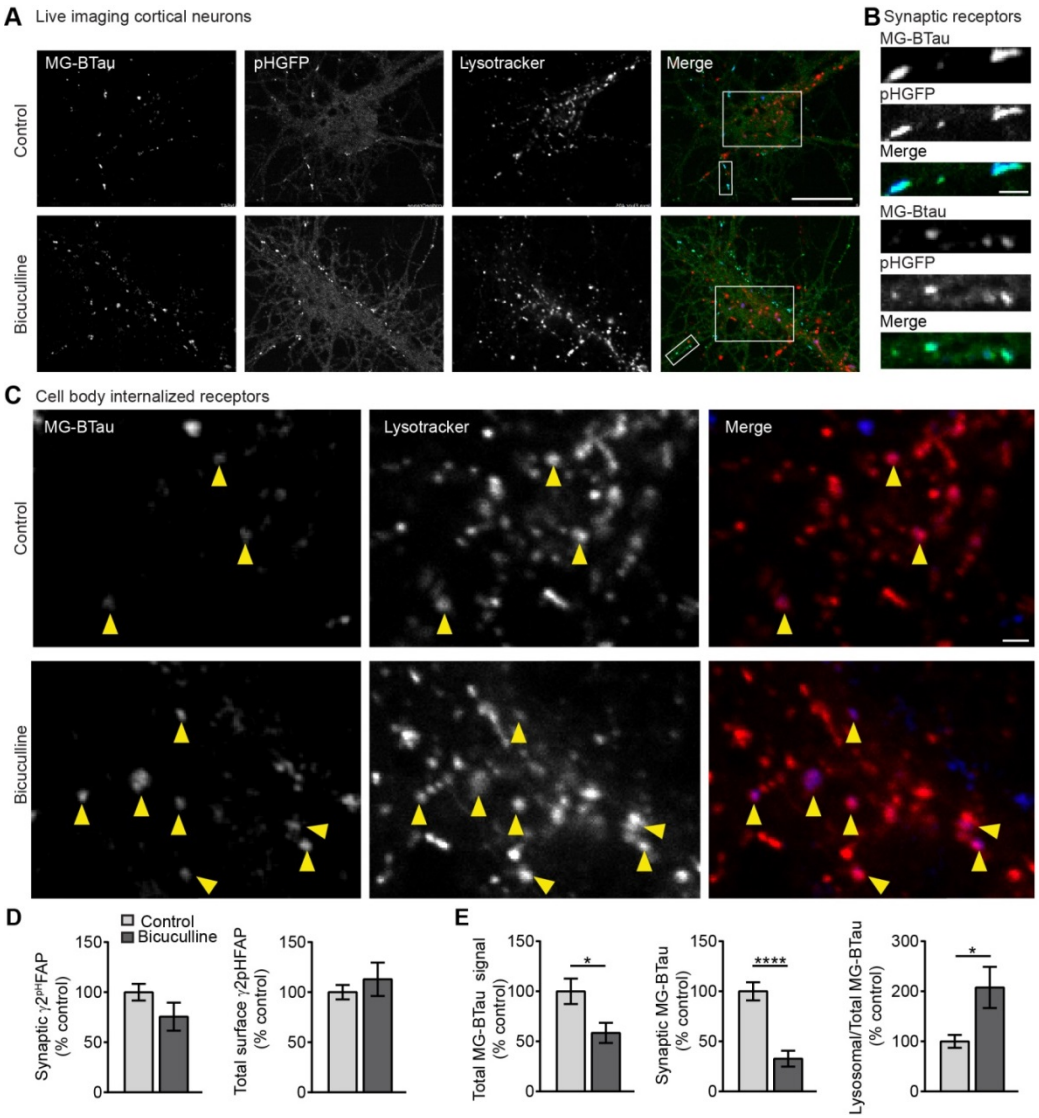


**Figure 10. γ2pHFAP Imaging Reveals Increased Internalization and Enhanced GABAAR Turnover Rates Following a Bicuculline-Induced Seizure Paradigm.**

(A) γ2$^{pH}$FAP neurons were pulse-labeled with 100 nM MG-BTau for 2 min then returned to 37°C conditioned media +/- 50 µM bicuculline for 1 h. LysoTracker (50 nM) was added directly to the media after 30 min to label lysosomes. pHGFP fluorescence is shown in green, LysoTracker in red, and MG-BTau in blue in the Merge panels. Smaller boxed areas in Merge panel identify surface synaptic receptors (enlarged in B). Larger boxed area identifies internalized receptors present in endosomes and lysosomes in cell body of neuron (enlarged in C). (B) Surface synaptic receptors on dendrites are seen with colocalization of MG-BTau and pHGFP signals. (C) Enlargements of cell body area show colocalization of internalized MG-BTau labeled $GABA_A$Rs and lysosomes. (D) Quantification of pHGFP signal showed synaptic and total surface levels were not changed following bicuculline treatment. (E) In contrast,

quantification of MG-BTau signal revealed reductions in total and synaptic receptor levels after the bicuculline seizure paradigm. Bicuculline treatment also enhanced the ratio of MG-BTau labeled receptors associated with lysosomes over total MG-BTau signal. (*$p < 0.05$, ****$p < 0.0001$, Student's t-test; synaptic measurements performed on three 10 μm regions located on dendrites; $n = 13$ neurons per treatment from 3 independent cultures; error bars represent ± S.E.M.). Scale bars: 20 μm in A and 2 μm in B,C.

mitigate this response. These results robustly demonstrate the versatility of the $\gamma2^{pH}$FAP-dye system and its ability to measure numerous trafficking events to address complex questions.

## 2.4 Discussion

Live-cell receptor tracking approaches offer critical information by revealing real-time alterations in protein trafficking. Here we describe a flexible paired $GABA_AR$ γ2-subunit optical reporter system that can be used to monitor multi-stage receptor trafficking. Compared to previously available methods that require reliable antibodies, conventional fluorophore tagging, or fluorescent α-bungarotoxin labeling, the $\gamma2^{pH}$FAP-dye system can allow for simultaneous monitoring of surface, synaptic, and intracellularly trafficking $GABA_ARs$ in real-time. The strength of this method lies in the ability to simply alternate FAP-compatible MG dyes to address the specific experimental question of interest.

We applied the pH sensor dye, Cy3pH(S/SA)-MG, to monitor internalization and constitutive endosomal and lysosomal trafficking of $GABA_ARs$ in neurons. We found that Cy3pH(S/SA)-MG labeled surface $\gamma2^{pH}$FAP receptors can be tracked to small EEA1-positive early endosomes (MG-BTau labeled receptors also identified at EEA1 endosomes; **Fig. 7**) and also to larger vesicular structures with low pH (likely lysosomes), generating high $MG_{561}/MG_{640}$ ratios **(Fig. 9B,C)**. Synaptic $GABA_AR$ endocytosis occurs primarily in a dynamin-dependent manner

(257) and can be identified within 30 minutes using an antibody feeding approach (137). Our results in **Fig. 9** demonstrate rapid internalization of receptors in endosomal/lysosomal pathways on this same time scale, a process reduced by the dynamin-inhibitor dynasore. As a result of the vesicle-level pH-sensitive measurement afforded by this tool, we were able to further generate a histogram plot identifying differences in the trafficking stages of $\gamma2^{pH}$FAP-positive vesicles. These analyses suggest internalized receptors favor early endosomal pathways, a finding supported by a previous study that determined over 70% of internalized $GABA_AR$s are recycled back to the cell surface within 1 h (143). Furthermore, dynasore treated neurons displayed vesicles with a distinct MG ratio profile, possibly resulting from acidification of endocytic pits/vesicles not released from the plasma membrane, non-dynamin dependent endocytosis of receptors, or dynasore off-target effects. $GABA_AR$s undergo both clathrin-dependent and -independent endocytosis pathways in heterologous cells (138), with both mechanisms being recently identified in neurons for glutamateric AMPA receptors (264, 265). Dynasore has also been shown to disrupt lysosomal fission by inhibiting dynamin-2 (266) as well as have other non-specific, dynamin independent effects (267, 268) that could result in different vesicle $MG_{561}/MG_{640}$ ratio profiles. Further studies investigating additional time points are necessary to identify the rate, equilibrium, and overall population dynamics of constitutive $GABA_AR$ internalization.

To test the utility of $\gamma2^{pH}$FAP in detecting pharmacologically-induced changes in $GABA_AR$ trafficking, we exposed neurons to a bicuculline-induced seizure paradigm following a MG-BTau pulse-labeling protocol **(Fig. 10)**. This unique dye labeling approach readily detected enhanced synaptic receptor turnover rates and lysosomal targeting that were not detectable by pHGFP fluorescence alone. Previous work has shown that more aggressive seizure protocols relying on

depolarization via high external potassium and/or agonist application targeting highly calcium permeable NMDA receptors reduces total surface $GABA_A$Rs in cultured neurons (157). It is likely that the mild seizure paradigm used here does not affect total surface receptor levels, but instead enhances surface turnover that is offset by increased receptor insertion rates. In support of this argument, another recent study (160) found that 1 h treatment with $GABA_A$R antagonists did not lead to a reduction in surface $GABA_A$R levels.

This paper lays the groundwork for future investigations of $GABA_A$R trafficking using the $\gamma2^{pH}$FAP sensor. Importantly, this technique can be further extended toward pharmacology focused efforts in high throughput screenings (234, 244), assay development based on flow cytometry (235, 243) or high resolution 96-well plate assays (250), and for *in vivo* protein labeling (237, 269). In summary, our $\gamma2^{pH}$FAP is the first protein-FAP conjugate characterized in primary neurons, providing a unique tool to monitor multistage $GABA_A$R trafficking in living cells with relevance both for basic science research and applied pharmacology.

## 3.0 Early Diazepam Exposure Alters $GABA_AR$ Intracellular Trafficking and Accelerates Synaptic Exchange

Chapter adapted from: Lorenz-Guertin, J. M., et al. (2019). Diazepam Accelerates GABAAR Synaptic Exchange and Alters Intracellular Trafficking. Front Cell Neurosci (270) https://doi.org/10.3389/fncel.2019.00163

JL-G performed the biochemistry, immunoprecipitation, bioinformatics analysis and fixed and live imaging acquisition and analysis. Matthew J. Bambino performed the FRET imaging and analysis. Joshua Lorenz-Guertin, Tija C. Jacob and Susan T. Weintraub designed the Mass spectrometry experiments. The Weintraub lab performed mass spectrometry and data was analyzed by Joshua Lorenz-Guertin, Tija C. Jacob and Susan T. Weintraub.

### 3.1 Introduction

The most prevalent synaptic $GABA_AR$ subtype is composed of two α, two β, and a γ2 subunit forming a heteropentamer (32). BZDs are a widely used clinical sedative-hypnotic drug class that selectively bind between the interface of a $GABA_AR$ γ2 subunit and either an α1/2/3/5 subunit (33). Receptors containing these α subunits are considered to be primarily synaptic, with the exception of α5, which is localized both synaptically and extrasynaptically (63). Positive allosteric modulation by BZD enhances $GABA_AR$ inhibition by increasing the binding affinity of GABA and increasing channel opening frequency (32). It is known that the potentiating effect of BZDs are lost after prolonged or high dose acute exposure (271, 272), characterized first by a loss of sedative/hypnotic activity followed by the anti-convulsant properties behaviorally (46, 273-275). The induction of BZD tolerance occurs in part due to the uncoupling of allosteric actions between GABA and BZD (276, 277), a process that appears to rely on $GABA_AR$ receptor internalization (278, 279). We have previously shown that 24 h BZD treatment leads to decreased

surface and total levels of the α2 subunit in cultured hippocampal neurons that was dependent on lysosomal-mediated degradation (169); however, the process by which the α2 subunit is selectively targeted to lysosomes is still unknown. $GABA_AR$ subunit ubiquitination and subsequent degradation at proteasomes or lysosomes modulates cell surface expression of receptors (117, 159, 170, 280, 281). Ubiquitination of the γ2 subunit is the only currently known mechanism identified to target internalized surface $GABA_ARs$ to lysosomes (159).

Another major regulator of $GABA_AR$ efficacy is postsynaptic scaffolding. Confinement at synaptic sites maintains receptors at GABA axonal release sites for activation. Furthermore, this limits receptor diffusion into the extrasynaptic space where internalization occurs (282, 283). The scaffolding protein gephyrin is the main organizer of $GABA_AR$ synaptic localization and density, as gephyrin knock-down and knock-out models show dramatic reductions in γ2- and α2-$GABA_AR$ clustering (54, 55). Evidence suggests gephyrin interacts directly with $GABA_AR$ α1, α2, α3, α5, β2, and β3 subunits (62, 63, 65, 284-286). Gephyrin recruitment is involved in inhibitory long term potentiation (iLTP) (77, 287), while its dispersal coincides with $GABA_AR$ diffusion away from synapses (54, 182). Extensive post-translational modifications influence gephyrin function (288, 289). Accordingly, expression of gephyrin phosphorylation site mutants revealed complex effects on $GABA_AR$ diffusion and gephyrin ultrastructure and scaffolding (289, 290). Phosphorylation at the gephyrin serine 270 (Ser270) site has been particularly characterized to negatively modulate scaffold clustering and density, in part by enhancing calpain-1 protease mediated degradation of gephyrin (73). Given the well-established interdependent relationship between gephyrin and the γ2 subunit in maintaining receptor synaptic integrity (54, 55, 67, 215, 291, 292), impaired postsynaptic scaffolding should affect both pre-existing and newly inserted $GABA_AR$ clustering

and ultimately the efficacy of inhibitory neurotransmission. Thus a central unanswered question is if BZD exposure causes changes in gephyrin phosphorylation or protein levels.

Here we demonstrate that 12-24 h treatment with the BZD diazepam (DZP) leads to a reduction in total γ2 subunit and full-length gephyrin levels *in vitro* and *in vivo*. This reduction occurred coincident with enhanced γ2 subunit ubiquitination, but resulted in no significant change in overall γ2 surface levels. Using our recently published dual fluorescent BZD-sensitive $GABA_AR$ reporter ($\gamma2^{pH}FAP$), we further show that cell surface γ2-$GABA_ARs$ are more frequently targeted to lysosomes after DZP exposure. Forester resonance energy transfer (FRET) experiments further confirmed specific loss of synaptic α2/γ2 $GABA_AR$ levels following DZP treatment. The scaffolding protein gephyrin also demonstrated augmented phosphorylation at Ser270, increased cleavage and was significantly decreased in membrane and cytosolic compartments. Fluorescence recovery after photobleaching (FRAP) assays identified that DZP treatment increased the simultaneous recovery of γ2-$GABA_AR$ and gephyrin at synaptic sites, indicating reduced receptor confinement and accelerated exchange between the synaptic and extrasynaptic $GABA_AR$ pool. This process was reversed by the BZD site antagonist Ro 15-1788. Lastly, co-immunoprecipitation, quantitative mass spectrometry and bioinformatics analysis revealed shifts in the γ2-$GABA_AR$ interactome towards trafficking pathways *in vivo.* Together, these data suggest that DZP exposure causes a compensatory decrease in inhibitory neurotransmission by reducing BZD-sensitive $GABA_AR$ and gephyrin confinement at synapses and via ubiquitination and lysosomal targeting of γ2 by reducing BZD-sensitive $GABA_AR$ and gephyrin confinement at synapses, and via ubiquitination and lysosomal targeting of γ2.

## 3.2 Methods and Materials

### 3.2.1 Cell Culture, Transfection, Expression Constructs and Mice

Cortical neurons were prepared from embryonic day 18 Sprague Dawley rats and nucleofected with constructs at plating (Amaxa). The $\gamma2^{pH}$FAP construct was characterized in (212) and RFP-gephyrin was described in (63). The $\gamma2^{RFP}$ construct was generated by PCR cloning and fully sequenced: the red fluorescent protein *mCherry* replaced *pHluorin* in the previously published $\gamma2^{pHGFP}$ construct (54). *GFP-ubiquitin* was a gift from Nico Dantuma (Addgene plasmid # 11928) (293). 8-10 week old male C57BL/6J mice (Jackson Laboratory) were maintained on a reverse 12 h dark/light schedule. Mouse cortical brain tissue was collected and flash frozen 12 h after I.P. injection with either vehicle or diazepam (in 40% PEG, 10% EtOH, 5% Na Benzoate, 1.5 % Benzyl alcohol (Hospira)). All procedures were approved by the University of Pittsburgh Institutional Animal Care and Use Committee.

### 3.2.2 Reagents, Antibodies, and MG Dye

Diazepam (cell culture, Sigma; injections, Hospira); Ro 15-1788 (Tocris Bioscience); calpain-1 inhibitor MDL-28170 (Santa Cruz); L-glutamic acid (Tocris Bioscience). Primary antibodies: rabbit GAPDH (WB) (14C10, Cell Signaling); guinea pig GAD-65 (IF) (198104, Synaptic Systems); rabbit γ2 $GABA_AR$ subunit (IF, WB, IP) (224003, Synaptic Systems); rabbit gephyrin (WB) (sc-14003, Santa Cruz); rabbit gephyrin (IF, total) (147002, Synaptic Systems); mouse gephyrin mAb7a (IF, phospho) (147011, Synaptic Systems); chicken GFP (WB) (GFP-1020, Aves); rabbit (P)ERK (WB) (4370, Cell Signaling); mouse ERK (WB) (9107, Cell

Signaling); rabbit (P)GSK3β (WB) (9322, Cell Signaling); rabbit GSK3β (WB) (9315. Cell Signaling); rabbit CDK5 (WB) (2506, Cell Signaling). MG-BTau dye prepared as in (212).

### 3.2.3 **Fixed and Live-Imaging**

Measurements were made on days *in vitro* (DIV) 15–19 cortical neurons. Live-imaging performed in Hepes-buffered saline (HBS), containing the following (in mM): 135 NaCl, 4.7 KCl, 10 Hepes, 11 glucose, 1.2 $MgCl_2$, and 2.5 $CaCl_2$ (adjusted to pH 7.4 with NaOH). Images were acquired using a Nikon A1 confocal microscope with a 60× oil objective (N.A., 1.49) at 3× zoom. Data were analyzed in NIS Elements software (Nikon, N.Y.). Measurements were taken from whole cell or averaged from three dendritic 10μm regions of interest (ROI) per cell. For fixed imaging, media was quickly removed and coverslips were washed twice with Dulbecco's Phosphate Buffered Saline (DPBS) and immediately fixed with 4% paraformaldehyde and then blocked in PBS containing 10% fetal bovine serum and 0.5% bovine serum albumin. Surface antibody staining was performed under non-permeabilized conditions overnight at 4°C. Intracellular staining was performed overnight at 4°C following 0.2% Triton-X permeabilization for 10 min in blocking solution. Synaptic sites were determined during analysis by binary thresholds and colocalization with GAD-65. Extrasynaptic intensity was measured by taking the total dendrite ROI sum intensity minus background and synaptic fluorescence intensity. Dendritic fluorescence was measured using binary thresholds. Experimental conditions were blinded during image acquisition and analysis. The ROUT test (Q=1%) or Grubbs' Test (alpha=0.05) was used to remove a single outlier from a data set.

### 3.2.4 **Lysosomal Targeting Assay**

Neuron surface and lysosomal-association assays utilized MG-BTau dye for surface receptor pulse-labeling. DIV 15-16 neurons were treated with vehicle or DZP for 8-12 h, then pulse labeled with 100 nM MG-BTau for 2 min at room temperature in HBS. Neurons were then washed 5x times with HBS and returned to conditioned media +/- DZP for 1 h. To identify lysosomal targeting, 50 nM LysoTracker Blue DND-22 (Life Technologies) and the lysosomal inhibitor, Leupeptin (200 μM Amresco), was added 30 min prior to imaging. Following incubation, neurons were washed and imaged in 4°C HBS. Two-three neurons were immediately imaged per culture dish within 10 min of washing. For image analysis, independent ROIs were drawn to capture the soma, three 10 μm sections of dendrite and the whole cell. Binary thresholds and colocalization measurements were performed to identify MG-BTau, pHGFP synaptic $GABA_AR$ clusters and lysosomes. Total surface pHGFP expression was determined by taking the entire cell surface signal following background subtraction.

### 3.2.5 **$NH_4Cl$ Intracellular Imaging**

DIV 15-16 neurons were washed and continuously perfused with HBS + treatment at room temperature. Multiposition acquisition was used to image 2-3 neurons per dish. An initial image was taken to identify surface $\gamma2^{pH}$FAP $GABA_ARs$. Neurons were then perfused with $NH_4Cl$ solution to collapse the cellular pH gradient and were reimaged. $NH_4Cl$ solution (in mM): 50 $NH_4Cl$, 85 NaCl, 4.7 KCl, 10 Hepes, 11 glucose, 1.2 $MgCl_2$, and 2.5 $CaCl_2$ (adjusted to pH 7.4 with NaOH). pHGFP intensity was measured following background subtraction and smoothing. Surface/total levels were determined by dividing the first image (surface only) from the second

image (total). The spot detection tool in Nikon Elements was used to selectively count larger intracellular vesicles positive for $\gamma2^{pH}$FAP. A stringent threshold was set to identify brightly fluorescent circular objects with a circumference of approximately 0.75 μm. Values reflect new vesicle objects that were only seen after $NH_4Cl$ perfusion (second image – first image).

### 3.2.6 **Intermolecular FRET Imaging, Characterization and Analysis**

The α2 pHGFP ($\alpha2^{pH}$) construct was previously published (65) and the $\gamma2^{RFP}$ construct was generated by PCR cloning and fully sequenced. DIV 15-16 neurons were treated with Veh or DZP for 20-28 h, then washed and continuously perfused with HBS at room temperature. Images were acquired with a 60x objective at 2x zoom. For each cell, an initial image was acquired containing two channels to identify surface $\alpha2^{pH}$ (excited by 488 laser, emission band pass filter 500-550) and $\gamma2^{RFP}$ participating in FRET (excited 488 FRET, emission band pass filter 575–625 nm, FRET channel). A second, single channel image was taken immediately following with only 561 nm excitation to reveal total $\gamma2^{RFP}$ levels (excited by 561 laser, emission band pass filter 575–625 nm). For synaptic quantifications, binary thresholding based on intensity was applied with smoothing and size exclusion (0-3 μm) factors. FRET and 561 channel binaries shared identical minimum and maximum binary threshold ranges. Individual synaptic ROIs were created to precisely target and measure synaptic clusters containing both $\alpha2^{pH}$ and $\gamma2^{RFP}$. Manual trimming and single pixel removal were used to remove signal not meeting the criteria of a receptor cluster. Restriction criteria were applied in the following order: 1) at least 15 synapses measured per cell, 2) FRET $\gamma2^{RFP}$: raw $\gamma2^{RFP}$ sum intensity ratio must be less than one, 3) synaptic $\alpha2^{pH}$ mean intensity of at least 500, and 4) $\alpha2^{pH}$ sum intensity limit of 300% of average sum intensity. ROI data was then

normalized to vehicle control as percent change. The percentage of RFP participating in FRET was also calculated using FRET RFP:Total RFP ratio.

FRET activity was directly assessed by acceptor ($\gamma2^{RFP}$) photobleaching. Photobleaching ROIs were implemented on 2 synapses per cell. Pre-bleaching images were acquired every 5 seconds, followed by a $\gamma2^{RFP}$ photobleaching event using 80% 561 nm laser power. After photobleaching, image capturing resumed without delay using pre-bleach laser power settings for 2 minutes. Image analysis incorporated background subtraction and the measurement of percent change in $\alpha2^{pH}$/FRET $\gamma2^{RFP}$ ratio over the time course. FRET efficacy measurements compared directly adjacent $\alpha2^{pH}$ and $\gamma2^{RFP}$ subunits in a $GABA_AR$ complex. Live-imaging with perfusion of pH 6.0 extracellular imaging saline solution (MES) was used to quench the pH-dependent GFP fluorescence from the $\alpha2^{pH}$ donor fluorophores and show the dependence of FRET on surface $\alpha2^{pH}$ fluorescence. Acidic extracellular saline solution, MES solution pH 6.0 (in mM): 10 MES, 135 NaCl, 4.7 KCl, 11 glucose, 1.2 $MgCl_2$, and 2.5 $CaCl_2$ (adjusted to pH 7.4 with NaOH). Images were collected under HBS conditions for 1 minute at 20 second intervals, and then followed by a 2 minute MES wash with the same imaging interval to quench donor emissions. FRET RFP mean intensity was measured under both conditions and normalized to HBS. Percent or fold change in FRET RFP emissions were reported. We confirmed loss of $\alpha2^{pH}$ donor lead to 90% loss of FRET $\gamma2^{RFP}$ emissions. $\gamma2^{RFP}$ emission from 488 laser excitation in the absence of donor was not tested. Measurements did not correct for channel bleed through.

### 3.2.7 **Synaptic Exchange Rate FRAP Imaging**

Neurons were washed and media was replaced with HBS + treatment. Imaging was performed in an enclosed chamber at 37°C. An initial image was taken for baseline

standardization. Photobleaching was performed by creating a stimulation ROI box encompassing two or more dendrites. This stimulation region was photobleached using the 488 and 561 lasers at 25% power for 1 minute. The same stimulation ROI was used for every cell in an experiment. Immediately following photobleaching, 10 nM MG-Tau dye was added to the cell culture dish to re-identify surface synaptic $GABA_AR$ clusters. Time-lapse imaging was then started every 2 min for 60 min. During image analysis, objects were only considered synaptic if they demonstrated colocalization with $\gamma2^{pH}$FAP pHGFP signal, RFP-gephyrin signal and had obvious surface MG-BTau fluorescence. ROIs were drawn measuring the rate of fluorescence recovery at 4-8 synaptic sites and one extrasynaptic site (10μm long region; Bezier tool) per cell. For data analysis, synapse post-bleach fluorescence intensity time point data was first normalized to pre-bleach fluorescence intensity (post-bleach/pre-bleach). Normalized synapse post-bleach data was then calculated as percent change from t0 ((tx/t0)*100, where x = min). Individual synapses were then averaged to calculate fluorescence recovery and statistically significant changes across time points.

### 3.2.8 **Quantitative PCR**

RNA was extracted from primary cultured neurons purified using a RNeasy mini kit (Qiagen). RNA concentration and purity were assessed using a Nanodrop spectrophotometer (Thermo Scientific). cDNA was synthesized from 320 ng of total RNA per reaction using the High Capacity cDNA Reverse Transcription Kit (Applied Biosystems). The Quantitative Polymerase Chain Reaction (qPCR) was performed using SYBR Green and the 7300 RealTimePCR system (Applied Biosystems Corp.), starting with 50°C for 2 min and 95°C for 10 min, followed by 40 cycles at 95°C for 15 s and 60°C for 1 min, and concluding with 15 s at 95°C, 60°C for 1 min and 95°C for 15 s to ensure a single product on melting curves; 1 μl of cDNA was used per well. All

data were analyzed using the ΔΔ*C*t approach as described previously (294). $GABA_AR$ β3 subunit primers: CATGTCCTTTGTGAAGGAGACG, GTCAAGCGTGAGGTTGAGAGG, product length 229 base pairs (BP); $GABA_AR$ γ2 subunit primers GCGCAGTTCTGTTGAAGTGG, CCATTGCTGTGACATAGGAGAC, product length 338 BP; Gephyrin primers: GCAGGGTATCTTGGATCCTCG, GCTCTGTCTTTGGAGGTAGC, product length 215 BP; 4) β-actin primers: AGCCATGTACGTAGCCATCC, ACCCTCATAGATGGGCACAG, product length 115 BP.

### 3.2.9 **Western Blot and Immunoprecipitation**

Protein concentration was determined by BCA protein assay for all biochemistry. Neurons were lysed in denaturing buffer for immunoprecipitation: 50mM Tris HCl, 1mM EDTA, 1% SDS, 2mM $Na_3VO_4$, 10mM NaF, 50mM N-ethylmaleimide, protease inhibitor cocktail (Sigma). Lysates were sonicated and heated at 50°C for 20 min, then diluted 1:5 in RIPA buffer (50mM Tris HCl pH 7.6, 150mM NaCl, 1% Igepal, 0.5 % Sodium deoxycholate, 1mM EDTA, 2mM $Na_3VO_4$, 10mM NaF, 50mM N-ethylmaleimide, protease inhibitor cocktail). Standard immunoprecipitation procedures were performed using overnight incubation with γ2 subunit antibody or rabbit IgG (sci2027; Sigma), 1 h incubation with Protein A Sepharose 4B beads (Invitrogen), three RIPA buffer washes, and loading for SDS-PAGE. After electrophoresis and transfer to nitrocellulose membrane, samples were probed with primary antibody overnight followed by the appropriate horseradish peroxide (HRP)-coupled secondary antibody.

### 3.2.10 **Membrane and Subcellular Fractionation**

Cultured neurons were lysed using fractionation buffer: 50mM Tris-HCl, 50mM NaCl, 1mM EDTA, 2mM $Na_3VO_4$, 10mM NaF, 320mM sucrose, 0.25% igepal, and protease inhibitor cocktail. Lysates were spun at 88,881*g* for 30 min at 4°C to separate pellet (membrane) from supernatant (cytosol). Fraction integrity was tested by localization specific markers in all experiments (270).

### 3.2.11 **Co-immunoprecipitation**

Mice were intraperitoneally (I.P.) injected with vehicle control or 10mg/kg DZP and sacrificed 12 h post-injection (n = 4 mice per treatment). Mouse cortical tissue was homogenized in co-IP buffer (50mM Tris HCl pH 7.6, 50mM NaCl, 0.25% Igepal, 1mM EDTA, 2mM $Na_3VO_4$, 10mM NaF, 50mM N-ethylmaleimide, and Sigma protease inhibitor cocktail) using a Dounce homogenizer. Tissue was solubilized with end-over-end mixing at 4°C for 15 min, and then spun at 1,000g to remove non-solubilized fractions. Each immunoprecipitation tube contained 375µg of tissue lysate brought up to 1ml volume using co-IP buffer. Lysates were precleared using Protein A Sepharose 4B beads (Invitrogen) for 1 h at 4°C. Lysate was then immunoprecipitated overnight with 2.5µg rabbit γ2 subunit antibody (224003, Synaptic Systems) or 2.5µg rabbit IgG (2027, Santa Cruz). The next day, 40 µl Protein A Sepharose slurry was added and mixed for 2 h at 4°C on a nutator. Beads were then washed 3x at 4°C on a nutator in 1ml co-IP buffer. Beads were denatured with SDS-PAGE loading buffer [Laemmli Sample buffer (Biorad) + β-mercaptoethanol] with heat at 70°C for 10 min and intermittent vortexing. Two immunoprecipitation reactions were

performed per animal and were pooled into a single tube without beads to be used for downstream in-gel digestion.

### 3.2.12 **Mass Spectrometry and Data Processing**

Immunoprecipitated proteins were separated by electrophoresis in Criterion XT MOPS 12% SDS-PAGE reducing gels (Bio-Rad), with subsequent protein visualization by staining with Coomassie blue. Each gel lane was divided into six slices. After de-staining, proteins in the gel slices were reduced with TCEP [tris(2-carboxyethyl)phosphine hydrochloride] and then alkylated with iodoacetamide before digestion with trypsin (Promega). HPLC-electrospray ionization-tandem mass spectrometry (HPLC-ESI-MS/MS) was accomplished by data-dependent acquisition on a Thermo Fisher Orbitrap Fusion Lumos Tribrid mass spectrometer. Mascot (Matrix Science; London, UK) was used to search the MS files against the mouse subset of the UniProt database combined with a database of common contaminants. Subset searching of the Mascot data, determination of probabilities of peptide assignments and protein identifications, were accomplished by Scaffold (v 4.8.4, Proteome Software). MS data files for each entire gel lane were combined via the "MudPIT" option. Identification criteria were: minimum of two peptides; 96% peptide threshold; 1% FDR; 99% protein threshold. One vehicle- and one DZP-treated animal were removed from analysis due to insufficient γ2 subunit pulldown relative to all other groups. N = 3 animals per condition were used for downstream analysis. Protein clustering was applied in Scaffold and weighted spectrum values and exclusive unique peptides were exported for manual excel analysis. Student's t-test analysis was performed using relative fold change (ratio) of DZP compared to vehicle group. In some cases peptides were only detected in vehicle or DZP treated groups, resulting in DZP/V ratio values of zero or undefined error (cannot divide by zero). These

were annotated as NF-DZP (not found in DZP samples) or NF-V (not found in vehicle samples) in the tables.

### 3.2.13 **Bioinformatics Analysis**

Ingenuity Pathways Analysis (IPA) (Ingenuity Systems) was used for cellular pathway analysis. Relative fold levels of DZP proteins compared to vehicle were used for analysis. To be suitable for IPA analysis, proteins NF-DZP were assigned a value of -1E+99, while proteins NF-V were assigned a value of 1E+99. Significant enrichment in protein networks were calculated by right tailed Fisher's exact test. Z-score analysis is a statistical measure of an expected relationship direction and observed protein/gene expression to predict pathway activation or inhibition. IPA core analysis was searched to determine direct and indirect relationships within 35 molecules per network and 25 networks per analysis. All data repositories available through IPA were used to determine experimentally observed and highly predicted interactions occurring in mammalian tissue and cell lines. Ratio data were converted to fold change values in IPA, where the negative inverse (-1/x) was taken for values between 0 and 1, while ratio values greater than 1 were not affected. Proteins found to be enhanced in their association with γ2 (Table 1) were searched in the *Mus musculus* GO Ontology database (released 2018-10-08) for GO biological process and GO molecular function and analyzed by the PANTHER overrepresentation test; significance was determined using Fisher’s Exact with Bonferroni correction for multiple testing.

### 3.2.14 **Statistics**

Relevant statistical test information is described in the figure legends or within the individual methods sections. *p* values are reported in the results section if significance is between 0.01 and < 0.05 or if the data is approaching significance.

## 3.3 Results

### 3.3.1 **12-24h Diazepam Decreases the GABA$_A$R γ2 Subunit and Gephyrin through Post-Translational Mechanisms**

We first examined if DZP exposure reduced surface levels of γ2-GABA$_A$Rs and altered gephyrin Ser270 phosphorylation in cortical neurons by immunofluorescence **(Fig. 11A)**. Cortical neurons were treated for 24 h with vehicle or 1 μM DZP, then immunostained for surface γ2, followed by permeabilization and immunostaining with GAD65 (glutamic acid decarboxylase 65, a marker for presynaptic GABAergic terminals) and the phospho-Ser270 specific gephyrin mAb7a antibody (72, 75). Image analysis identified no sizable change in surface synaptic (91.6 ± 5.3%) or extrasynaptic (93.3 ± 3.8%) γ2 intensity in DZP treated neurons relative to control, but DZP induced a significant 18.9 ± 7.4% ($p = 0.033$) increase in synaptic phospho-gephyrin **(Fig. 11B)**. No change in extrasynaptic phosphorylated Ser270 gephyrin was measured. We repeated this DZP treatment and examined total and phospho-gephyrin levels in dendrites **(Fig. 11C)**. Again DZP significantly enhanced phospho-Ser270 gephyrin compared to vehicle (132 ± 12%; $p = 0.013$), while a decrease in overall gephyrin levels was found (69.7 ± 5.4%) **(Fig. 11D)**.

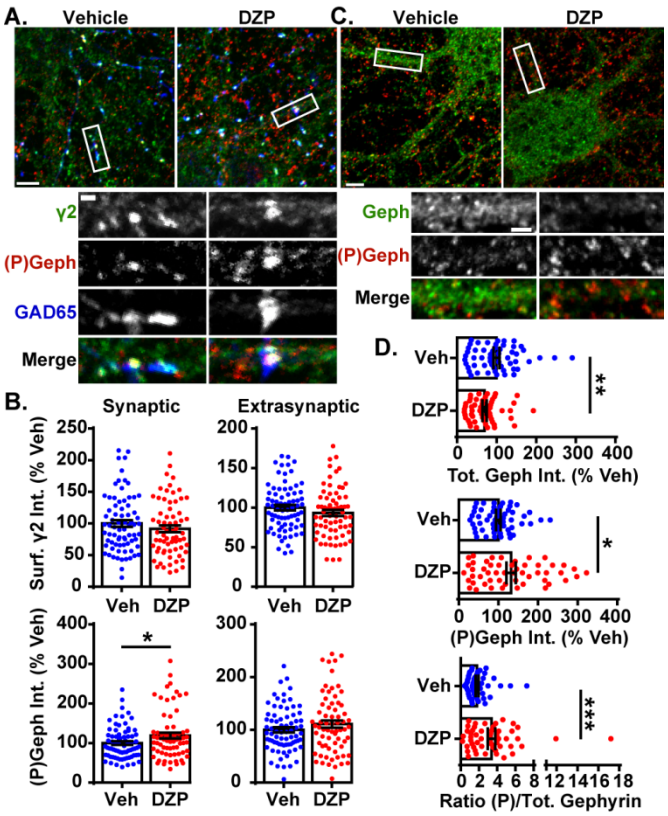


**Figure 11. DZP Downregulates Gephyrin Independent of γ2 Surface Levels**.

(A) Cortical neurons were treated for 24 h with vehicle or 1 μM DZP, then immunostained for surface γ2 $GABA_AR$ (green), followed by permeabilization and immunostaining for (P)Ser270 gephyrin (red), and GAD65 (blue). Panels below show enlargements of $GABA_AR$ synapses on dendrites. (B) Dendrite surface synaptic and extrasynaptic γ2 levels are not significantly altered by DZP. Synaptic phospho-gephyrin was enhanced in response to DZP (n = 69-74 neurons; 4 independent cultures). (C) Neurons were treated as in A followed by antibody staining for total gephyrin (green) and (P)Ser270 gephyrin (red). Panels below show enlargements of dendrite region. (D) The dendritic pool of gephyrin was decreased, while (P)Ser270 gephyrin levels were augmented, resulting in a dramatic increase in the ratio of phosphorylated gephyrin to total gephyrin (n = 52-59 neurons; 3 independent cultures). Int. = fluorescence intensity. Image scale bars: main panels = 5 μm, enlargements = 1 μm. *$p \leq 0.05$, **$p < 0.01$, ***$p < 0.001$, Student's t-test; error bars ± S.E.M.

Accordingly, the mean ratio of phospho/total gephyrin was 78.1± 21% higher following DZP **(Fig. 11D)**. Complimentary biochemical studies using membrane fractionation were used to compare cytosolic, membrane, and total protein pools in cortical neurons. In agreement with immunofluorescence data, membrane levels of γ2 (0.929 ± 0.06) were not reduced after 1 μM DZP, although the total pool of γ2 was diminished (0.793 ± 0.07) **(Fig. 12A,B)** compared to vehicle. Cytosolic levels of γ2 (1.03 ± 0.06) were also unchanged. Comparatively, DZP reduced full-length gephyrin in every compartment measured relative to control (cytosol: 0.871 ± 0.03; membrane: 0.722 ± 0.06, total: 0.695 ± 0.05). We confirmed the integrity of our fractions using cytosolic and membrane specific markers (Supplemental Figure 2; (270)).

Next we assessed if the decrease in gephyrin and γ2 total levels at 24 hours was a result of altered gene expression. qRT-PCR experiments revealed no difference in gephyrin ($p = 0.206$), γ2, or control $GABA_AR$ β3 subunit mRNA levels between vehicle and DZP treated neurons **(Fig. 12C)**. To determine if post-translational modification of γ2 also occurs coincident with decreased γ2 protein levels, we examined ubiquitination of γ2 in response to DZP exposure. We reasoned that changes in ubiquitination of γ2 would likely precede the loss of total γ2 seen at 24 h **(Fig. 12A,B)**. GFP-ubiquitin transfected cortical neurons were treated with vehicle or 1 μM DZP for 12 h. Neurons were lysed under denaturing conditions to isolate the γ2 subunit from the receptor complex. Immunoprecipitation of the γ2 subunit revealed a 2.13 fold increase ($p = 0.015$) in ubiquitination in DZP treated neurons relative to vehicle **(Fig. 12D,E)**. Furthermore, just as observed with 24 h DZP treatment, a reduced total pool of γ2 was also found at 12 h ($p = 0.020$) **(Fig. 12D,E)**. Notably, this is the first demonstration of endogenous γ2 ubiquitination occurring in neurons (previous findings were of recombinant receptors in HEK cells) (159, 170). To investigate mechanisms underlying reduced full-length gephyrin levels, we examined gephyrin cleavage.

Gephyrin is degraded post-translationally by the protease calpain-1 (73, 295, 296), and gephyrin Ser270 phosphorylation promotes cleavage by calpain-1 (73). Consistent with the enhanced gephyrin Ser270 phosphorylation **(Fig.11)** and reduced full-length levels **(Fig. 11,12)** we found a significant increase in the ratio of cleaved/full length gephyrin after 24 h DZP *in vitro* **(Fig. 12F,G)**. We confirmed the identity of the gephyrin cleavage product using a well-characterized glutamate stimulation protocol that induces gephyrin cleavage in cultured neurons (295, 296), a process blocked by calpain-1 inhibition **(Fig. 13)**.

Finally, we wanted to determine if similar mechanisms occur *in vivo* following DZP treatment. Prior publications show BZDs and metabolites are not present 24 h post-injection due to rapid drug metabolism in rodents (297-300). Furthermore, BZD uncoupling does not persist 24 h after a single dose (15 mg/kg) or 2 week daily DZP treatment, whereas uncoupling can be seen 12 h after a single injection, indicating this is the appropriate time point for measuring *in vivo* loss of γ2-$GABA_AR$ function (271). Accordingly, mice were given a single intraperitoneal (IP) injection of 10 mg/kg DZP or vehicle control, and cortex tissues were harvested 12 h later. We found DZP significantly reduced the total pool of γ2 (87.3 ± 3.0%) and full-length gephyrin (73.9 ± 9.1%; p=0.046) relative to vehicle treated mice at 12 h post injection **(Fig. 12H,I)**. Plasma membrane compartment specific loss of these proteins was further assessed using subcellular fractionation of mouse cortical tissue. Synaptic **(Fig. 14A)** and extrasynaptic **(Fig. 14B)** membrane fractions were unable to detect a robust loss of γ2 subunit or gephyrin at either localization after DZP treatment although a near significant decrease in extrasynaptic γ2 levels was found (-12.8% ± 4.0; p=0.053) **(Fig. 14C)**. These findings indicate both BZD-sensitive $GABA_ARs$ and full-length gephyrin are downregulated by post-translational mechanisms after initial DZP treatment *in vitro* and *in vivo* to temper potentiation of $GABA_AR$ function.

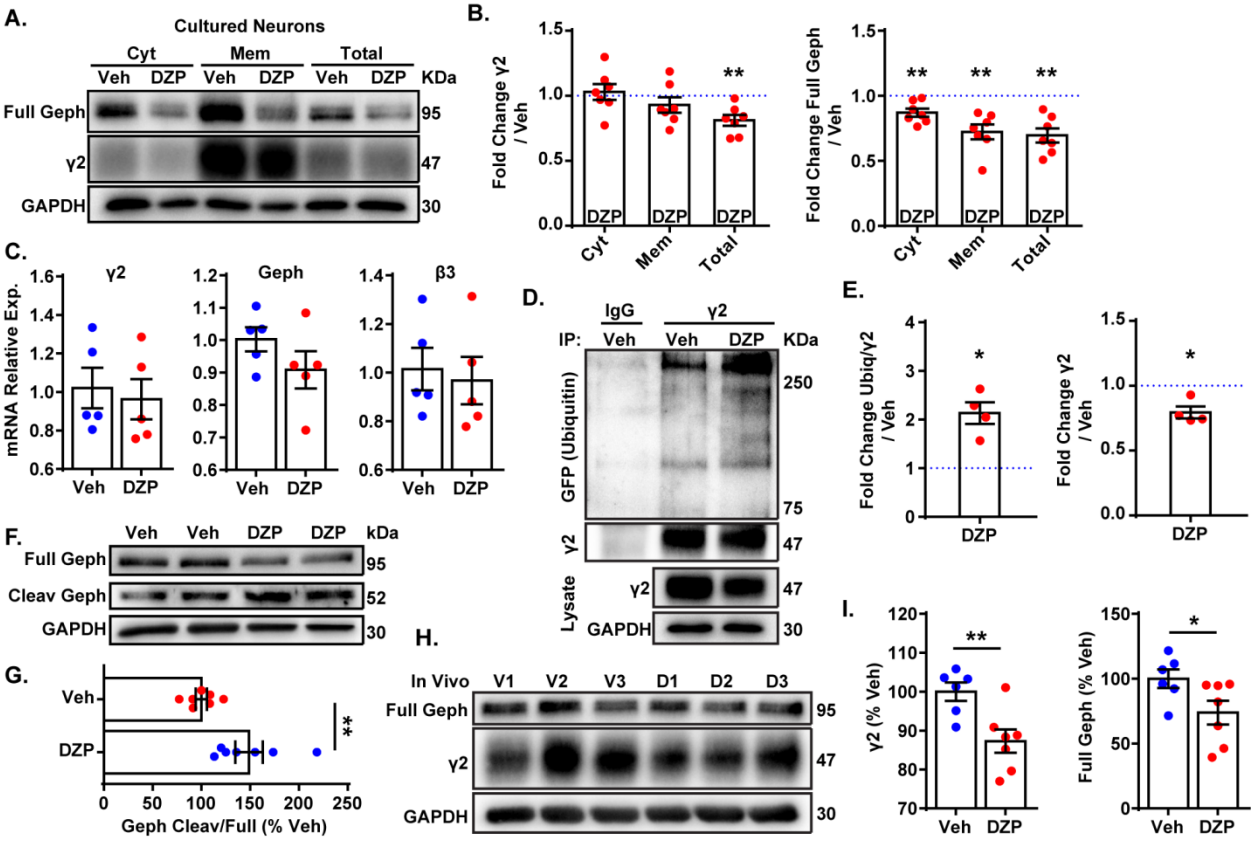


**Figure 12. DZP Induces Degradation of γ2 and Gephyrin *In Vitro* and *In Vivo*.**

(A) Cortical neurons exposed to 1 μM DZP or vehicle for 24 h were subjected to membrane fraction and western blot analysis. (B) Total γ2 subunit and cytosolic, membrane, and total gephyrin were significantly reduced after DZP (n=4 independent cultures). (C) Quantitative RT-PCR revealed no change in γ2 subunit, β3 subunit or gephyrin mRNA expression following 24 h DZP *in vitro* (n=5 independent cultures). (D) GFP-ubiquitin transfected neurons were treated with vehicle or DZP for 12 h. Lysates were immunoprecipitated with control IgG or γ2 antibody, followed by blotting with anti-GFP, γ2 and GAPDH. (E) DZP treatment increased the levels of γ2 ubiquitin conjugates and decreased γ2 total levels. (F,G) DZP treatment enhanced the ratio of cleaved gephyrin fragments/full length gephyrin (n=4 independent cultures). (H) Representative western blots of cortical tissue collected from mice 12 h after a single IP injection of 10 mg/kg DZP or vehicle. Three mice shown from each treatment. (I) γ2 subunit and gephyrin totals are significantly reduced in DZP-treated animals (6-7 mice per condition). (*$p \leq 0.05$, **$p < 0.01$, ****$p < 0.0001$, Student's t-test; error bars ± S.E.M.)

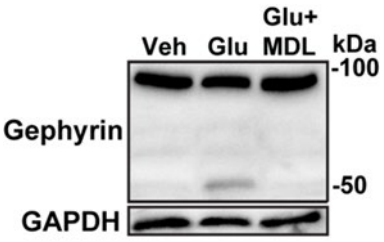


**Figure 13. Calpain-1 Dependent Gephyrin Cleavage upon Glutmate Stimulation.**

DIV 16 neurons were treated with vehicle or 100µM glutamate for 30min in HBS +/- 10µM calpain-1 inhibitor MDL-28170 (MDL). Neurons were then returned to conditioned media for 1.5 h prior to lysis. MDL-28170 treated neurons were in presence of inhibitor throughout experiment. Calpain-1 inhibition mitigates glutamate induced cleavage of gephyrin. Top band indicates full length gephyrin (95 kDa), bottom band indicates cleaved gephyrin (~50 kDA).

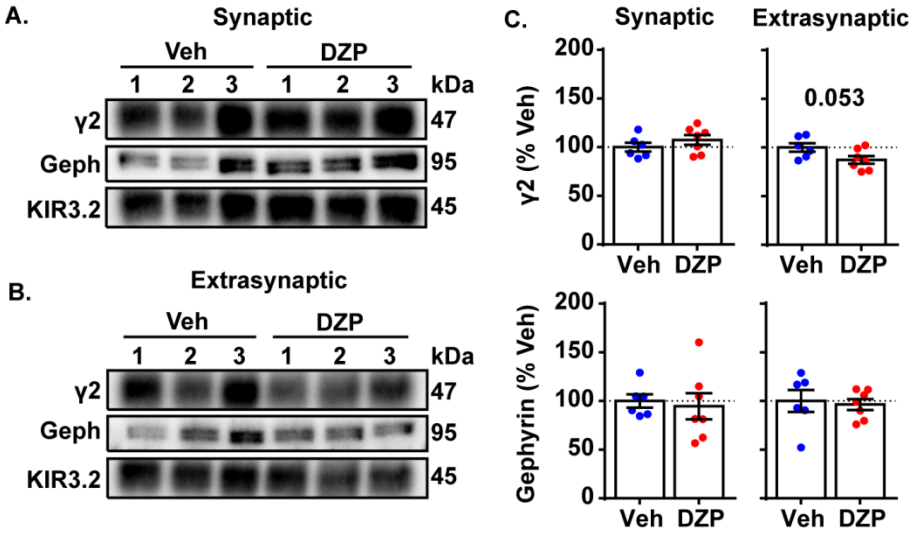


**Figure 14. Subcellular Fractionation of DZP Treated Mice.**

Cortical tissue collected from mice 12 h after a single IP injection of 10 mg/kg DZP or vehicle were subjected to subcellular fractionation to separate synaptic (A) and extrasynaptic fractions (B). Representative blots shown from animals 1-3 for each treatment. Western blot analysis was used to examine γ2 subunit and gephyrin levels. KIR 3.2, an inward-rectifier potassium channel present at equal distribution in the plasma membrane (at both synaptic and extrasynaptic regions) was used as loading control. (C) Quantification of synaptic and extrasynaptic γ2 subunit and gephyrin (6-7 mice per condition). (*$p \leq 0.05$, Student's t-test; error bars ± S.E.M.).

### 3.3.2 **$GABA_AR$ Composition and Intracellular and Surface Trafficking are Changed by DZP *In Vitro***

We then investigated if surface γ2-containing $GABA_ARs$ are more frequently targeted to lysosomes after DZP exposure by live-imaging. For these experiments we used our recently characterized optical sensor for synaptic $GABA_AR$ ($\gamma2^{pH}FAP$). This dual reporter is composed of a γ2 subunit tagged with an N-terminal pH-sensitive GFP, myc, and the fluorogen-activating peptide DL5 (212). The pH-sensitive GFP tag selectively identifies cell surface $GABA_ARs$ and the DL5 FAP binds malachite green (MG) dye derivatives including MG-BTau (233, 240, 301). MG-BTau is cell impermeable and non-fluorescent until bound by DL5. Upon binding, MG-BTau fluoresces in the far red spectral region (~670 nM). This FAP-dye system allows for selective labeling of surface γ2-containing $GABA_ARs$ which can then be tracked through various phases of trafficking (212). As previously shown, $\gamma2^{pH}FAP$ $GABA_ARs$ are expressed on the neuronal surface, form synaptic clusters, do not perturb neuronal development and show equivalent functional responsiveness to GABA and DZP both in the absence and presence of MG dyes (212). We transfected neurons with *$\gamma2^{pH}FAP$* and treated them with DZP for 8-16 h. Neurons were then pulse-labeled with 100 nM MG-BTau dye and returned to conditioned media at 37°C +/- DZP for 1 h. The lysosomal inhibitor leupeptin (200 μM) and the lysosomal specific dye, Lysotracker (50 nM), were added after 30 min. At the end of the incubation, neurons were washed in 4°C saline to inhibit trafficking and immediately used for live-imaging experiments. Representative images demonstrate MG-BTau labeled $\gamma2^{pH}FAP$-$GABA_ARs$ localized on the cell surface **(Fig. 15A)** and at synaptic clusters on dendrites **(Fig. 15B)** based on colocalization with surface specific pHGFP signal. MG-BTau further reveals internalized receptors at lysosomes **(Fig. 15C)**. Image quantification showed synaptic γ2-$GABA_AR$ intensity remained largely unchanged (**Fig. 15D**).

Importantly, we found a significant 8.0 ± 2.5% ($p$ = 0.015) enhancement in the mean intensity of $GABA_ARs$ labeled with MG-BTau at lysosomes following DZP **(Fig. 15E)**. The area of $GABA_ARs$ colocalized at lysosomes trended towards an increase in DZP treated cells (140.2 ± 23.6%; $p$ = 0.144) but did not reach significance.

We complemented these lysosomal targeting studies with an $NH_4Cl$ live-imaging approach that allows us to compare the ratio of cell surface vs. intracellular $GABA_ARs$ in living neurons. $\gamma2^{pH}FAP$ expressing neurons were treated with vehicle or DZP for 24 h. Additional control groups included the BZD antagonist Ro 15-1788 (1-2 h) to reverse the effects of DZP. Neurons were actively perfused with HEPES buffered saline (HBS) treatment and an initial image was taken of surface pHGFP receptor signal **(Fig. 15F)**. Neurons were then exposed to pH 7.4 $NH_4Cl$ solution to neutralize the pH gradient of all intracellular membrane compartments, revealing internal pools of γ2 containing $GABA_ARs$. Analysis revealed no change in surface γ2 levels between treatments **(Fig. 15G)** consistent with Fig. 11 and 12. However, the number of large intracellular vesicles (circular area ~0.75 μm) containing receptors was significantly enhanced ($p$ = 0.047) **(Fig. 15H)**, consistent with increased localization in intracellular vesicles. Ro 15-1788 and DZP + Ro 15-1788 treated neurons were not significantly different from vehicle. Overall, these findings suggest γ2-$GABA_AR$ ubiquitination, intracellular accumulation, lysosomal targeting and degradation are part of the adaptive response to DZP.

To determine if γ2 subunit ubiquitination is key for lysosomal targeting of $GABA_ARs$ following DZP exposure, we created lysine to arginine mutated γ2 subunits to block ubiquitination. Importantly, the lysine residues in the large intracellular domain have been implicated in γ2 subunit degradation (159, 170). We created a construct of the γ2 long isoform where eight closely compacted lysine residues previously found to be important for ubiquitination were mutated

(*γ2$^{pH}$FAPK8R*). Two additional lysine residues in the ICD at more distant locations may also be subject to ubiquitination; therefore an additional *γ2$^{pH}$FAPK10R* construct with these residues mutated was generated. First we examined if the *γ2$^{pH}$FAPK8R* and *γ2$^{pH}$FAPK10R* constructs could be expressed in primary cultured neurons **(Fig. 16 A,B)** and HEK293 cells **(Fig. 16 C,D)**. We found that full length γ2$^{pH}$FAPK8R and γ2$^{pH}$FAPK10R are expressed in both cell types but at significantly lower levels in neurons (K8R: -65.0%; K10R: -70.8%) and in HEK293 cells (K8R: -22.3%; K10R: -35.1%) relative to wild type. This suggests that the eight closely encoded lysine residues in the γ2 subunit may have a role in subunit stability during biosynthesis.

Given the similar expression levels of γ2$^{pH}$FAPK8R and γ2$^{pH}$FAPK10R in our biochemical data, we proceeded with the γ2$^{pH}$FAPK10R construct with two additional lysine residues mutated as it should conceivably be more resistant to ubiquitination. Cultured neurons expressing wild-type γ2$^{pH}$FAP and γ2$^{pH}$FAPK10R were exposed to DZP for 20-28 h and then pulse-labeled with MG-BTau dye and returned to conditioned media at 37°C +/- DZP for 1.5 h. At the end of the incubation, neurons were washed in 4°C saline to inhibit trafficking and immediately used for live-imaging experiments. Lysotracker (50 nM), was added 10 min prior to imaging. Representative images demonstrate MG-BTau labeled γ2$^{pH}$FAP and γ2$^{pH}$FAPK10R $GABA_A$Rs localized on the cell surface **(Fig. 16E)** and at synaptic clusters on dendrites **(Fig. 16F)** indicating the γ2$^{pH}$FAPK10R traffics to the plasma membrane. As seen previously in **Fig. 15**, DZP increases MG-BTau labeled γ2$^{pH}$FAP $GABA_A$R colocalization at lysosomes **(Fig. 16G)**. Enhanced association of γ2$^{pH}$FAPK10R with lysosomes was also observed after DZP. Image quantification **(Fig. 16H,I)** confirmed that DZP caused a significant increase in the intensity (+174.0% ± 72.5) and near significant increase in the area of (+153.1% ± 65.5) of MG-

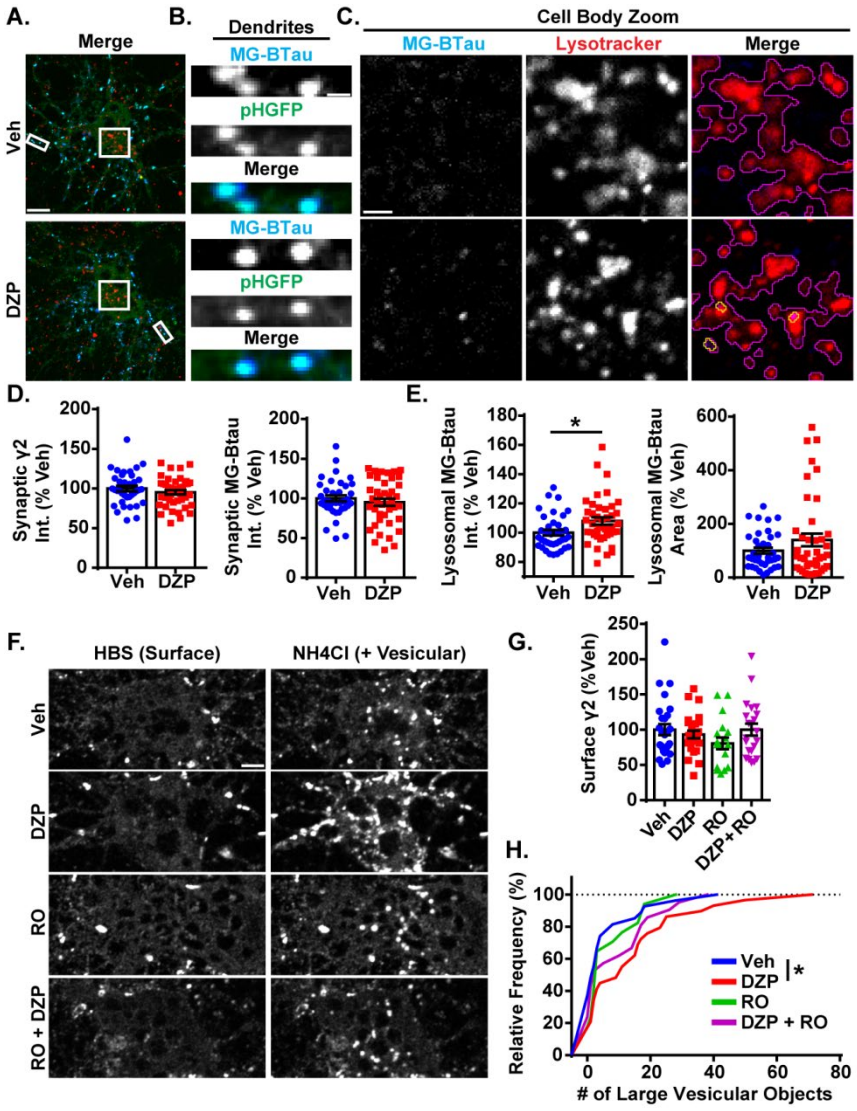


**Figure 15. Lysosomal Targeting and Vesicular Accumulation of γ2-GABA$_A$Rs in Response to DZP.**

(A) γ2$^{pH}$FAP neurons were pretreated for 12-18 h with 1 μM DZP, then pulse-labeled with 100 nM MG-BTau dye for 2 min, and returned to conditioned media at 37°C +/- DZP for 1 h. 50 nM Lysotracker dye was added at the 30 min mark to identify lysosomes. MG-BTau = blue; pHGFP = green; Lysotracker = red. (n=37-42 neurons; 5 independent cultures). (B) Dendrite zoom images show MG-BTau labeling at γ2$^{pH}$FAP synapses. (C) Cell body zoom images highlighting colocalization of MG-BTau labeled GABA$_A$Rs (yellow trace) at lysosomes (purple trace). (D) pHGFP and MG-BTau measurements reveal surface synaptic γ2-GABA$_A$R levels are not altered by DZP. (E) The pool of internalized MG-BTau GABA$_A$Rs colocalized at lysosomes was enhanced in DZP treated neurons as measured by intensity (*$p \leq 0.05$, Student's t-test; error bars ± S.E.M.). (F) Neurons treated 20-28 h with vehicle or DZP. The DZP

site antagonist Ro 15-1788 (5 μM) was added 1-2 h prior to imaging to inhibit DZP binding at $GABA_ARs$. Neurons were first imaged in HBS, and then perfused with $NH_4Cl$ (pH 7.4) to reveal intracellular $\gamma2^{pH}FAP$ receptors. DZP treated neurons accumulated more γ2-$GABA_ARs$ in large vesicular structures compared to vehicle. (n=20-27 neurons; 3-4 independent cultures). (G) Surface intensity of $\gamma2^{pH}FAP$ was not different between treatments (one-way ANOVA; error bars ± S.E.M.). (H) DZP-treated neurons more frequently demonstrated accumulation of $\gamma2^{pH}FAP$ in large vesicles (*$p \leq 0.05$ Kolmogorov-Smirnov statistical test). Scale bars in μm: A=10; B=1;C=2, F=5.

BTau labeled $\gamma2^{pH}FAP$ $GABA_ARs$ at lysosomes compared to vehicle wild type. Dye-labeled $\gamma2^{pH}FAPK10R$ receptors also demonstrated an increase in intensity (+128.2% ± 63.8) and area (+81.1% ± 35.4) of colocalization with lysosomes relative to vehicle control. No significant difference in synaptic cluster measurements were found for either group. This data suggests that redundant ubiquitination of other $GABA_AR$ subunits in complex with γ2 likely mediates DZP-induced lysosomal targeting and that γ2 ubiquitination alone is not a key step in this process.

Despite the increase in ubiquitination and lysosomal targeting of γ2-$GABA_ARs$ after DZP, we did not detect decreased overall surface or synaptically localized surface γ2 levels. This suggested two possibilities, one being that DZP treatment only reduced total γ2 levels to 80% of control in cultured cortical neurons and 85% *in vivo*, making a slight decrease in surface γ2-$GABA_ARs$ challenging to detect with current methods. Alternatively, there could be an increase in γ2 subunit assembly with BZD-insensitive α subunits (γ2α4β) (302) with a concomitant reduction in surface levels of BZD-sensitive receptors (γ2α1/2/3/5β). Our previous work showed 24 h BZD exposure in hippocampal neurons causes decreased total and surface levels of the α2 $GABA_AR$ subunit via lysosomal mediated degradation, without any changes in receptor insertion or removal rate (169). To determine if α2/γ2 $GABA_ARs$ are specifically decreased by DZP treatment, we developed and employed an intermolecular FRET assay, using pH-sensitive GFP

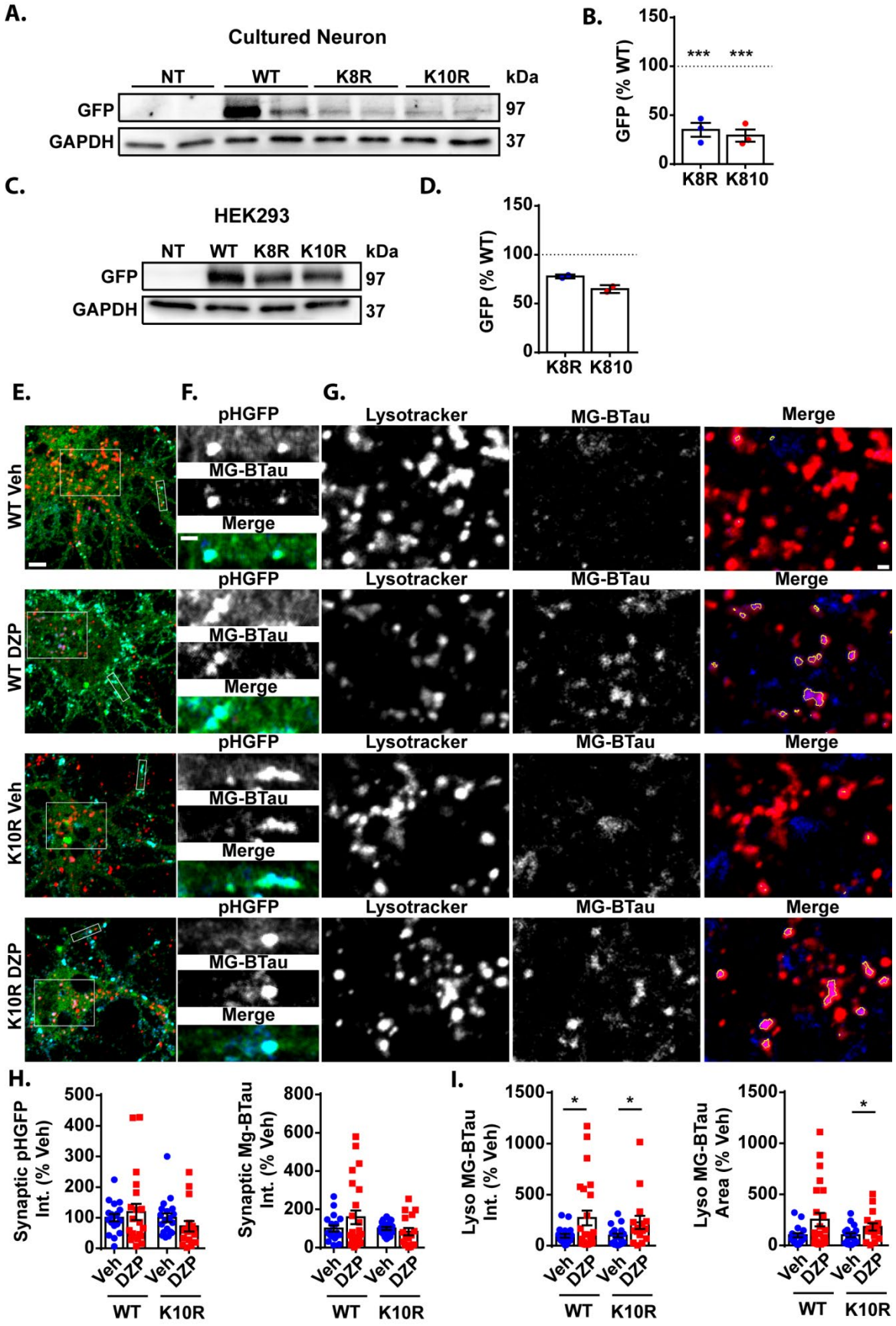
A.
Cultured Neuron
NT
WT
K8R
K10R
kDa
GFP
GAPDH
97
37
B.
GFP (% WT)
150
100
50
0
***
***
K8R
K810
C.
HEK293
NT
WT
K8R
K10R
kDa
GFP
GAPDH
97
37
D.
GFP (% WT)
150
100
50
0
K8R
K810
E.
F.
G.
pHGFP
MG-BTau
Merge
Lysotracker
MG-BTau
Merge
WT Veh
WT DZP
K10R Veh
K10R DZP
H.
Synaptic pHGFP Int. (% Veh)
Synaptic Mg-BTau Int. (% Veh)
Veh
DZP
WT
K10R
I.
Lyso MG-BTau Int. (% Veh)
Lyso MG-BTau Area (% Veh)
*

**Figure 16. Characterization and Lysosomal Targeting of Lysine Mutant γ2 in Response to DZP.**

(A) Cortical neurons transfected with wild type (*WT*), *K8R* or *K10R γ2$^{pH}$FAP* constructs were assessed for full-length protein expression. NT = non-transfected. (B) Quantifcation revealed the K8R and K10R γ2$^{pH}$FAP were expressed at a signifgantly lower level than wild-type (n = 3 independent cultures; one-way ANOVA with post-hoc Tukey's Test; error bars ± S.E.M.; ***p ≤ 0.001). (C) Western blot analysis of HEK293 cells transfected with GABA$_A$R *β3* subunit along with *WT*, *K8R* or *K10R γ2$^{pH}$FAP* subunits or NT negative control. (D) Quantification determined full-length K8R and K10R γ2$^{pH}$FAP subunits are also expressed at lower levels in HEK293 cells relative to WT γ2$^{pH}$FAP (n = 2 independent cultures). (E) *WT γ2$^{pH}$FAP* and *K10R γ2$^{pH}$FAP* transfected neurons were pretreated for 12-18 h with 1 μM DZP, then pulse-labeled with 100 nM MG-BTau dye for 2 min, and returned to conditioned media at 37°C +/- DZP for 1.5 h. 50 nM Lysotracker dye was added 10 min prior to live-imaging to identify lysosomes. MG-BTau = blue; pHGFP = green; Lysotracker = red. (n = 16-24 neurons; 4 independent cultures). (F) Dendrite zoom images show MG-BTau labeling at γ2$^{pH}$FAP synapses. (G) Cell body zoom images highlighting colocalization of MG-BTau labeled WT and K10R γ2$^{pH}$FAP GABA$_A$Rs (yellow trace) at lysosomes. (H) pHGFP and MG-BTau measurements reveal surface synaptic γ2-GABA$_A$R levels are not altered by DZP when compared against matching vehicle control in either WT or K10R γ2$^{pH}$FAP cells. (I) The intensity of internalized MG-BTau labeled GABA$_A$Rs colocalized at lysosomes was enhanced in both γ2$^{pH}$FAP WT and K10R cells after DZP treatment relative to their respective vehicle controls (*p ≤ 0.05, Student's t-test; error bars ± S.E.M.). A signifgant increase in the area of MG-BTau lysosomal colocalization was also detected for γ2$^{pH}$FAP K10R neurons. Scale bars in μm: E=5; F=1;G=1.

tagged α2$^{pH}$ (65) as a donor fluorophore and a red fluorescent protein (RFP) tagged γ2 subunit (γ2$^{RFP}$) as an acceptor. FRET is an accurate measurement of molecular proximity at distances of 10-100 Å and is highly efficient if donor and acceptor are within the Förster radius, typically 30-60 Å (3-6 nM), with the efficiency of FRET being dependent on the inverse sixth power of intermolecular separation (303). Synaptic GABA$_A$Rs exist as five subunits assembled in γ2-α-β-α-β order forming a heteropentameric ion channel **(Fig. 17A)**. We first expressed *α2$^{pH}$* and *γ2$^{RFP}$* in neurons and examined their ability to participate in intermolecular FRET. Photobleaching of the

acceptor $\gamma2^{RFP}$ channel enhanced donor $\alpha2^{pH}$ signal (Supplementary Figure 4; (270)), confirming energy transfer from $\alpha2^{pH}$ to $\gamma2^{RFP}$. Next, we confirmed measurable FRET only occurs between $\alpha2^{pH}/\gamma2^{RFP}$ in surface $GABA_AR$ at synaptic sites; FRET was blocked with quenching of donor $\alpha2^{pH}$ when the extracellular pH was reduced from 7.4 to 6.0 **(Fig.17A,B)**. Following FRET assay validation, $\alpha2^{pH}/\gamma2^{RFP}$ $GABA_AR$ neurons were treated for 24 h with vehicle or DZP and examined for total synaptic $\alpha2^{pH}$ and $\gamma2^{RFP}$ fluorescence as well as the γ2 FRET signal **(Fig. 17C)**. These studies identified a DZP-induced reduction in synaptic α2 (-12.6%), synaptic γ2 (-14.3%) and diminished association of α2 with γ2 in synaptic $GABA_ARs$ as measured by decreased FRET γ2 signal (-10.6%) **(Fig. 17D)**. In summary, this sensitive FRET method indicates that cortical neurons show a similar susceptibility for α2 subunit downregulation by BZD treatment as seen in hippocampal neurons (169). Furthermore it identifies a DZP-induced decrease in a specific pool of surface synaptic BZD-sensitive γ2-$GABA_AR$.

To gain additional mechanistic insight into the molecular mechanisms controlling phosphorylation and degradation of gephyrin observed in Fig. 11 and 12, we performed a DZP time series experiment to measure changes in expression or activation of the gephyrin regulating kinases ERK, GSK3β, and CDK5. CDK5 and GSK3β phosphorylate gephyrin at the Ser270 site (74, 75), while ERK phosphorylates a neighboring Ser268 residue (73). We first measured ERK activation by examining ERK phosphorylation across time points. DZP treatment caused a significant decrease in ERK phosphorylation at 45 min (-50.2%), 3 h (-44.5%) and 6 h (-51.2%), with a recovery in phosphorylation to vehicle levels occurring around 12 h and 24 h (Figure 5A,B). Total ERK levels were unchanged after DZP, except for a significant enhancement in expression at the 12 h time point, coinciding with recovery of ERK phosphorylation. We did not detect a change in the phosphorylation or total levels of GSK3β **(Fig.18C,D)** or expression of CDK5

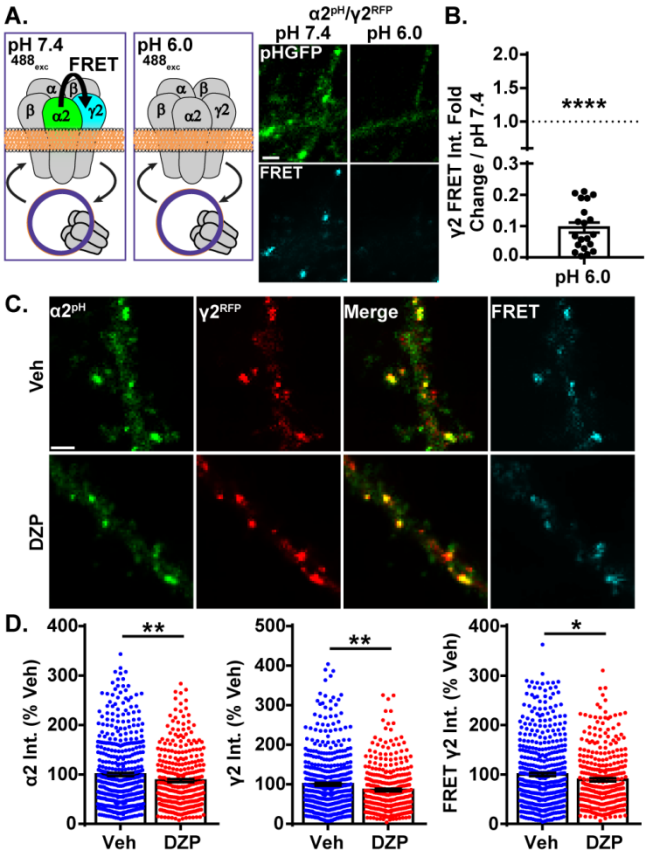


**Figure 17. Intermolecular FRET Reveals Decreased Synaptic α2/γ2 Surface GABA$_A$Rs after DZP.**

(A) Diagram and time-series images of cortical neurons expressing donor α2$^{pH}$ (green) and acceptor γ2$^{RFP}$ during imaging and with imaging saline at pH 7.4 and pH 6.0. Surface α2$^{pH}$ (green) signal and intermolecular FRET (teal) between α2/γ2 subunits occurs at pH 7.4, but is eliminated by brief wash with pH 6.0 extracellular saline and quenching of the α2$^{pH}$ donor pHGFP fluorescence. (B) Quantification of relative FRET at pH 7.4 and pH 6.0 (n = 20 synapses). (C) Neurons α2$^{pH}$ (green) and γ2$^{RFP}$ (red) were treated with vehicle or DZP for 20-28 h +/- and then subjected to live-imaging. For each cell, an initial image used 488 nm laser excitation to identify surface α2$^{pH}$ and FRET γ2$^{RFP}$. A second image was taken immediately afterwards to acquire γ2$^{RFP}$ total levels (561 nm laser excitation). Dendritic lengths show multiple synaptic clusters with α2/γ2 surface GABA$_A$Rs. (D) Synaptic cluster intensity quantification of α2$^{pH}$, γ2$^{RFP}$ and FRET γ2$^{RFP}$ (at least 15 synapses per cell; n = 335-483 synapses; 6 independent cultures). Image scale bars = 2 μm (*p ≤ 0.05, **p < 0.01, ****p < 0.0001, paired t-test (B), Student's t-test (D); error bars ± S.E.M.).

**(Fig. 18E,F)**. This data suggests that kinases involved in gephyrin phosphorylation at Ser270 do not demonstrate global changes after DZP, suggesting that the kinases may be recruited to gephyrin, or that an unknown phosphatase responsible for dephosphorylating Ser270 is inhibited after DZP exposure. Conversely, ERK inactivation by DZP is predicted to decrease phosphorylation of the functionally relevant Ser268 site of gephyrin, which has also been implicated in gephyrin synaptic remodeling (73). Gephyrin point mutant studies suggest reduced phosphorylation at Ser268 coupled with enhanced Ser270 phosphorylation, or the inverse, promotes calpain-1 degradation and scaffold remodeling (73). This data provides evidence that a known kinase pathway responsible for fine-tuning $GABA_AR$ synapse dynamics (304) and scaffold (73) is robustly inactivated by DZP.

We previously found 24 h BZD exposure reduces the amplitude of miniature inhibitory postsynaptic currents (mIPSCs) (169), suggesting changes in synaptic $GABA_AR$ function. Having identified both reductions in full-length gephyrin **(Fig. 11,12)** and BZD sensitive $GABA_ARs$ **(Fig. 12, 15)**, we next tested if DZP treatment altered the synaptic retention properties of gephyrin and/or $GABA_ARs$. Neurons expressing $\gamma2^{pH}FAP$ and RFP-gephyrin were used for live-imaging fluorescence recovery after photobleaching experiments (FRAP) to measure synaptic and extrasynaptic exchange following exposure to vehicle, 1 μm DZP, 5 μm Ro 15-1788, or DZP + Ro 15-1788. After an initial image was taken, dendrites were photobleached, and signal recovery was measured every 2 min over 30 min at synaptic sites and extrasynaptic regions (**Fig. 19A** synapses panel; **Fig.19B** larger dendritic region with white arrows denoting extrasynaptic region). MG-BTau dye was added directly after the photobleaching step to immediately re-identify the photobleached surface synaptic $GABA_ARs$, and improve spatial measurements **(Fig. 19B)**. These experiments revealed synaptic γ2 turnover rates were nearly doubled in DZP treated neurons, a

process reversed by Ro 15-1788 co-treatment **(Fig. 19C)**. DZP also accelerated gephyrin synaptic exchange rates compared to vehicle, with Ro 15-1788 co-treatment restoring exchange to control levels. No significant correlation was found between cluster area measured and fluorescence recovery rates of γ2 and gephyrin across all conditions, suggesting synaptic exchange rate is independent of cluster size (data not shown). Moreover, no statistical difference was found in γ2 or gephyrin extrasynaptic exchange rates **(Fig.19D)**. These findings suggest concurrent reduction of gephyrin and $GABA_AR$ synaptic confinement is a compensatory response to mitigate prolonged DZP potentiation of $GABA_ARs$.

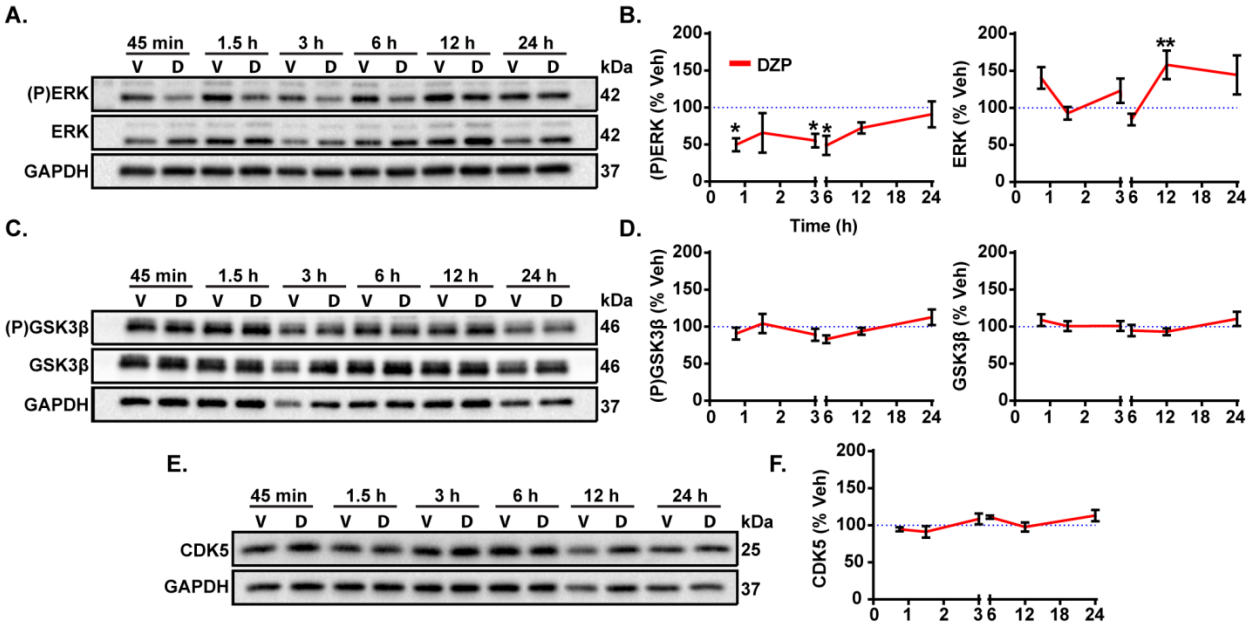


**Figure 18. Gephyrin Regulating Kinases Following DZP Treatment.**

DIV 16 cortical neurons were treated with vehicle (V) or DZP (D) at multiple time points. Known kinase regulators of gephyrin synaptic clustering were tested for total protein levels and activation status with phospho-specific antibodies as indicated. (P)ERK and total ERK (A,B), (P)GSK3β and total GSK3β (C,D) and CDK5 (E,F) western blot and quantification (n = 4 independent cultures). DZP inhibited ERK phosphorylation across multiple time points while GSK3β activation and total levels did not change. CDK5 total levels were also unchanged by DZP treatment. (*p ≤ 0.05, **p < 0.01, Two-way ANOVA followed by Sidak's multiple comparisons test; error bars ± S.E.M.).

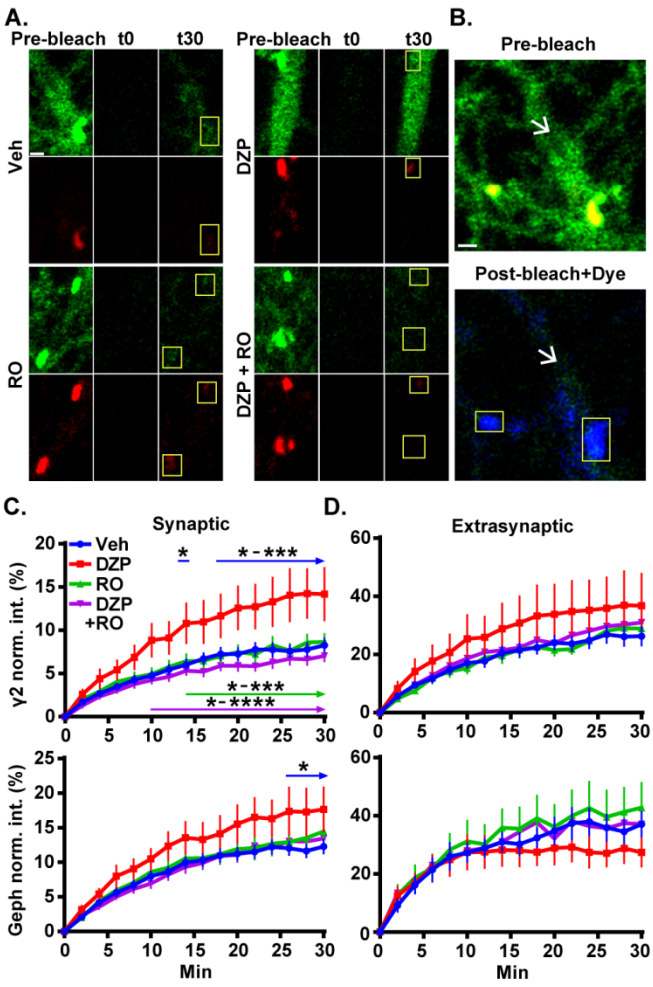


**Figure 19. Prolonged DZP Exposure Accelerates γ2 GABA$_A$R and Gephyrin Synaptic Exchange.**

(A) Neurons expressing γ2$^{pH}$FAP (green) and RFP-gephyrin (red) were treated with vehicle or DZP for 20-28 h +/- Ro 15-1788 for the last 1-2 h. Neurons were imaged at 37°C in constant presence of treatment. Initial image of dendrites taken prior to photobleaching (Pre-bleach), then imaged post-bleach (t0) every 2 min for 30 min. Images of dendritic regions show synaptic cluster sites (yellow boxes) and extrasynaptic regions. (B) 10 nM MG-BTau dye (blue) was added immediately after bleaching events in A to resolve bleached γ2$^{pH}$FAP GABA$_A$Rs and provide spatial accuracy for time series measurements. Panels show enlargement of vehicle dendritic regions identified in A. Yellow boxes indicate synaptic clusters and arrows indicate extrasynaptic region seen by pHGFP fluorescence in pre-bleach (green) followed by post-bleach labeling with MG-Btau (blue). (C, D) Fluorescence recovery of γ2 GABA$_A$R and gephyrin measured at synaptic sites and extrasynaptic sites from A. Synapse = γ2$^{pH}$FAP cluster colocalized with

gephyrin cluster. Int. = fluorescence intensity. Image scale bars = 1 μm (*$p \leq 0.05$, **$p < 0.01$, ***$p < 0.001$, ****$p < 0.0001$, two-way ANOVA; Tukey's multiple comparisons test; 4-8 synapses and one 10 μm extrasynaptic region per cell; n = 51-56 synapses from 16 neurons per treatment; 4 independent cultures; error bars ± S.E.M.).

### 3.3.3 Label-Free Quantitative Proteomics of γ2 $GABA_AR$ Following DZP Injection *In Vivo*

We next sought to observe DZP-induced changes in receptor trafficking *in vivo*. As an orthogonal approach, we utilized label-free quantitative proteomics to measure changes in the quantities of proteins associated with γ2-$GABA_ARs$ in the cortex of mice after DZP. Cortical tissue was collected from DZP- or vehicle-treated mice 12 h post injection, lysed, and immunoprecipitated with anti-γ2 subunit antibody or IgG control. Following label-free mass spectrometry analysis, spectrum counts were used to assess relative abundance of γ2-associated proteins. A total of 395 proteins were identified using our inclusion criteria: minimum of two peptides; identified in at least three samples overall or in two of three samples in a specific treatment group; demonstrated at least 3:1 enrichment over IgG control across at least three samples overall (Dataset 1; not included). The relative abundance of γ2-$GABA_AR$ associated proteins in the DZP group compared to vehicle was used to determine which proteins were increased **(Table 1)** or decreased **(Table 2)**. As a result we identified 46 proteins with elevated levels of interaction with γ2-$GABA_ARs$, including 10 proteins that were only found in the DZP treated group (Table 1, not found in vehicle samples, NF-V). Notably, we found a significant ($p < 0.05$) increase in γ2 association with 14-3-3 protein family members tyrosine 3-monooxygenase/tryptophan 5-monooxygenase activation protein gamma (also known as 14-3-3γ) and tyrosine 3-monooxygenase/tryptophan 5-monooxygenase activation protein epsilon (also

known as 14-3-3ε), the phosphatase protein phosphatase 3 catalytic subunit alpha (also known as calcineurin/PPP3CA) and a near significant increase in the $GABA_AR$ α5 subunit ($p$ = 0.057), suggesting DZP induced changes in $GABA_AR$ surface trafficking (305, 306), synaptic retention (162, 180, 182, 183, 307), and receptor composition (308). In contrast, 23 proteins were found to co-immunoprecipitate with γ2 less in DZP animals relative to control, seven of which were only present in the vehicle treatment group (**Table 2**, not found in DZP, NF-DZP). Interestingly, the calcium-sensitive kinase CaMKIIα, which can regulate $GABA_AR$ membrane insertion, synaptic retention and drug binding properties (26, 70-72), was found to be significantly decreased in interaction with γ2-$GABA_AR$ following DZP injection *in vivo*.

To better understand the consequences of the DZP-induced shift in the γ2-$GABA_AR$ protein interaction network, protein fold change data was subjected to core Ingenuity Pathway Analysis (IPA). Top enriched canonical pathways with –log(p-value) > 6.2 are shown in Figure 20. Notably, GABA receptor signaling pathways were highly enriched, as expected, although IPA was unable to determine pathway activation status by z-score analysis. γ2-$GABA_AR$ association with proteins involved in 14-3-3 mediated signaling and Ras homolog gene family, member A (RhoA) signaling pathways were greatly increased after DZP (**Fig. 20A**, orange), while interaction with proteins involved in eukaryotic initiation factor 2 (EIF2) signaling and sirtuin signaling pathways were reduced (**Fig. 20A**, blue) relative to vehicle. We further examined alterations in functional network association relevant to receptor trafficking by checking the predicted activation status of select pathways when only using proteins which were found to be increased or decreased **(Table 1, 2)**. **Fig. 20B** lists γ2-$GABA_AR$ major functional pathways found to be altered by DZP, contributing to processes such as endocytosis (z-score = 2.626), organization of cytoskeleton (z-score = 0.672), and development of neurons (z-score = -0.293). Significant protein changes ($p$ <

0.05) conserved between two or more pathways include decreased γ2-$GABA_AR$ association with CAMKIIα and CDK5 and enhanced association with calcineurin/PPP3CA, the intracellular trafficking protein RAB35 and the cytoskeletal protein NEFH (also known as heavy neurofilament protein). As an additional measurement, we performed gene ontology (GO) database analysis of proteins which were found to be increased in DZP treated mice relative to vehicle control **(Table 3)**. GO analysis identified enrichment in γ2 association with proteins involved in intracellular trafficking and cellular localization biological pathways after DZP, consistent with IPA analysis findings. Taken together, these results suggest DZP modifies intracellular and surface trafficking of γ2-$GABA_ARs$ both *in vitro* and *in vivo*.

**Table 1. Proteins Demonstrating Increased Association with γ2-GABA$_A$Rs after DZP *In Vivo* by Mass Spectrometry.**

Ratio DZP/V is fold change in DZP animals' peptide spectral counts (SC) relative to control vehicle treated animals. NF-V = not found in vehicle samples. N = 3 animals per treatment condition, $p < 0.1$, t-test.

| *Ratio DZP/V* | *P-Value* | *UniProtKB* | *Gene ID* | *Entrez Gene Name* | *Location* | *Type(s)* |
|---|---|---|---|---|---|---|
| 9.6 | 8.9E-02 | Q14BI2 | GRM2 | glutamate metabotropic receptor 2 | Plasma Membrane | G-protein coupled receptor |
| 9.5 | 4.3E-02 | P12960 | CNTN1 | contactin 1 | Plasma Membrane | enzyme |
| 7.0 | 5.9E-02 | P11276 | FN1 | fibronectin 1 | Extracellular Space | enzyme |
| 5.4 | 2.7E-02 | E9Q4P0 | KXD1 | KxDL motif containing 1 | Cytoplasm | other |
| 5.4 | 3.1E-02 | Q62277 | SYP | synaptophysin | Cytoplasm | transporter |
| 5.0 | 5.0E-03 | Q9QXY6 | EHD3 | EH domain containing 3 | Cytoplasm | other |
| 5.0 | 7.8E-02 | P48774 | GSTM3 | glutathione S-transferase mu 3 | Cytoplasm | enzyme |
| 4.9 | 1.9E-05 | P38647 | HSPA9 | heat shock protein family A (Hsp70) member 9 | Cytoplasm | other |
| 4.7 | 6.4E-02 | Q91V41 | RAB14 | RAB14, member RAS oncogene family | Cytoplasm | enzyme |
| 4.2 | 6.4E-02 | P48758 | CBR1 | carbonyl reductase 1 | Cytoplasm | enzyme |
| 4.2 | 7.2E-02 | Q8K3F6 | KCNQ3 | potassium voltage-gated channel subfamily Q member 3 | Plasma Membrane | ion channel |
| 4.2 | 3.3E-02 | A0A0R4J036 | Nefm | neurofilament, medium polypeptide | Plasma Membrane | other |
| 4.0 | 7.9E-02 | Q921I1 | TF | transferrin | Extracellular Space | transporter |
| 3.8 | 8.6E-02 | Q9CYZ2 | TPD52L2 | tumor protein D52 like 2 | Cytoplasm | other |
| 3.3 | 4.2E-02 | Q99KI0 | ACO2 | aconitase 2 | Cytoplasm | enzyme |
| 2.6 | 8.0E-02 | Q9EQF6 | DPYSL5 | dihydropyrimidinase like 5 | Cytoplasm | enzyme |
| 2.4 | 2.2E-02 | P56480 | ATP5F1B | ATP synthase F1 subunit beta | Cytoplasm | transporter |
| 2.4 | 9.2E-02 | P46096 | SYT1 | synaptotagmin 1 | Cytoplasm | transporter |
| 2.4 | 3.7E-02 | Q6P1J1 | CRMP1 | collapsin response mediator protein 1 | Cytoplasm | enzyme |
| 2.2 | 3.8E-02 | Q9DB20 | ATP5PO | ATP synthase peripheral stalk subunit OSCP | Cytoplasm | transporter |
| 1.9 | N.A. | P61027 | RAB10 | RAB10, member RAS oncogene family | Cytoplasm | enzyme |
| 1.8 | 9.6E-02 | P63017 | HSPA8 | heat shock protein family A (Hsp70) member 8 | Cytoplasm | enzyme |
| 1.8 | 1.8E-02 | P63011 | RAB3A | RAB3A, member RAS oncogene family | Cytoplasm | enzyme |
| 1.8 | 1.3E-02 | P17426-2 | AP2A1 | adaptor related protein complex 2 subunit alpha 1 | Cytoplasm | transporter |
| 1.7 | 9.1E-02 | P18760 | CFL1 | cofilin 1 | Nucleus | other |
| | | | | | | |

**Table 1. Continued**

| | | | | | | |
|---|---|---|---|---|---|---|
| 1.7 | 8.2E-02 | Q9Z2I9 | SUCLA2 | succinate-CoA ligase ADP-forming beta subunit | Cytoplasm | enzyme |
| 1.7 | 4.0E-02 | P63328 | PPP3CA | protein phosphatase 3 catalytic subunit alpha | Cytoplasm | phosphatase |
| 1.7 | 7.1E-02 | Q8R191 | SYNGR3 | synaptogyrin 3 | Plasma Membrane | other |
| 1.6 | 5.7E-02 | Q8BHJ7 | GABRA5 | gamma-aminobutyric acid type A receptor alpha5 subunit | Plasma Membrane | ion channel |
| 1.6 | 1.8E-02 | O35129 | PHB2 | prohibitin 2 | Cytoplasm | transcription regulator |
| 1.6 | 1.6E-02 | P61982 | YWHAG | tyrosine 3-monooxygenase/tryptophan 5-monooxygenase activation protein gamma (14-3-3 gamma) | Cytoplasm | other |
| 1.5 | 5.3E-02 | P07901 | HSP90AA1 | heat shock protein 90 alpha family class A member 1 | Cytoplasm | enzyme |
| 1.5 | 7.8E-03 | P67778 | PHB | prohibitin | Nucleus | transcription regulator |
| 1.5 | 8.1E-02 | Q3UGC7 | EIF3J | eukaryotic translation initiation factor 3 subunit J | Cytoplasm | translation regulator |
| 1.5 | 7.5E-02 | Q8VEM8 | SLC25A3 | solute carrier family 25 member 3 | Cytoplasm | transporter |
| 1.3 | 3.3E-02 | P60710 | ACTB | actin beta | Cytoplasm | other |
| NF-V | 7.9E-04 | P62259 | YWHAE | tyrosine 3-monooxygenase/tryptophan 5-monooxygenase activation protein epsilon (14-3-3 epsilon) | Cytoplasm | other |
| NF-V | 1.0E-02 | P63044 | VAMP2 | vesicle associated membrane protein 2 | Plasma Membrane | other |
| NF-V | 1.6E-02 | P46660 | INA | internexin neuronal intermediate filament protein alpha | Cytoplasm | other |
| NF-V | 3.7E-02 | Q9QYM9 | TMEFF2 | transmembrane protein with EGF like and two follistatin like domains 2 | Cytoplasm | other |
| NF-V | 4.1E-02 | Q6PHN9 | RAB35 | RAB35, member RAS oncogene family | Cytoplasm | enzyme |
| NF-V | 6.0E-02 | P19246 | NEFH | neurofilament heavy | Cytoplasm | other |
| NF-V | 6.3E-02 | Q9CZ13 | UQCRC1 | ubiquinol-cytochrome c reductase core protein 1 | Cytoplasm | enzyme |
| NF-V | 1.2E-06 | Q9CQQ7 | ATP5PB | ATP synthase peripheral stalk-membrane subunit b | Cytoplasm | transporter |
| NF-V | 2.8E-06 | P80317 | CCT6A | chaperonin containing TCP1 subunit 6A | Cytoplasm | other |
| NF-V | 2.8E-06 | Q9CWS0 | DDAH1 | dimethylarginine dimethylaminohydrolase 1 | Cytoplasm | enzyme |

**Table 2. Proteins Demonstrating Decreased Association with γ2-GABA$_A$Rs after DZP *In Vivo* by Mass Spectrometry.**

Ratio DZP/V is fold change in DZP animals' peptide SC relative to control vehicle treated animals. NF-DZP = not found in DZP samples. N = 3 animals per treatment condition, $p < 0.1$, t-test.

| *Ratio DZP/V* | *P-Value* | *UniProtKB* | *Gene ID* | *Entrez Gene Name* | *Location* | *Type(s)* |
|---|---|---|---|---|---|---|
| 0.2 | 3.4E-02 | P62717 | RPL18A | ribosomal protein L18a | Cytoplasm | other |
| 0.2 | 3.9E-02 | P62874 | GNB1 | G protein subunit beta 1 | Plasma Membrane | enzyme |
| 0.2 | 4.2E-02 | Q60900-2 | ELAVL3 | ELAV like RNA binding protein 3 | Nucleus | other |
| 0.2 | 5.8E-02 | Q920I9 | WDR7 | WD repeat domain 7 | Cytoplasm | other |
| 0.3 | 2.0E-02 | P53026 | RPL10A | ribosomal protein L10a | Nucleus | other |
| 0.3 | 3.4E-02 | Q91VM5 | Rbmxl1 | RNA binding motif protein, X-linked like-1 | Nucleus | other |
| 0.4 | 6.9E-02 | P49312 | Hnrnpa1 | heterogeneous nuclear ribonucleoprotein A1 | Nucleus | other |
| 0.4 | 8.5E-02 | Q8BG05 | Hnrnpa3 | heterogeneous nuclear ribonucleoprotein A3 | Nucleus | transporter |
| 0.4 | 7.9E-02 | Q922F4 | TUBB6 | tubulin beta 6 class V | Cytoplasm | other |
| 0.5 | 5.2E-02 | P62334 | PSMC6 | proteasome 26S subunit, ATPase 6 | Nucleus | peptidase |
| 0.5 | 2.9E-04 | P11798 | CAMK2A | calcium/calmodulin dependent protein kinase II alpha | Cytoplasm | kinase |
| 0.5 | 3.6E-02 | E9PV14 | EPB41L1 | erythrocyte membrane protein band 4.1 like 1 | Plasma Membrane | other |
| 0.7 | 6.8E-02 | P16330 | CNP | 2',3'-cyclic nucleotide 3' phosphodiesterase | Cytoplasm | enzyme |
| 0.7 | 7.6E-02 | O35643 | AP1B1 | adaptor related protein complex 1 subunit beta 1 | Cytoplasm | transporter |
| 0.8 | 1.4E-02 | P68369 | TUBA1A | tubulin alpha 1a | Cytoplasm | other |
| 0.8 | 8.0E-02 | P52480 | PKM | pyruvate kinase M1/2 | Cytoplasm | kinase |
| NF-DZP | 1.5E-02 | P61358 | RPL27 | ribosomal protein L27 | Cytoplasm | other |
| NF-DZP | 3.5E-02 | Q9Z1X4-3 | ILF3 | interleukin enhancer binding factor 3 | Nucleus | transcription regulator |
| NF-DZP | 5.5E-02 | Q80UJ0 | ELAVL2 | ELAV like RNA binding protein 2 | Cytoplasm | other |
| NF-DZP | 2.8E-06 | Q3UHB8 | CCDC177 | coiled-coil domain containing 177 | Other | other |
| NF-DZP | 2.8E-06 | P49615 | CDK5 | cyclin dependent kinase 5 | Nucleus | kinase |
| NF-DZP | 2.8E-06 | Q6ZWV3 | RPL10 | ribosomal protein L10 | Cytoplasm | translation regulator |
| NF-DZP | 2.8E-06 | Q9CQ69 | UQCRQ | ubiquinol-cytochrome c reductase complex III subunit VII | Cytoplasm | enzyme |

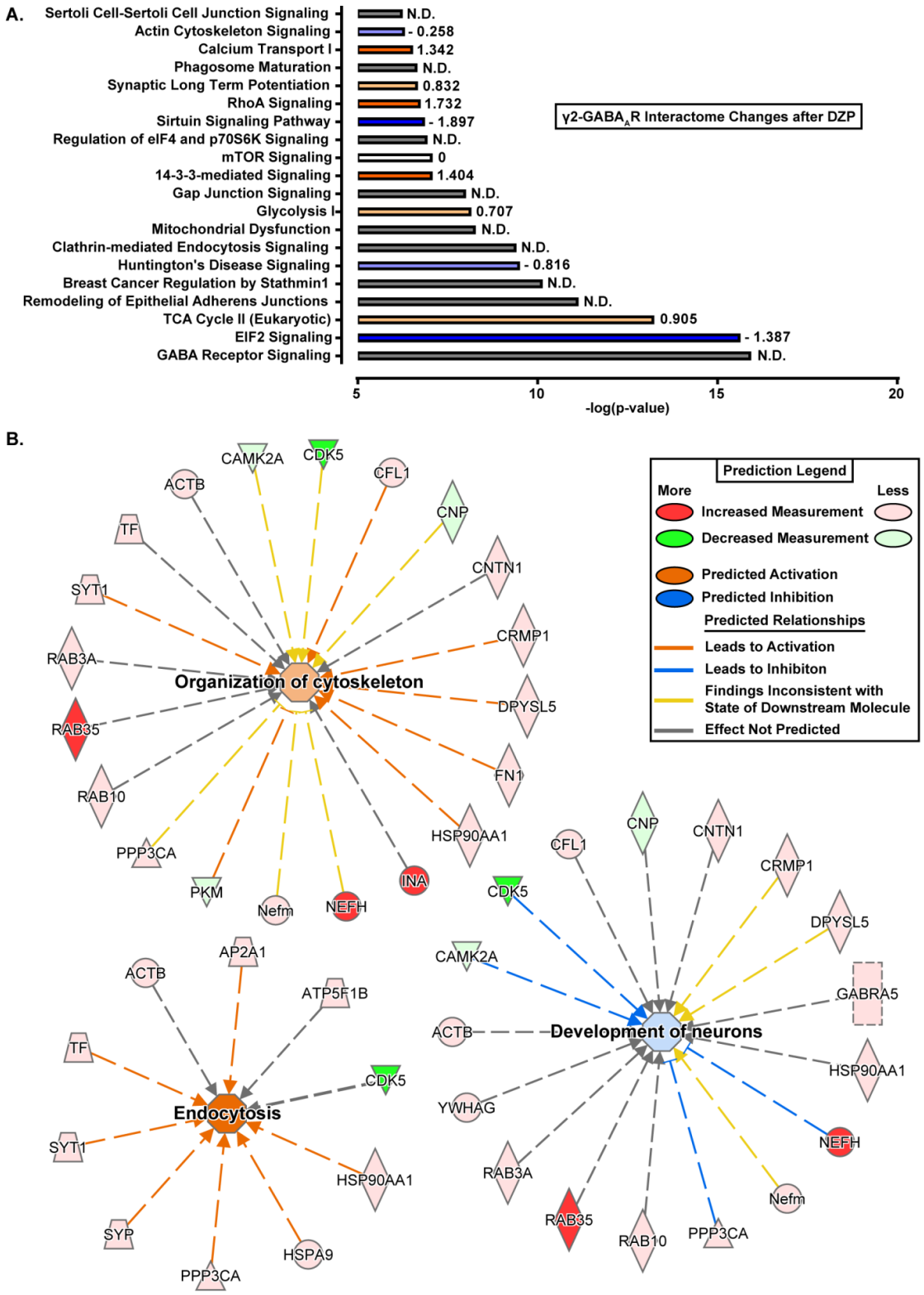


**Figure 20. Ingenuity Pathway Analysis Reveals Shifts in Protein Interaction Networks After DZP Exposure.**

(A) Canonical pathways found to be enriched with γ2-$GABA_A$Rs and differentially expressed following DZP administration *in vivo*. Enriched pathways with –log(p-value) greater than 6.2 were considered as calculated by Fisher's exact test right-tailed. Values to right of bars represent pathway activation z-score. Positive z-score represents predicted upregulation of a pathway (orange), negative z-score predicts inhibition (blue), z-score = 0 represents no change in pathway (white), while not determined (N.D.) conveys the analysis program was unable to determine a significant change (grey). Intensity of color represents size of z-score value. (B) Functional network association of select pathways when using proteins which were found to be increased or decreased with a $p < 0.1$. Major functional pathways altered by DZP include endocytosis (z-score = 2.626), organization of cytoskeleton (z-score = 0.672), and development of neurons (z-score = -0.293). Significant protein changes ($p < 0.05$) conserved between two or more pathways include decreased γ2-$GABA_A$R association with CAMKIIα and CDK5 and enhanced association with calcineurin/PPP3CA, the intracellular trafficking protein RAB35 and the cytoskeletal protein NEFH (also known as heavy neurofilament protein). Red = increased measurement, green = decreased measurement, orange = activation of pathway, blue = inhibition of pathway, yellow = findings inconsistent with state of downstream molecule, grey = effect not predicted.

**Table 3. GO Analysis Reveals Enrichment of Intracellular Trafficking, Transport, and Protein Localization Pathways after DZP.**

Proteins found to have enhanced association ($p < 0.1$) with γ2-$GABA_A$Rs during Scaffold analysis were searched in the GO Ontology database for biological process pathway enrichments. PANTHER Overrepresentation test and Fisher's Exact test with Bonferroni correction for multiple testing for significance.

| *GO Biological Process* | *GO Term ID* | *Fold Enrichment* | *P-Value* |
|---|---|---|---|
| transport | GO:0006810 | 4.2 | 9.8E-09 |
| establishment of localization | GO:0051234 | 4.0 | 2.5E-08 |
| establishment of localization in cell | GO:0051649 | 6.8 | 2.0E-07 |
| localization | GO:0051179 | 3.3 | 2.5E-07 |
| intracellular transport | GO:0046907 | 7.2 | 1.6E-06 |
| regulation of localization | GO:0032879 | 4.3 | 3.7E-06 |
| intracellular protein transport | GO:0006886 | 9.1 | 7.8E-06 |
| regulation of transport | GO:0051049 | 5.1 | 2.2E-05 |
| cellular localization | GO:0051641 | 4.8 | 4.8E-05 |
| protein transport | GO:0015031 | 6.1 | 2.2E-04 |

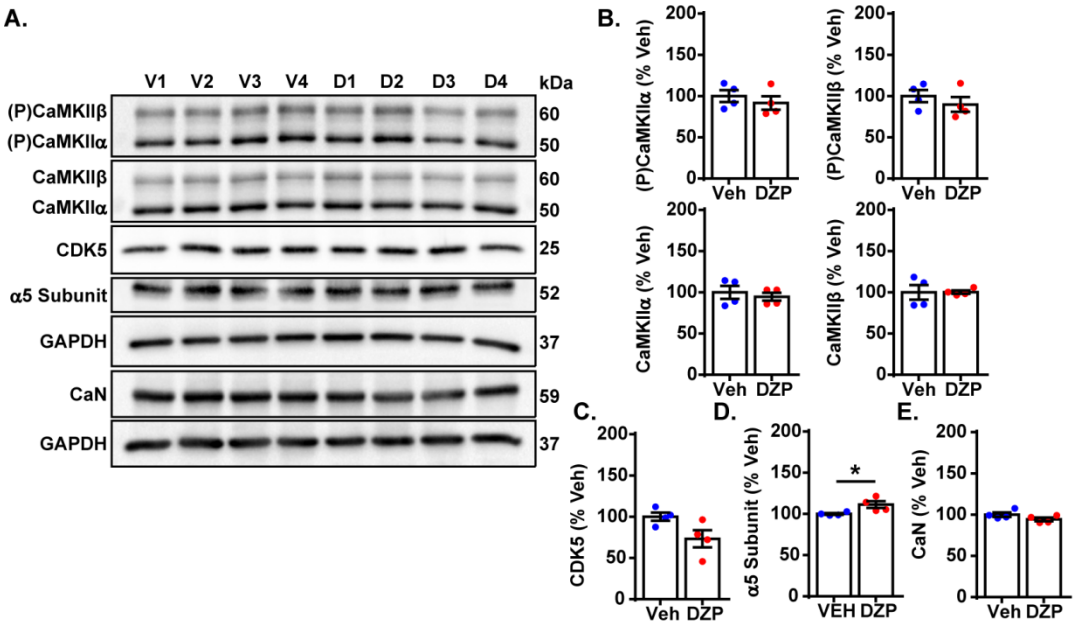


**Figure 21. Biochemical Evaluation of Proteins Found to be Altered in their Association with γ2-GABA$_A$Rs after DZP by Proteomics.**

Western blot analysis (A) of cortical tissue from mice treated with vehicle or DZP for 12 h. Quantification of T286/T287 (P)CaMKII and overall CaMKII α/β subunits (B), CDK5 (C), GABA$_A$R α5 (D) subunit and calcineurin (CaN) (E). The α5 subunit demonstrated a global increase in protein levels after DZP, while no other proteins were signifigantly altered (*$p \leq 0.05$, Student's t-test; n = 4 mice per treatment; error bars ± S.E.M.).

To determine if the changes in association with key proteins identified to be altered in their association with γ2 after DZP was a result of changes in total overall protein levels, we performed western blot analysis of cortical tissue from mice treated with vehicle or DZP for 12 h **(Fig. 21)**. Quantification revealed that phosphorylated T286/T287 ((P)CaMKII) and overall CaMKIIα/β subunits, CDK5 and CaN were not significantly altered by DZP. In contrast, the α5 subunit exhibited a statistically significant increase in response to DZP relative to vehicle. These findings suggest that higher levels of expression of the α5 subunit leads to increased α5/γ2 containing

$GABA_ARs$, while a change in localization or interaction of CaMKIIα/β, CDK5 and CaN underlie the diminished association with γ2 after DZP exposure seen by proteomics.

## 3.4 Discussion

This work identifies key trafficking pathways involved in $GABA_AR$ neuroplasticity in response to initial DZP exposure. Using a combination of biochemical and imaging techniques, we identified total γ2 subunit levels are diminished in response to 12-24 h of DZP exposure *in vitro* and *in vivo*. Concurrent with the decrease in the overall γ2 pool, we found DZP treatment enhanced ubiquitination of this subunit. Use of an innovative optical sensor for BZD sensitive $GABA_AR$ ($\gamma2^{pH}FAP$) in combination with MG dye pulse-labeling approaches revealed DZP exposure moderately enhanced targeting of surface γ2-$GABA_ARs$ to lysosomes. Live-imaging experiments with pH 7.4 $NH_4Cl$ revealed increased intracellular receptor pools, providing further evidence that DZP enhances γ2-$GABA_AR$ lysosomal accumulation, a response reversed by BZD antagonist Ro 15-1788 treatment. We used novel intersubunit FRET based live-imaging to identify that surface synaptic α2/γ2 $GABA_ARs$ were specifically decreased after DZP, suggesting these receptor complexes were subjected to ubiquitination, lysosomal targeting, and degradation. In addition to DZP modulation of receptor trafficking, the postsynaptic scaffolding protein gephyrin demonstrated significant plasticity including increased Ser270 phosphorylation and production of gephyrin proteolytic fragments, concurrent with a decrease in total and membrane full-length gephyrin levels and ERK inactivation. Given the fundamental role of gephyrin in scaffolding $GABA_ARs$ and regulating synaptic confinement, we used simultaneous FRAP live-imaging of receptors and scaffold in neurons to monitor inhibitory synaptic dynamics. We found ~24 h DZP

exposure accelerates both the rate of gephyrin and $GABA_AR$ exchange at synapses as shown by enhanced fluorescence recovery rates. Control experiments using the BZD antagonist Ro 15-1788 were able to reverse the DZP induced loss of synaptic confinement, reducing gephyrin and $GABA_AR$ mobility back to vehicle levels. Finally, we used label-free quantitative mass spectrometry and bioinformatics to identify key changes in γ2-$GABA_AR$ protein association *in vivo* suggesting alterations in trafficking at the cell surface and intracellularly. Collectively, this work defines a DZP-induced reduction of gephyrin scaffolding coupled with increased synaptic exchange of gephyrin and $GABA_ARs$. This dynamic flux of $GABA_ARs$ between synapses and the extrasynaptic space was associated with enhanced γ2-$GABA_AR$ accumulation in intracellular vesicles and γ2-$GABA_AR$ subtype specific lysosomal degradation. We propose DZP treatment alters these key intracellular and surface trafficking pathways ultimately diminishing responsiveness to DZP.

Numerous classical studies have examined gene and protein expression adaptations in $GABA_AR$ subunits after BZD exposure with minimal agreement that a specific change occurs (32, 33, 46). Here molecular mechanistic insight is provided, through direct measurements of enhanced ubiquitination of the γ2 subunit **(Fig. 12)**, lysosomal targeting **(Fig. 14,15)**, reduced surface synaptic α2/γ2 $GABA_AR$ levels **(Fig. 17)**, and reduced synaptic confinement **(Fig. 19)** of DZP-sensitive $GABA_ARs$. Together this suggests BZD exposure primarily decreases synaptic retention of γ2 containing $GABA_AR$ while downregulating surface levels of the α2 subunit. Ubiquitination of the γ2 subunit by the E3 ligase Ring Finger Protein 34 (RNF 34) (170) is the only currently known mechanism targeting internalized synaptic $GABA_ARs$ to lysosomes (159). Due to the requirement of the γ2 subunit in all BZD-sensitive $GABA_ARs$, it is likely that ubiquitination of the γ2 subunit is a contributing factor for increased lysosomal-mediated degradation in response to

DZP, although not required **(Fig. 16)**. Despite a small decrease in the γ2 total protein, changes in surface levels were not significant by biochemical approaches, consistent with evidence that γ2-$GABA_AR$ surface levels are tightly regulated to maintain baseline inhibition and prevent excitotoxicity. For example, in heterozygous γ2 knockout mice a 50% reduction in γ2 levels appears to be compensated by increased cell surface trafficking, resulting in only an approximately 25% reduction in BZD binding sites in the cortex and a limited reduction in synaptic $GABA_AR$ clusters (309, 310). In contrast, homozygous γ2 knockout mice show a complete loss of behavioral drug response to BZD and over 94% of the BZD sites in the brain (GABA binding sites unchanged) and early lethality (311). Similarly, studies have shown that prolonged $GABA_AR$ agonist or BZD application increases γ2 $GABA_AR$ internalization in cultured neurons, with inconsistent changes in surface $GABA_AR$ levels detected (160, 312). Importantly, by using high sensitivity surface $GABA_AR$ intersubunit FRET measurements we were able to detect a decrease in BZD sensitive α2/γ2 $GABA_ARs$ (**Fig. 17**).

The role of inhibitory scaffolding changes in responsiveness to BZD has been largely under investigated. Phosphorylation of gephyrin at Ser270 is mediated by CDK5 and GSK3β, while a partnering and functionally relevant Ser268 site is regulated by ERK (73). DZP time series experiments revealed a global decrease in ERK phosphorylation but not GSK3β, without a change in total kinase levels of ERK, GSK3β or CDK5 over the course of the assay (except 12 h ERK) **(Fig. 18)**. A previous model by Tyagarajan SK, et al. (2013) using gephyrin point mutants at Ser268 and Ser270 suggested that enhanced Ser270 phosphorylation coupled with decreased Ser268 phosphorylation by ERK promotes gephyrin remodeling and calpain-1 degradation. This is consistent with the ERK inactivation measured in our data and the increase in gephyrin Ser270 phosphorylation demonstrated by immunofluorescence after DZP **(Fig. 11)**, enhanced gephyrin

degradation and decreased full-length gephyrin levels **(Fig. 11,12)**. Calpain-1 mediated gephyrin cleavage can occur within 1 minute in hippocampal membranes (313), and cleavage products are increased following *in vitro* ischemia at 30 min and up to 48 hours following ischemic events *in vivo* (295). Gephyrin cleavage may be occurring at earlier time points than the DZP 24 h mark measured here **(Fig. 12 F,G)**, coinciding with ERK dephosphorylation as early as 45 min (Figure 5A,B). One limitation of our results is that measuring total and phospho levels of these kinases does not directly address changes in association or regulation of gephyrin, although it does provide an additional piece of evidence supporting gephyrin cleavage by calpain-1 and scaffold remodeling. Accordingly, our previous work found 30 min treatment with the $GABA_AR$ agonist muscimol in immature neurons (depolarizing) leads to ERK/BDNF signaling and decreased Ser270 phosphorylated gephyrin levels at synapses and overall (304). Thus, ERK activation status negatively correlates with the level of phosphorylation at gephyrin Ser270.

Recent work has demonstrated 12 h DZP treatment of organotypic hippocampal slices expressing eGFP-gephyrin causes enhanced gephyrin mobility at synapses and reduced gephyrin cluster size (314). Here we found the synaptic exchange rate of γ2 $GABA_ARs$ and gephyrin to be nearly doubled at synapses in cortical neurons after ~24 h DZP exposure **(Fig. 19)**. γ2 extrasynaptic fluorescence recovery in DZP treated neurons was variable but also trended towards an increase relative to controls **(Fig. 19)**, which could be a result of increased diffusion of receptors out of the synaptic space. This effect occurred coincident with the formation of truncated gephyrin cleavage products **(Fig. 12)**, which has previously been shown to decrease γ2 synaptic levels (295). These findings are also consistent with our previous work showing RNAi gephyrin knockdown doubles the rate of γ2-$GABA_AR$ turnover at synaptic sites (54). Later quantum dot single particle tracking studies confirmed γ2 synaptic residency time is linked to gephyrin scaffolding levels (252).

Importantly, $GABA_AR$ diffusion dynamics also reciprocally regulate gephyrin scaffolding levels (307), suggesting gephyrin and $GABA_ARs$ synaptic residency are often functionally coupled. Accordingly, γ2 subunit and gephyrin levels both decrease in responses to other stimuli including status epilepticus (315) or prolonged inhibition of $IP_3$ receptor-dependent signaling (180). Additionally, chemically-induced inhibitory long-term potentiation (iLTP) protocols demonstrate gephyrin accumulation occurs concurrent with the synaptic recruitment of $GABA_ARs$ within 20 min (287). Collectively, these proteins display a high degree of interdependence across different experimental paradigms of inhibitory synapse plasticity occurring over minutes to days.

Increasing receptor synaptic retention enhances synaptic currents, while enhanced receptor diffusion via decreased scaffold interactions reduces synaptic currents. For example, reduction of gephyrin binding by replacement of the α1 $GABA_AR$ subunit gephyrin binding domain with non gephyrin binding homologous region of the α6 subunit results in faster receptor diffusion rates and a direct reduction in mIPSC amplitude (285). Similarly, enhanced diffusion of $GABA_ARs$ following estradiol treatment also reduces mIPSCs in cultured neurons and in hippocampal slices (316). In contrast, brief DZP exposure (< 1h) reduces $GABA_AR$ synaptic mobility (69) without a change in surface levels (70), consistent with initial synaptic potentiation of $GABA_AR$ neurotransmission by DZP. Together with our current findings, this suggests post-translational modifications on $GABA_AR$ subunits or gephyrin that enhance receptor diffusion are a likely key step leading to functional tolerance to BZD drugs.

It is a significant technical challenge to examine dynamic alterations in receptor trafficking occurring *in vivo*. To overcome this we examined changes in γ2-$GABA_AR$ protein association following DZP injection in mice using quantitative proteomics and bioinformatics analysis. This work revealed shifts toward γ2-$GABA_AR$ association with protein pathway networks associated

with endocytosis and organization of cytoskeleton **(Fig. 20B, Table 3)**, confirming similar fluctuations in membrane and intracellular trafficking occur *in vivo* and *in vitro* after DZP. We also found that shifts in association of proteins involved in the development of neurons (CaMKIIα, CDK5, NEFH, calcineurin/PPP3CA) suggested an inhibition in this pathway after DZP **(Fig. 20B)**. When considering all protein hits between vehicle and DZP, γ2-$GABA_AR$ association with proteins involved in 14-3-3 mediated signaling and RhoA signaling pathways were greatly increased after DZP (**Fig. 20A**, orange), while interaction with proteins involved in EIF2 signaling and sirtuin signaling pathways were reduced (**Fig. 20A**, blue). 14-3-3 proteins are heavily linked in $GABA_AR$ intracellular to surface trafficking (305, 306), and the RhoA signaling pathway is directly involved in actin cytoskeleton organization (317) and α5-$GABA_AR$ anchoring (106), providing further evidence of $GABA_AR$ shifts in membrane and cytosolic trafficking after DZP exposure.

Recent inhibitory synapse proteomics studies have identified a number of new protein synaptic constituents or modulators of $GABA_AR$ function (87, 318-321). We show here that proteins known to have roles in synaptic function and trafficking of membrane receptors show changes in their association with γ2-receptors. For example, the calcium-sensitive kinase CaMKIIα was found to be significantly decreased in interaction with γ2-$GABA_AR$ following DZP, which can regulate $GABA_AR$ membrane insertion, synaptic retention and drug binding properties (119, 178, 287, 322) (Table 2). Calcineurin/PPP3CA has been recognized as a key regulator of $GABA_AR$ synaptic retention and plasticity (162, 180, 182, 183, 307) and has been linked to the response to DZP *in vitro* (312). Here we provide the first evidence that DZP exposure enhances the association of calcineurin with γ2-$GABA_ARs$ *in vivo*. Furthermore, DZP was found to enhance γ2 association with 14-3-3 protein family members **(Table 1)**, which are known mediators of

$GABA_AR$ surface and intracellular trafficking (305, 306). α5 subunit coassembly with γ2 **(Table 1)** and overall levels **(Fig. 21)** were elevated after DZP. Interestingly, the α5 subunit is required for the development of BZD sedative tolerance in mice (308). It is notable that our proteomic studies are in part limited by the specificity of our antibody used and general downstream effects of reduced neuronal activity. Future follow up studies using the DZP site antagonist R015-1788 will be needed to dissect the individual roles of proteins found to be significantly altered in their association with $GABA_AR$, and their physiological and pharmacological importance to BZD tolerance and inhibitory neurotransmission.

Through application of novel and highly sensitive fluorescence imaging approaches combined with *in vivo* proteomics, we provide unprecedented resolution of $GABA_AR$ synapse plasticity induced by BZDs at both the level of the single neuron and cortex. Our study reveals that sustained initial DZP treatment diminishes synaptic BZD sensitive $GABA_AR$ availability through multiple fundamental cellular mechanisms: through reduction of the post-synaptic scaffolding protein gephyrin; shifts toward intracellular trafficking pathways and targeting of receptors for lysosomal degradation; and enhanced synaptic exchange of both gephyrin and $GABA_ARs$. Proteomic and bioinformatics studies using DZP-treated mouse brain tissue provide further evidence that altered γ2-$GABA_AR$ surface and intracellular trafficking mechanisms play a critical role to the response to DZP *in vivo*. These results define key events leading to BZD irresponsiveness in initial sustained drug exposure. Future studies utilizing this dual approach will address the neuroadaptations produced by long term BZD use to systematically identify the effects of a critical drug class that has seen a tripling in prescription numbers over the last two decades (323).

# 4.0 Inhibitory and Excitatory Synaptic Neuroadaptations in the Diazepam Tolerant Brain

Joshua Lorenz-Guertin performed animal injections, sample collection, biochemistry data collection and analysis, behavior, mass spectrometry data analysis. Megan L. Brady performed an open-field behavioral assay. Sabya Das performed biochemistry experiments on tissue from seven day treated animals and assisted with behavioral experiments. Tija C. Jacob, Matthew J. Bambino, Katarina Vajn and Matthew L. MacDonald assisted with mass spectrometry data analysis. Tija C. Jacob and Matthew L. MacDonald built and curated SRM libraries. The Macdonald laboratory performed mass spectrometry experiments. Nadezda Povysheva performed electrophysiology experiments and analysis.

## 4.1 Introduction

BZDs are positive allosteric modulators that potentiate $GABA_AR$ inhibition by increasing the binding affinity of GABA and increasing channel opening frequency (32). Sustained treatment with BZD drugs is intimately associated with the development of tolerance, dependence, withdrawal and addiction (33). BZD efficacy diminishes after prolonged or high dose acute exposure (271, 272), with tolerance to the sedative/hypnotic effects and anti-convulsant properties forming most quickly (46, 273-275). Since the development of BZDs in the early 1960s, intense research efforts have attempted to understand the adaptive response to BZDs. Direct comparison of these studies has proved challenging due to inconsistent findings likely as a result of methodological differences (33). Regardless, three important key characteristics were identified: BZD drugs demonstrate reduced affinity for the $GABA_AR$ after prolonged exposure (allosteric uncoupling; described in section 3.1), the effects of BZD could be reversed by concurrent treatment with the BZD site antagonist flumazenil (including behavioral dependence, withdrawal and tolerance (324-326)), and DNA/RNA level changes of $GABA_AR$ subunit expression are

inconsistent across experimental models (32). Considering these findings en masse, it is likely that rapidly tunable post-translational modifications, protein levels of $GABA_AR$ subunits, or other non-$GABA_AR$ inhibitory synapse components, may provide important mechanistic information underlying BZD irresponsiveness. For instance, BZD potentiation of recombinant $GABA_ARs$ in HEK293 cells is reduced when γ2 subunit Ser327 residue is phosphorylated (150) and 7-14 days of DZP treatment in rats causes increased phosphorylation at this site (327). Moreover, protein level changes in $GABA_AR$ subunit composition dictates the ability to bind BZD drugs (2), impacts localization at synapses and interacting proteins (328) and determines general channel properties (329). $GABA_ARs$ exist primarily in heteropentamers composed of two α, two β and a γ2 subunit, possibly containing two different α subunits, which impacts receptor pharmacology (330-332). As stated in previous sections, α1/2/3/5 subunits directly adjacent to γ2 form the BZD binding pocket, while α4 and α6 are BZD insensitive. Notably, α4/β/γ2 $GABA_ARs$ exist in small α subunit heterogeneous populations (333, 334), and increased expression of these BZD-insensitive $GABA_ARs$ could shift receptor pharmacology and contribute to tolerance by reducing BZD binding.

Neurotransmission relies on a delicate balance of both inhibitory and excitatory input, and thus synaptic neuronal proteins involved in both of these processes are likely involved in the response to BZDs. Excitatory glutamatergic receptors consist of ionotropic and metabotropic subtypes. Ionotropic glutamate receptors are heteromeric ligand-gated cation channels inwardly permeable to $K^+$, $Na^+$, or $Ca^{2+}$ ions following glutamate binding. The NMDA (N-methyl-D-aspartate) receptor class is crucial for synaptic plasticity and is comprised of two obligatory GluN1 subunits and two GluN2/3 subunits with differing regulatory characteristics. The predominant GluN2 isoforms are GluN2A and GluN2B. GluN2B is predominantly expressed in

the early postnatal brain and remains open longer after activation compared to GluN2A, which is expressed at higher levels later in over development (335). As a result, NMDA receptor function and role in synaptic plasticity is closely correlated with dynamic changes in the composition of GluN2 subunit isoforms. AMPA (alpha-amino-3-hydroxy-5-methyl-4-isoxazole-4-propionic acid) receptors are heterotetrameric ligand-gated ion channels composed of multiple subunits (GluR1-4). AMPA receptors are also important for the establishment of long-term excitatory potentiation and synaptic plasticity. AMPA receptors exhibit faster kinetics and lower glutamate affinity than NMDA receptors, thus the balance of AMPA/NMDA receptors is key to neuronal excitatory neurotransmission for short-term integration of synaptic inputs and long-term transformation of circuits (336-338).

Glutamatergic sensitization or upregulation has been postulated to be important in the development of BZD tolerance and addiction/withdrawal (339), as excessive excitation could require BZDs to be administered persistently or at higher doses to achieve the intended therapeutic effect. Early mouse studies using the AMPA antagonist GYKI 52466 and the NMDA receptor antagonist CPP revealed BZD withdrawal syndromes occur in separate AMPA and NMDA dependent phases (340). NMDAR current has also been shown to be decreased two days post cessation of one week treatment with the BZD flurazepam in CA1 hippocampal neurons, although this effect could be reversed by treatment with the non-competitive NMDAR antagonist MK-801 one day after BZD cessation (299). Multiple studies support the role of enhanced NMDA receptor function in withdrawal behaviors (341-343) and upregulation of GluN1 and GluN2B NMDAR subunits after DZP by [3H]MK801 binding and biochemistry (344, 345). Moreover, MK801 and ifenprodil (GluN2B subtype NMDAR antagonist) suppressed withdrawal-induced

pentylenetetrazole (PTZ) seizure susceptibility in DZP treated mice (342), cumulatively supporting the idea of NMDAR upregulation in response to DZP withdrawal.

Fewer studies have focused on the role of NMDAR contribution to the formation BZD tolerance. Importantly, NMDARs are implicated in tolerance to a number of other pharmacological drug classes including opioids (346), ethanol (347) and barbiturates (348). Some behavioral data suggests co-administration of the highly potent NMDAR competitive antagonist CPP, but not the AMPAR antagonist GYKI 52466, prevents development of DZP sedative behavioral tolerance in mice (349). MK801 also prevented the development of tolerance to locomotor effects (350) of DZP in rats, while tolerance to the anticonvulsant response of the BZD lorazepam was moderately prevented by CPP in mice (341). Interestingly, lorazepam reduced binding of the BZD binding site agent [3H]flumazenil in multiple brain regions, an effect that was not reversed by CPP co-treatment, suggesting downregulation of $GABA_A$Rs was not reversible by NMDAR inhibition. This finding could imply distinct contributions of $GABA_A$Rs and NMDARs to neuroadaptations in BZD tolerance.

Understanding the role of both GABAergic and glutamatergic contributions in BZD withdrawal and tolerance studies has been limited by using non-comprehensive experimental approaches. Moreover, these studies lack insight about the key molecular signaling networks undermining functional changes in synaptic function. To gain a more holistic perspective of the neuroadaptive changes occurring during BZD tolerance, we analyzed inhibitory and excitatory synaptic protein levels and function by biochemical and electrophysiology approaches in mice who demonstrate DZP sedative tolerance behaviorally. To generate a more complete understanding of DZP-induced neuroplasticity, we used state of the art selected reaction monitoring (SRM) mass spectrometry to quantify over 500 proteins, interrogating glutamatergic,

GABAergic and other signaling pathways. No existing studies have used a high-throughput quantitative and targeted proteomics based method to reveal the complex neuroadaptations of the BZD tolerant rodent brain. We assessed our proteomic findings using bioinformatics analysis to determine changes in activation states of key biological pathways to predict changes in cellular activity and function. Collectively our findings reveal complex alterations in both synaptic inhibitory and excitatory neurotransmission that share overlapping mechanisms with ethanol and opiate tolerance.

## 4.2 Methods and Materials

### 4.2.1 **Mice**

All experiments were approved by the Institutional Animal Care and Use Committee of the University of Pittsburgh and conducted in accordance with the National Institutes of Health Guidelines for the Care and Use of Laboratory Animals. C57BL/6J 8-10 week old male mice (Jackson Laboratory) were maintained on a reverse 12 h dark/light schedule. Mice were habituated to the University of Pittsburgh animal facility for at least three days prior to initiation of experiments. Mice were housed under 12 h light/dark cycles and had ad libitum access to food.

### 4.2.2 **Diazepam Treatment and Open-Field Behavior Assay**

Mice were randomly assigned to vehicle (40% PEG, 10% EtOH, 5% Na Benzoate, 1.5 % Benzyl alcohol) or DZP (Hospira) treatments. All animals received a saline injection at day -1 and

vehicle injection at day 0. On day 1, mice received either a DZP (10mg/kg) or vehicle injection and this treatment continued once daily for seven days in the morning. Mice were injected with vehicle or DZP approximately 45 min prior to testing for locomotor activity in an open field using automated activity monitors (Med Associates, St Albans, VT). Mice were allowed to freely explore the chamber for 20 min during which time ambulatory distance traveled was recorded. Brain tissue was immediately collected and flash frozen following day 7 behavior studies where applicable. Mice that were only used for biochemistry experiments were given the same dosing regimen, including a dose approximately 45 min prior to sacrifice (two treatments total for 24 h timepoint mice and four treatments total for 72 h timepoint mice).

### 4.2.3 **Antibodies**

Primary antibodies: rabbit GAPDH (WB) (14C10, Cell Signaling); rabbit CaMKII α/β Phospho Thr286 (WB) (p1005-286, Phosphosolutions); rabbit CaMKII pan (WB) (4436, Cell Signaling); rabbit GluN1 (WB) (5704, Cell Signaling); mouse GluN2B (WB) (610417, BD Biosciences); rabbit GluN2A (WB) (1500, Phosphosolutions), rabbit $GABA_AR$ α1 subunit (WB) (06-868, Millipore); rabbit $GABA_AR$ α4 subunit (WB) (845-GA4C, Phoshposolutions); rabbit $GABA_AR$ α5 subunit (WB) (2224503, Synaptic Systems); rabbit $GABA_AR$ β3 subunit (WB) (863-GB3C, Phoshposolutions); rabbit γ2 $GABA_AR$ subunit (WB) (224003, Synaptic Systems); rabbit gephyrin (WB) (sc-14003, Santa Cruz); rabbit KIR3.2 (WB) (APC-006, Alomone Labs).

### 4.2.4 **Subcellular Fractionation**

Subcellular fractionation was performed as previously described (351). Mouse cortical tissue was homogenized using a dounce homogenizer in homogenization buffer (HB) (in mM): 20 Tris-HCl, 2 EDTA, 640 Sucrose, 40 Na pyrophosphate, 20 NaF, 40 β-glycerophosphate, 4 $Na_3VO_4$, Sigma protease inhibitor cocktail (adjusted to pH 7.4 with NaOH at 4°C). After homogenization, samples were spun 1000rcf for 10mins at 4°C. The supernatant was removed and was either stored (Total) or used for subcellular fractionation. Samples were spun at 15,000 rcf for 30 min at 4°C. The supernatant was removed and the pellet was resuspended in 496 µL $H_20$ with protease inhibitor and sat on ice for 15 min. 3.75 µL 1M HEPES NaOH was then added and lysis continued on ice for 15 min. Samples were then spun for 20 min at 25,000 rpm at 4°C. Supernatant was discarded and 75 µL HB was added followed by addition of 75 µL 2x Triton buffer (final concentration in mM): 20 Tris-HCl, 2 EDTA, 2 EGTA, 20 NaF, 4 $Na_3VO_4$, Sigma protease inhibitor cocktail). Samples were sonicated at 25%, 3 pulses, 5s each under ice to dissolve the pellet. 150 µL 1x Triton buffer (with 1% Triton X-100) was then added and incubated for 30 min on ice. Next, samples were spun 100,000 rcf for 60 min at 4°C; the supernatant (extrasynaptic fraction) was removed and stored on ice. The pellet was homogenized in HB and sonicated, followed by the addition of 1% SDS prior to storage at -80°C (Synaptic). The extrasynaptic fraction was concentrated using acetone precipitation overnight, followed by homogenization in HB, sonication, and addition of 1% SDS. Samples were run using SDS-PAGE and transferred to nitrocellulose membrane. Samples were probed with primary antibody overnight followed by the appropriate horseradish peroxide (HRP)-coupled secondary antibody.

### 4.2.5 **Electrophysiological Recordings**

Experiments were performed on prefrontal cortex (PFC) slices from 3-7 month old C57BL/6J male mice. Mice were deeply anesthetized with chloral hydrate and decapitated. The brain was quickly removed and immersed in ice-cold pre-oxygenated artificial cerebrospinal fluid (ACSF). Coronal slices containing PFC were made as previously described (352). Throughout experiments, ACSF (31-32°C, perfused with a 95% $O_2$/5% $CO_2$) of the following composition was used (in mM): 126 NaCl, 2.5 or 10 KCl, 1.25 $NaH_2PO_4$, 1 $MgSO_4$, 2 $CaCl_2$, 24 $NaHCO_3$, 10-20 glucose; pH~7.3.

Whole-cell recordings were performed from layer 2-3 neurons visualized by IR-DIC video microscopy as previously described (353). Pyramidal neurons were identified by their apical dendrites and triangular somata. Patch electrodes (5-10 MΩ open-tip resistance) were filled with a solution containing (in mM): 140 CsCl, 0.1 $CaCl_2$, 2 $MgCl_2$, 2.5 Phosphocreatine, 1.1 EGTA, 2 ATP-Mg, 1 GTP-Na and 10 HEPES, adjusted to 7.2 with 1 M CsOH. Voltage and current recordings were performed with a Multi-Clamp 700A amplifier (Axon Instruments, Union City, CA). Signals were filtered at 2 kHz and acquired at a sampling rate of 10 kHz using Clampex 10.2 software (Molecular Devices Corporation, Sunnyvale, CA). Access resistance typically was 10-20 MΩ and remained relatively stable during experiments (≤30% increase). Corrections were made for liquid junction potential (-13 mV). We used: gabazine (10 μM) and picrotoxin (100 μM) to inhibit $GABA_AR$; 2,3-dihydroxy-6-nitro-7-sulfamoylbenzo(F)quinoxaline (NBQX; 20 μM) to inhibit kainate and α-amino-3-hydroxy-5-methyl-4-isoxazolepropionic acid receptors (AMPARs); D-2-amino-5-phospho-pentanoic acid (AP-5; 50 μM) to inhibit NMDARs; tetrodotoxin (TTX; 1 μM) to inhibit voltage-gated $Na^+$ channels; diazepam (3 μM) and GABA (20 μM) as an $GABA_AR$

agonist. Gabazine, picrotoxin, GABA, diazepam, NBQX, and AP-5 were purchased from Abcam (Cambridge, MA); TTX from Sigma (St. Louis, MO).

Miniature inhibitory postsynaptic currents (mIPSCs) were recorded at -70 mV in NBQX, AP-5, TTX. Miniature excitatory post-synaptic currents (mEPSCs) were recorded at -70 mV in Gabazine and TTX. Spontaneous and miniature events were analyzed using the MiniAnalysis Program (Synaptosoft, Decatur, GA) as previously described (353).

To record evoked AMPA/NMDA receptor EPSC (eEPSC), a bipolar stimulating electrode was placed on the border of white matter and layer 6 (352) with pulses delivered at 0.1 Hz frequency. eEPSCs were recorded at +40 mV in the presence of gabazine to block $GABA_AR$ mediated currents. After eEPSCs were recorded for ~5 min, AP-5 was added to isolate AMPAR mediated responses. The AMPA/NMDA ratio was calculated as previously described (354). First, the average NMDAR current was calculated by subtracting the average isolated AMPAR current from the initial average eEPSC prior to AP-5 application. Second, the AMPA/NMDA ratio was calculated as a ratio of the peak amplitude of the currents. Amplitude of evoked synaptic responses was measured on averaged traces as the most positive current value compared to baseline current using Clampfit.

Tonic $GABA_AR$ current was measured as the shift in baseline produced by the application of $GABA_AR$ blocker picrotoxin in the presence of NBQX, AP-5, TTX and GABA. The baseline current was measured in the Clampfit during three consecutive 0.2-min intervals before the application of pictrotoxin and 3 min after its application when baselines reach plateau.

Two-tailed paired t-test was used for group comparisons using Excel (Microsoft Corp., Redmond, WA). Values are presented as mean ± SEM.

### 4.2.6 **Mass Spectrometry**

Mouse cortical tissue from 10 vehicle and 10 DZP treated mice was homogenized individually using a dounce homogenizer in HB (in mM): 20 Tris-HCl, 2 EDTA, 640 Sucrose, 40 Na pyrophosphate, 20 NaF, 40 β-glycerophosphate, 4 $Na_3VO_4$, Sigma protease inhibitor cocktail (adjusted to pH 7.4 with NaOH at 4°C). After homogenization, samples were spun 1000 rcf for 10 min at 4°C. The supernatant (total) was used for downstream mass spectrometry. Total protein concentration in the homogenate preparations were assessed by micro BCA (Pierce). Targeted MS was performed in a similar fashion as described previously (355):10 µg homogenate or pooled controls were mixed with 10 µg of [$^{13}C_6$]brain ISTD (355) prepared from stable isotope labeling in mammals (SILAM) mouse cortex tissue (Cambridge Isotopes). The [$^{13}C_6$]lysine-labeled brain proteome internal standard ([$^{13}C_6$]brain ISTD) was prepared by homogenizing cerebral cortex tissue from a Stable Isotope Labeling in Mammals (SILAM) mouse (Cambridge Isotopes). These animals were raised on a diet in which the only source of Lysine was $^{13}C_6$ labeled, resulting in near complete (99%) labeling of the animal proteome in three generations. Labeling efficiency of each [$^{13}C_6$]brain ISTD preparation was confirmed prior to use.

Mass spectrometry analyses were conducted on a TSQ Quantiva triple stage quadrupole mass spectrometer (ThermoFisher Scientific, Location) with an Ultimate 3000 HPLC (Dionex). Two µl (~1 µg protein) was loaded on to a 3 µm 120A; 105mm REPROSIL-Pur C18 Picochip (New Objective) at 1 µl/min for 12 min and eluted at 400nl/min over a 25 min gradient from 3-35% mobile phase B (Acetonitrile, 0.1% formic acid). Selected reaction monitoring (SRM) transitions were scheduled with 60 second windows. Transitions were monitored, allowing for a cycle time of 1 sec, resulting in a dynamic dwell time never falling below 10 msec. The MS instrument parameters were as follows: capillary temperature 275°C, spray voltage 1350 V, and a

collision gas of 1.4 mTorr (argon). The resolving power of the instrument was set to 0.7 Da (Full Width Half Maximum) for the first and third quadrupole. Data were acquired using a Chrom Filter peak width of 4.0 sec.

Method development began by building upon our previously described SRM libraries (355-358) with the selection of additional proteins of interest included in published multidimensional MS/MS analyses of synaptic enrichments from mouse and human brain tissue (355, 359, 360) as well as the NIST Tandem Mass Spectral Library and the library generated by pilot immunoprecipitation-proteomic studies of γ2-$GABA_A$Rs. Targets for inclusion in the LC-SRM/MS assay were selected with a bias toward well annotated synaptic proteins, such as glutamate receptors, kinases, phosphatases, vesicular fusion, amino acid metabolism, protein trafficking and scaffolding as well as proteins found to interact with the $GABA_A$R. Peptides for proteins of interest were then filtered based on the following criteria: 1) presence of lysine and 2) non-redundant to a selected protein or protein group (determined by BLAST search). Acceptable peptide sequences, along with MS2 spectra, were imported into Skyline (361). Initially, five mass transitions were selected for each target peptide and its "heavy" counter-part. To ensure that the desired peptide was assayed, rigorous selection criteria were employed for the inclusion of peptide SRM transitions. Candidate "light"/"heavy" peptide SRMs were evaluated manually in Skyline for A) retention time, B) similar y-ion ratios (within 25%) to each other and database MS2 spectra, and D) a signal-to-noise ratio greater than 3. Peptide SRM pairs for which more than one identical peak was observed was omitted. Ultimately, 961 peptides unique to 571 proteins (or protein groups) were quantified in mouse samples. Statistics were performed by Student's t-test analysis in Excel.

### 4.2.7 **Bioinformatics Analysis**

Ingenuity Pathways Analysis (IPA) (Ingenuity Systems) was used for cellular pathway analysis. Proteins with peptides which were found to have increased or decreased DZP/Veh ratios with a $p < 0.1$ were used for analysis. This statistical cutoff was used to achieve adequate numbers of proteins to be used for comparison and prediction based analysis. Duplicate proteins were averaged within IPA to determine relative ratio changes. Significant enrichment in protein networks were calculated by right tailed Fisher's exact test. Z-score analysis is a statistical measure of an expected relationship direction and observed protein/gene expression to predict pathway activation or inhibition. IPA core analysis was searched to determine direct and indirect relationships within 35 molecules per network and 25 networks per analysis. All data repositories available through IPA were used to determine experimentally observed and highly predicted interactions occurring in mammalian tissue and cell lines. Ratio data were converted to fold change values in IPA, where the negative inverse (-1/x) was taken for values between 0 and 1, while ratio values greater than 1 were not affected.

### 4.2.8 **Statistics**

Relevant statistical test information is described in the figure legends or within the individual methods sections.

## 4.3 Results

### 4.3.1 Mice Rapidly Form Tolerance to the Sedation Actions of DZP

We first sought to establish a model of DZP sedative tolerance in mice. All animals received a saline injection at day -1 and vehicle injection at day 0. On day 1, mice received either a DZP (10mg/kg) or vehicle injection. DZP-treated mice demonstrated sedation and a significant decrease in distance traveled compared to vehicle treated animals **(Fig. 22)**. By day 3, the distance traveled was not significantly different between groups, indicating DZP-treated mice had become tolerant to the sedative effects of DZP. Similar rapidly forming behavioral tolerance to the sedative actions of DZP has been reported by multiple groups (47, 297, 349, 362). To confirm functional loss of DZP sensitivity in the cortex, we measured miniature inhibitory postsynaptic currents (mIPSCs) and potentiation by DZP using slice electrophysiology at the end of the seven day protocol **(Fig. 23A)**. There was no significant difference between vehicle (Veh) and DZP treated animals mIPSC amplitude **(Fig. 23B)**, frequency **(Fig. 23C)** or tau (decay) **(Fig. 23D)**, suggesting no major change in pre- or post-synaptic GABAergic neurotransmission. In contrast, DZP potentiation **(Fig. 23E)** of current amplitude **(Fig. 23F)** and tau decay **(Fig. 22G)** in vehicle animals was significantly higher than animals treated for seven days with DZP, suggesting functional tolerance to the positive allosteric effects of the drug. These results are consistent with previous publications suggesting loss of DZP sensitivity occurs independent of changes in basal GABAergic neurotransmission (363-365).

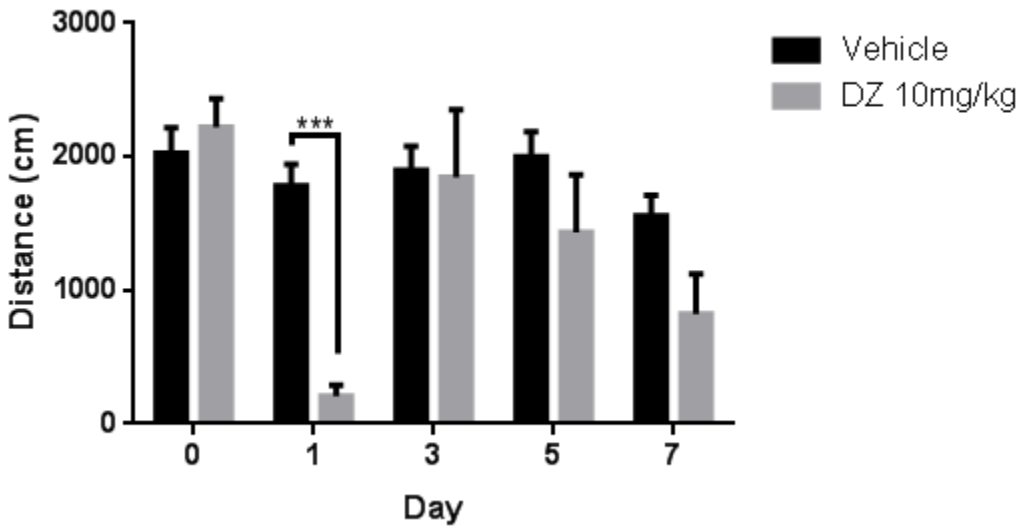


**Figure 22. Repeated DZP Treatment Rapidly Leads to Sedative Tolerance in Mice.**

Animals were administered treatment by IP injection once daily and then tested for sedative tolerance 45min later in the open field behavioral test on the days indicated. All animals received a saline injection at day -1 and vehicle injection at day 0. Mice received either a DZP (10mg/kg) or vehicle injection on days 1-7. DZP-treated mice demonstrated sedation and a significant decrease in distance traveled compared to vehicle treated animals. By day 3, the distance traveled was not significantly different between groups, indicating DZP-treated mice had become tolerant to the sedative effects of DZP. Two-way ANOVA found a significant effect of time ($p < 0.0001$), treatment ($p = 0.0261$), and a significant interaction ($p = 0.0020$), with a post-hoc Sidak test indicating a significant difference between vehicle and DZP treated animals at day 1 ($p < 0.001$), n=16 vehicle treated mice, n=14 DZP-treated mice.

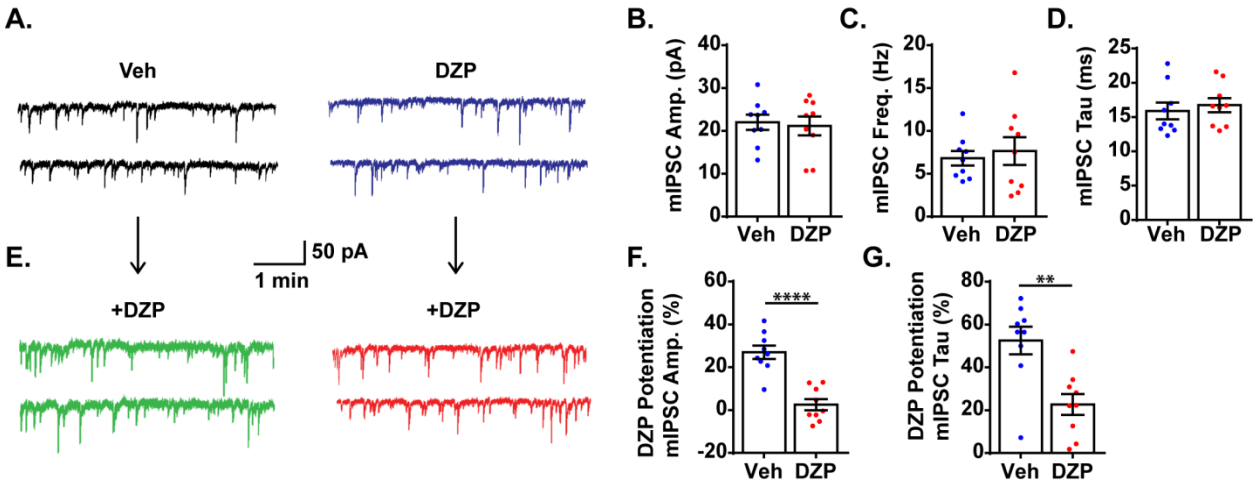


**Figure 23. Repeated DZP Exposure Leads to Loss of DZP Potentiation of GABA$_A$R Synaptic Currents.**

(A) mIPSCs in vehicle (Veh) (black and green) and DZP (blue and red) treated mice (Vhold = -70 mV). (B) mIPSC amplitude, (C) frequency and (D) tau were not different in DZP treated mice compared to Veh. (E,F,G) DZP potentiation of current amplitude and tau is signifantly larger in Veh animals relative to DZP (**p ≤ 0.01, ****p ≤ 0.0001 Student's t-test; n=9 per treatment group ; error bars ± S.E.M.).

### 4.3.2 **Inhibitory Synapse Protein Levels and Localization after DZP**

We next sought to determine if GABA$_A$R subunits involved in the sedation response to DZP (308, 366, 367) were altered by seven day drug treatment. Levels of gephyrin, the key synaptic scaffolding protein for GABAergic synapses, the DZP-insensitive GABA$_A$R α4 subunit, and the highly expressed GABA$_A$R β3 subunit were also measured. Subcellular fractionation (351) was used to measure the total, synaptic and extrasynaptic cortical levels of these proteins to determine membrane localization and overall changes **(Fig. 24A,B,C)**. Unexpectedly, this analysis revealed a significant increase in the overall pool of GABA$_A$R α1 (+71.4% ± 11.6), β3 (+48.8% ± 7.2) and γ2 (+32.9% ± 5.7) subunits in the DZP group relative to the vehicle animals

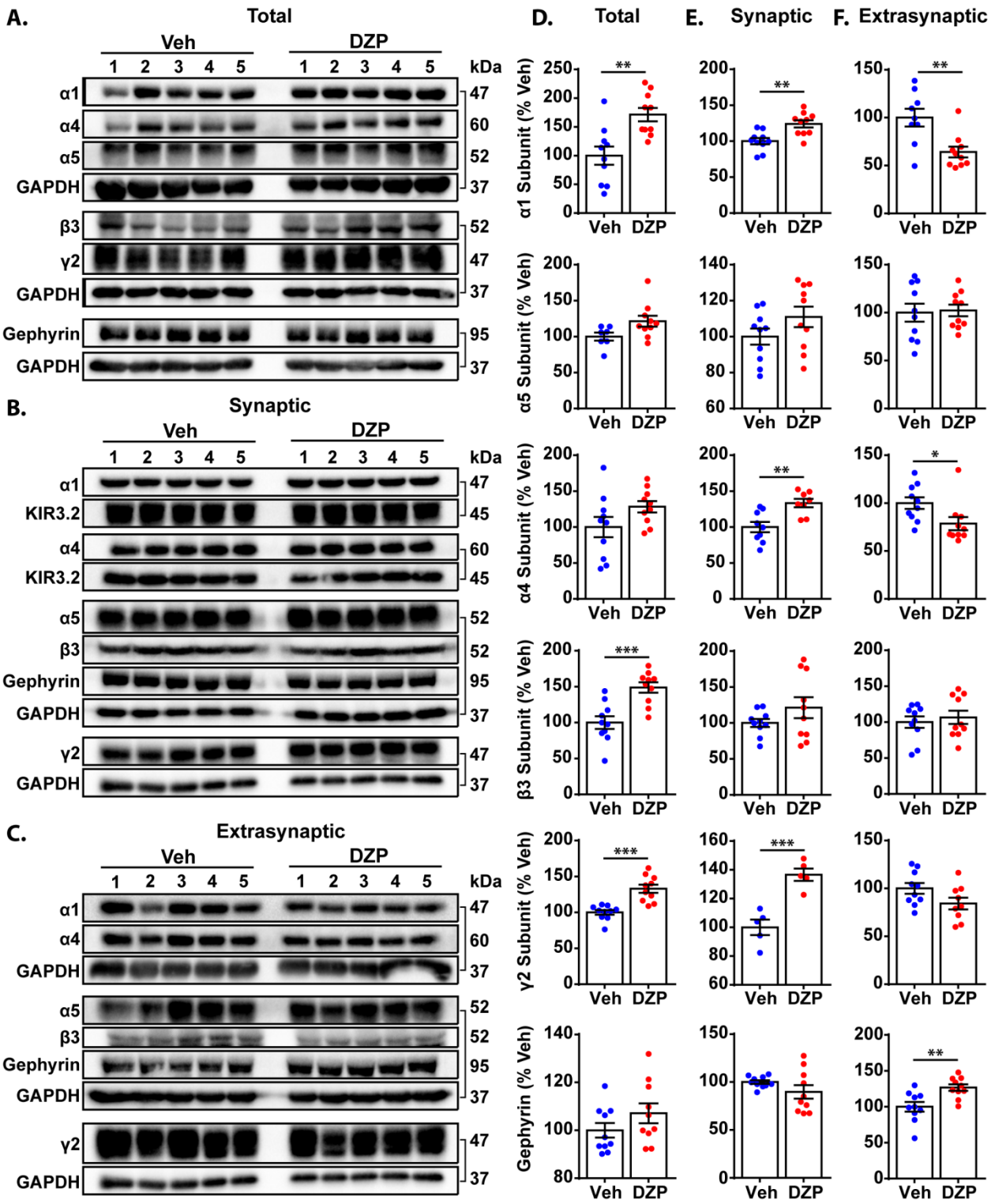


**Figure 24. GABA$_A$R Subunits and Gephyrin are Altered by Seven Day DZP Treatment *In Vivo*.**

Mice treated IP once daily for seven days with vehicle or DZP were assessed for GABA$_A$R subunit and gephyrin cortical tissue total (A), synaptic (B), and extrasynaptic levels (C) by western blot analysis. Representative blots show

mice 1-5 from each treatment. Quantification revealed a significant increase in the overall levels of α1, β3, γ2 subunits (D). Synaptic levels of (E) α1, α4 and γ2 subunits were also enhanced, while extrasynaptically α1 and α4 were decreased (F). DZP also increased extrasynaptic gephyrin (*p ≤ 0.05, **p < 0.01, ***p < 0.001, Student's t-test; n = 10 mice per treatment (experimental error resulted in n < 10 for some measurements); error bars ± S.E.M.).

**(Fig. 24D)**. An increase in α5 subunit levels also approached statistical significance (+21.4% ± 7.6; p = 0.054). No change in α4 or gephyrin total levels was detected **(Fig. 24A,D)**. Synaptic fractions revealed an enrichment of α1 (+24.1% ± 5.0), the DZP-insensitive α4 subunit (+33.4 % ± 5.8) and γ2 (+36.6% ± 4.3) at synaptic sites **(Fig. 24B,E)**. The enhancement of α1 and α4 subunits in the synaptic fraction also occurred concomitantly with a significant reduction in the extrasynaptic pools of these subunits **(Fig. 23C,F)**, suggesting a recruitment of these subunits to synapses away from extrasynaptic sites during seven day DZP exposure. A significant increase in extrasynaptic gephyrin levels (+26.7% ± 4.6) was also detected, indicating inhibitory scaffold function or clustering may be altered as well.

Next we performed slice electrophysiology recordings to determine if the DZP-induced shift of α1 and α4 subunits away from the extrasynaptic space and into the synapse would alter tonic inhibition. Whole-cell patch clamp recordings in cortical slices were used to measure changes in the tonic current. Bath application of the $GABA_AR$ pore blocker picrotoxin revealed a dramatic decrease in the tonic current of neurons from DZP treated mice compared to vehicle **(Fig. 25)**. Whole-cell current change, measured as a difference between baseline before and after picrotoxin application was used for control. These experiments revealed seven day DZP exposure produces a shift in synaptic $GABA_AR$ composition where α4 and α1 subunits are

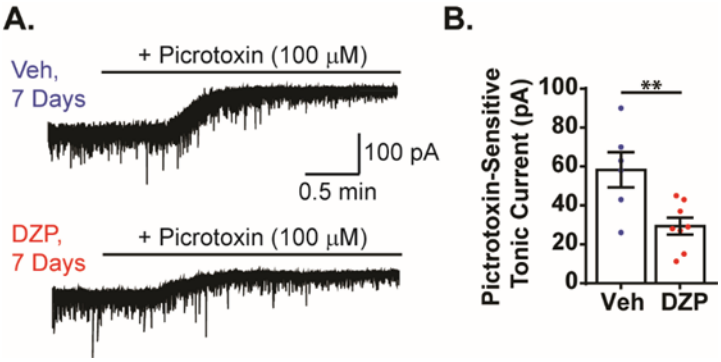


**Figure 25. Tonic Inhibition is Reduced in DZP Treated Mice.**

(A) Picrotoxin-sensitive changes in holding current were used to measure tonic inhibition in cortical slices from vehicle or DZP treated mice. (B) Quantification revealed a signifigant reduction in DZP (n = 8) treated animals tonic inhibtion relative to vehicle (n = 6) injected mice (**p ≤ 0.01, Student's t-test; error bars ± S.E.M.).

elevated and a corresponding reductions of these subunits at extrasynaptic sites occurs concurrent with decreased baseline tonic inhibition.

### 4.3.3 DZP Treatment Increases NMDA Receptor Levels and Function

Given the neuroadaptations seen in inhibitory $GABA_AR$ subunit synaptic proteins and prior evidence for glutamatergic system sensitization in the development of BZD tolerance, we hypothesized that an equivalent increase in excitation may also occur to achieve appropriate E/I balance in a homeostatic manner. Moreover, previous studies link enhanced NMDAR function to various types of drug tolerance (346-348), including evidence it has a role in DZP behavioral sedative tolerance (349, 350). We examined the subunit levels of this receptor after seven day DZP treatment. Analysis revealed increased total levels of GluN2A (+17.8% ± 4.7) and GluN2B (+53.7% ± 13.4) subunits in the cortex of DZP treated mice relative to vehicle **(Fig. 26A,C)** with an enrichment of GluN2A subunit (21.6 ± 4.1) at synapses **(Fig. 26B, D)**. Collectively this data

suggests compensatory upregulation of excitatory receptors occurs after DZP exposure. Next we examined functional changes in excitatory neurotransmission by first measuring AMPA miniature excitatory postsynaptic currents (mEPSC) **(Fig. 27A)**. We found no significant difference between treatment groups in AMPA mEPSC amplitude **(Fig. 27B)**, frequency **(Fig. 27C)** and tau **(Fig. 27D)**, suggesting pre- and post-synaptic mechanisms regulating AMPA receptor activation were not altered by seven day DZP exposure. In contrast, we found that the AMPA/NMDA ratio in DZP treated mice was nearly half that of vehicle in evoked excitatory postsynaptic current (eEPSC) measurements **(Fig. 27E,F)**, consistent with upregulation of NMDAR functional activity. Together these functional results, combined with biochemical data indicate GluN2A and GluN2B NMDAR subunit upregulation, enhanced synaptic GluN2A levels and increased NMDAR activity following seven day DZP injections.

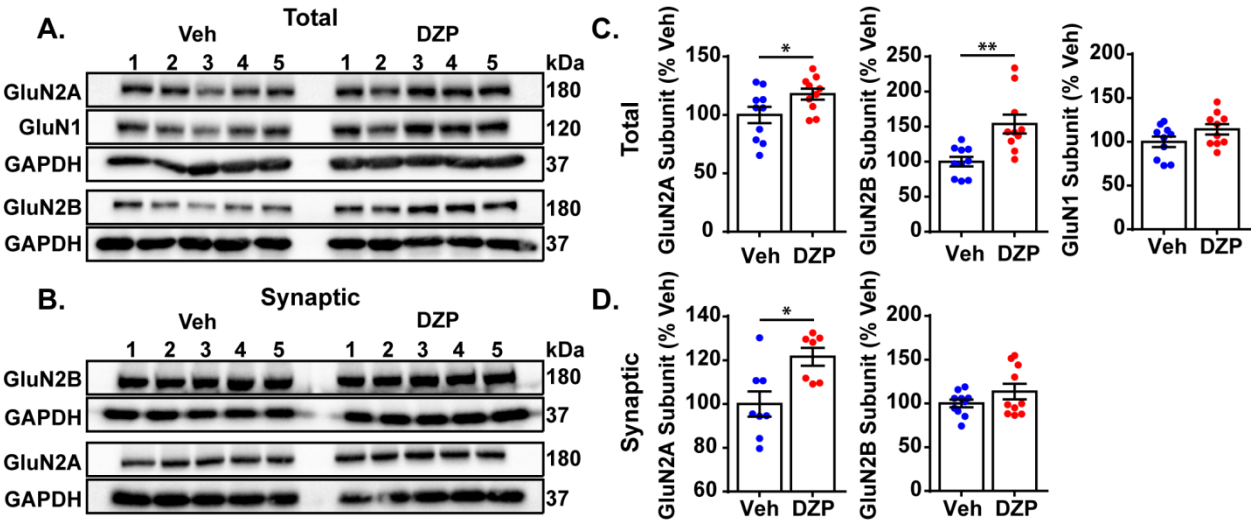


**Figure 26. NMDA Receptor Subunit Levels are Increased by Seven Day DZP Treatment *In Vivo*.**

Mice treated IP once daily for seven days with vehicle or DZP were assessed for NMDA receptor subunit cortical tissue total (A) and synaptic (B) levels by western blot analysis. Representative blots for mice 1-5. Quantification revealed a significant increase in the overall levels of the GluN2A and GluN2B subunits (C). GluN2A synaptic levels were also found to be significantly enhanced after DZP exposure (D) (*$p \leq 0.05$, **$p < 0.01$, Student's t-test; $n = 10$ mice per treatment (experimental error resulted in $n < 10$ for some measurements); error bars ± S.E.M.).

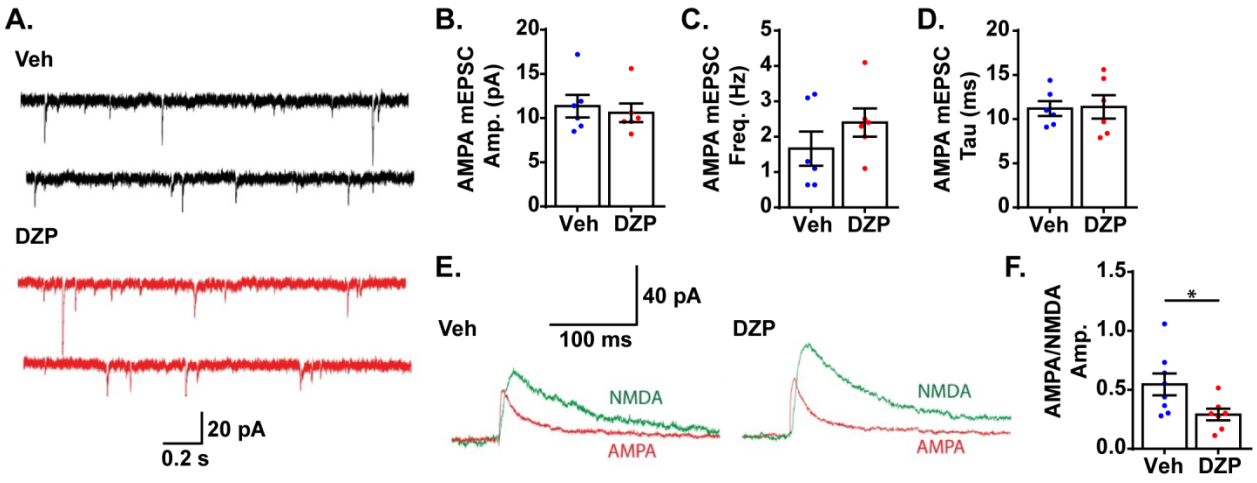


**Figure 27. NMDAR Function is Increased in DZP Treated Mice.**

(A) AMPAR EPSC traces in vehicle (black) and DZP (red) treated animals (Vhold= -70 mV). (B) AMPAR mEPSC (B) amplitude, (C) frequency and (D) decay were unchanged at day seven of DZP treatment (n=6). (*p ≤ 0.05, Student's t-test; error bars ± S.E.M.). (E,F) The AMPA/NMDA ratio (Vhold= +40 mV) was significantly lower ($p < 0.05$, Student's t test) in DZP treated (n = 7) compared to vehicle-treated mice (n = 8).

### 4.3.4 **Inhibitory and Excitatory Proteins Adaptions Occur at Earlier DZP Timepoints**

To determine if key inhibitory and excitatory proteins altered after seven day DZP treatment are also changed at earlier stages of drug exposure, we tested the cortical tissue of mice treated for a 24 h period (two treatments) or 72h period (four treatments) with vehicle or DZP. This experiment revealed a significant increase in total $GABA_AR$ α1 (+49.5% ± 16.0), α4 (+25.3% ± 5.5) and α5 (+32.0% ± 4.4) subunits after 24 h DZP exposure relative to vehicle **(Fig. 28A,B)**. $GABA_AR$ β3 subunit, γ2 subunit, and gephyrin were not significantly altered. Increased α1 subunit levels persisted across 72 h of DZP treatment, while α4 and α5 subunits were not detectably different than vehicle. Notably, β3 and γ2 subunit overall levels were enhanced at 72 h in the DZP treated group, consistent with findings at day seven **(Fig. 24)**.

The excitatory NMDA receptor subunit GluN2A was upregulated after 24 h of DZP treatment (+21.1% ± 4.4), without a detectable change in GluN1 or GluN2B subunits **(Fig. 28C,D)**. In contrast, DZP elevated the GluN1 (+30.3% ± 3.3) and GluN2B (+35.2% ± 11.8) subunits after 72 h, but the GluN2A subunit returned to vehicle levels.

Collectively, these results suggest that $GABA_AR$ subunits found to be elevated after seven day DZP treatment can be detected at higher levels earlier in the DZP treatment timeline axis. Notably the $GABA_AR$ α1 subunit is elevated as early as the 24 h time point and persists through day seven. NMDA receptor subunits are also found to be differentially increased at earlier DZP treatment time points, suggesting NMDA receptor plasticity at multiple stages following drug exposure.

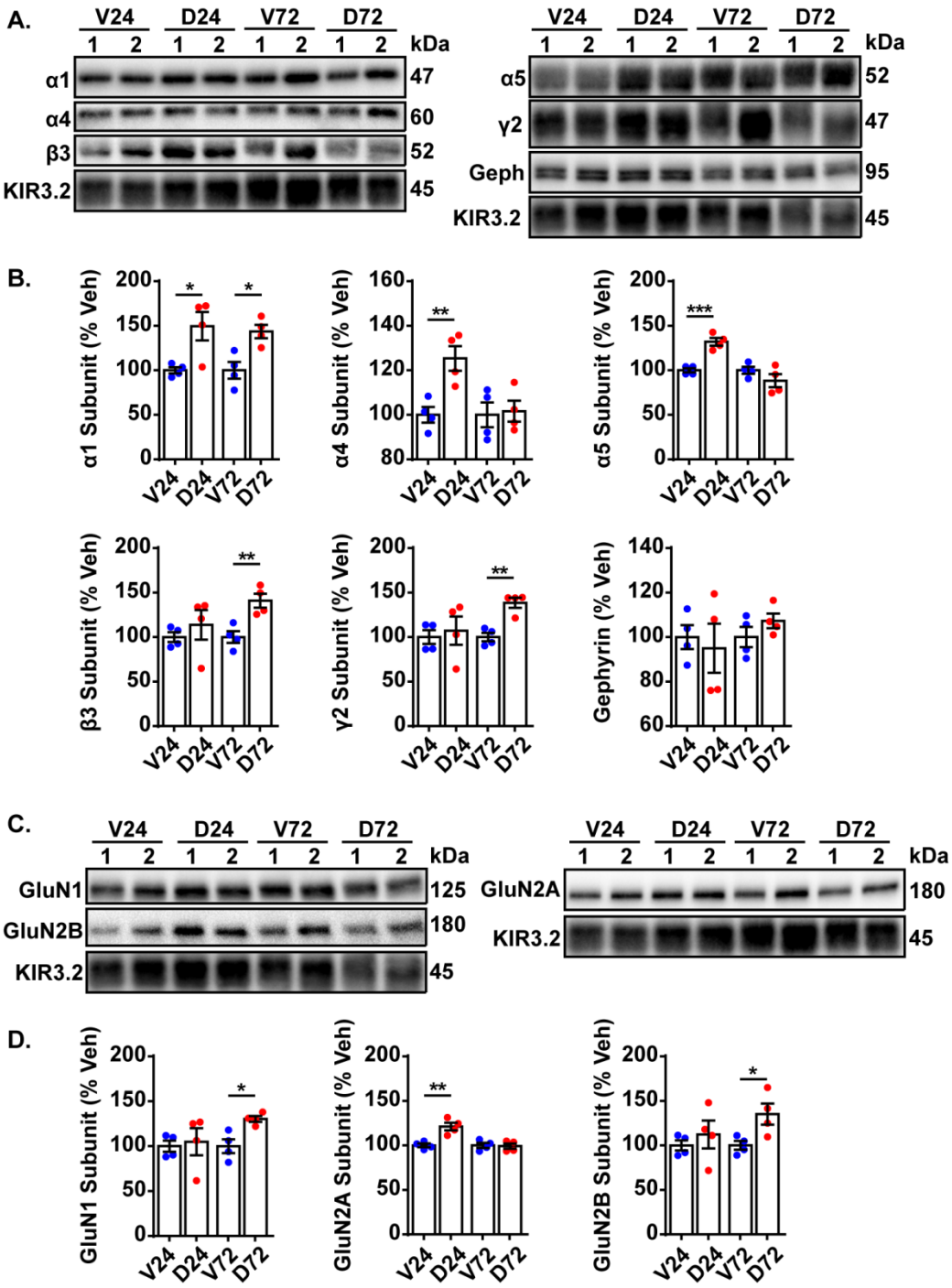


**Figure 28. Key Inhibitory and Excitatory Proteins are Upregulated at Earlier DZP Treatment Timepoints.**

Mice were treated with DZP or vehicle for 24 h (two doses) or 72 h (four doses). Total cortical lysates of $GABA_AR$ subunits and gephyrin (A,B) and NMDAR subunits (C,D) were examined by western blot. Representative blots for mice 1-2 from each treatment. Quantification revealed significantly increased levels of α1, α4 and α5 $GABA_AR$ subunits and NMDAR GluN2A subunit after 24 h DZP. The α1 subunit remained elevated after 72 h DZP treatment,

while α4, α5 and GluN2A subuntis returned to vehicle levels. Conversely, the $GABA_AR$ subunits β3 and γ2, and NMDAR subunits GluN2B and GluN1, were increased at the 72 h DZP treatment time point (*$p \leq 0.05$, **$p < 0.01$, ***$p < 0.001$, Student's t-test; n = 4 mice per treatment; error bars ± S.E.M.).

### 4.3.5 Quantitative Mass Spectrometry Identifies Changes in Neuronal Synaptic Proteome with DZP Treatment

Changes in the major $GABA_AR$ and NMDAR subunits contributing to inhibitory and excitatory neurotransmission are only a small fraction of the possible signaling network altered by DZP treatment. To gain a more comprehensive understanding of the protein profile of a DZP tolerant brain, we performed a quantitative proteomic screening against 500+ key synaptic proteins in vehicle versus DZP treated cortical tissue. This experiment identified a total of 962 unique peptides across 10 vehicle and 10 DZP samples. The peptide abundance of proteins in the DZP group compared to vehicle was used to determine which proteins were increased **(Table 4)** or decreased **(Table 5)**. As a result we identified 108 protein peptides with elevated levels of interaction in seven day DZP treated animals, while 16 protein peptides were decreased. These experiments revealed robust changes in the $Ca^{2+}$/calmodulin-dependent protein kinase II (CaMKII), a dodecameric holoenzyme that regulates key processes including synaptic plasticity. CaMKII is expressed in four isoforms α/β/δ/γ, with α and β being the most highly expressed in the forebrain at a ratio of about three α per β subunit (368). Individual CAMKII subunits can have distinct regulatory properties (369), localization (370), and developmental expression in neurons, for instance the δ and γ subunits are highly and selectively expressed early in development but strongly decrease in expression over time (371). Here we identified highly elevated peptide levels

of the α, β and δ subunits in cortical tissue of DZP treated mice, suggesting a global upregulation of CaMKII function or activity **(Table 4)**.

Protein kinase C (PKC) is critical for NMDAR function and trafficking alongside CaMKII (372, 373), and PKC epsilon (1.20 fold increase, $p = 0.0060$) and gamma (1.30 fold increase, $p = 0.026$) isozymes were significantly enriched in DZP treated mice **(Table 4)**. PKCε reduces $GABA_AR$ sensitivity to ethanol and BZDs *in vitro* and *in vivo* by phosphorylating the γ2 subunit S327 residue (150), while PKCγ is critical in tolerance mechanisms to other drugs like opioids (374, 375). DZP also significantly increased the levels of the growth associated protein 43 (GAP-43) (1.50 fold increase, $p = 0.019$) **(Table 4)** which is involved in excitatory neuron driven epileptogenesis (376), is integral for growth cone dynamics (377-379) and PKC phosphorylation of GAP-43 promotes excitatory long-term potentiation (380, 381). Increased levels of other pro-excitatory synapse proteins including discs large MAGUK scaffold protein 2 (DLGAP2) (382) (1.20 fold increase, $p = 0.027$) and the protein tyrosine kinase 2 beta (FAK2/CAKβ/Pyk2) (1.30 fold increase, $p = 0.0036$) were also measured. FAK2 can be recruited to excitatory synapses to mediate PSD-95 scaffolding maintenance, promotes NMDA receptor levels, upregulate NMDAR function by activating Src and is involved in long term potentiation (LTP) (383-386).

Interestingly, DZP evoked presynaptic plasticity is also suggested by increases in piccolo peptides (1.60 fold increase, $p = 0.033$), which functions as a large scaffold protein that redundantly contributes to the synaptic vesicle readily releasable pool with bassoon (387). Importantly, combined knockdown of piccolo and bassoon does not affect basic synaptic vesicle release (387, 388). The synaptotagmin 7 (SYT7) and 1 (SYT1) proteins were also enriched in DZP treated animals. SYT7 is a major regulator of the readily releasable neurotransmitter pool and was recently identified to work postsynaptically with SYT1 in hippocampal neurons as

redundant $Ca^{2+}$-sensors for $Ca^{2+}$-dependent exocytosis of AMPA-receptors during LTP (389), although no change in mEPSCs was detected. Combined knockout of SYT1 and SYT7 is needed to block LTP, and SYT1/SYT7 double knockout does not alter mEPSCs, suggesting no change in baseline synaptic AMPAR activity, consistent with our electrophysiology data showing no changes in AMPAR mEPSC after DZP **(Fig. 27)**. Elevated peptide levels of the membrane trafficking RAB3A protein (1.10 fold increase, $p = 0.0036$) were also measured, which regulates exocytosis of synaptic vesicles and is the most abundant RAB in the brain (390). Conversely, DZP animals exhibited decreased Dynamin 3 expression **(Table 5)**, which is a large GTPase crucial for presynaptic endocytosis and neurotransmission (391), is a component of the metabotropic glutamate receptor excitatory postsynapse (392), and mediates developmental synaptogenesis (393).

Cyclic nucleotide (namely cAMP and cGMP) levels are tightly regulated by phosphodiesterases (PDEs) (394) and we identified a DZP-induced enrichment (1.40 fold increase, $p = 0.042$) of the PDE2 enzyme which is particularly key for the regulation of performance and cognitive functions (395, 396) and inhibition of this enzyme is a key target for ongoing cognitive therapies (397). Interestingly, a decrease in the $GABA_AR$ subunit beta family (isoform 1/2/3) was determined by our analysis **(Table 5)**. Our biochemical data predicts a significant increase in β3 subunit levels, suggesting a decrease in either isoform β1 and/or β2, which is consistent with multiple studies showing decreased β2 subunit mRNA after BZD exposure (32). We were unable to detect a statistically significant difference in other $GABA_AR$ subunits or NMDAR subunits using our quantitative proteomics method in part due to variability and the limitations of our methodology in measuring hydrophobic membrane proteins (398).

**Table 4. Protein Peptides Demonstrating Increased Levels after DZP Treatment by Mass Spectrometry.**

Ratio D/V is fold change in DZP animals' relative peptide levels to control vehicle treated animals, t-test. Significant ($p < 0.05$) and near significant results ($p < 0.1$) shown.

| D/V | P-Value | Uniprot | Entrez Gene Name | Peptide Sequence | Location | Type(s) |
|---|---|---|---|---|---|---|
| 1.6 | 3.27E-02 | Q9QYX7 | piccolo presynaptic cytomatrix protein | ASPVPAPAEPPPQK | Cytoplasm | transporter |
| 1.6 | 6.57E-04 | P28652 | calcium/calmodulin dependent protein kinase II beta | FYFENLLAK | Cytoplasm | kinase |
| 1.6 | 4.01E-02 | Q9R0N7 | synaptotagmin 7 | VDLTQMQTFWK | Cytoplasm | transporter |
| 1.6 | 5.28E-02 | O35136 | neural cell adhesion molecule 2 | IIELSQTTAK | Plasma Membrane | other |
| 1.5 | 5.61E-02 | P55095 | glucagon | AQDFVQWLMNTK | Cytoplasm | other |
| 1.5 | 1.63E-03 | Q6PHZ2 | calcium/calmodulin dependent protein kinase II delta | QETVDCLK | Cytoplasm | kinase |
| 1.5 | 3.69E-04 | P11798 | calcium/calmodulin dependent protein kinase II alpha | FTEEYQLFEELGK | Cytoplasm | kinase |
| 1.5 | 2.98E-04 | P11798 | calcium/calmodulin dependent protein kinase II alpha | AGAYDFPSPEWDTVTPEAK | Cytoplasm | kinase |
| 1.5 | 3.46E-04 | P11798 | calcium/calmodulin dependent protein kinase II alpha | VLAGQEYAAK | Cytoplasm | kinase |
| 1.5 | 1.88E-02 | P06837 | growth associated protein 43 | QADVPAAVTDAAATTPAAEDAATK | Plasma Membrane | other |
| 1.4 | 1.11E-03 | P28652 | calcium/calmodulin dependent protein kinase II beta | FTDEYQLYEDIGK | Cytoplasm | kinase |
| 1.4 | 3.70E-03 | Q6PHZ2 | calcium/calmodulin dependent protein kinase II delta | FTDEYQLFEELGK | Cytoplasm | kinase |
| 1.4 | 1.49E-03 | P11798 | calcium/calmodulin dependent protein kinase II alpha | ITAAEALK | Cytoplasm | kinase |
| 1.4 | 1.16E-03 | P11798 | calcium/calmodulin dependent protein kinase II alpha | VTEQLIEAISNGDFESYTK | Cytoplasm | kinase |
| 1.4 | 9.09E-02 | Q91XM9 | discs large MAGUK scaffold protein 2 | VNEVDVSEVSHSK | Plasma Membrane | kinase |
| 1.4 | 1.44E-02 | P46096 | synaptotagmin 1 | LTVVILEAK | Cytoplasm | transporter |
| 1.4 | 4.26E-02 | Q922S4 | phosphodiesterase 2A | EFFSQGDLEK | Cytoplasm | enzyme |
| 1.4 | 6.94E-02 | Q6P9K8 | CASK interacting protein 1 | VGYFPSSLGEAIVK | Nucleus | transcription regulator |
| 1.4 | 6.25E-02 | Q80Z24 | neuronal growth regulator 1 | CYLEDGASK | Plasma Membrane | other |
| 1.3 | 4.26E-02 | Q922D8 | methylenetetrahydrofolate dehydrogenase, cyclohydrolase and formyltetrahydrofolate synthetase 1 | GDLNDCFIPCTPK | Cytoplasm | enzyme |
| 1.3 | 6.86E-02 | Q9CS84 | neurexin 1 | SADYVNLALK | Plasma Membrane | transporter |
| 1.3 | 4.93E-02 | Q9Z140 | copine 6 | SDPFMEIYK | Plasma Membrane | transporter |
| 1.3 | 5.14E-02 | P60879 | synaptosome associated protein 25 | FCGLCVCPCNK | Plasma Membrane | transporter |
| 1.3 | 3.60E-03 | Q9QVP9 | protein tyrosine kinase 2 beta/proline-rich tyrosine kinase 2 | DMPHNALDK | Cytoplasm | kinase |

**Table 4. Continued**

| | | | | | | |
|---|---|---|---|---|---|---|
| 1.3 | 8.31E-02 | P46660 | internexin neuronal intermediate filament protein alpha | NLQSAEEWYK | Cytoplasm | other |
| 1.3 | 1.61E-02 | P08551 | neurofilament light | NMQNAEEWFK | Cytoplasm | other |
| 1.3 | 7.76E-02 | P06837 | growth associated protein 43 | EGDGSATTDAA PATSPK | Plasma Membrane | other |
| 1.3 | 3.20E-02 | Q8CHH9 | septin 8 | SLSLGGHVGFD SLPDQLVSK | Extracellul ar Space | other |
| 1.3 | 4.17E-02 | Q8R3V5 | SH3 domain containing GRB2 like, endophilin B2 | VEEFLYEK | Cytoplasm | other |
| 1.3 | 3.92E-02 | P46096 | synaptotagmin 1 | VPYSELGGK | Cytoplasm | transporter |
| 1.3 | 9.14E-02 | O35526 | syntaxin 1A | HSAILASPNPDE K | Cytoplasm | transporter |
| 1.3 | 8.00E-03 | Q9Z1G4 | ATPase H+ transporting V0 subunit a1 | QAEIENPLEDPV TGDYVHK | Cytoplasm | transporter |
| 1.3 | 2.63E-02 | P63318 | protein kinase C gamma | GSDELYAIK | Cytoplasm | kinase |
| 1.2 | 8.66E-02 | A2A9R6 | ELAV like RNA binding protein 4 | DANLYVSGLPK | Cytoplasm | translation regulator |
| 1.2 | 2.72E-02 | Q8BJ42 | DLG associated protein 2 | SSWSTLTVSQA K | Plasma Membrane | other |
| 1.2 | 7.60E-03 | Q9JME5 | adaptor related protein complex 3 subunit beta 2 | LLTQYVLSLAK | Cytoplasm | transporter |
| 1.2 | 1.22E-02 | Q8BUV3 | gephyrin | TLIINLPGSK | Plasma Membrane | enzyme |
| 1.2 | 8.44E-02 | Q922S4 | phosphodiesterase 2A | ATDQVVALACAF NK | Cytoplasm | enzyme |
| 1.2 | 9.81E-02 | P46097 | synaptotagmin 2 | VFLLPDK | Cytoplasm | transporter |
| 1.2 | 2.11E-02 | Q3TXX4 | solute carrier family 17 member 7 | YIEDAIGESAK | Plasma Membrane | transporter |
| 1.2 | 2.51E-02 | P25444 | ribosomal protein S2 | TYSYLTPDLWK | Cytoplasm | other |
| 1.2 | 9.67E-02 | P53994 | RAB2A, member RAS oncogene family | YIIIGDTGVGK | Cytoplasm | enzyme |
| 1.2 | 1.51E-02 | P46460 | N-ethylmaleimide sensitive factor, vesicle fusing ATPase | GILLYGPPGCGK | Cytoplasm | transporter |
| 1.2 | 6.90E-02 | Q9CQC9 | secretion associated Ras related GTPase 1B | LVFLGLDNAGK | Cytoplasm | enzyme |
| 1.2 | 1.14E-02 | P35276 | RAB3D, member RAS oncogene family | LVDIICDK | Cytoplasm | enzyme |
| 1.2 | 6.55E-02 | Q01097 | glutamate ionotropic receptor NMDA type subunit 2B | VFASTGYGIAIQ K | Plasma Membrane | ion channel |
| 1.2 | 5.96E-03 | P16054 | protein kinase C epsilon | DFIWGVIGK | Cytoplasm | kinase |
| 1.2 | 6.29E-02 | P58281 | OPA1 mitochondrial dynamin like GTPase | VVVVGDQSAGK | Cytoplasm | enzyme |
| 1.2 | 8.40E-03 | Q91V41 | RAB14, member RAS oncogene family | TGENVEDAFLEA AK | Cytoplasm | enzyme |
| 1.2 | 7.25E-02 | Q9WUK 2 | eukaryotic translation initiation factor 4H | GFCYVEFDEVD SLK | Cytoplasm | translation regulator |
| 1.2 | 4.51E-02 | Q8BMS1 | hydroxyacyl-CoA dehydrogenase trifunctional multienzyme complex subunit alpha | FVDLYGAQK | Cytoplasm | enzyme |
| 1.2 | 5.28E-02 | P63318 | protein kinase C gamma | ITDFGMCK | Cytoplasm | kinase |
| 1.2 | 6.06E-02 | Q925E7 | protein phosphatase 2 regulatory subunit Bdelta | FLESPDFQPNIA K | Nucleus | other |

**Table 4. Continued**

| | | | | | | |
|---|---|---|---|---|---|---|
| 1.2 | 3.69E-02 | P46460 | N-ethylmaleimide sensitive factor, vesicle fusing ATPase | TTIAQQVK | Cytoplasm | transporter |
| 1.2 | 2.70E-02 | Q91V92 | ATP citrate lyase | FGGALDAAAK | Cytoplasm | enzyme |
| 1.2 | 6.57E-02 | P31324 | protein kinase cAMP-dependent type II regulatory subunit beta | VVDVIGTK | Cytoplasm | kinase |
| 1.2 | 1.59E-02 | Q80TJ1 | calcium dependent secretion activator | DIVTPVPQEEVK | Plasma Membrane | other |
| 1.2 | 7.03E-02 | P60766 | cell division cycle 42 | WVPEITHHCPK | Plasma Membrane | enzyme |
| 1.2 | 4.32E-02 | P47857 | phosphofructokinase, muscle | VLVVHDGFEGLAK | Cytoplasm | kinase |
| 1.2 | 2.73E-02 | P28474 | alcohol dehydrogenase 5 (class III), chi polypeptide | GTAFGGWK | Cytoplasm | enzyme |
| 1.2 | 8.97E-02 | Q6PGN3 | doublecortin like kinase 2 | TAHSFEQVLTDITEAIK | Cytoplasm | kinase |
| 1.1 | 6.85E-03 | Q9CVB6 | actin related protein 2/3 complex subunit 2 | IIEETLALK | Cytoplasm | other |
| 1.1 | 7.61E-02 | O08539 | bridging integrator 1 | LNQNLNDVLVSLEK | Nucleus | other |
| 1.1 | 2.42E-02 | Q76MZ3 | protein phosphatase 2 scaffold subunit Aalpha | VLELDNVK | Cytoplasm | phosphatase |
| 1.1 | 7.81E-03 | P62761 | visinin like 1 | STEFNEHELK | Cytoplasm | other |
| 1.1 | 7.33E-02 | P17710 | hexokinase 1 | FLLSESGSGK | Cytoplasm | kinase |
| 1.1 | 4.10E-02 | P14869 | ribosomal protein lateral stalk subunit P0 | TSFFQALGITTK | Cytoplasm | other |
| 1.1 | 5.69E-02 | O88935 | synapsin I | IHGEIDIK | Plasma Membrane | transporter |
| 1.1 | 5.65E-02 | O88935 | synapsin I | TYATAEPFIDAK | Plasma Membrane | transporter |
| 1.1 | 2.83E-02 | P63011 | RAB3A, member RAS oncogene family | LVDVICEK | Cytoplasm | enzyme |
| 1.1 | 4.81E-02 | Q62351 | transferrin receptor | DAWGPGAAK | Plasma Membrane | transporter |
| 1.1 | 5.65E-02 | Q63844 | mitogen-activated protein kinase 3 | DVYIVQDLMETDLYK | Cytoplasm | kinase |
| 1.1 | 9.08E-02 | Q9CQE8 | RNA transcription, translation and transport factor | NFIVWLEDQK | Nucleus | other |
| 1.1 | 8.04E-02 | P11499 | heat shock protein 90 alpha family class B member 1 | YESLTDPSK | Cytoplasm | enzyme |
| 1.1 | 2.01E-02 | P17710 | hexokinase 1 | NILIDFTK | Cytoplasm | kinase |
| 1.1 | 2.48E-02 | Q63844 | mitogen-activated protein kinase 3 | APEIMLNSK | Cytoplasm | kinase |
| 1.1 | 9.53E-02 | Q8K0T0 | reticulon 1 | SVLQAVQK | Cytoplasm | other |
| 1.1 | 9.69E-02 | Q76MZ3 | protein phosphatase 2 scaffold subunit Aalpha | LTQDQDVDVK | Cytoplasm | phosphatase |
| 1.1 | 9.26E-02 | P70168 | karyopherin subunit beta 1 | SSAYESLMEIVK | Nucleus | transporter |
| 1.1 | 5.94E-02 | P62827 | RAN, member RAS oncogene family | LVLVGDGGTGK | Nucleus | enzyme |
| 1.1 | 5.75E-02 | P68254 | tyrosine 3-monooxygenase/tryptophan 5-monooxygenase activation protein theta | YDDMATCMK | Cytoplasm | other |
| 1.1 | 7.56E-02 | P39053 | dynamin 1 | LQSQLLSIEK | Cytoplasm | enzyme |

**Table 4. Continued**

| | | | | | | |
|---|---|---|---|---|---|---|
| 1.1 | 7.43E-02 | P68368 | tubulin alpha 4a | TIGGGDDSFTTF FCETGAGK | Cytoplasm | other |
| 1.1 | 9.39E-02 | P40124 | cyclase associated actin cytoskeleton regulatory protein 1 | NSLDCEIVSAK | Plasma Membrane | other |
| 1.1 | 2.46E-02 | P62631 | eukaryotic translation elongation factor 1 alpha 2 | QLIVGVNK | Cytoplasm | translation regulator |
| 1.1 | 1.16E-02 | P49615 | cyclin dependent kinase 5 | DLLQNLLK | Nucleus | kinase |
| 1.1 | 4.38E-02 | Q7TMM 9 | tubulin beta 2A class IIa | INVYYNEAAGNK | Cytoplasm | other |
| 1.1 | 9.45E-02 | P05213 | tubulin alpha 1b | SIQFVDWCPTGF K | Cytoplasm | other |
| 1.1 | 6.81E-02 | Q8CHC4 | synaptojanin 1 | NQTLTDWLLDA PK | Cytoplasm | phosphatase |
| 1.1 | 2.10E-02 | P68369 | tubulin alpha 1a | GHYTIGK | Cytoplasm | other |
| 1.1 | 9.94E-02 | P39054 | dynamin 2 | LQSQLLSLEK | Plasma Membrane | enzyme |
| 1.1 | 3.91E-02 | P84078 | ADP ribosylation factor 1 | DAVLLVFANK | Cytoplasm | enzyme |

**Table 5. Protein Peptides Demonstrating Decreased Levels after DZP Treatment by Mass Spectrometry.**

Ratio D/V is fold change in DZP animals' relative peptide levels to control vehicle treated animals, t-test. Significant ($p < 0.05$) and near significant results ($p < 0.1$) shown.

| D/V | P-Value | Uniprot | Entrez Gene Name | Peptide Sequence | Location | Type(s) |
|---|---|---|---|---|---|---|
| 0.6 | 1.65E-02 | Q8BZ98 | dynamin 3 | RPLVLQLVTSK | Cytoplasm | enzyme |
| 0.7 | 4.19E-02 | P63080 | gamma-aminobutyric acid type A receptor beta1/2/3 subunit | VADQLWVPDT YFLNDK | Plasma Membrane | ion channel |
| 0.7 | 5.99E-02 | P61027 | RAB10, member RAS oncogene family | SFENISK | Cytoplasm | enzyme |
| 0.7 | 2.21E-02 | Q9D6M3 | solute carrier family 25 member 22 | GAAVNLTLVTP EK | Cytoplasm | transporter |
| 0.7 | 8.23E-02 | P84096 | ras homolog family member G | YLECSALQQD GVK | Cytoplasm | enzyme |
| 0.7 | 7.25E-02 | Q60597 | oxoglutarate dehydrogenase | VIPENGPAAQD PHK | Cytoplasm | enzyme |
| 0.7 | 3.36E-02 | P63038 | heat shock protein family D (Hsp60) member 1/HSP60 | GIIDPTK | Cytoplasm | enzyme |
| 0.8 | 8.65E-02 | P35436 | glutamate ionotropic receptor NMDA type subunit 2A | FSYIPEAK | Plasma Membrane | ion channel |
| 0.8 | 2.99E-02 | O08915 | aryl hydrocarbon receptor interacting protein | EGEIAQFLCDI K | Nucleus | transcription regulator |
| 0.9 | 9.43E-02 | P15105 | glutamate-ammonia ligase | ACLYAGVK | Cytoplasm | enzyme |
| 0.9 | 6.64E-02 | Q02053 | ubiquitin like modifier activating enzyme 1 | QFLDYFK | Cytoplasm | enzyme |
| 0.9 | 7.17E-02 | P05063 | aldolase, fructose-bisphosphate C | DNAGAATEEFI K | Cytoplasm | enzyme |
| 0.9 | 9.88E-02 | Q9D051 | pyruvate dehydrogenase E1 beta subunit | VVSPWNSEDA K | Cytoplasm | enzyme |
| 0.9 | 9.71E-02 | Q8BG32 | proteasome 26S subunit, non-ATPase 11 | EQSILELGSLL AK | Cytoplasm | other |
| 0.9 | 1.71E-02 | P35979 | ribosomal protein L12 | QAQIEVVPSAS ALIIK | Nucleus | other |
| 0.9 | 5.53E-02 | P19096 | fatty acid synthase | AGLYGLPK | Cytoplasm | enzyme |

To gain a more complete understanding of the functional outcome of DZP-induced changes in the synaptic proteome, we subjected our quantitative proteomics data to IPA bioinformatics analysis. Top enriched canonical pathways with –log(p-value) > 6.2 are shown in **(Fig. 29A)**. Analysis determined the synaptogenesis signaling pathway to be the most abundantly enriched and was predicted to be robustly upregulated as determined by z-score analysis. Synaptic LTP and CREB signaling in neurons pathways were also found to be activated, suggesting increased synaptic remodeling and strengthening of excitatory synapses, consistent with increased peptide levels for actin related protein 2/3 complex subunit 2 (ARP 2/3) **(Table 4)**, an important driver of

dendritic spine maturation and synapse unsilencing (399). Predicted activation of other interesting pathways including 14-3-3 mediated signaling, melatonin signaling and Huntington's disease signaling was also observed.

We further examined alterations in functional network association by checking the predicted activation status of select pathways when only using proteins which were found to be increased or decreased with a $p < 0.1$ **(Table 4,5)**. Functional network association of key biological pathways **(Fig. 29B)** predicted activation of the release of neurotransmitter (z-score = 3.112), development of neurons (z-score = 2.886), and long-term potentiation (z-score = 1.902) pathways in DZP mice relative to vehicle control. Significant protein changes ($p < 0.05$) conserved between two or more pathways include increased peptide levels of CaMKII subunits α/β, PRKCG (PKCγ) and RAB3A. Taken together, these results suggest seven day DZP treatment *in vivo* results in synaptic remodeling, pre- and post-synaptic plasticity and strengthening of excitatory synapses.

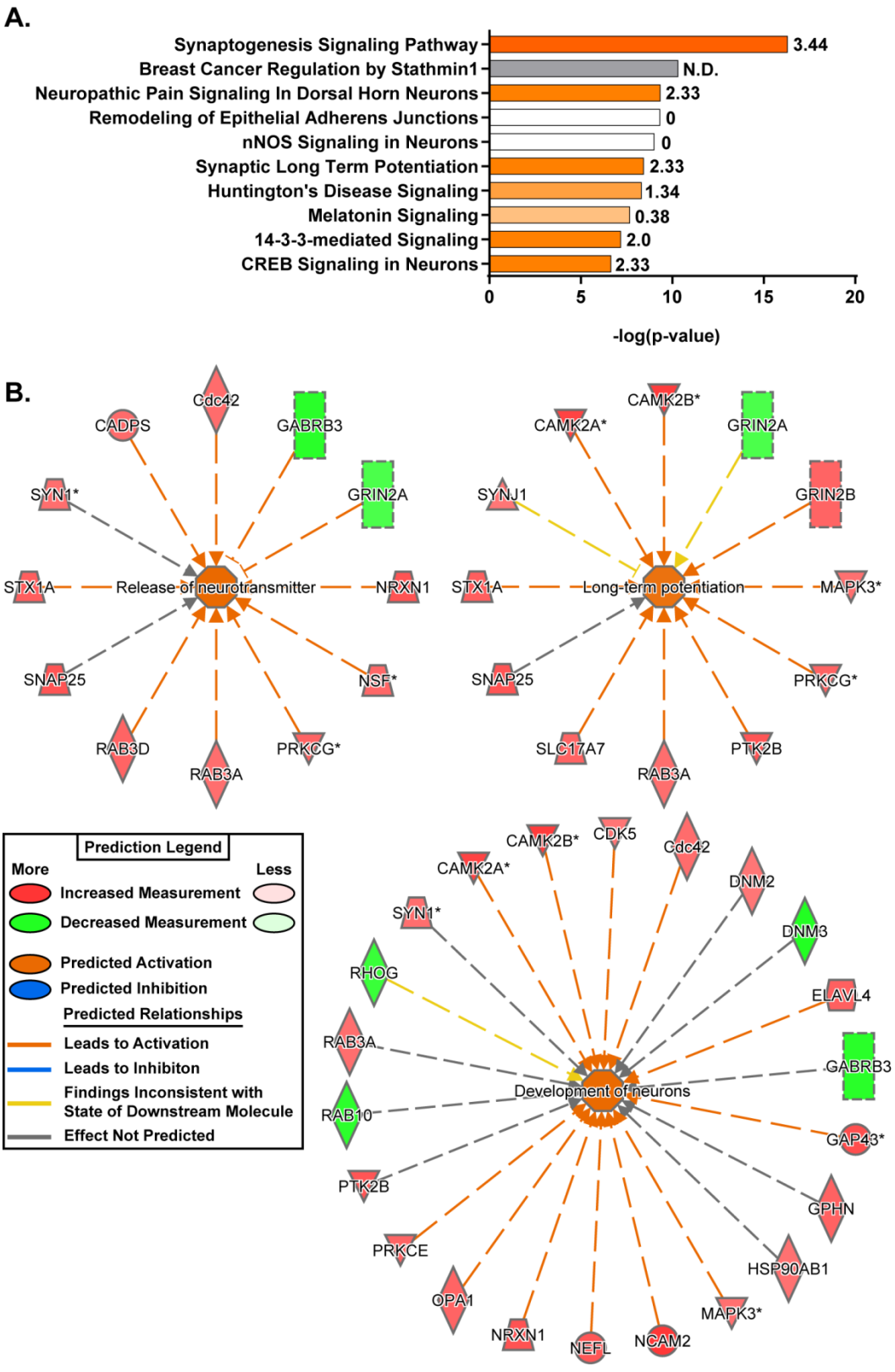


**Figure 29. IPA Analysis Reveals Activation of Key Biological Networks Following DZP Treatment.**

(A) Canonical pathways found to be differentially expressed following DZP administration *in vivo*. Enriched pathways with –log(p-value) greater than 6.2 were considered as calculated by Fisher's exact test right-tailed. Values to right of bars represent pathway activation z-score. Positive z-score represents predicted upregulation of a pathway (orange), negative z-score predicts inhibition (blue), z-score = 0 represents no change in pathway (white), while not determined (N.D.) conveys the analysis program was unable to determine a significant change (grey). Intensity of color represents size of z-score value. (B) Functional network association of select pathways when using proteins which were found to be increased or decreased with a $p < 0.1$. Major functional pathways altered by DZP include release of neurotransmitter (z-score = 3.112), development of neurons (z-score = 2.886), and long-term potentiation (z-score = 1.902). Significant protein changes ($p < 0.05$) conserved between two or more pathways include increased peptide levels of CaMKII subunits α/β, PRKCG (PKCγ) and RAB3A. Red = increased measurement, green = decreased measurement, orange = activation of pathway, blue = inhibition of pathway, yellow = findings inconsistent with state of downstream molecule, grey = effect not predicted.

### 4.3.6 **Western Blot Analysis of CaMKII Activation and Levels**

To further validate the observed increase in CaMKII subunit peptide levels after DZP treatment in our proteomics data **(Table 4)**, we performed western blot analysis on the cortical tissue of these mice. As an additional measure we also examined activation of CaMKII based on the phosphorylation state of the Thr286/287 residue, which is important for autonomous activation of the kinase (400), targeting to specific subcellular domains such as excitatory synapses (401) and regulation of LTP (402, 403). These experiments were unable to detect a statistical difference in the total α/β/δ or Thr286/287 phosphorylation levels of α/β CaMKII **(Fig. 30A,B)**. The inability to measure a change in CaMKII subunit levels equivalent to that seen in mass spectrometry experiments could be a result of the constraints of western blot analysis when considering antibody detection limitations and single molecular weight band measurements that may not comprehensively represent all forms of a protein including splice variants or various post-

translational modifications (368). Collectively, further tests will be needed to confirm that the alterations in CaMKII observed after DZP by proteomics are not false positive findings.

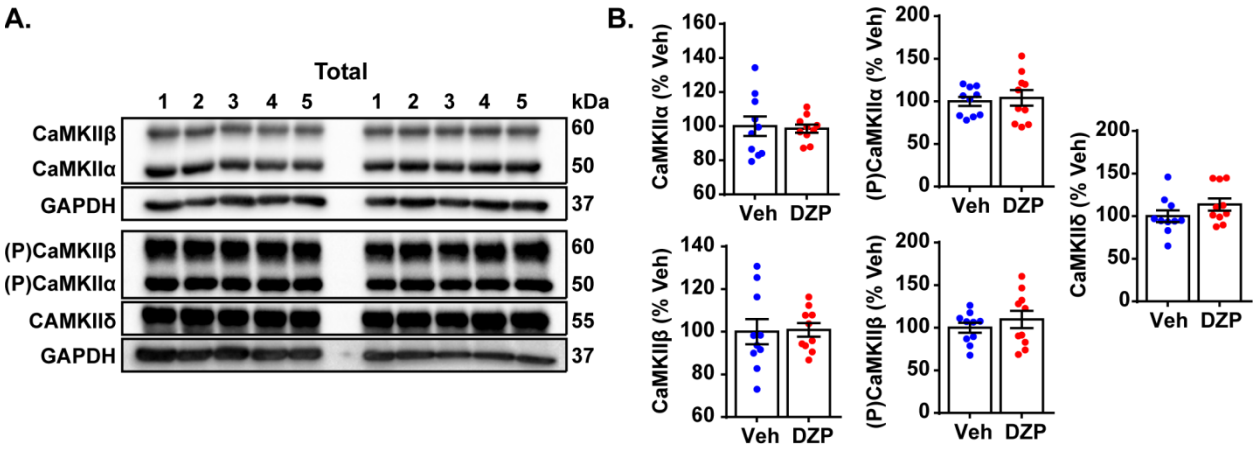


**Figure 30. Western Blot Analysis was Unable to Detect a Change in CaMKII Subunit Expression after DZP.** Mice treated seven days with vehicle or DZP were assessed for phosphorylation status of CaMKII Thr286/287 residues and total CaMKII subunit cortical tissue levels (A). (B) Quantification revealed no change in phosphorylation or subunit levels of CaMKII (Student's t-test; n = 10 mice per treatment; error bars ± S.E.M.).

## 4.4 Discussion

The neuroadaptive signature of a DZP tolerant brain has been elusive for researchers in part due to experimental limitations. Herein we find mice with tolerance to the sedative actions of DZP have modified $GABA_AR$ subunit protein levels and localization in the cortex, highlighted by the DZP-insensitive α4 subunit and the highly abundant α1 subunit moving away from the extrasynaptic space into the synapse **(Fig. 24)**. Slice electrophysiology experiments confirmed DZP insensitivity in animals treated for seven days with this drug, while no significant change in mIPSC amplitude was detected between treatments **(Fig. 23)**. This suggests the total numbers of

$GABA_AR$s at synapses are not changed but a modification of the receptor pharmacological profile had occurred, consistent with increased incorporation of α4 into γ2 $GABA_AR$s. Further supporting this proposed shift in $GABA_AR$ subtypes away from the extrasynaptic space, DZP treated animals demonstrated a marked reduction in tonic inhibitory current **(Fig. 25)**. Biochemical analysis of cortical tissue further revealed an enrichment of NMDAR subunits GluN2A and GluN2B **(Fig. 26)**, culminating with an decrease in AMPA/NMDA ratio in slice electrophysiology studies without a change in AMPA mEPSCs **(Fig. 27)**, suggesting overall increased NMDAR activity. Examining total levels of key inhibitory and excitatory proteins at earlier DZP treatment time points identified increases in $GABA_AR$ β3, γ2 and NMDAR GluN2B subunit by day three of DZP exposure, concomitant with behavioral sedative tolerance **(Fig. 28)**. Quantitative proteomic experiments screening hundreds of pivotal synaptic proteins in the cortex of vehicle versus DZP treated mice revealed upregulation of a number of proteins involved in synaptogenesis and remodeling, excitatory LTP and drug tolerance **(Table 4 and Fig. 29)**. The most robust increase found by mass spectrometry was the pro-excitatory CaMKII kinase α/β/δ subunit levels **(Table 4)**, where all measured peptides were elevated by around 1.5 fold (number of peptides for CaMKII kinase α/β/δ subunits were 4/2/2). Our inability to detect this by western blot analysis is likely due to methodological limitations including antibody specificity, limitations in sensitivity of measurements with highly abundant proteins, and single molecular weight band measurements **(Fig. 30)**. In summary, our work demonstrates DZP sedative tolerance is associated with synaptic $GABA_AR$ compositional changes, increased NMDAR levels and activity, enhanced expression of positive NMDAR modulators and synapse remodeling and excitatory synapse strengthening. These findings are clear factors that would contribute to a hyperexcitable and DZP-insensitive

brain state promoting symptoms observed during BZD withdrawal: heightened seizure susceptibility, anxiety, panic, and sleep disturbances.

One key finding in this study was the apparent shift in the α4 subunit to the synapse away from the extrasynaptic space. The α4 subunit does not bind classical BZD agonists like DZP, and receptor function is enhanced, rather than inhibited, by antagonists/inverse agonists at the BZD binding site and also is sensitive to modulation by neurosteroids, anesthetics, and ethanol (1, 219, 302, 404). Interestingly, the expression of the α4 subunit is highly malleable to a number of stimuli including alcohol exposure withdrawal (219, 405-407), progesterone-withdrawal (408, 409), social isolation in rats (410), electroshock seizures (411), absence seizures induced by gamma-hydroxybutyric acid (412) and pilocarpine-induced seizures (413). Chronic intermittent ethanol (CIE) treatments leads to a reduced behavioral hypnotic response to BZDs, associated with increased α4 and γ2 total levels and decreased decay time of $GABA_AR$-mediated mIPSCs and potentiation by DZP (407). Similarly, we identified a DZP-induced increase in synaptic α4 and γ2 subunit levels by western blot analysis **(Fig. 24)** coupled with minimal potentiation by DZP in electrophysiology studies **(Fig. 23)**. Dorsal ganglion cells (DGCs) from temporal lobe epilepsy animal models also show diminished DZP responsiveness following accumulation of α4 at synaptic sites (414). Furthermore, electrophysiology recordings in hippocampal slices found an extrasynaptic to synaptic switch of α4 appears after CIE, demonstrating potentiation by RO 15-4513, which acts as a partial agonist at α4/γ2 $GABA_ARs$, but functions as an inverse agonist at receptors with classical BZD pharmacology (α1/α2/α5β2). This was further confirmed by electron microscopy studies identifying increased α4 but not δ subunit within GABAergic synapses. It is important to note RO 15-4513 has high selectivity for the α5 subunit over other alpha subunits, and is used as a relatively selective marker for α5-$GABA_AR$ subtypes (415-417). Interestingly,

rapid ethanol tolerance paradigms examining CA1 area slices show increased surface synaptic α4 levels, decreased DZP enhancement of mIPSCs and faster mIPSC kinetics after ethanol withdrawal (219). As the quantitative proteomic data here identified increased expression of the PKCε and PKCγ isoforms **(Table 4)**, this suggests a PKC mediated mechanistic link between increased synaptic α4 subunit observed biochemically (**Fig. 24**) and the decrease in tonic inhibition by electrophysiology **(Fig. 25)** after DZP. Future studies examining the synaptic composition of $GABA_AR$s *in vivo* will be needed to fully elucidate the role of α4 in DZP insensitivity.

Surprisingly, a similar extrasynaptic to synaptic accumulation was seen with the α1 subunit, which also demonstrated increased overall levels **(Fig. 24)**. The majority of BZD-sensitive $GABA_AR$s in the brain contain the α1 subunit (418). The DZP sedative response is mediated by the α1 subunit as demonstrated by studies using knock-in mice expressing an α1 subunit H101R mutation, which disrupts BZD binding (366). Increased BZD-sensitive γ2-$GABA_AR$ internalization and trafficking *in vivo* has been implicated with sustained DZP exposure (270). Accordingly, increased expression of PKCγ **(Table 4)** in DZP treated mice may promote increased α1-$GABA_AR$ internalization, as is seen with ethanol treatment (149). An elevated rate of extrasynaptic endocytosis of α1 receptors may also provide context to the observed reduction in $GABA_AR$ tonic current **(Fig. 25)**. Additionally, the increase in total and synaptic $GABA_AR$ γ2 subunit levels observed biochemically **(Fig. 24, Fig. 28)** may be an adaptive response to rescue inhibition as a result of augmented endocytosis rates of α1-$GABA_AR$s and lead to incorporation of atypical $GABA_AR$ subtypes (α4/γ2) at synapses.

Enhanced inhibition via DZP-mediated $GABA_AR$ potentiation would likely result in a homeostatic upregulation of excitation to restore E/I balance. Importantly, over the last twenty years, the majority of studies have focused on hippocampal plasticity found following 2 days of

BZD withdrawal, leaving the BZD adapted cortex before drug withdrawal relatively uncharacterized. Due to the many confounds and changes induced with the evolving hyperexcitability of the withdrawal state and the prolonged removal of BZD drugs, the glutamatergic receptor adaptations shown for sedative tolerance here may be distinct from withdrawal studies. For example, NMDAR currents are reduced in two day flurazepam withdrawn rats in the CA1 hippocampus (299, 419), potentially due to reduced GluN2B but not GluN2A receptor levels (420), while AMPAR-mediated miniature excitatory postsynaptic current (mEPSC) amplitude are diminished after one and two-day withdrawal (299, 421). Behaviorally, AMPAR current amplitude and anxiety-like behavior measured in the elevated plus-maze in one-day FZP-withdrawn rats is enhanced (422). GluN2B levels are not decreased after one day of flurazepam withdrawal, suggesting down regulation of NMDAR function does not occur until later (423). Conversely, a single *in vivo* dose of DZP increased the AMPA/NMDA current ration in ventral tegmental area dopaminergic neurons that lasted up to 72 hours, suggesting brain region and time-dependent plasticity (354).

Here we identify in a seven day DZP treatment sedative tolerance paradigm, where animals are not in a withdrawal state, enhanced cortical NMDAR subunit levels by western blot analysis **(Fig. 26)** and decreased AMPA/NMDA amplitude ratio without changes in AMPA mEPSCs **(Fig. 27)**, suggesting selectively increased NMDAR function. In agreement, behavioral data suggests co-administration of the highly potent competitive antagonist NMDAR CPP, but not the AMPAR antagonist GYKI 52466, prevents development of sedative behavioral tolerance after DZP in mice (349). MK801, a non-competitive NMDAR agonist also prevents the development of tolerance to locomotor effects (350) of DZP. These findings are consistent with a generalized role of increased

NMDAR function in tolerance to a number of pharmacological drug classes including opioids (346), ethanol (347) and barbiturates (348).

To gain a more holistic understanding of the mechanisms leading to DZP tolerance, both directly and indirectly related to the changes observed in our biochemical and electrophysiology findings, we performed a quantitative proteomics screen against 500+ key synaptic proteins. We found a enrichment in a number of kinase pathways associated with increased NMDAR function including elevated CaMKII subunit levels (424), PKC isozymes (372, 373) and protein tyrosine kinase 2 beta (383-385). Interestingly, CaMKII inhibition in two-day flurazepam withdrawn rats reverses increased AMPAR single-channel conductance (425). This was later connected to CaMKIIα-mediated GluA1 Ser831 phosphorylation in the postsynaptic density of two-day FZP-withdrawn rats without changes in (P)T286 CaMKIIα levels (426). This may suggest a general increase in CAMKII levels during both tolerance and withdrawal. This increase in CaMKII appears to occur after prolonged DZP treatment, as a single dose decreased transcript levels of CAMKIIα in mice cortex (427), and our lab found decreased association of $GABA_AR$s with CAMKIIα 12h following DZP injection (270).

Interestingly we found both the PKCγ isoform and CaMKII subunits to be increased after seven day DZP treatment. Multiple studies implicate both of these kinases as essential for the generation and maintenance of opioid tolerance and dependence (374, 428-435). PKC activation by 4beta-phorbol-12,13-dibutyrate (PDBu; 100nM, 10 min) in endogenous $GABA_AR$s of NT2-N neurons caused a rightward shift of the concentration-response curve for DZP positive allosteric enhancement without affecting the maximal response, suggesting decreased allosteric coupling of DZP and GABA sites (436). Our proteomic studies also found elevated PKCε isozyme levels after DZP **(Table 4)**, which has been described to reduce $GABA_AR$ sensitivity to ethanol and BZDs *in*

*vitro* and *in vivo* by acting at a γ2 S327 residue (150) and negatively regulates cell surface $GABA_AR$s levels through the membrane fusion ATPase N-ethylmaleimide-sensitive factor (NSF) (437). Importantly, a significant increase in NSF protein peptides after DZP exposure was also seen **(Table 4)**. Both PKCγ and PKCε knock-out mice exhibit altered ethanol potentiation of $GABA_AR$ mediated $Cl^-$ flux (438), where chronic ethanol consumption decreases association of PKCγ association with α1 but increases its association with α4 (439). Short (4 h) ethanol exposure induces internalization of α1-containing $GABA_AR$s (149) coinciding with an increase in surface levels of the α4 subunit (440) with both adaptations occurring in a PKCγ dependent manner. Notably, PKCγ is recruited to the membrane after opioid exposure (441, 442) and PKCγ kinase mutant mice demonstrate reduced tolerance (374) and blocks delayed pronociceptive sensitivity to opioid agents (375). Herein we observed increased α1 subunit and PKCγ levels after seven days DZP treatment, suggesting an increase in surface $GABA_AR$ populations undergoing drug-induced endocytosis and intracellular trafficking in agreement with our previous findings at earlier DZP treatment time points (270).

We further analyzed our proteomics data by using IPA bioinformatics analysis to determine changes in pathway activation or enrichment. Canonical pathway analysis revealed strong predicted activation of synaptogenesis signaling, synaptic LTP and CREB signaling in neurons pathways **(Fig. 29A)**. Individual biological pathway assessment suggested the release of neurotransmitter, development of neurons, and long-term potentiation favored an activated state **(Fig. 29B)**. Statistically significant protein peptide changes with the most robust difference between DZP and vehicle animals support these changes including growth cone regulator GAP-43 (377-379), the $Ca^{2+}$-sensors Syt1 and Syt7 that contribute to both presynaptic synaptic vesicle ready releasable pool and postsynaptic trafficking to support LTP (443), piccolo (387), dynamin-

3 (391) and RAB3A (390) and the critical phosphodiesterase enzyme PDE2 (395, 396). The collective bioinformatics and proteomics analysis supports synaptic plasticity, in part through NMDAR pathway upregulation and function.

Here we leverage a comprehensive experimental approach utilizing behavioral testing, biochemistry, quantitative proteomics and electrophysiology to examine the neuronal adaptions occurring in response to DZP tolerance *in vivo*. Our study reveals complex alterations in both inhibitory and excitatory neurotransmission that have similar profiles to ethanol and opiate tolerance. We find an increase in the synaptic levels of α1, γ2 and the DZP-insensitive α4 subunit, resistance to DZP potentiation and no change in GABA mIPSC amplitude or frequency. Moreover, an increase in NMDAR levels and function was observed by western blot analysis and by electrophysiology. These changes occurred coincidently with an increase in the levels of multiple CaMKII subunits and the PKCγ isozyme, known positive regulators of NMDAR function. These results define key aspects of the neuroadaptive signature of a brain with sedative BZD tolerance. Future studies will need to identify if other BZD class drugs with different pharmacokinetic and pharmacodynamics profiles relative to DZP elicit similar changes found here. Moreover, the FDA approved NMDAR inhibitor memantine poses an interesting candidate to inhibit or reverse the DZP induced adaptations, as it has been show to alleviate some negative side effects resulting from opioid (444) and alcohol intake (445, 446). Advancing our understanding and identifying possible targets for treatments for the neuroadaptations produced by long-term BZD are critical for clinical care considering that during the last two decades prescription dosage and/or length of treatment has steadily risen (323).

# 5.0 Final Conclusions

A deeper molecular understanding of the factors influencing the pharmacological profile of $GABA_AR$s is crucial for current clinical practices and future drug development. $GABA_AR$ regulatory mechanisms including trafficking, post-translational modifications and composition directly and dynamically tune receptor activity and function during neuronal scaling. Herein we investigated the compensatory neuroadaptations occurring after initial and prolonged treatment with the highly utilized clinical drug, DZP, where functional and behavioral tolerance to DZP has occurred. This work included the generation and characterization of a novel dual reporter $GABA_AR$ optical tool with multiple imaging based applications. The $\gamma2^{pH}$FAP construct aided our ability to detect elusive trafficking changes in receptors after initial DZP and an *in vitro* epilepsy paradigm, and this tool will remain highly useful for future studies into $GABA_AR$ trafficking regulation. The comprehensive use of advanced imaging techniques, biochemistry and label-free quantitative proteomics revealed a complex array of trafficking and regulatory mechanisms dampening inhibitory synapse function in response to one day DZP exposure. Compromised gephyrin scaffolding, increased internalization and lysosomal targeting of select $GABA_AR$ subtypes, and enhanced $\gamma2$-$GABA_AR$ association with intracellular and surface trafficking protein mediators *in vivo* defined this work.

Many classical studies have attempted to solve the molecular fingerprint of a BZD tolerant brain, but conclusive evidence remains undetermined due to differences in research paradigm, brain-region and experimental tool limitations (32). Our work utilized a comprehensive experimental strategy in a behaviorally-validated DZP tolerance model to measure protein level changes in inhibitory and excitatory receptors, functional validation by electrophysiology and a

targeted synaptic proteome screening. These findings revealed alterations in subunit specific synaptic and extrasynaptic $GABA_AR$ localization coupled with a general increase in $GABA_AR$ subunits. Additionally, we identified enhanced NMDAR subunit levels and function, and an upregulation of proteins regulating neuronal remodeling, development, and excitatory synapse strengthening. The use of SRM based quantitative proteomic methods afforded us detection of a number of key kinase mediators altered by DZP including CAMKII and PKC subtypes that have also been determined to be important in the adaptive drug response to ethanol and opiates. Importantly, we identified a unique response profile between early and sustained DZP treatment, including opposing changes in $GABA_AR$ subunit levels and the inhibitory scaffolding protein gephyrin. This work highlights the necessity of multiple experimental approaches and emphasizes the importance of understanding drug effects at different stages of treatment exposure. Current clinical and new $GABA_AR$ modulating therapies will have to strongly consider the short- and long-term consequences of manipulating $GABA_AR$ function and the brains fundamental mechanisms to compensate for robust changes in the E/I balance.

## Bibliography


1. Lorenz-Guertin JM & Jacob TC (2018) GABA type a receptor trafficking and the architecture of synaptic inhibition. *Developmental neurobiology* 78(3):238-270.

2. Olsen RW & Sieghart W (2009) GABA A receptors: subtypes provide diversity of function and pharmacology. *Neuropharmacology* 56(1):141-148.

3. Sieghart W (2006) Structure, pharmacology, and function of GABAA receptor subtypes. *Adv Pharmacol* 54:231-263.

4. Minier F & Sigel E (2004) Techniques: Use of concatenated subunits for the study of ligand-gated ion channels. *Trends in pharmacological sciences* 25(9):499-503.

5. Baur R, Minier F, & Sigel E (2006) A GABA(A) receptor of defined subunit composition and positioning: concatenation of five subunits. *FEBS letters* 580(6):1616-1620.

6. Cellot G & Cherubini E (2013) Functional role of ambient GABA in refining neuronal circuits early in postnatal development. *Frontiers in Neural Circuits* 7.

7. Deng L*, et al.* (2007) Sequential postsynaptic maturation governs the temporal order of GABAergic and glutamatergic synaptogenesis in rat embryonic cultures. *J Neurosci* 27(40):10860-10869.

8. Cellot G & Cherubini E (2013) Functional role of ambient GABA in refining neuronal circuits early in postnatal development. *Frontiers in neural circuits* 7:136.

9. Ben-Ari Y, Gaiarsa JL, Tyzio R, & Khazipov R (2007) GABA: a pioneer transmitter that excites immature neurons and generates primitive oscillations. *Physiological reviews* 87(4):1215-1284.

10. Mohler H (2012) The GABA system in anxiety and depression and its therapeutic potential. *Neuropharmacology* 62(1):42-53.

11. Nuss P (2015) Anxiety disorders and GABA neurotransmission: a disturbance of modulation. *Neuropsychiatric Disease and Treatment* 11:165-175.

12. Pehrson AL & Sanchez C (2015) Altered γ-aminobutyric acid neurotransmission in major depressive disorder: a critical review of the supporting evidence and the influence of serotonergic antidepressants. *Drug Design, Development and Therapy* 9:603-624.

13. Luscher B, Shen Q, & Sahir N (2011) The GABAergic deficit hypothesis of major depressive disorder. *Mol Psychiatry* 16(4):383-406.

14. Pitman RK*, et al.* (2012) Biological Studies of Posttraumatic Stress Disorder. *Nature reviews. Neuroscience* 13(11):769-787.

15. Trousselard M*, et al.* (2016) Is plasma GABA level a biomarker of Post-Traumatic Stress Disorder (PTSD) severity? A preliminary study. *Psychiatry Research* 241:273-279.

16. Möller AT, Bäckström T, Nyberg S, Söndergaard HP, & Helström L (2016) Women with PTSD have a changed sensitivity to GABA-A receptor active substances. *Psychopharmacology* 233(11):2025-2033.

17. Bandelow B*, et al.* (2017) Biological markers for anxiety disorders, OCD and PTSD: A consensus statement. Part II: Neurochemistry, neurophysiology and neurocognition. *The world journal of biological psychiatry : the official journal of the World Federation of Societies of Biological Psychiatry* 18(3):162-214.

18. Chao HT*, et al.* (2010) Dysfunction in GABA signalling mediates autism-like stereotypies and Rett syndrome phenotypes. *Nature* 468(7321):263-269.

19. Coghlan S*, et al.* (2012) GABA system dysfunction in autism and related disorders: from synapse to symptoms. *Neuroscience and biobehavioral reviews* 36(9):2044-2055.

20. Robertson Caroline E, Ratai E-M, & Kanwisher N (Reduced GABAergic Action in the Autistic Brain. *Current Biology* 26(1):80-85.

21. Robertson CE, Ratai EM, & Kanwisher N (2016) Reduced GABAergic Action in the Autistic Brain. *Current biology : CB* 26(1):80-85.

22. Wang H, Pati S, Pozzo-Miller L, & Doering LC (2015) Targeted pharmacological treatment of autism spectrum disorders: fragile X and Rett syndromes. *Frontiers in cellular neuroscience* 9:55.

23. Lozano R, Martinez-Cerdeno V, & Hagerman RJ (2015) Advances in the Understanding of the Gabaergic Neurobiology of FMR1 Expanded Alleles Leading to Targeted Treatments for Fragile X Spectrum Disorder. *Current pharmaceutical design* 21(34):4972-4979.

24. Bristow GC, Bostrom JA, Haroutunian V, & Sodhi MS (2015) Sex differences in GABAergic gene expression occur in the anterior cingulate cortex in schizophrenia. *Schizophrenia research* 167(0):57-63.

25. Wijtenburg SA, Yang S, Fischer BA, & Rowland LM (2015) In Vivo Assessment of Neurotransmitters and Modulators with Magnetic Resonance Spectroscopy: Application to Schizophrenia. *Neuroscience and biobehavioral reviews* 51:276-295.

26. Gonzalez-Burgos G, Hashimoto T, & Lewis DA (2010) Alterations of Cortical GABA Neurons and Network Oscillations in Schizophrenia. *Current psychiatry reports* 12(4):335-344.

27. Scharfman HE & Brooks-Kayal AR (2014) Is Plasticity of GABAergic Mechanisms Relavant to Epileptogenesis? *Advances in experimental medicine and biology* 813:133-150.

28. Blicher JU*, et al.* (2015) GABA Levels Are Decreased After Stroke and GABA Changes During Rehabilitation Correlate With Motor Improvement. *Neurorehabilitation and neural repair* 29(3):278-286.

29. Carmichael ST (2012) Brain Excitability in Stroke: The Yin and Yang of Stroke Progression. *Archives of neurology* 69(2):161-167.

30. Wu C & Sun D (2015) GABA receptors in brain development, function, and injury. *Metabolic brain disease* 30(2):367-379.

31. Guerriero RM, Giza CC, & Rotenberg A (2015) Glutamate and GABA imbalance following traumatic brain injury. *Current neurology and neuroscience reports* 15(5):27-27.

32. Uusi-Oukari M & Korpi ER (2010) Regulation of GABA(A) receptor subunit expression by pharmacological agents. *Pharmacological reviews* 62(1):97-135.

33. Vinkers CH & Olivier B (2012) Mechanisms Underlying Tolerance after Long-Term Benzodiazepine Use: A Future for Subtype-Selective GABA(A) Receptor Modulators? *Advances in pharmacological sciences* 2012:416864.

34. Olsen RW (2018) GABAA receptor: Positive and negative allosteric modulators. *Neuropharmacology* 136(Pt A):10-22.

35. Miller PS & Aricescu AR (2014) Crystal structure of a human GABAA receptor. *Nature* 512(7514):270-275.

36. Zhu S*, et al.* (2018) Structure of a human synaptic GABAA receptor. *Nature* 559(7712):67-72.

37. Miller PS*, et al.* (2017) Structural basis for GABAA receptor potentiation by neurosteroids. *Nature structural & molecular biology* 24(11):986-992.

38. Laverty D*, et al.* (2019) Cryo-EM structure of the human alpha1beta3gamma2 GABAA receptor in a lipid bilayer. *Nature* 565(7740):516-520.

39. Masiulis S*, et al.* (2019) GABAA receptor signalling mechanisms revealed by structural pharmacology. *Nature* 565(7740):454-459.

40. Phulera S*, et al.* (2018) Cryo-EM structure of the benzodiazepine-sensitive α1β1γ2S tri-heteromeric GABAA receptor in complex with GABA. *eLife* 7:e39383.

41. Walters RJ, Hadley SH, Morris KD, & Amin J (2000) Benzodiazepines act on GABAA receptors via two distinct and separable mechanisms. *Nature neuroscience* 3(12):1274-1281.

42. Wick JY (2013) The history of benzodiazepines. *The Consultant pharmacist : the journal of the American Society of Consultant Pharmacists* 28(9):538-548.

43. Calcaterra NE & Barrow JC (2014) Classics in chemical neuroscience: diazepam (valium). *ACS chemical neuroscience* 5(4):253-260.

44. Olfson M, King M, & Schoenbaum M (2015) Benzodiazepine use in the United States. *JAMA psychiatry* 72(2):136-142.

45. Maust DT, Lin LA, & Blow FC (2019) Benzodiazepine Use and Misuse Among Adults in the United States. *Psychiatric services (Washington, D.C.)* 70(2):97-106.

46. Bateson AN (2002) Basic pharmacologic mechanisms involved in benzodiazepine tolerance and withdrawal. *Current pharmaceutical design* 8(1):5-21.

47. Pratt JA, Brett RR, & Laurie DJ (1998) Benzodiazepine dependence: from neural circuits to gene expression. *Pharmacology, biochemistry, and behavior* 59(4):925-934.

48. Cameron OG*, et al.* (2007) Reduced gamma-aminobutyric acid(A)-benzodiazepine binding sites in insular cortex of individuals with panic disorder. *Archives of general psychiatry* 64(7):793-800.

49. Blumenfeld RS & Ranganath C (2007) Prefrontal cortex and long-term memory encoding: an integrative review of findings from neuropsychology and neuroimaging. *The Neuroscientist : a review journal bringing neurobiology, neurology and psychiatry* 13(3):280-291.

50. Muzur A, Pace-Schott EF, & Hobson JA (2002) The prefrontal cortex in sleep. *Trends in cognitive sciences* 6(11):475-481.

51. Gallager DW, Lakoski JM, Gonsalves SF, & Rauch SL (1984) Chronic benzodiazepine treatment decreases postsynaptic GABA sensitivity. *Nature* 308(5954):74-77.

52. Marley RJ & Gallager DW (1989) Chronic diazepam treatment produces regionally specific changes in GABA-stimulated chloride influx. *European journal of pharmacology* 159(3):217-223.

53. Luscher B, Fuchs T, & Kilpatrick CL (2011) GABAA receptor trafficking-mediated plasticity of inhibitory synapses. *Neuron* 70(3):385-409.

54. Jacob TC*, et al.* (2005) Gephyrin regulates the cell surface dynamics of synaptic GABAA receptors. *The Journal of neuroscience : the official journal of the Society for Neuroscience* 25(45):10469-10478.

55. Kneussel M*, et al.* (1999) Loss of postsynaptic GABA(A) receptor clustering in gephyrin-deficient mice. *The Journal of neuroscience : the official journal of the Society for Neuroscience* 19(21):9289-9297.

56. Kneussel M*, et al.* (2001) Gephyrin-independent clustering of postsynaptic GABA(A) receptor subtypes. *Molecular and cellular neurosciences* 17(6):973-982.

57. Levi S, Logan SM, Tovar KR, & Craig AM (2004) Gephyrin is critical for glycine receptor clustering but not for the formation of functional GABAergic synapses in hippocampal neurons. *The Journal of neuroscience : the official journal of the Society for Neuroscience* 24(1):207-217.

58. Giesemann T*, et al.* (2003) Complex formation between the postsynaptic scaffolding protein gephyrin, profilin, and Mena: a possible link to the microfilament system. *The Journal of neuroscience : the official journal of the Society for Neuroscience* 23(23):8330-8339.

59. Tretter V*, et al.* (2012) Gephyrin, the enigmatic organizer at GABAergic synapses. *Front Cell Neurosci* 6:23.

60. Kneussel M & Betz H (2000) Clustering of inhibitory neurotransmitter receptors at developing postsynaptic sites: the membrane activation model. *Trends in neurosciences* 23(9):429-435.

61. Saiyed T*, et al.* (2007) Molecular basis of gephyrin clustering at inhibitory synapses: role of G- and E-domain interactions. *The Journal of biological chemistry* 282(8):5625-5632.

62. Kowalczyk S*, et al.* (2013) Direct binding of GABAA receptor beta2 and beta3 subunits to gephyrin. *The European journal of neuroscience* 37(4):544-554.

63. Brady ML & Jacob TC (2015) Synaptic localization of alpha5 GABA (A) receptors via gephyrin interaction regulates dendritic outgrowth and spine maturation. *Developmental neurobiology* 75(11):1241-1251.

64. Wu X*, et al.* (2012) gamma-Aminobutyric acid type A (GABAA) receptor alpha subunits play a direct role in synaptic versus extrasynaptic targeting. *J Biol Chem* 287(33):27417-27430.

65. Tretter V*, et al.* (2008) The clustering of GABA(A) receptor subtypes at inhibitory synapses is facilitated via the direct binding of receptor alpha 2 subunits to gephyrin. *The Journal of neuroscience : the official journal of the Society for Neuroscience* 28(6):1356-1365.

66. Gunther U*, et al.* (1995) Benzodiazepine-insensitive mice generated by targeted disruption of the gamma 2 subunit gene of gamma-aminobutyric acid type A receptors. *Proc Natl Acad Sci U S A* 92(17):7749-7753.

67. Essrich C, Lorez M, Benson JA, Fritschy JM, & Luscher B (1998) Postsynaptic clustering of major GABAA receptor subtypes requires the gamma 2 subunit and gephyrin. *Nature neuroscience* 1(7):563-571.

68. Kerti-Szigeti K, Nusser Z, & Eyre MD (2014) Synaptic GABA<sub>A</sub> Receptor Clustering without the γ2 Subunit. *The Journal of Neuroscience* 34(31):10219-10233.

69. Levi S, Le Roux N, Eugene E, & Poncer JC (2015) Benzodiazepine ligands rapidly influence GABAA receptor diffusion and clustering at hippocampal inhibitory synapses. *Neuropharmacology* 88:199-208.

70. Gouzer G, Specht CG, Allain L, Shinoe T, & Triller A (2014) Benzodiazepine-dependent stabilization of GABA(A) receptors at synapses. *Mol Cell Neurosci* 63:101-113.

71. Herweg J & Schwarz G (2012) Splice-specific glycine receptor binding, folding, and phosphorylation of the scaffolding protein gephyrin. *The Journal of biological chemistry* 287(16):12645-12656.

72. Kuhse J*, et al.* (2012) Phosphorylation of gephyrin in hippocampal neurons by cyclin-dependent kinase CDK5 at Ser-270 is dependent on collybistin. *The Journal of biological chemistry* 287(37):30952-30966.

73. Tyagarajan SK*, et al.* (2013) Extracellular signal-regulated kinase and glycogen synthase kinase 3beta regulate gephyrin postsynaptic aggregation and GABAergic synaptic function in a calpain-dependent mechanism. *J Biol Chem* 288(14):9634-9647.

74. Tyagarajan SK*, et al.* (2011) Regulation of GABAergic synapse formation and plasticity by GSK3beta-dependent phosphorylation of gephyrin. *Proceedings of the National Academy of Sciences of the United States of America* 108(1):379-384.

75. Kalbouneh H, Schlicksupp A, Kirsch J, & Kuhse J (2014) Cyclin-dependent kinase 5 is involved in the phosphorylation of gephyrin and clustering of GABAA receptors at inhibitory synapses of hippocampal neurons. *PloS one* 9(8):e104256.

76. Wuchter J*, et al.* (2012) A comprehensive small interfering RNA screen identifies signaling pathways required for gephyrin clustering. *The Journal of neuroscience : the official journal of the Society for Neuroscience* 32(42):14821-14834.

77. Flores CE*, et al.* (2015) Activity-dependent inhibitory synapse remodeling through gephyrin phosphorylation. *Proceedings of the National Academy of Sciences of the United States of America* 112(1):E65-72.

78. Varoqueaux F*, et al.* (2006) Neuroligins determine synapse maturation and function. *Neuron* 51(6):741-754.

79. Graf ER, Zhang X, Jin SX, Linhoff MW, & Craig AM (2004) Neurexins induce differentiation of GABA and glutamate postsynaptic specializations via neuroligins. *Cell* 119(7):1013-1026.

80. Krueger DD, Tuffy LP, Papadopoulos T, & Brose N (2012) The role of neurexins and neuroligins in the formation, maturation, and function of vertebrate synapses. *Current opinion in neurobiology* 22(3):412-422.

81. Zhang C*, et al.* (2010) Neurexins physically and functionally interact with GABA(A) receptors. *Neuron* 66(3):403-416.

82. Dong N, Qi J, & Chen G (2007) Molecular reconstitution of functional GABAergic synapses with expression of neuroligin-2 and GABAA receptors. *Molecular and cellular neurosciences* 35(1):14-23.

83. Hoon M*, et al.* (2009) Neuroligin 2 controls the maturation of GABAergic synapses and information processing in the retina. *The Journal of neuroscience : the official journal of the Society for Neuroscience* 29(25):8039-8050.

84. Fu Z & Vicini S (2009) Neuroligin-2 accelerates GABAergic synapse maturation in cerebellar granule cells. *Molecular and cellular neurosciences* 42(1):45-55.

85. Brown LE*, et al.* (2014) Inhibitory synapse formation in a co-culture model incorporating GABAergic medium spiny neurons and HEK293 cells stably expressing GABAA receptors. *Journal of visualized experiments : JoVE* (93):e52115.

86. Chubykin AA*, et al.* (2007) Activity-dependent validation of excitatory versus inhibitory synapses by neuroligin-1 versus neuroligin-2. *Neuron* 54(6):919-931.

87. Nakamura Y*, et al.* (2016) Proteomic characterization of inhibitory synapses using a novel pHluorin-tagged GABAAR alpha2 subunit knock-in mouse. *The Journal of biological chemistry*.

88. Uezu A*, et al.* (2016) Identification of an elaborate complex mediating postsynaptic inhibition. *Science* 353(6304):1123-1129.

89. Saxena NC & Macdonald RL (1996) Properties of putative cerebellar gamma-aminobutyric acid A receptor isoforms. *Molecular pharmacology* 49(3):567-579.

90. Haas KF & Macdonald RL (1999) GABAA receptor subunit gamma2 and delta subtypes confer unique kinetic properties on recombinant GABAA receptor currents in mouse fibroblasts. *The Journal of physiology* 514 ( Pt 1):27-45.

91. Ke Y, Cohen BM, Bang JY, Yang M, & Renshaw PF (2000) Assessment of GABA concentration in human brain using two-dimensional proton magnetic resonance spectroscopy. *Psychiatry research* 100(3):169-178.

92. Bianchi MT, Haas KF, & Macdonald RL (2001) Structural determinants of fast desensitization and desensitization-deactivation coupling in GABAa receptors. *The Journal of neuroscience : the official journal of the Society for Neuroscience* 21(4):1127-1136.

93. Brown N, Kerby J, Bonnert TP, Whiting PJ, & Wafford KA (2002) Pharmacological characterization of a novel cell line expressing human alpha(4)beta(3)delta GABA(A) receptors. *British journal of pharmacology* 136(7):965-974.

94. Terpstra M, Ugurbil K, & Gruetter R (2002) Direct in vivo measurement of human cerebral GABA concentration using MEGA-editing at 7 Tesla. *Magnetic resonance in medicine* 47(5):1009-1012.

95. Glykys J & Mody I (2007) The main source of ambient GABA responsible for tonic inhibition in the mouse hippocampus. *The Journal of physiology* 582(Pt 3):1163-1178.

96. Liu QY, Schaffner AE, Chang YH, Maric D, & Barker JL (2000) Persistent activation of GABA(A) receptor/Cl(-) channels by astrocyte-derived GABA in cultured embryonic rat hippocampal neurons. *Journal of neurophysiology* 84(3):1392-1403.

97. Kozlov AS, Angulo MC, Audinat E, & Charpak S (2006) Target cell-specific modulation of neuronal activity by astrocytes. *Proceedings of the National Academy of Sciences of the United States of America* 103(26):10058-10063.

98. Olah S*, et al.* (2009) Regulation of cortical microcircuits by unitary GABA-mediated volume transmission. *Nature* 461(7268):1278-1281.

99. Wlodarczyk AI*, et al.* (2013) GABA-independent GABAA receptor openings maintain tonic currents. *The Journal of neuroscience : the official journal of the Society for Neuroscience* 33(9):3905-3914.

100. Brunig I, Scotti E, Sidler C, & Fritschy JM (2002) Intact sorting, targeting, and clustering of gamma-aminobutyric acid A receptor subtypes in hippocampal neurons in vitro. *The Journal of comparative neurology* 443(1):43-55.

101. Crestani F*, et al.* (2002) Trace fear conditioning involves hippocampal alpha5 GABA(A) receptors. *Proceedings of the National Academy of Sciences of the United States of America* 99(13):8980-8985.

102. Serwanski DR*, et al.* (2006) Synaptic and nonsynaptic localization of GABAA receptors containing the alpha5 subunit in the rat brain. *The Journal of comparative neurology* 499(3):458-470.

103. Zarnowska ED, Keist R, Rudolph U, & Pearce RA (2009) GABAA receptor alpha5 subunits contribute to GABAA,slow synaptic inhibition in mouse hippocampus. *Journal of neurophysiology* 101(3):1179-1191.

104. Loebrich S, Bahring R, Katsuno T, Tsukita S, & Kneussel M (2006) Activated radixin is essential for GABAA receptor alpha5 subunit anchoring at the actin cytoskeleton. *Embo J* 25(5):987-999.

105. Barberis A (2019) Postsynaptic plasticity of GABAergic synapses. *Neuropharmacology*:107643.

106. Hausrat TJ*, et al.* (2015) Radixin regulates synaptic GABAA receptor density and is essential for reversal learning and short-term memory. *Nat Commun* 6:6872.

107. Gerrow K & Triller A (2014) GABAA receptor subunit composition and competition at synapses are tuned by GABAB receptor activity. *Molecular and cellular neurosciences* 60:97-107.

108. Carlson SL, Bohnsack JP, & Morrow AL (2016) Ethanol Regulation of Synaptic GABAA alpha4 Receptors Is Prevented by Protein Kinase A Activation. *The Journal of pharmacology and experimental therapeutics* 357(1):10-16.

109. Carlson SL, Bohnsack JP, Patel V, & Morrow AL (2016) Regulation of Extrasynaptic GABAA alpha4 Receptors by Ethanol-Induced Protein Kinase A, but Not Protein Kinase C Activation in Cultured Rat Cerebral Cortical Neurons. *The Journal of pharmacology and experimental therapeutics* 356(1):148-156.

110. Krishek BJ, Moss SJ, & Smart TG (1996) Homomeric beta 1 gamma-aminobutyric acid A receptor-ion channels: evaluation of pharmacological and physiological properties. *Mol Pharmacol* 49(3):494-504.

111. Wooltorton JR, Moss SJ, & Smart TG (1997) Pharmacological and physiological characterization of murine homomeric beta3 GABA(A) receptors. *Eur J Neurosci* 9(11):2225-2235.

112. Angelotti TP & Macdonald RL (1993) Assembly of GABAA receptor subunits: alpha 1 beta 1 and alpha 1 beta 1 gamma 2S subunits produce unique ion channels with dissimilar single-channel properties. *The Journal of neuroscience : the official journal of the Society for Neuroscience* 13(4):1429-1440.

113. Draguhn A, Verdorn TA, Ewert M, Seeburg PH, & Sakmann B (1990) Functional and molecular distinction between recombinant rat GABAA receptor subtypes by Zn2+. *Neuron* 5(6):781-788.

114. Wong LW, Tae HS, & Cromer BA (2015) Assembly, trafficking and function of alpha1beta2gamma2 GABAA receptors are regulated by N-terminal regions, in a subunit-specific manner. *Journal of neurochemistry* 134(5):819-832.

115. Bradley CA, Taghibiglou C, Collingridge GL, & Wang YT (2008) Mechanisms involved in the reduction of GABAA receptor alpha1-subunit expression caused by the epilepsy mutation A322D in the trafficking-competent receptor. *The Journal of biological chemistry* 283(32):22043-22050.

116. Gallagher MJ, Ding L, Maheshwari A, & Macdonald RL (2007) The GABAA receptor alpha1 subunit epilepsy mutation A322D inhibits transmembrane helix formation and causes proteasomal degradation. *Proc Natl Acad Sci U S A* 104(32):12999-13004.

117. Saliba RS, Michels G, Jacob TC, Pangalos MN, & Moss SJ (2007) Activity-dependent ubiquitination of GABA(A) receptors regulates their accumulation at synaptic sites. *The Journal of neuroscience : the official journal of the Society for Neuroscience* 27(48):13341-13351.

118. Saliba RS, Gu Z, Yan Z, & Moss SJ (2009) Blocking L-type voltage-gated Ca2+ channels with dihydropyridines reduces gamma-aminobutyric acid type A receptor expression and synaptic inhibition. *The Journal of biological chemistry* 284(47):32544-32550.

119. Saliba RS, Kretschmannova K, & Moss SJ (2012) Activity-dependent phosphorylation of GABAA receptors regulates receptor insertion and tonic current. *Embo j* 31(13):2937-2951.

120. Huang X, Hernandez CC, Hu N, & Macdonald RL (2014) Three epilepsy-associated GABRG2 missense mutations at the gamma+/beta- interface disrupt GABAA receptor assembly and trafficking by similar mechanisms but to different extents. *Neurobiology of disease* 68:167-179.

121. Cossette P*, et al.* (2002) Mutation of GABRA1 in an autosomal dominant form of juvenile myoclonic epilepsy. *Nat Genet* 31(2):184-189.

122. Crider A, Pandya CD, Peter D, Ahmed AO, & Pillai A (2014) Ubiquitin-proteasome dependent degradation of GABAAalpha1 in autism spectrum disorder. *Molecular autism* 5:45.

123. Fang C*, et al.* (2006) GODZ-mediated palmitoylation of GABA(A) receptors is required for normal assembly and function of GABAergic inhibitory synapses. *The Journal of neuroscience : the official journal of the Society for Neuroscience* 26(49):12758-12768.

124. Keller CA*, et al.* (2004) The gamma2 subunit of GABA(A) receptors is a substrate for palmitoylation by GODZ. *The Journal of neuroscience : the official journal of the Society for Neuroscience* 24(26):5881-5891.

125. Kilpatrick CL*, et al.* (2016) Dissociation of Golgi-Associated DHHC-Type Zinc Finger Protein (GODZ) and Sertoli Cell Gene with a Zinc Finger Domain-β (SERZ-β)-Mediated Palmitoylation by Loss of Function Analyses in Knockout Mice. *Journal of Biological Chemistry*.

126. Gu Y*, et al.* (2016) Differential vesicular sorting of AMPA and GABAA receptors. *Proceedings of the National Academy of Sciences* 113(7):E922-E931.

127. Charych EI*, et al.* (2004) The brefeldin A-inhibited GDP/GTP exchange factor 2, a protein involved in vesicular trafficking, interacts with the beta subunits of the GABA receptors. *Journal of neurochemistry* 90(1):173-189.

128. Wang H, Bedford FK, Brandon NJ, Moss SJ, & Olsen RW (1999) GABA(A)-receptor-associated protein links GABA(A) receptors and the cytoskeleton. *Nature* 397(6714):69-72.

129. Charych EI, *et al.* (2004) A four PDZ domain-containing splice variant form of GRIP1 is localized in GABAergic and glutamatergic synapses in the brain. *The Journal of biological chemistry* 279(37):38978-38990.

130. Kittler JT, Arancibia-Carcamo IL, & Moss SJ (2004) Association of GRIP1 with a GABA(A) receptor associated protein suggests a role for GRIP1 at inhibitory synapses. *Biochemical pharmacology* 68(8):1649-1654.

131. Uji A, *et al.* (2002) Molecules interacting with PRIP-2, a novel Ins(1,4,5)P3 binding protein type 2: Comparison with PRIP-1. *Life sciences* 72(4-5):443-453.

132. Kanematsu T, *et al.* (2002) Role of the PLC-related, catalytically inactive protein p130 in GABA(A) receptor function. *Embo j* 21(5):1004-1011.

133. Beck M, *et al.* (2002) Identification, molecular cloning, and characterization of a novel GABAA receptor-associated protein, GRIF-1. *The Journal of biological chemistry* 277(33):30079-30090.

134. Smith KR, *et al.* (2010) Identification and characterisation of a Maf1/Macoco protein complex that interacts with GABAA receptors in neurons. *Mol Cell Neurosci* 44(4):330-341.

135. Goto H, *et al.* (2005) Direct interaction of N-ethylmaleimide-sensitive factor with GABA(A) receptor beta subunits. *Mol Cell Neurosci* 30(2):197-206.

136. Twelvetrees AE, *et al.* (2010) Delivery of GABAARs to synapses is mediated by HAP1-KIF5 and disrupted by mutant huntingtin. *Neuron* 65(1):53-65.

137. Kittler JT, *et al.* (2000) Constitutive endocytosis of GABAA receptors by an association with the adaptin AP2 complex modulates inhibitory synaptic currents in hippocampal neurons. *The Journal of neuroscience : the official journal of the Society for Neuroscience* 20(21):7972-7977.

138. Cinar H & Barnes EM, Jr. (2001) Clathrin-independent endocytosis of GABA(A) receptors in HEK 293 cells. *Biochemistry* 40(46):14030-14036.

139. Rowland AM, Richmond JE, Olsen JG, Hall DH, & Bamber BA (2006) Presynaptic terminals independently regulate synaptic clustering and autophagy of GABAA receptors in Caenorhabditis elegans. *The Journal of neuroscience : the official journal of the Society for Neuroscience* 26(6):1711-1720.

140. McDonald BJ, *et al.* (1998) Adjacent phosphorylation sites on GABAA receptor beta subunits determine regulation by cAMP-dependent protein kinase. *Nature neuroscience* 1(1):23-28.

141. Brandon N, Jovanovic J, & Moss S (2002) Multiple roles of protein kinases in the modulation of gamma-aminobutyric acid(A) receptor function and cell surface expression. *Pharmacology & therapeutics* 94(1-2):113-122.

142. Brandon NJ, *et al.* (2003) A-kinase anchoring protein 79/150 facilitates the phosphorylation of GABA(A) receptors by cAMP-dependent protein kinase via selective interaction with receptor beta subunits. *Molecular and cellular neurosciences* 22(1):87-97.

143. Kittler JT, *et al.* (2005) Phospho-dependent binding of the clathrin AP2 adaptor complex to GABAA receptors regulates the efficacy of inhibitory synaptic transmission. *Proceedings of the National Academy of Sciences of the United States of America* 102(41):14871-14876.

144. Smith KR, *et al.* (2008) Regulation of inhibitory synaptic transmission by a conserved atypical interaction of GABA(A) receptor beta- and gamma-subunits with the clathrin AP2 adaptor. *Neuropharmacology* 55(5):844-850.

145. Herring D, Huang R, Singh M, Dillon GH, & Leidenheimer NJ (2005) PKC modulation of GABAA receptor endocytosis and function is inhibited by mutation of a dileucine motif within the receptor beta 2 subunit. *Neuropharmacology* 48(2):181-194.

146. Smith KR, *et al.* (2012) Stabilization of GABA(A) receptors at endocytic zones is mediated by an AP2 binding motif within the GABA(A) receptor beta3 subunit. *The Journal of neuroscience : the official journal of the Society for Neuroscience* 32(7):2485-2498.

147. Jacob TC, *et al.* (2009) GABA(A) receptor membrane trafficking regulates spine maturity. *Proceedings of the National Academy of Sciences of the United States of America* 106(30):12500-12505.

148. Vien TN, *et al.* (2015) Compromising the phosphodependent regulation of the GABAAR beta3 subunit reproduces the core phenotypes of autism spectrum disorders. *Proc Natl Acad Sci U S A* 112(48):14805-14810.

149. Kumar S, *et al.* (2010) Ethanol reduces GABAA alpha1 subunit receptor surface expression by a protein kinase Cgamma-dependent mechanism in cultured cerebral cortical neurons. *Molecular pharmacology* 77(5):793-803.

150. Qi ZH, *et al.* (2007) Protein kinase C epsilon regulates gamma-aminobutyrate type A receptor sensitivity to ethanol and benzodiazepines through phosphorylation of gamma2 subunits. *The Journal of biological chemistry* 282(45):33052-33063.

151. Brandon NJ, Delmas P, Hill J, Smart TG, & Moss SJ (2001) Constitutive tyrosine phosphorylation of the GABA(A) receptor gamma 2 subunit in rat brain. *Neuropharmacology* 41(6):745-752.

152. Jurd R, Tretter V, Walker J, Brandon NJ, & Moss SJ (2010) Fyn kinase contributes to tyrosine phosphorylation of the GABA(A) receptor gamma2 subunit. *Molecular and cellular neurosciences* 44(2):129-134.

153. Kittler JT, *et al.* (2008) Regulation of synaptic inhibition by phospho-dependent binding of the AP2 complex to a YECL motif in the GABAA receptor gamma2 subunit. *Proceedings of the National Academy of Sciences of the United States of America* 105(9):3616-3621.

154. Tretter V, *et al.* (2009) Deficits in spatial memory correlate with modified {gamma}-aminobutyric acid type A receptor tyrosine phosphorylation in the hippocampus. *Proceedings of the National Academy of Sciences of the United States of America* 106(47):20039-20044.

155. Vithlani M, *et al.* (2013) The ability of BDNF to modify neurogenesis and depressive-like behaviors is dependent upon phosphorylation of tyrosine residues 365/367 in the GABA(A)-receptor gamma2 subunit. *The Journal of neuroscience : the official journal of the Society for Neuroscience* 33(39):15567-15577.

156. Naylor DE, Liu H, & Wasterlain CG (2005) Trafficking of GABA(A) receptors, loss of inhibition, and a mechanism for pharmacoresistance in status epilepticus. *The Journal of neuroscience : the official journal of the Society for Neuroscience* 25(34):7724-7733.

157. Goodkin HP, Joshi S, Mtchedlishvili Z, Brar J, & Kapur J (2008) Subunit-specific trafficking of GABA(A) receptors during status epilepticus. *The Journal of neuroscience : the official journal of the Society for Neuroscience* 28(10):2527-2538.

158. Goodkin HP, Yeh JL, & Kapur J (2005) Status epilepticus increases the intracellular accumulation of GABAA receptors. *The Journal of neuroscience : the official journal of the Society for Neuroscience* 25(23):5511-5520.

159. Arancibia-Carcamo IL, *et al.* (2009) Ubiquitin-dependent lysosomal targeting of GABA(A) receptors regulates neuronal inhibition. *Proceedings of the National Academy of Sciences of the United States of America* 106(41):17552-17557.

160. Chaumont S, *et al.* (2013) Agonist-dependent endocytosis of gamma-aminobutyric acid type A (GABAA) receptors revealed by a gamma2(R43Q) epilepsy mutation. *The Journal of biological chemistry* 288(39):28254-28265.

161. Joshi S, *et al.* (2015) Phosphatase inhibition prevents the activity-dependent trafficking of GABAA receptors during status epilepticus in the young animal. *Epilepsia* 56(9):1355-1365.

162. Eckel R, Szulc B, Walker MC, & Kittler JT (2015) Activation of calcineurin underlies altered trafficking of alpha2 subunit containing GABAA receptors during prolonged epileptiform activity. *Neuropharmacology* 88:82-90.

163. Chávez AE, Hernández VM, Rodenas-Ruano A, Chan CS, & Castillo PE (2014) Compartment-Specific Modulation of GABAergic Synaptic Transmission by TRPV1 Channels in the Dentate Gyrus. *The Journal of Neuroscience* 34(50):16621-16629.

164. Pribiag H & Stellwagen D (2013) TNF-alpha downregulates inhibitory neurotransmission through protein phosphatase 1-dependent trafficking of GABA(A) receptors. *The Journal of neuroscience : the official journal of the Society for Neuroscience* 33(40):15879-15893.

165. Ulrich D (2015) Amyloid-beta Impairs Synaptic Inhibition via GABA(A) Receptor Endocytosis. *The Journal of neuroscience : the official journal of the Society for Neuroscience* 35(24):9205-9210.

166. Kittler JT*, et al.* (2004) Huntingtin-associated protein 1 regulates inhibitory synaptic transmission by modulating gamma-aminobutyric acid type A receptor membrane trafficking. *Proceedings of the National Academy of Sciences of the United States of America* 101(34):12736-12741.

167. Mele M, Aspromonte MC, & Duarte CB (2017) Downregulation of GABAA Receptor Recycling Mediated by HAP1 Contributes to Neuronal Death in In Vitro Brain Ischemia. *Molecular neurobiology* 54(1):45-57.

168. Yuan X*, et al.* (2008) Calcium-modulating cyclophilin ligand regulates membrane trafficking of postsynaptic GABA(A) receptors. *Molecular and cellular neurosciences* 38(2):277-289.

169. Jacob TC*, et al.* (2012) Benzodiazepine treatment induces subtype-specific changes in GABA(A) receptor trafficking and decreases synaptic inhibition. *Proceedings of the National Academy of Sciences of the United States of America* 109(45):18595-18600.

170. Jin H*, et al.* (2014) Ring finger protein 34 (RNF34) interacts with and promotes gamma-aminobutyric acid type-A receptor degradation via ubiquitination of the gamma2 subunit. *The Journal of biological chemistry* 289(42):29420-29436.

171. Liu T, Li H, Hong W, & Han W (2016) Brefeldin A-inhibited guanine nucleotide exchange protein 3 is localized in lysosomes and regulates GABA signaling in hippocampal neurons. *Journal of neurochemistry* 139(5):748-756.

172. Flores CE & Méndez P (2014) Shaping inhibition: activity dependent structural plasticity of GABAergic synapses. *Frontiers in cellular neuroscience* 8:327.

173. Maguire J (2014) Stress-induced plasticity of GABAergic inhibition. *Frontiers in cellular neuroscience* 8:157.

174. Nakamura Y, Darnieder LM, Deeb TZ, & Moss SJ (2015) Regulation of GABAARs by phosphorylation. *Advances in pharmacology (San Diego, Calif.)* 72:97-146.

175. Wang RA, Cheng G, Kolaj M, & Randic M (1995) Alpha-subunit of calcium/calmodulin-dependent protein kinase II enhances gamma-aminobutyric acid and inhibitory synaptic responses of rat neurons in vitro. *Journal of neurophysiology* 73(5):2099-2106.

176. Nusser Z, Hajos N, Somogyi P, & Mody I (1998) Increased number of synaptic GABA(A) receptors underlies potentiation at hippocampal inhibitory synapses. *Nature* 395(6698):172-177.

177. Marsden KC, Beattie JB, Friedenthal J, & Carroll RC (2007) NMDA Receptor Activation Potentiates Inhibitory Transmission through GABA Receptor-Associated Protein-Dependent Exocytosis of GABAA Receptors. pp 14326-14337.

178. Marsden KC, Shemesh A, Bayer KU, & Carroll RC (2010) Selective translocation of Ca2+/calmodulin protein kinase IIalpha (CaMKIIalpha) to inhibitory synapses. *Proceedings of the National Academy of Sciences of the United States of America* 107(47):20559-20564.

179. Petrini EM*, et al.* (2014) Synaptic recruitment of gephyrin regulates surface GABAA receptor dynamics for the expression of inhibitory LTP. *Nat Commun* 5:10.1038/ncomms4921.

180. Bannai H*, et al.* (2015) Bidirectional Control of Synaptic GABAAR Clustering by Glutamate and Calcium. *Cell reports* 13(12):2768-2780.

181. Marsden KC, Beattie JB, Friedenthal J, & Carroll RC (2007) NMDA receptor activation potentiates inhibitory transmission through GABA receptor-associated protein-dependent exocytosis of GABA(A) receptors. *The Journal of neuroscience : the official journal of the Society for Neuroscience* 27(52):14326-14337.

182. Bannai H*, et al.* (2009) Activity-dependent tuning of inhibitory neurotransmission based on GABAAR diffusion dynamics. *Neuron* 62(5):670-682.

183. Muir J*, et al.* (2010) NMDA receptors regulate GABAA receptor lateral mobility and clustering at inhibitory synapses through serine 327 on the gamma2 subunit. *Proceedings of the National Academy of Sciences of the United States of America* 107(38):16679-16684.

184. Lu YM, Mansuy IM, Kandel ER, & Roder J (2000) Calcineurin-mediated LTD of GABAergic inhibition underlies the increased excitability of CA1 neurons associated with LTP. *Neuron* 26(1):197-205.

185. Wang J*, et al.* (2003) Interaction of calcineurin and type-A GABA receptor gamma 2 subunits produces long-term depression at CA1 inhibitory synapses. *The Journal of neuroscience : the official journal of the Society for Neuroscience* 23(3):826-836.

186. Morishita W & Sastry BR (1996) Postsynaptic mechanisms underlying long-term depression of GABAergic transmission in neurons of the deep cerebellar nuclei. *Journal of neurophysiology* 76(1):59-68.

187. Ouardouz M & Sastry BR (2000) Mechanisms underlying LTP of inhibitory synaptic transmission in the deep cerebellar nuclei. *Journal of neurophysiology* 84(3):1414-1421.

188. Specht Christian G*, et al.* (2013) Quantitative Nanoscopy of Inhibitory Synapses: Counting Gephyrin Molecules and Receptor Binding Sites. *Neuron* 79(2):308-321.

189. Kilman V, van Rossum MC, & Turrigiano GG (2002) Activity deprivation reduces miniature IPSC amplitude by decreasing the number of postsynaptic GABA(A) receptors clustered at neocortical synapses. *J Neurosci* 22(4):1328-1337.

190. Fuchs JL & Salazar E (1998) Effects of whisker trimming on GABAA receptor binding in the barrel cortex of developing and adult rats. *The Journal of Comparative Neurology* 395(2):209-216.

191. Gainey MA, Wolfe R, Pourzia O, & Feldman DE (2016) Whisker Deprivation Drives Two Phases of Inhibitory Synapse Weakening in Layer 4 of Rat Somatosensory Cortex. *PLoS ONE* 11(2):e0148227.

192. Micheva KD & Beaulieu C (1995) Neonatal sensory deprivation induces selective changes in the quantitative distribution of GABA-immunoreactive neurons in the rat barrel field cortex. *J Comp Neurol* 361(4):574-584.

193. Jasinska M*, et al.* (2010) Rapid, learning-induced inhibitory synaptogenesis in murine barrel field. *The Journal of neuroscience : the official journal of the Society for Neuroscience* 30(3):1176-1184.

194. Chen JL*, et al.* (2012) Clustered dynamics of inhibitory synapses and dendritic spines in the adult neocortex. *Neuron* 74(2):361-373.

195. Maffei A, Nataraj K, Nelson SB, & Turrigiano GG (2006) Potentiation of cortical inhibition by visual deprivation. *Nature* 443(7107):81-84.

196. Kurotani T, Yamada K, Yoshimura Y, Crair MC, & Komatsu Y (2008) State-dependent bidirectional modification of somatic inhibition in neocortical pyramidal cells. *Neuron* 57(6):905-916.

197. Chhatwal JP, Myers KM, Ressler KJ, & Davis M (2005) Regulation of gephyrin and GABAA receptor binding within the amygdala after fear acquisition and extinction. *The Journal of neuroscience : the official journal of the Society for Neuroscience* 25(2):502-506.

198. Lin HC, Mao SC, & Gean PW (2009) Block of gamma-aminobutyric acid-A receptor insertion in the amygdala impairs extinction of conditioned fear. *Biological psychiatry* 66(7):665-673.

199. Kang Y*, et al.* (2014) A Combined Transgenic Proteomic Analysis and Regulated Trafficking of Neuroligin-2. *Journal of Biological Chemistry* 289(42):29350-29364.

200. Loh KH*, et al.* (2016) Proteomic Analysis of Unbounded Cellular Compartments: Synaptic Clefts. *Cell* 166(5):1295-1307.e1221.

201. Lin WC*, et al.* (2014) Engineering a light-regulated GABAA receptor for optical control of neural inhibition. *ACS chemical biology* 9(7):1414-1419.

202. Lin WC*, et al.* (2015) A Comprehensive Optogenetic Pharmacology Toolkit for In Vivo Control of GABA(A) Receptors and Synaptic Inhibition. *Neuron* 88(5):879-891.

203. Oh WC, Lutzu S, Castillo PE, & Kwon HB (2016) De novo synaptogenesis induced by GABA in the developing mouse cortex. *Science (New York, N.Y.)* 353(6303):1037-1040.

204. Petrini EM & Barberis A (2014) Diffusion dynamics of synaptic molecules during inhibitory postsynaptic plasticity. *Frontiers in cellular neuroscience* 8:300.

205. Pennacchietti F*, et al.* (2017) Nanoscale molecular reorganization of the inhibitory postsynaptic density is a determinant of GABAergic synaptic potentiation. *The Journal of Neuroscience*.

206. Gross GG*, et al.* (2016) An E3-ligase-based method for ablating inhibitory synapses. *Nat Meth* 13(8):673-678.

207. Gross GG*, et al.* (2013) Recombinant probes for visualizing endogenous synaptic proteins in living neurons. *Neuron* 78(6):971-985.

208. Maric HM*, et al.* (2017) Gephyrin-binding peptides visualize postsynaptic sites and modulate neurotransmission. *Nature chemical biology* 13(2):153-160.

209. Smith KR*, et al.* (2014) GIT1 and betaPIX are essential for GABA(A) receptor synaptic stability and inhibitory neurotransmission. *Cell reports* 9(1):298-310.

210. Tseng WC, Jenkins PM, Tanaka M, Mooney R, & Bennett V (2015) Giant ankyrin-G stabilizes somatodendritic GABAergic synapses through opposing endocytosis of GABAA receptors. *Proceedings of the National Academy of Sciences of the United States of America* 112(4):1214-1219.

211. Lorenz-Guertin JM, Bambino MJ, Das S, Weintraub ST, & Jacob TC (2019) Diazepam Accelerates GABAAR Synaptic Exchange and Alters Intracellular Trafficking. *Frontiers in cellular neuroscience* 13(163).

212. Lorenz-Guertin JM*, et al.* (2017) A versatile optical tool for studying synaptic GABAA receptor trafficking. *J Cell Sci*.

213. Schweizer C (2003) The γ2 subunit of GABAA receptors is required for maintenance of receptors at mature synapses. *Molecular and Cellular Neuroscience* 24(2):442-450.

214. Sumegi M*, et al.* (2012) Virus-mediated swapping of zolpidem-insensitive with zolpidem-sensitive GABA(A) receptors in cortical pyramidal cells. *The Journal of physiology* 590(7):1517-1534.

215. Alldred MJ, Mulder-Rosi J, Lingenfelter SE, Chen G, & Luscher B (2005) Distinct gamma2 subunit domains mediate clustering and synaptic function of postsynaptic GABAA receptors and gephyrin. *The Journal of neuroscience : the official journal of the Society for Neuroscience* 25(3):594-603.

216. Rovo Z*, et al.* (2014) Phasic, nonsynaptic GABA-A receptor-mediated inhibition entrains thalamocortical oscillations. *The Journal of neuroscience : the official journal of the Society for Neuroscience* 34(21):7137-7147.

217. Möhler H, Crestani F, & Rudolph U (2001) GABAA-receptor subtypes: a new pharmacology. *Current Opinion in Pharmacology* 1(1):22-25.

218. Jacob TC, Moss SJ, & Jurd R (2008) GABA(A) receptor trafficking and its role in the dynamic modulation of neuronal inhibition. *Nature reviews. Neuroscience* 9(5):331-343.

219. Liang J*, et al.* (2007) Mechanisms of reversible GABAA receptor plasticity after ethanol intoxication. *The Journal of neuroscience : the official journal of the Society for Neuroscience* 27(45):12367-12377.

220. Shen Y*, et al.* (2011) Plasticity of GABAA receptors after ethanol pre-exposure in cultured hippocampal neurons. *Molecular pharmacology* 79(3):432-442.

221. Tehrani MH & Barnes EM, Jr. (1991) Agonist-dependent internalization of gamma-aminobutyric acidA/benzodiazepine receptors in chick cortical neurons. *Journal of neurochemistry* 57(4):1307-1312.

222. Hablitz JJ, Tehrani MH, & Barnes EM, Jr. (1989) Chronic exposure of developing cortical neurons to GABA down-regulates GABA/benzodiazepine receptors and GABA-gated chloride currents. *Brain research* 501(2):332-338.

223. Tehrani MH & Barnes EM, Jr. (1988) GABA down-regulates the GABA/benzodiazepine receptor complex in developing cerebral neurons. *Neuroscience letters* 87(3):288-292.

224. Calkin PA & Barnes EM, Jr. (1994) gamma-Aminobutyric acid-A (GABAA) agonists down-regulate GABAA/benzodiazepine receptor polypeptides from the surface of chick cortical neurons. *The Journal of biological chemistry* 269(2):1548-1553.

225. Carver CM & Reddy DS (2013) Neurosteroid interactions with synaptic and extrasynaptic GABA(A) receptors: regulation of subunit plasticity, phasic and tonic inhibition, and neuronal network excitability. *Psychopharmacology* 230(2):151-188.

226. Wan Q*, et al.* (1997) Recruitment of functional GABA(A) receptors to postsynaptic domains by insulin. *Nature* 388(6643):686-690.

227. Arancibia-Carcamo IL, Fairfax BP, Moss SJ, & Kittler JT (2006) Frontiers in Neuroscience Studying the Localization, Surface Stability and Endocytosis of Neurotransmitter Receptors by Antibody Labeling and Biotinylation Approaches. *The Dynamic Synapse: Molecular Methods in Ionotropic Receptor Biology*, eds Kittler JT & Moss SJ (CRC Press/Taylor & Francis, Taylor & Francis Group, LLC., Boca Raton (FL)).

228. Kirchhausen T (2009) Imaging endocytic clathrin structures in living cells. *Trends in cell biology* 19(11):596-605.

229. Sankaranarayanan S, De Angelis D, Rothman JE, & Ryan TA (2000) The use of pHluorins for optical measurements of presynaptic activity. *Biophysical journal* 79(4):2199-2208.

230. Asokan A & Cho MJ (2002) Exploitation of intracellular pH gradients in the cellular delivery of macromolecules. *Journal of pharmaceutical sciences* 91(4):903-913.

231. Brady ML, Moon CE, & Jacob TC (2014) Using an alpha-bungarotoxin binding site tag to study GABA A receptor membrane localization and trafficking. *Journal of visualized experiments : JoVE* (85).

232. Hannan S, Mortensen M, & Smart TG (2015) Snake neurotoxin alpha-bungarotoxin is an antagonist at native GABA(A) receptors. *Neuropharmacology* 93:28-40.

233. Szent-Gyorgyi C*, et al.* (2008) Fluorogen-activating single-chain antibodies for imaging cell surface proteins. *Nature biotechnology* 26(2):235-240.

234. Fisher GW*, et al.* (2014) Self-Checking Cell-Based Assays for GPCR Desensitization and Resensitization. *Journal of biomolecular screening* 19(8):1220-1226.

235. Saunders MJ*, et al.* (2012) Fluorogen activating proteins in flow cytometry for the study of surface molecules and receptors. *Methods* 57(3):308-317.

236. Grover A*, et al.* (2012) Genetically encoded pH sensor for tracking surface proteins through endocytosis. *Angew Chem Int Ed Engl* 51(20):4838-4842.

237. Zhang M*, et al.* (2015) Fluoromodule-based reporter/probes designed for in vivo fluorescence imaging. *The Journal of clinical investigation* 125(10):3915-3927.

238. Perkins LA*, et al.* (2017) Genetically Targeted Ratiometric and Activated pH Indicator Complexes (TRApHIC) for Receptor Trafficking. *bioRxiv*.

239. Yan Q*, et al.* (2015) Near-instant surface-selective fluorogenic protein quantification using sulfonated triarylmethane dyes and fluorogen activating proteins. *Organic & biomolecular chemistry* 13(7):2078-2086.

240. Szent-Gyorgyi C*, et al.* (2013) Malachite green mediates homodimerization of antibody VL domains to form a fluorescent ternary complex with singular symmetric interfaces. *Journal of molecular biology* 425(22):4595-4613.

241. Pratt CP, He J, Wang Y, Barth AL, & Bruchez MP (2015) Fluorogenic Green-Inside Red-Outside (GIRO) Labeling Approach Reveals Adenylyl Cyclase-Dependent Control of BKalpha Surface Expression. *Bioconjugate chemistry* 26(9):1963-1971.

242. Fisher GW*, et al.* (2010) Detection and quantification of beta2AR internalization in living cells using FAP-based biosensor technology. *Journal of biomolecular screening* 15(6):703-709.

243. Wu Y, Tapia PH, Jarvik J, Waggoner AS, & Sklar LA (2014) Real-time detection of protein trafficking with high-throughput flow cytometry (HTFC) and fluorogen-activating protein (FAP) base biosensor. *Current protocols in cytometry / editorial board, J. Paul Robinson, managing editor ... [et al.]* 67:Unit 9 43.

244. Snyder JC*, et al.* (2015) A rapid and affordable screening platform for membrane protein trafficking. *BMC biology* 13:107.

245. He J*, et al.* (2016) A genetically targetable near-infrared photosensitizer. *Nature methods* 13(3):263-268.

246. Saunders MJ*, et al.* (2013) Engineering fluorogen activating proteins into self-assembling materials. *Bioconjugate chemistry* 24(5):803-810.

247. Kittler JT*, et al.* (2000) Analysis of GABAA receptor assembly in mammalian cell lines and hippocampal neurons using gamma 2 subunit green fluorescent protein chimeras. *Mol Cell Neurosci* 16(4):440-452.

248. Bedford FK*, et al.* (2001) GABA(A) receptor cell surface number and subunit stability are regulated by the ubiquitin-like protein Plic-1. *Nat Neurosci* 4(9):908-916.

249. Lawe DC, Patki V, Heller-Harrison R, Lambright D, & Corvera S (2000) The FYVE domain of early endosome antigen 1 is required for both phosphatidylinositol 3-phosphate and Rab5 binding. Critical role of this dual interaction for endosomal localization. *The Journal of biological chemistry* 275(5):3699-3705.

250. Larsen MB, Hu J, Frizzell RA, & Watkins SC (2016) Simple image-based no-wash method for quantitative detection of surface expressed CFTR. *Methods* 96:40-45.

251. Blanpied TA, Boeckman FA, Aizenman E, & Johnson JW (1997) Trapping channel block of NMDA-activated responses by amantadine and memantine. *Journal of neurophysiology* 77(1):309-323.

252. Renner M, Schweizer C, Bannai H, Triller A, & Levi S (2012) Diffusion barriers constrain receptors at synapses. *PloS one* 7(8):e43032.

253. Connolly CN, Krishek BJ, McDonald BJ, Smart TG, & Moss SJ (1996) Assembly and cell surface expression of heteromeric and homomeric gamma-aminobutyric acid type A receptors. *The Journal of biological chemistry* 271(1):89-96.

254. Mortensen M, Patel B, & Smart TG (2011) GABA Potency at GABA(A) Receptors Found in Synaptic and Extrasynaptic Zones. *Frontiers in cellular neuroscience* 6:1.

255. Yushchenko DA, Zhang M, Yan Q, Waggoner AS, & Bruchez MP (2012) Genetically targetable and color-switching fluorescent probe. *Chembiochem : a European journal of chemical biology* 13(11):1564-1568.

256. Szent-Gyorgyi C, Schmidt BF, Fitzpatrick JA, & Bruchez MP (2010) Fluorogenic dendrons with multiple donor chromophores as bright genetically targeted and activated probes. *Journal of the American Chemical Society* 132(32):11103-11109.

257. Herring D*, et al.* (2003) Constitutive GABAA receptor endocytosis is dynamin-mediated and dependent on a dileucine AP2 adaptin-binding motif within the beta 2 subunit of the receptor. *The Journal of biological chemistry* 278(26):24046-24052.

258. Macia E*, et al.* (2006) Dynasore, a cell-permeable inhibitor of dynamin. *Developmental cell* 10(6):839-850.

259. Khalilov I, Khazipov R, Esclapez M, & Ben-Ari Y (1997) Bicuculline induces ictal seizures in the intact hippocampus recorded in vitro. *European journal of pharmacology* 319(2-3):R5-6.

260. Colombi I, Mahajani S, Frega M, Gasparini L, & Chiappalone M (2013) Effects of antiepileptic drugs on hippocampal neurons coupled to micro-electrode arrays. *Frontiers in neuroengineering* 6:10.

261. Hongo Y*, et al.* (2015) Heterogeneous effects of antiepileptic drugs in an in vitro epilepsy model--a functional multineuron calcium imaging study. *The European journal of neuroscience* 42(2):1818-1829.

262. Chauvette S, Soltani S, Seigneur J, & Timofeev I (2016) In vivo models of cortical acquired epilepsy. *Journal of neuroscience methods* 260:185-201.

263. Terunuma M*, et al.* (2008) Deficits in phosphorylation of GABA(A) receptors by intimately associated protein kinase C activity underlie compromised synaptic inhibition during status epilepticus. *The Journal of neuroscience : the official journal of the Society for Neuroscience* 28(2):376-384.

264. Glebov OO, Tigaret CM, Mellor JR, & Henley JM (2015) Clathrin-independent trafficking of AMPA receptors. *The Journal of neuroscience : the official journal of the Society for Neuroscience* 35(12):4830-4836.

265. Zheng N, Jeyifous O, Munro C, Montgomery JM, & Green WN (2015) Synaptic activity regulates AMPA receptor trafficking through different recycling pathways. *eLife* 4:e06878.

266. Schulze RJ*, et al.* (2013) Lipid droplet breakdown requires dynamin 2 for vesiculation of autolysosomal tubules in hepatocytes. *The Journal of cell biology* 203(2):315-326.

267. Park RJ*, et al.* (2013) Dynamin triple knockout cells reveal off target effects of commonly used dynamin inhibitors. *Journal of Cell Science* 126(22):5305-5312.

268. Preta G, Cronin JG, & Sheldon IM (2015) Dynasore - not just a dynamin inhibitor. *Cell Communication and Signaling : CCS* 13:24.

269. Liu W*, et al.* (2016) Local retention of antibodies in vivo with an injectable film embedded with a fluorogen-activating protein. *Journal of controlled release : official journal of the Controlled Release Society* 230:1-12.

270. Lorenz-Guertin JM, Bambino MJ, Das S, Weintraub ST, & Jacob TC (2019) Diazepam Accelerates GABAAR Synaptic Exchange and Alters Intracellular Trafficking. *bioRxiv*:514133.

271. Holt RA, Bateson AN, & Martin IL (1999) Decreased GABA enhancement of benzodiazepine binding after a single dose of diazepam. *Journal of neurochemistry* 72(5):2219-2222.

272. Tietz EI, Chiu TH, & Rosenberg HC (1989) Regional GABA/benzodiazepine receptor/chloride channel coupling after acute and chronic benzodiazepine treatment. *European journal of pharmacology* 167(1):57-65.

273. File SE, Wilks LJ, & Mabbutt PS (1988) Withdrawal, tolerance and sensitization after a single dose of lorazepam. *Pharmacology, biochemistry, and behavior* 31(4):937-940.

274. Wong PT, Yoong YL, & Gwee MC (1986) Acute tolerance to diazepam induced by benzodiazepines. *Clinical and experimental pharmacology & physiology* 13(1):1-8.

275. Lister RG & Nutt DJ (1986) Mice and rats are sensitized to the proconvulsant action of a benzodiazepine-receptor inverse agonist (FG 7142) following a single dose of lorazepam. *Brain research* 379(2):364-366.

276. Gallager DW, Lakoski JM, Gonsalves SF, & Rauch SL (1984) Chronic benzodiazepine treatment decreases postsynaptic GABA sensitivity. *Nature* 308:74.

277. Marley RJ & Gallager DW (1989) Chronic diazepam treatment produces regionally specific changes in GABA-stimulated chloride influx. *European journal of pharmacology* 159(3):217-223.

278. Gutierrez ML, Ferreri MC, & Gravielle MC (2014) GABA-induced uncoupling of GABA/benzodiazepine site interactions is mediated by increased GABAA receptor internalization and associated with a change in subunit composition. *Neuroscience* 257:119-129.

279. Ali NJ & Olsen RW (2001) Chronic benzodiazepine treatment of cells expressing recombinant GABA(A) receptors uncouples allosteric binding: studies on possible mechanisms. *Journal of neurochemistry* 79(5):1100-1108.

280. Di XJ, *et al.* (2016) Grp94 Protein Delivers gamma-Aminobutyric Acid Type A (GABAA) Receptors to Hrd1 Protein-mediated Endoplasmic Reticulum-associated Degradation. *The Journal of biological chemistry* 291(18):9526-9539.

281. Crider A, Pandya CD, Peter D, Ahmed AO, & Pillai A (2014) Ubiquitin-proteasome dependent degradation of GABAAα1 in autism spectrum disorder. *Molecular autism* 5(1):1-10.

282. Bogdanov Y, *et al.* (2006) Synaptic GABAA receptors are directly recruited from their extrasynaptic counterparts. *The EMBO journal* 25(18):4381-4389.

283. Gu Y, *et al.* (2016) Differential vesicular sorting of AMPA and GABAA receptors. *Proceedings of the National Academy of Sciences of the United States of America* 113(7):E922-931.

284. Tyagarajan SK & Fritschy JM (2014) Gephyrin: a master regulator of neuronal function? *Nature reviews. Neuroscience* 15(3):141-156.

285. Mukherjee J, *et al.* (2011) The residence time of GABA(A)Rs at inhibitory synapses is determined by direct binding of the receptor alpha1 subunit to gephyrin. *The Journal of neuroscience : the official journal of the Society for Neuroscience* 31(41):14677-14687.

286. Maric HM, Mukherjee J, Tretter V, Moss SJ, & Schindelin H (2011) Gephyrin-mediated gamma-aminobutyric acid type A and glycine receptor clustering relies on a common binding site. *The Journal of biological chemistry* 286(49):42105-42114.

287. Petrini EM, *et al.* (2014) Synaptic recruitment of gephyrin regulates surface GABAA receptor dynamics for the expression of inhibitory LTP. *Nature communications* 5:3921.

288. Zacchi P, Antonelli R, & Cherubini E (2014) Gephyrin phosphorylation in the functional organization and plasticity of GABAergic synapses. *Frontiers in cellular neuroscience* 8:103.

289. Ghosh H, *et al.* (2016) Several posttranslational modifications act in concert to regulate gephyrin scaffolding and GABAergic transmission. *Nat Commun* 7:13365.

290. Battaglia S, *et al.* (2018) Activity-Dependent Inhibitory Synapse Scaling Is Determined by Gephyrin Phosphorylation and Subsequent Regulation of GABAA Receptor Diffusion. *eNeuro* 5(1).

291. Schweizer C, *et al.* (2003) The gamma 2 subunit of GABA(A) receptors is required for maintenance of receptors at mature synapses. *Molecular and cellular neurosciences* 24(2):442-450.

292. Li RW, *et al.* (2005) Disruption of postsynaptic GABA receptor clusters leads to decreased GABAergic innervation of pyramidal neurons. *Journal of neurochemistry* 95(3):756-770.

293. Dantuma NP, Groothuis TA, Salomons FA, & Neefjes J (2006) A dynamic ubiquitin equilibrium couples proteasomal activity to chromatin remodeling. *The Journal of cell biology* 173(1):19-26.

294. Coffey EE, Beckel JM, Laties AM, & Mitchell CH (2014) Lysosomal alkalization and dysfunction in human fibroblasts with the Alzheimer's disease-linked presenilin 1 A246E mutation can be reversed with cAMP. *Neuroscience* 263:111-124.

295. Costa JT*, et al.* (2015) Gephyrin Cleavage in In Vitro Brain Ischemia Decreases GABA Receptor Clustering and Contributes to Neuronal Death. *Molecular neurobiology*.

296. Kumar A*, et al.* (2017) S-sulfocysteine/NMDA receptor-dependent signaling underlies neurodegeneration in molybdenum cofactor deficiency. *The Journal of clinical investigation*.

297. Yoong YL, Lee HS, Gwee MC, & Wong PT (1986) Acute tolerance to diazepam in mice: pharmacokinetic considerations. *Clinical and experimental pharmacology & physiology* 13(2):153-158.

298. Xie XH & Tietz EI (1992) Reduction in potency of selective gamma-aminobutyric acidA agonists and diazepam in CA1 region of in vitro hippocampal slices from chronic flurazepam-treated rats. *The Journal of pharmacology and experimental therapeutics* 262(1):204-211.

299. Van Sickle BJ, Xiang K, & Tietz EI (2004) Transient plasticity of hippocampal CA1 neuron glutamate receptors contributes to benzodiazepine withdrawal-anxiety. *Neuropsychopharmacology : official publication of the American College of Neuropsychopharmacology* 29(11):1994-2006.

300. Markowitz GJ, Kadam SD, Boothe DM, Irving ND, & Comi AM (2010) The pharmacokinetics of commonly used antiepileptic drugs in immature CD1 mice. *Neuroreport* 21(6):452-456.

301. Pratt CP*, et al.* (2017) Tagging of Endogenous BK Channels with a Fluorogen-Activating Peptide Reveals beta4-Mediated Control of Channel Clustering in Cerebellum. *Frontiers in cellular neuroscience* 11:337.

302. Wafford KA*, et al.* (1996) Functional characterization of human gamma-aminobutyric acidA receptors containing the alpha 4 subunit. *Molecular pharmacology* 50(3):670-678.

303. Förster T (1965) *Delocalized excitation and excitation transfer* (Academic Press Inc., New York).

304. Brady ML*, et al.* (2017) Depolarizing, inhibitory GABA type A receptor activity regulates GABAergic synapse plasticity via ERK and BDNF signaling. *Neuropharmacology* 128:324-339.

305. Nakamura T*, et al.* (2016) PX-RICS-deficient mice mimic autism spectrum disorder in Jacobsen syndrome through impaired GABAA receptor trafficking. *Nat Commun* 7:10861.

306. Qian Z, Micorescu M, Yakhnitsa V, & Barmack NH (2012) Climbing fiber activity reduces 14-3-3-theta regulated GABA(A) receptor phosphorylation in cerebellar Purkinje cells. *Neuroscience* 201:34-45.

307. Niwa F*, et al.* (2012) Gephyrin-independent GABA(A)R mobility and clustering during plasticity. *PloS one* 7(4):e36148.

308. van Rijnsoever C*, et al.* (2004) Requirement of alpha5-GABAA receptors for the development of tolerance to the sedative action of diazepam in mice. *The Journal of neuroscience : the official journal of the Society for Neuroscience* 24(30):6785-6790.

309. Crestani F*, et al.* (1999) Decreased GABAA-receptor clustering results in enhanced anxiety and a bias for threat cues. *Nature neuroscience* 2(9):833-839.

310. Ren Z*, et al.* (2015) Defects in dendrite and spine maturation and synaptogenesis associated with an anxious-depressive-like phenotype of GABAA receptor-deficient mice. *Neuropharmacology* 88:171-179.

311. Gunther U*, et al.* (1995) Benzodiazepine-insensitive mice generated by targeted disruption of the gamma 2 subunit gene of gamma-aminobutyric acid type A receptors. *Proceedings of the National Academy of Sciences of the United States of America* 92(17):7749-7753.

312. Nicholson MW*, et al.* (2018) Diazepam-induced loss of inhibitory synapses mediated by PLCδ/ Ca2+/calcineurin signalling downstream of GABAA receptors. *Molecular psychiatry*.

313. Kawasaki BT, Hoffman KB, Yamamoto RS, & Bahr BA (1997) Variants of the receptor/channel clustering molecule gephyrin in brain: distinct distribution patterns, developmental profiles, and proteolytic cleavage by calpain. *Journal of neuroscience research* 49(3):381-388.

314. Vlachos A, Reddy-Alla S, Papadopoulos T, Deller T, & Betz H (2013) Homeostatic regulation of gephyrin scaffolds and synaptic strength at mature hippocampal GABAergic postsynapses. *Cerebral cortex* 23(11):2700-2711.

315. Gonzalez MI, Cruz Del Angel Y, & Brooks-Kayal A (2013) Down-regulation of gephyrin and GABAA receptor subunits during epileptogenesis in the CA1 region of hippocampus. *Epilepsia* 54(4):616-624.

316. Mukherjee J*, et al.* (2017) Estradiol modulates the efficacy of synaptic inhibition by decreasing the dwell time of GABAA receptors at inhibitory synapses. *Proceedings of the National Academy of Sciences of the United States of America* 114(44):11763-11768.

317. Negishi M & Katoh H (2002) Rho family GTPases as key regulators for neuronal network formation. *Journal of biochemistry* 132(2):157-166.

318. Ge Y, *et al.* (2018) Clptm1 Limits Forward Trafficking of GABAA Receptors to Scale Inhibitory Synaptic Strength. *Neuron* 97(3):596-610.e598.

319. Uezu A, *et al.* (2016) Identification of an elaborate complex mediating postsynaptic inhibition. *Science (New York, N.Y.)* 353(6304):1123-1129.

320. Kang Y, *et al.* (2014) A combined transgenic proteomic analysis and regulated trafficking of neuroligin-2. *The Journal of biological chemistry* 289(42):29350-29364.

321. Butko MT, *et al.* (2013) In vivo quantitative proteomics of somatosensory cortical synapses shows which protein levels are modulated by sensory deprivation. *Proceedings of the National Academy of Sciences of the United States of America* 110(8):E726-735.

322. Churn SB, *et al.* (2002) Calcium/calmodulin-dependent kinase II phosphorylation of the GABAA receptor alpha1 subunit modulates benzodiazepine binding. *Journal of neurochemistry* 82(5):1065-1076.

323. Bachhuber MA, Hennessy S, Cunningham CO, & Starrels JL (2016) Increasing Benzodiazepine Prescriptions and Overdose Mortality in the United States, 1996-2013. *American journal of public health* 106(4):686-688.

324. Nutt DJ & Costello MJ (1988) Rapid induction of lorazepam dependence and reversal with flumazenil. *Life sciences* 43(13):1045-1053.

325. Hood SD, Norman A, Hince DA, Melichar JK, & Hulse GK (2014) Benzodiazepine dependence and its treatment with low dose flumazenil. *British journal of clinical pharmacology* 77(2):285-294.

326. Savic I, Widen L, & Stone-Elander S (1991) Feasibility of reversing benzodiazepine tolerance with flumazenil. *Lancet (London, England)* 337(8734):133-137.

327. Ferreri MC, Gutierrez ML, & Gravielle MC (2015) Tolerance to the sedative and anxiolytic effects of diazepam is associated with different alterations of GABAA receptors in rat cerebral cortex. *Neuroscience* 310:152-162.

328. Mody I & Pearce RA (2004) Diversity of inhibitory neurotransmission through GABA(A) receptors. *Trends in neurosciences* 27(9):569-575.

329. Gingrich KJ, Roberts WA, & Kass RS (1995) Dependence of the GABAA receptor gating kinetics on the alpha-subunit isoform: implications for structure-function relations and synaptic transmission. *The Journal of physiology* 489 ( Pt 2):529-543.

330. Ju YH, *et al.* (2009) Distinct properties of murine α5 γ-aminobutyric acid type a receptors revealed by biochemical fractionation and mass spectroscopy. *Journal of Neuroscience Research* 87(8):1737-1747.

331. del Rio JC, Araujo F, Ramos B, Ruano D, & Vitorica J (2001) Prevalence between different alpha subunits performing the benzodiazepine binding sites in native heterologous GABA(A) receptors containing the alpha2 subunit. *Journal of neurochemistry* 79(1):183-191.

332. Araujo F, Ruano D, & Vitorica J (1999) Native gamma-aminobutyric acid type A receptors from rat hippocampus, containing both alpha 1 and alpha 5 subunits, exhibit a single benzodiazepine binding site with alpha 5 pharmacological properties. *J Pharmacol Exp Ther* 290(3):989-997.

333. Sur C*, et al.* (1999) Preferential coassembly of alpha4 and delta subunits of the gamma-aminobutyric acidA receptor in rat thalamus. *Molecular pharmacology* 56(1):110-115.

334. Benke D, Michel C, & Mohler H (1997) GABA(A) receptors containing the alpha4-subunit: prevalence, distribution, pharmacology, and subunit architecture in situ. *Journal of neurochemistry* 69(2):806-814.

335. Paoletti P, Bellone C, & Zhou Q (2013) NMDA receptor subunit diversity: impact on receptor properties, synaptic plasticity and disease. *Nature reviews. Neuroscience* 14(6):383-400.

336. Cho KK, Khibnik L, Philpot BD, & Bear MF (2009) The ratio of NR2A/B NMDA receptor subunits determines the qualities of ocular dominance plasticity in visual cortex. *Proceedings of the National Academy of Sciences of the United States of America* 106(13):5377-5382.

337. Bagetta V*, et al.* (2012) Rebalance of striatal NMDA/AMPA receptor ratio underlies the reduced emergence of dyskinesia during D2-like dopamine agonist treatment in experimental Parkinson's disease. *The Journal of neuroscience : the official journal of the Society for Neuroscience* 32(49):17921-17931.

338. Myme CI, Sugino K, Turrigiano GG, & Nelson SB (2003) The NMDA-to-AMPA ratio at synapses onto layer 2/3 pyramidal neurons is conserved across prefrontal and visual cortices. *Journal of neurophysiology* 90(2):771-779.

339. Allison C & Pratt JA (2003) Neuroadaptive processes in GABAergic and glutamatergic systems in benzodiazepine dependence. *Pharmacology & therapeutics* 98(2):171-195.

340. Stephens DN & Turski L (1993) Kindling to the benzodiazepine receptor inverse agonist, FG 7142: evidence for involvement of NMDA, but not non-NMDA, glutamatergic receptors. *Neuropharmacology* 32(10):1011-1017.

341. Koff JM, Pritchard GA, Greenblatt DJ, & Miller LG (1997) The NMDA receptor competitive antagonist CPP modulates benzodiazepine tolerance and discontinuation. *Pharmacology* 55(5):217-227.

342. Tsuda M, Suzuki T, & Misawa M (1997) Recovery of decreased seizure threshold for pentylenetetrazole during diazepam withdrawal by NMDA receptor antagonists. *European journal of pharmacology* 324(1):63-66.

343. Tsuda M, Suzuki T, & Misawa M (1998) NMDA receptor antagonists potently suppress the spontaneous withdrawal signs induced by discontinuation of long-term diazepam treatment in Fischer 344 rats. *Brain research* 790(1-2):82-90.

344. Tsuda M, Chiba Y, Suzuki T, & Misawa M (1998) Upregulation of NMDA receptor subunit proteins in the cerebral cortex during diazepam withdrawal. *European journal of pharmacology* 341(2-3):R1-2.

345. Tsuda M, Suzuki T, & Misawa M (1998) Region-specific changes in [3H]dizocilpine binding in diazepam-withdrawn rats. *Neuroscience letters* 240(2):113-115.

346. Price DD, Mayer DJ, Mao J, & Caruso FS (2000) NMDA-receptor antagonists and opioid receptor interactions as related to analgesia and tolerance. *Journal of pain and symptom management* 19(1 Suppl):S7-11.

347. Nagy J (2008) Alcohol related changes in regulation of NMDA receptor functions. *Current neuropharmacology* 6(1):39-54.

348. Khanna JM, Kalant H, Chau A, & Shah G (1998) Effect of NMDA antagonists on development of rapid tolerance to various barbiturates. *Alcohol (Fayetteville, N.Y.)* 15(1):9-18.

349. Steppuhn KG & Turski L (1993) Diazepam dependence prevented by glutamate antagonists. *Proceedings of the National Academy of Sciences of the United States of America* 90(14):6889-6893.

350. File SE & Fernandes C (1994) Dizocilpine prevents the development of tolerance to the sedative effects of diazepam in rats. *Pharmacology, biochemistry, and behavior* 47(4):823-826.

351. Brady ML*, et al.* (2013) Moderate prenatal alcohol exposure reduces plasticity and alters NMDA receptor subunit composition in the dentate gyrus. *The Journal of neuroscience : the official journal of the Society for Neuroscience* 33(3):1062-1067.

352. Povysheva NV*, et al.* (2006) Properties of excitatory synaptic responses in fast-spiking interneurons and pyramidal cells from monkey and rat prefrontal cortex. *Cerebral cortex* 16(4):541-552.

353. Povysheva NV & Johnson JW (2012) Tonic NMDA receptor-mediated current in prefrontal cortical pyramidal cells and fast-spiking interneurons. *Journal of neurophysiology* 107(8):2232-2243.

354. Heikkinen AE, Moykkynen TP, & Korpi ER (2009) Long-lasting modulation of glutamatergic transmission in VTA dopamine neurons after a single dose of benzodiazepine agonists. *Neuropsychopharmacology : official publication of the American College of Neuropsychopharmacology* 34(2):290-298.

355. MacDonald ML, *et al.* (2012) Biochemical fractionation and stable isotope dilution liquid chromatography-mass spectrometry for targeted and microdomain-specific protein quantification in human postmortem brain tissue. *Molecular & cellular proteomics : MCP* 11(12):1670-1681.

356. MacDonald ML, *et al.* (2019) Laser capture microdissection-targeted mass spectrometry: a method for multiplexed protein quantification within individual layers of the cerebral cortex. *Neuropsychopharmacology* 44(4):743-748.

357. Krivinko JM, *et al.* (2018) Synaptic Proteome Compensation and Resilience to Psychosis in Alzheimer's Disease. *Am J Psychiatry* 175(10):999-1009.

358. MacDonald ML, *et al.* (2015) Altered glutamate protein co-expression network topology linked to spine loss in the auditory cortex of schizophrenia. *Biol Psychiatry* 77(11):959-968.

359. Trinidad JC, *et al.* (2008) Quantitative analysis of synaptic phosphorylation and protein expression. *Molecular {\&} Cellular Proteomics* 7(4):684-696.

360. Chang-Gyu H, *et al.* (2009) The Post-Synaptic Density of Human Postmortem Brain Tissues: An Experimental Study Paradigm for Neuropsychiatric Illnesses. *Public Library of Sciences* (Journal Article).

361. MacLean B, *et al.* (2010) Skyline: an open source document editor for creating and analyzing targeted proteomics experiments. *Bioinformatics* 26(7):966-968.

362. Vinkers CH, *et al.* (2012) GABA(A) receptor alpha subunits differentially contribute to diazepam tolerance after chronic treatment. *PloS one* 7(8):e43054.

363. Brett RR & Pratt JA (1995) Changes in benzodiazepine-GABA receptor coupling in an accumbens-habenula circuit after chronic diazepam treatment. *British journal of pharmacology* 116(5):2375-2384.

364. Hu XJ & Ticku MK (1994) Chronic benzodiazepine agonist treatment produces functional uncoupling of the gamma-aminobutyric acid-benzodiazepine receptor ionophore complex in cortical neurons. *Molecular pharmacology* 45(4):618-625.

365. Roca DJ, *et al.* (1990) gamma-Aminobutyric acidA receptor regulation in culture: altered allosteric interactions following prolonged exposure to benzodiazepines, barbiturates, and methylxanthines. *Molecular pharmacology* 37(5):710-719.

366. Rudolph U, *et al.* (1999) Benzodiazepine actions mediated by specific gamma-aminobutyric acid(A) receptor subtypes. *Nature* 401(6755):796-800.

367. McKernan RM*, et al.* (2000) Sedative but not anxiolytic properties of benzodiazepines are mediated by the GABA(A) receptor alpha1 subtype. *Nature neuroscience* 3(6):587-592.

368. Tombes RM, Faison MO, & Turbeville JM (2003) Organization and evolution of multifunctional Ca(2+)/CaM-dependent protein kinase genes. *Gene* 322:17-31.

369. Liu XB & Murray KD (2012) Neuronal excitability and calcium/calmodulin-dependent protein kinase type II: location, location, location. *Epilepsia* 53 Suppl 1:45-52.

370. Takeuchi Y, Nomura K, & Fukunaga K (2004) Differential subcellular distribution of Ca2+/calmodulin-dependent protein kinase II isoforms in the striatum and NG108-15 cells. *Journal of neuroscience research* 75(4):480-490.

371. Bayer KU, Lohler J, Schulman H, & Harbers K (1999) Developmental expression of the CaM kinase II isoforms: ubiquitous gamma- and delta-CaM kinase II are the early isoforms and most abundant in the developing nervous system. *Brain research. Molecular brain research* 70(1):147-154.

372. Lin Y, Jover-Mengual T, Wong J, Bennett MV, & Zukin RS (2006) PSD-95 and PKC converge in regulating NMDA receptor trafficking and gating. *Proceedings of the National Academy of Sciences of the United States of America* 103(52):19902-19907.

373. Yan JZ*, et al.* (2011) Protein kinase C promotes N-methyl-D-aspartate (NMDA) receptor trafficking by indirectly triggering calcium/calmodulin-dependent protein kinase II (CaMKII) autophosphorylation. *The Journal of biological chemistry* 286(28):25187-25200.

374. Zeitz KP, Malmberg AB, Gilbert H, & Basbaum AI (2001) Reduced development of tolerance to the analgesic effects of morphine and clonidine in PKC gamma mutant mice. *Pain* 94(3):245-253.

375. Celerier E, Simonnet G, & Maldonado R (2004) Prevention of fentanyl-induced delayed pronociceptive effects in mice lacking the protein kinase Cgamma gene. *Neuropharmacology* 46(2):264-272.

376. Nemes AD*, et al.* (2017) Growth Associated Protein 43 (GAP-43) as a Novel Target for the Diagnosis, Treatment and Prevention of Epileptogenesis. *Sci Rep* 7(1):17702.

377. Goslin K, Schreyer DJ, Skene JH, & Banker G (1988) Development of neuronal polarity: GAP-43 distinguishes axonal from dendritic growth cones. *Nature* 336(6200):672-674.

378. Liu YC, Chapman ER, & Storm DR (1991) Targeting of neuromodulin (GAP-43) fusion proteins to growth cones in cultured rat embryonic neurons. *Neuron* 6(3):411-420.

379. Meiri KF & Gordon-Weeks PR (1990) GAP-43 in growth cones is associated with areas of membrane that are tightly bound to substrate and is a component of a membrane skeleton subcellular fraction. *The Journal of neuroscience : the official journal of the Society for Neuroscience* 10(1):256-266.

380. Gianotti C, Nunzi MG, Gispen WH, & Corradetti R (1992) Phosphorylation of the presynaptic protein B-50 (GAP-43) is increased during electrically induced long-term potentiation. *Neuron* 8(5):843-848.

381. Nelson RB, Linden DJ, Hyman C, Pfenninger KH, & Routtenberg A (1989) The two major phosphoproteins in growth cones are probably identical to two protein kinase C substrates correlated with persistence of long-term potentiation. *The Journal of neuroscience : the official journal of the Society for Neuroscience* 9(2):381-389.

382. Jiang-Xie LF*, et al.* (2014) Autism-associated gene Dlgap2 mutant mice demonstrate exacerbated aggressive behaviors and orbitofrontal cortex deficits. *Molecular autism* 5:32.

383. Zhao C*, et al.* (2015) The upregulation of NR2A-containing N-methyl-D-aspartate receptor function by tyrosine phosphorylation of postsynaptic density 95 via facilitating Src/proline-rich tyrosine kinase 2 activation. *Molecular neurobiology* 51(2):500-511.

384. Giralt A*, et al.* (2017) Pyk2 modulates hippocampal excitatory synapses and contributes to cognitive deficits in a Huntington's disease model. *Nat Commun* 8:15592.

385. Afonso P & De Luca P (2019) BDNF increases synaptic NMDA receptor abundance by enhancing the local translation of Pyk2 in cultured hippocampal neurons. 12(586).

386. Huang Y*, et al.* (2001) CAKbeta/Pyk2 kinase is a signaling link for induction of long-term potentiation in CA1 hippocampus. *Neuron* 29(2):485-496.

387. Mukherjee K*, et al.* (2010) Piccolo and bassoon maintain synaptic vesicle clustering without directly participating in vesicle exocytosis. *Proceedings of the National Academy of Sciences of the United States of America* 107(14):6504-6509.

388. Parthier D, Kuner T, & Korber C (2018) The presynaptic scaffolding protein Piccolo organizes the readily releasable pool at the calyx of Held. *The Journal of physiology* 596(8):1485-1499.

389. Wu D*, et al.* (2017) Postsynaptic synaptotagmins mediate AMPA receptor exocytosis during LTP. *Nature* 544(7650):316-321.

390. Hutagalung AH & Novick PJ (2011) Role of Rab GTPases in membrane traffic and cell physiology. *Physiological reviews* 91(1):119-149.

391. Wu Y*, et al.* (2014) A dynamin 1-, dynamin 3- and clathrin-independent pathway of synaptic vesicle recycling mediated by bulk endocytosis. *Elife* 3:e01621.

392. Gray NW*, et al.* (2003) Dynamin 3 is a component of the postsynapse, where it interacts with mGluR5 and Homer. *Current biology : CB* 13(6):510-515.

393. Fan F, Funk L, & Lou X (2016) Dynamin 1- and 3-Mediated Endocytosis Is Essential for the Development of a Large Central Synapse In Vivo. *The Journal of Neuroscience* 36(22):6097-6115.

394. Conti M & Beavo J (2007) Biochemistry and physiology of cyclic nucleotide phosphodiesterases: essential components in cyclic nucleotide signaling. *Annual review of biochemistry* 76:481-511.

395. Sierksma AS*, et al.* (2013) Chronic phosphodiesterase type 2 inhibition improves memory in the APPswe/PS1dE9 mouse model of Alzheimer's disease. *Neuropharmacology* 64:124-136.

396. Xu Y, Zhang HT, & O'Donnell JM (2011) Phosphodiesterases in the central nervous system: implications in mood and cognitive disorders. *Handbook of experimental pharmacology* (204):447-485.

397. Gomez L & Breitenbucher JG (2013) PDE2 inhibition: potential for the treatment of cognitive disorders. *Bioorganic & medicinal chemistry letters* 23(24):6522-6527.

398. Barrera NP & Robinson CV (2011) Advances in the mass spectrometry of membrane proteins: from individual proteins to intact complexes. *Annual review of biochemistry* 80:247-271.

399. Spence EF & Kanak DJ (2016) The Arp2/3 Complex Is Essential for Distinct Stages of Spine Synapse Maturation, Including Synapse Unsilencing. 36(37):9696-9709.

400. Miller SG & Kennedy MB (1986) Regulation of brain type II Ca2+/calmodulin-dependent protein kinase by autophosphorylation: a Ca2+-triggered molecular switch. *Cell* 44(6):861-870.

401. Woolfrey KM & Dell'Acqua ML (2015) Coordination of Protein Phosphorylation and Dephosphorylation in Synaptic Plasticity. *Journal of Biological Chemistry* 290(48):28604-28612.

402. Pi HJ*, et al.* (2010) CaMKII control of spine size and synaptic strength: role of phosphorylation states and nonenzymatic action. *Proceedings of the National Academy of Sciences of the United States of America* 107(32):14437-14442.

403. Lledo PM*, et al.* (1995) Calcium/calmodulin-dependent kinase II and long-term potentiation enhance synaptic transmission by the same mechanism. *Proceedings of the National Academy of Sciences of the United States of America* 92(24):11175-11179.

404. Zhou X & Smith SS (2009) Expression levels of the alpha4 subunit of the GABA(A) receptor in differentiated neuroblastoma cells are correlated with GABA-gated current. *Neuropharmacology* 56(6-7):1041-1053.

405. Mahmoudi M, Kang MH, Tillakaratne N, Tobin AJ, & Olsen RW (1997) Chronic intermittent ethanol treatment in rats increases GABA(A) receptor alpha4-subunit expression: possible relevance to alcohol dependence. *Journal of neurochemistry* 68(6):2485-2492.

406. Devaud LL, Fritschy JM, Sieghart W, & Morrow AL (1997) Bidirectional alterations of GABA(A) receptor subunit peptide levels in rat cortex during chronic ethanol consumption and withdrawal. *Journal of neurochemistry* 69(1):126-130.

407. Cagetti E, Liang J, Spigelman I, & Olsen RW (2003) Withdrawal from chronic intermittent ethanol treatment changes subunit composition, reduces synaptic function, and decreases behavioral responses to positive allosteric modulators of GABAA receptors. *Molecular pharmacology* 63(1):53-64.

408. Smith SS*, et al.* (1998) GABA(A) receptor alpha4 subunit suppression prevents withdrawal properties of an endogenous steroid. *Nature* 392(6679):926-930.

409. Smith SS*, et al.* (1998) Withdrawal from 3alpha-OH-5alpha-pregnan-20-One using a pseudopregnancy model alters the kinetics of hippocampal GABAA-gated current and increases the GABAA receptor alpha4 subunit in association with increased anxiety. *The Journal of neuroscience : the official journal of the Society for Neuroscience* 18(14):5275-5284.

410. Serra M*, et al.* (2006) Social isolation-induced increase in alpha and delta subunit gene expression is associated with a greater efficacy of ethanol on steroidogenesis and GABA receptor function. *Journal of neurochemistry* 98(1):122-133.

411. Clark M (1998) Sensitivity of the rat hippocampal GABA(A) receptor alpha 4 subunit to electroshock seizures. *Neuroscience letters* 250(1):17-20.

412. Banerjee PK*, et al.* (1998) Alterations in GABAA receptor alpha 1 and alpha 4 subunit mRNA levels in thalamic relay nuclei following absence-like seizures in rats. *Experimental neurology* 154(1):213-223.

413. Brooks-Kayal AR, Shumate MD, Jin H, Rikhter TY, & Coulter DA (1998) Selective changes in single cell GABA(A) receptor subunit expression and function in temporal lobe epilepsy. *Nature medicine* 4(10):1166-1172.

414. Sun C, Mtchedlishvili Z, Erisir A, & Kapur J (2007) Diminished neurosteroid sensitivity of synaptic inhibition and altered location of the alpha4 subunit of GABA(A) receptors in an animal model of epilepsy. *The Journal of neuroscience : the official journal of the Society for Neuroscience* 27(46):12641-12650.

415. Hadingham KL*, et al.* (1993) Cloning of cDNA sequences encoding human alpha 2 and alpha 3 gamma-aminobutyric acidA receptor subunits and characterization of the benzodiazepine pharmacology of recombinant alpha 1-, alpha 2-, alpha 3-, and alpha 5-containing human gamma-aminobutyric acidA receptors. *Molecular pharmacology* 43(6):970-975.

416. Lingford-Hughes A*, et al.* (2002) Imaging the GABA-benzodiazepine receptor subtype containing the alpha5-subunit in vivo with [11C]Ro15 4513 positron emission tomography. *Journal of cerebral blood flow and metabolism : official journal of the International Society of Cerebral Blood Flow and Metabolism* 22(7):878-889.

417. Maeda J*, et al.* (2003) Visualization of alpha5 subunit of GABAA/benzodiazepine receptor by 11C Ro15-4513 using positron emission tomography. *Synapse (New York, N.Y.)* 47(3):200-208.

418. McKernan RM & Whiting PJ (1996) Which GABAA-receptor subtypes really occur in the brain? *Trends in neurosciences* 19(4):139-143.

419. Van Sickle BJ, Cox AS, Schak K, Greenfield LJ, Jr., & Tietz EI (2002) Chronic benzodiazepine administration alters hippocampal CA1 neuron excitability: NMDA receptor function and expression(1). *Neuropharmacology* 43(4):595-606.

420. Das P, Zerda R, Alvarez FJ, & Tietz EI (2010) Immunogold electron microscopic evidence of differential regulation of GluN1, GluN2A, and GluN2B, NMDA-type glutamate receptor subunits in rat hippocampal CA1 synapses during benzodiazepine withdrawal. *The Journal of comparative neurology* 518(21):4311-4328.

421. Van Sickle BJ & Tietz EI (2002) Selective enhancement of AMPA receptor-mediated function in hippocampal CA1 neurons from chronic benzodiazepine-treated rats. *Neuropharmacology* 43(1):11-27.

422. Xiang K & Tietz EI (2007) Benzodiazepine-induced hippocampal CA1 neuron alpha-amino-3-hydroxy-5-methylisoxasole-4-propionic acid (AMPA) receptor plasticity linked to severity of withdrawal anxiety: differential role of voltage-gated calcium channels and N-methyl-D-aspartic acid receptors. *Behavioural pharmacology* 18(5-6):447-460.

423. Shen G & Tietz EI (2011) Down-regulation of synaptic GluN2B subunit-containing N-methyl-D-aspartate receptors: a physiological brake on CA1 neuron alpha-amino-3-hydroxy-5-methyl-4-isoxazolepropionic acid hyperexcitability during benzodiazepine withdrawal. *The Journal of pharmacology and experimental therapeutics* 336(1):265-273.

424. Zalcman G, Federman N, & Romano A (2018) CaMKII Isoforms in Learning and Memory: Localization and Function. *Frontiers in molecular neuroscience* 11:445.

425. Shen G, Mohamed MS, Das P, & Tietz EI (2009) Positive allosteric activation of GABAA receptors bi-directionally modulates hippocampal glutamate plasticity and behaviour. *Biochemical Society transactions* 37(Pt 6):1394-1398.

426. Shen G, Van Sickle BJ, & Tietz EI (2010) Calcium/calmodulin-dependent protein kinase II mediates hippocampal glutamatergic plasticity during benzodiazepine withdrawal. *Neuropsychopharmacology : official publication of the American College of Neuropsychopharmacology* 35(9):1897-1909.

427. Huopaniemi L, Keist R, Randolph A, Certa U, & Rudolph U (2004) Diazepam-induced adaptive plasticity revealed by alpha1 GABAA receptor-specific expression profiling. *Journal of neurochemistry* 88(5):1059-1067.

428. Bilsky EJ, Bernstein RN, Wang Z, Sadee W, & Porreca F (1996) Effects of naloxone and D-Phe-Cys-Tyr-D-Trp-Arg-Thr-Pen-Thr-NH2 and the protein kinase inhibitors H7 and H8 on acute morphine dependence and antinociceptive tolerance in mice. *The Journal of pharmacology and experimental therapeutics* 277(1):484-490.

429. Fan GH, Wang LZ, Qiu HC, Ma L, & Pei G (1999) Inhibition of calcium/calmodulin-dependent protein kinase II in rat hippocampus attenuates morphine tolerance and dependence. *Molecular pharmacology* 56(1):39-45.

430. Granados-Soto V, Kalcheva I, Hua X, Newton A, & Yaksh TL (2000) Spinal PKC activity and expression: role in tolerance produced by continuous spinal morphine infusion. *Pain* 85(3):395-404.

431. Mayer DJ, Mao J, & Price DD (1995) The development of morphine tolerance and dependence is associated with translocation of protein kinase C. *Pain* 61(3):365-374.

432. Tang L, Shukla PK, Wang LX, & Wang ZJ (2006) Reversal of morphine antinociceptive tolerance and dependence by the acute supraspinal inhibition of Ca(2+)/calmodulin-dependent protein kinase II. *The Journal of pharmacology and experimental therapeutics* 317(2):901-909.

433. Wang Z, Bilsky EJ, Porreca F, & Sadee W (1994) Constitutive mu opioid receptor activation as a regulatory mechanism underlying narcotic tolerance and dependence. *Life sciences* 54(20):Pl339-350.

434. Wang ZJ, Tang L, & Xin L (2003) Reversal of morphine antinociceptive tolerance by acute spinal inhibition of Ca(2+)/calmodulin-dependent protein kinase II. *European journal of pharmacology* 465(1-2):199-200.

435. Shukla PK, Tang L, & Wang ZJ (2006) Phosphorylation of neurogranin, protein kinase C, and Ca2+/calmodulin dependent protein kinase II in opioid tolerance and dependence. *Neuroscience letters* 404(3):266-269.

436. Gao L & Greenfield LJ (2005) Activation of protein kinase C reduces benzodiazepine potency at GABAA receptors in NT2-N neurons. *Neuropharmacology* 48(3):333-342.

437. Chou WH*, et al.* (2010) GABAA receptor trafficking is regulated by protein kinase C(epsilon) and the N-ethylmaleimide-sensitive factor. *The Journal of neuroscience : the official journal of the Society for Neuroscience* 30(42):13955-13965.

438. Proctor WR*, et al.* (2003) Ethanol differentially enhances hippocampal GABA A receptor-mediated responses in protein kinase C gamma (PKC gamma) and PKC epsilon null mice. *The Journal of pharmacology and experimental therapeutics* 305(1):264-270.

439. Kumar S, Sieghart W, & Morrow AL (2002) Association of protein kinase C with GABA(A) receptors containing alpha1 and alpha4 subunits in the cerebral cortex: selective effects of chronic ethanol consumption. *Journal of neurochemistry* 82(1):110-117.

440. Werner DF*, et al.* (2011) PKCgamma is required for ethanol-induced increases in GABA(A) receptor alpha4 subunit expression in cultured cerebral cortical neurons. *Journal of neurochemistry* 116(4):554-563.

441. Cui W*, et al.* (2009) Systemic lidocaine inhibits remifentanil-induced hyperalgesia via the inhibition of cPKCgamma membrane translocation in spinal dorsal horn of rats. *Journal of neurosurgical anesthesiology* 21(4):318-325.

442. Rodriguez-Munoz M, de la Torre-Madrid E, Sanchez-Blazquez P, Wang JB, & Garzon J (2008) NMDAR-nNOS generated zinc recruits PKCgamma to the HINT1-RGS17 complex bound to the C terminus of Mu-opioid receptors. *Cellular signalling* 20(10):1855-1864.

443. Chang S, Trimbuch T, & Rosenmund C (2018) Synaptotagmin-1 drives synchronous Ca(2+)-triggered fusion by C2B-domain-mediated synaptic-vesicle-membrane attachment. *Nature neuroscience* 21(1):33-40.

444. Popik P & Skolnick P (1996) The NMDA antagonist memantine blocks the expression and maintenance of morphine dependence. *Pharmacology, biochemistry, and behavior* 53(4):791-797.

445. Maler JM*, et al.* (2005) Memantine inhibits ethanol-induced NMDA receptor up-regulation in rat hippocampal neurons. *Brain research* 1052(2):156-162.

446. Krupitsky EM*, et al.* (2007) Effect of memantine on cue-induced alcohol craving in recovering alcohol-dependent patients. *The American journal of psychiatry* 164(3):519-523.